I. APPLICATION OF NORMAL MODE THEORY TO SEISMIC SOURCE AND STRUCTURE PROBLEMS

II. SEISMIC INVESTIGATIONS OF UPPER MANTLE LATERAL HETEROGENEITY

Thesis by

Emile André Okal

In Partial Fulfillment of the Requirements

for the Degree of

Doctor of Philosophy

California Institute of Technology

Pasadena, California

1978

(Submitted April 13, 1978)

Toujours l'intérieur de la Terre travaille,

Son flanc universel incessamment tressaille...

Victor Hugo,

Les Feuilles d'Automne.

I am grateful to my advisor, David G. Harkrider, whose personal interest in my work contributed greatly to the achievement of this study. Dave and Janna also introduced me to the American tradition of Thanksgiving parties, which have been very nice and quite enjoyable.

My early interest in lateral heterogeneity was stimulated by Don L. Anderson, who constantly encouraged me in this work, and decisively sharpened my curiosity about the Earth (and, occasionally, other celestial bodies).

A large part of the present research evolved and greatly benefited from discussions with Hiroo Kanamori. Hiroo introduced me to the Earth's normal modes, and his universal interest for a wide range of geophysical problems has been a constant source of inspiration. Being a Teaching Assistant in his class was an especially exciting experience, and I am particularly indebted to him for this opportunity.

My association with Robert J. Geller and Seth Stein into the 'Gang of Modes' has been extremely enlightening. I was very fortunate to work with Bob on many aspects of Part I. His criticism and suggestions, during countless nights of working together or discussing over breakfast, provided much emulation into this work. Bob has also been a devoted friend in being concerned with my future plans, and I am very grateful to him in that respect. Meanwhile, Seth helped keep my scientific interests balanced through exciting joint ventures in Plate Tectonics.

I have benefited considerably from regular interaction with many members of the Seismological Laboratory community. Discussion on some

of the present material with Christine Powell, Donald V. Helmberger, J. Bernard Minster, Yoshio Fukao and Katsuyuki Abe is especially acknowledged. I am also grateful to Ralph Gilman, who built and watchfully cares after the ultra-long period systems at Kresge, and who took me there on a pilgrimage for a check of their responses.

Most of the mode data used in this study was kindly made available on a tape by Freeman Gilbert. I also made use of Robert Hart's file of excitation functions.

I am particularly grateful to Keiiti Aki for fruitful discussions, the most recent one over lunch in Cambridge.

Would it not be for the skilled work of Mrs. Marla Turner, few theses would ever see the light at the Lab. She did a marvelous job of typing this one, and so did Laszlo Lenches and Joe Galvan, who drafted some of the figures in Part II.

Financial support over my four years at Caltech has come from NASA, under Contract NGL-05-002-069, and the National Science Fundation, most recently under Grant EAR77-14675, and is gratefully acknowledged.

I was fortunate to be able to carry on the present work while fulfilling my national duties by teaching French, under the Volontariat au Service National Actif of the Ministère de la Coopération.

Finally, a special word of appreciation goes to Antoine Auquier, Guy Kuster and Bernard Minster. During the grim Winter and Spring of 1974, their friendship was instrumental in helping me reach an important personal decision.

Abstract

In Part I, the theory of the normal modes of the Earth is investigated and used to build synthetic seismograms in order to solve source and structural problems. After a study of the physical properties of spheroidal modes leading to a rational classification, two specific problems are addressed: the observability of deep isotropic seismic sources and the investigation of the physical properties of the Earth in the neighborhood of the Core-Mantle boundary, using SH waves diffracted at the core's surface.

In Chapter 1, it is shown that five different families of spheroidal modes can be isolated on the basis of their physical properties, including group velocities, attenuation and excitation functions. Except for a few hybrid modes, these families are arranged in "pseudo-overtone" branches, along which physical properties vary smoothly. The simplified model of a spherical, non-gravitating Earth is used to give a theoretical description of the properties of modes with low angular orders. Their group velocity is shown to be consistent with the physical concept of dispersion along a pseudo-overtone branch, thereby justifying the use of asymptotic expansions along them in generating synthetic seismograms. An interpretation of the existence of the various families in terms of an increase in mode-coupling with angular order is presented. A formal classification of the spheroidal modes into the five families is made, and a new nomenclature reflecting the physical properties of the modes is proposed.

In Chapter 2, the relative excitation of body and surface waves

by isotropic and deviatoric sources is studied as a function of depth and frequency. Since the fundamental Rayleigh wave excitation dies off faster as a function of frequency and depth for isotropic than for deviatoric sources, an ultra-long period record at Pasadena of the Colombian deep shock of 1970 (for which a compressional precursor was proposed), is studied and compared to synthetic seismograms calculated for several source models. The best agreement is obtained for a pure double-couple source. Linear combinations of synthetics for deviatoric and isotropic sources are tested for a wide range of relative amplitudes, showing the data to be little sensitive to the presence of a reasonably large isotropic component.

In Chapter 3, profiles of seismic shear waves diffracted around the core (Sd) for three deep events recorded at stations across North America and the Atlantic Ocean are used to determine the properties of the lower mantle in the vicinity of the core-mantle boundary. The S wave velocity above the surface of the core is found to be 7.22 ± 0.1 km/s, in agreement with gross Earth models, but higher than previously reported values from direct measurements of Sd. No evidence for a low-velocity zone in the lower mantle is found. Synthetic seismograms for Sd are easily generated through normal mode summation. A comparison of the present data with a synthetic profile for Earth model 1066A gives excellent agreement at periods greater than 45 seconds. Synthetics for other models confirm the absence of a strong low-velocity zone at the base of the mantle, and are used to strongly constrain any possible rigidity of the uppermost layers of the core.

In Part II, data sets of seismic body and surface waves are used in a search for possible deep lateral heterogeneities in the mantle. In both cases, it is found that seismic data do not require structural differences between oceans and continents to extend deeper than 250 km. In general, differences between oceans and continents are found to be on the same order of magnitude as the intrinsic lateral heterogeneity in the oceanic plate brought about by the aging of the oceanic lithosphere. A consistent similarity is inferred between stable shields and the oldest parts of the oceans.

In Chapter 1, an analysis of records of multiply reflected ScS phases from ten deep focus earthquakes yields near-vertical one-way travel-time residuals ranging from -3.5 to +5.0 seconds. Continental and oceanic residuals overlap, and both indicate large lateral variations. Similar values are found for the older oceanic basins (Western Pacific, Brazil Basin) and continental shields. Most, if not all, of the variations can be attributed to differences in the lithosphere and asthenosphere, down to a depth of 200 km, and the present results are in good agreement with local models derived by independent means. Oceanic islands are found to be anomalous with respect to the neighboring ocean floor, the mantle beneath Hawaii, Iceland and Trindade (South Atlantic) being exceptionally slow.

In Chapter 2, Rayleigh wave phase velocities at very long periods (185 to 290 seconds) are investigated and regionalized, taking into account the lateral heterogeneities in the oceanic plates revealed by earlier studies at shorter periods. The two-station method is applied to a few 'pure-age' oceanic paths, and is shown to

be compatible with an average gross Earth model below depths of 180 km. Under this assumed oceanic model, regionalized for age above 180 km, continental velocities are derived from a set of experimental great-circle values, both new or taken from previously published studies. The results basically agree with the earlier studies by Kanamori or Dziewonski, and it is suggested that the assumption of a uniform oceanic model may have been responsible for some scatter in Kanamori's solution. The results of the present inversion are successfully checked against a set of values derived by the two-station method from a pure continental, tectonic, path. A recent event in Indonesia is then used as a further independent check, in what is believed to be the first experimental determination of Rayleigh wave phase velocities over a pure shield path at very long periods. The shield velocities fall within the range of variation of their oceanic counterparts with the age of the plate, in agreement with the results of Chapter 1. This makes velocities derived theoretically from models involving deep continent vs. ocean lateral heterogeneities inconsistent with the present set of experimental data. Finally, it is shown that Dziewonski's model S2 reconciles all experimental seismic data relative to shields without being significantly different from oceanic models below 240 km.

Table of Contents

I. APPLICATION OF NORMAL MODE THEORY TO SEISMIC SOURCE AND STRUCTURE PROBLEMS

INTRODUCTION

In studying the propagation of a seismic disturbance through the Earth, there exist two alternate approaches: In wave theory, one considers mainly the local properties of the immediate neighborhood of the wavefront, and how they affect the propagation, ignoring as much as possible the finite size of the planet. In the other approach, one focuses on the description of the instantaneous motion of the Earth as a whole, ignoring as much as possible its regional deviations from a satisfactory gross model. This latter approach makes use of normal mode theory.

Like any other physical body of finite size, the Earth possesses a discrete number of eigenmodes, which form a complete set upon which the planet's response to any excitation can be expanded. Early interest in the Earth's normal modes was purely theoretical (Lamb, 1882; Love, 1911), until their identification was claimed by Benioff et al. (1954) following the great Kamchatka earthquake of November 4, 1952. The advent of high-speed computers at the end of the 1950's allowed realistic calculations for different models and made feasible the investigation of the excitation of the various modes by a given seismic source. After a number of case studies (Alterman et al., 1959; Jobert, 1962; Takeuchi et al., 1963), Saito (1967) presented general expressions of the excitation of the planet's mode by any single force, single couple or double couple. This now classic paper has remained the basis for all later developments in mode theory, especially in the domain of seismogram synthesis.

Extensive work has been done on the subject of ray-mode duality (Brune, 1964; Ben-Menahem, 1964; Woodhouse, 1978). However, both

theories retain their own advantages and drawbacks, their own domains of applicability and, above all, of efficiency. The present work examines a few areas in which normal mode theory can be used with most proficiency.

The natural domain of normal mode theory is, of course, the low-frequency end of the spectrum, where the eigenmodes of the Earth are fewest and geometrically simplest. This range of frequencies ($\nu < 0.003$ Hz) has been the subject of much recent interest since Kanamori (1976, 1977a) has proposed that slow deformations and/or aseismic creep make up a substantial part of the lithospheric subduction. Another domain where normal mode theory can be very helpful is the investigation of diffraction phenomena, such as along the core-mantle boundary, in violation of geometrical optics. Such studies are directly linked to the structural properties of the deep mantle of the Earth, which are of crucial importance in our understanding of the core differentiation process, and therefore of the formation of the Earth and other planets.

The present work consists of three chapters. In Chapter 1, we investigate the physical properties of spheroidal modes and show that they can be used to present a coherent classification of the modes into five families, greatly simplifying the handling and use of a large number of modes in synthetizing seismograms, and giving better physical insight into some aspects of mode theory. In Chapter 2, we study the influence of frequency and depth of source on the efficiency of an isotropic seismic source. The results are applied to the deep-Colombian earthquake of July 31, 1970 and it is concluded from a

series of time- and frequency-domain analyses that the seismic data do not warrant the existence of a slow compressional precursor to the main shock. In Chapter 3, we use profiles of SH waves diffracted around the core over a large distance (up to 55^{o}) to investigate the properties of the deep mantle. The S-wave velocity at the core mantle boundary is found to be in agreement with gross Earth models, but incompatible with a proposed low-velocity zone extending over 100 km or more. Synthetic seismograms obtained by normal mode summation confirm this result, and are used to strongly constrain any possible rigidity of the uppermost layer of the core.

Most of the present results are in the process of being published: Chapter 1 as Okal (1978a), Chapter 2 and 3 as Okal and Geller (1978 a, b).

CHAPTER 1

A Physical Classification of the Earth's Spheroidal Modes.

1.0 Introduction

The purpose of this chapter is to disentangle the physical properties of the spheroidal modes and to propose a classification and possible new nomenclature for them. In the conventional nomenclature, modes of similar angular order number ℓ are sorted by increasing frequencies. The physical properties of the modes (group velocity U, attenuation factor Q, particle motion at the surface, excitation functions) can vary dramatically with small changes in either ℓ or the overtone number n. It is shown that most of the spheroidal modes can be classified into several families offering regular, although different, trends in their physical properties. Specifically, one can isolate the Inner Core and Stoneley modes; then, among the remaining modes, for low ℓ, or equivalently, at high phase velocities, there are two completely different sets of spheroidal modes. The first is a family of highly attenuated modes, for which the group velocity is slow (usually $\leq$ 5 km/s), and the main component of the displacement colatitudinal. The eigenfunctions of these modes (and therefore, their periods, group velocities, Q's and excitation functions) are strikingly similar to those of torsional modes of the same angular order. The second family consists of modes with higher Q's, whose group velocities are higher (usually $\geq$ 10 km/s), for which the displacement is mainly vertical, and whose physical properties are continuous with those of the so-called "radial" modes ${}_nS_0$. At high ℓ (lower phase velocities), total coupling occurs between the vertical and colatitudinal modes, leading to a single family, whose physical properties are extremely regular, and can directly be compared to Rayleigh waves. At

intermediate ℓ, coupling occurs irregularly and it is not possible to define any strong trend in the physical properties.

Section 1.1 describes the irregular variations if the modes' properties with small variations of either n or ℓ, when the conventional nomenclature is used. The empirical analysis of a set of computed data introduces the idea of several families of spheroidal modes. In section 1.2, we adapt the results of Alterman et al. (1959) to the simplified case of a homogeneous Earth and of total decoupling between radial and horizontal displacements. We extend the results of Anderssen et al. (1975) and of Gilbert (1975), to discuss the values of the group velocities, inside the various families at low ℓ. A comparison is made with the values computed for a realistic Earth model. Section 1.3 formally presents the classification of spheroidal modes and proposed new nomenclature.

1.1 A Critical Review of Spheroidal Modes

The theoretical problem of the vibrations of an elastic sphere dates back to Lamb (1882). A complete review of the literature on this subject is beyond the scope of this work and we shall only summarize the following milestones in the development of mode theory: Love (1911), and later Pekeris and Jarosch (1958) discussed the eigenfunctions of a uniform, gravitating sphere; Alterman et al. (1959) first calculated the excitation coefficients of the various spheroidal oscillations of the Earth for a simple source; Satô and Usami (1962a, b,c) and Landisman et al. (1970) extensively studied the problem of the oscillations of a homogeneous sphere. Ray-mode duality was also investigated by Brune (1964), Ben-Menahem (1964), and more recently Woodhouse (1978).

Saito (1967) presented general results, applicable to any seismic source, and introduced a variational method of solving the differential equations. Kanamori and Cipar (1974) gave a simplified expression of the excitation of both T and S modes by any double-couple, and Kanamori and Stewart (1976) introduced asymptotic expansions, which help to avoid having to sum a forbidding number of modes at higher frequencies. Experimental identifications of the normal modes of the Earth were systematically carried out by Dziewonski and Gilbert (1972) and Gilbert and Dziewonski (1975). A theoretical investigation of the asymptotic behavior of ${}_{n}S_{\ell}$, at constant ℓ, was given by Anderssen et al. (1975) and by Gilbert (1975). However, these authors have limited their investigation to $\omega \to \infty$ at constant ℓ, thus neglecting the study of the modes' group velocity, which is of crucial importance

in the approach of Kanamori and Stewart, as the group velocity is the quantity associated with the variation of physical properties with wavenumber (or equivalently angular order).

1.1.1 The following briefly summarizes Saito's (1967) results in the simplified version of Kanamori and Cipar (1974).

The displacement $\vec{u}$ at a point (r,θ,ϕ) in the Earth, generated by an earthquake, can be expanded into a sum of the normal modes ${}_nS_\ell^m$ of the Earth (ℓ : angular order; m : azimuthal number; n : overtone number); the amplitude of excitation of a given mode by a particular source can be separated into radiation pattern factors (p_R, q_R, s_R), depending only on the mechanism of the earthquake, and excitation coefficients (K_0, K_1, K_2; N_0), depending only on the source depth and on the particular mode considered. The notation will always be that of Saito (1967) and Kanamori and Cipar (1974). However, the angular order number will always be ℓ. Also, N_0 is the excitation coefficient for a purely compressional source, adapted from Takeuchi and Saito (1972):

$$N_0 = - \frac{2\ell + 1}{4\pi \; {}_n\omega_\ell^2 \; (I_1 + L^2 I_2)} \cdot D(r_s) \; , \qquad (1.1)$$

where $D(r_s)\, Y_\ell^m(\theta,\phi) = \varepsilon_{ii} = \varepsilon_{rr} + \varepsilon_{\theta\theta} + \varepsilon_{\phi\phi}$ is the trace of the strain tensor or deformation:

$$D(r_s) = \frac{4\,\mu_s}{(\lambda_s+2\mu_s) r_s} \; y_1(r_s) + \frac{y_2(r_s)}{\lambda_s+2\mu_s} - \frac{L^2}{r_s} \cdot \frac{2\,\mu_s}{\lambda_s+2\mu_s} \; y_3(r_s). \qquad (1.2)$$

Following Kanamori and Cipar (1974) and Kanamori and Stewart (1976), we will always normalize $y_1(a)$ to unity and the excitation functions will always be computed assuming a double-couple moment of 10^{27} dynes-cm (or a purely compressional moment of 10^{27} dynes-cm for each of the three equivalent dipoles in the case of a compressional source).

The computed data set used in this study consists of some 5200 theoretical eigenfunctions for the Earth, computed by Buland and Gilbert (1976) for model 1066A (Gilbert and Dziewonski, 1975). This data set includes 1936 torsional and 3271 spheroidal modes, representing all solutions with angular order less than 151 and periods greater than 45 seconds. For periods larger than 150 seconds, the solutions for all torsional modes and most spheroidal ones were checked against an independent recomputation by the author, using model C2 (Anderson and Hart, 1976), and the program developed by Kanamori and Abe (1968). The eigenfunctions were processed to obtain the periods (T), phase velocities (C), group velocities (U), attenuation factors (Q), surface transverse displacements ($y_3(a)$, with $y_1(a)=1$, to be abbreviated below as y_3). The excitation functions N_0, K_0, K_1 and K_2 (L_1 and L_2 in the case of T modes) were obtained for 23 standard focal depths between 0 and 750 km.

It should be noted that the group velocity U is computed here as outlined by Jeffreys (1961):

$$U = (J_1 + J_2/k) / J_0 C , \qquad (1.3)$$

where $k = (\ell+\frac{1}{2})/a$ is the wavenumber, and the J's are energy integrals involving the eigenfunction and its derivative with respect to r. The concept of group velocity assumes the existence of a set of modes (generating a wave), whose physical properties vary smoothly enough that they can be easily followed and considered as continuous with frequency, despite the discrete layout of the modes. The group velocity $d\omega/dk$ is then used in the interpolation of physical properties of the modes (Kanamori and Stewart, 1976). In the case of spheroidal modes, this assumption might sometimes be inappropriate along an overtone branch n = constant. We shall return to this point below.

The values of Q were obtained both from the MM8 model of Anderson et al. (1965), and from the more recent SL2 model described by Anderson and Hart (1978). The primary difference between these two models is the presence in model SL2 of a zone of low Q at the base of the mantle, and of low values of Q in the inner core.

1.1.2 Difficulties with the conventional nomenclature ${}_nS_\ell$.

In the conventional nomenclature, modes of identical ℓ are assigned an overtone number by increasing frequency: the mode with the longest period is called ${}_0S_\ell$, the next one ${}_1S_\ell$, and so on. (The first mode with $\ell=1$, ${}_0S_1$, which represents a rigid body translation of the whole Earth, and for which ${}_0\omega_1=0$, is not usually included in any compilation of S modes, although it is tacitly part of the conventional nomenclature.) A similar method is used for torsional modes ${}_nT_\ell$. However, the torsional nomenclature does not

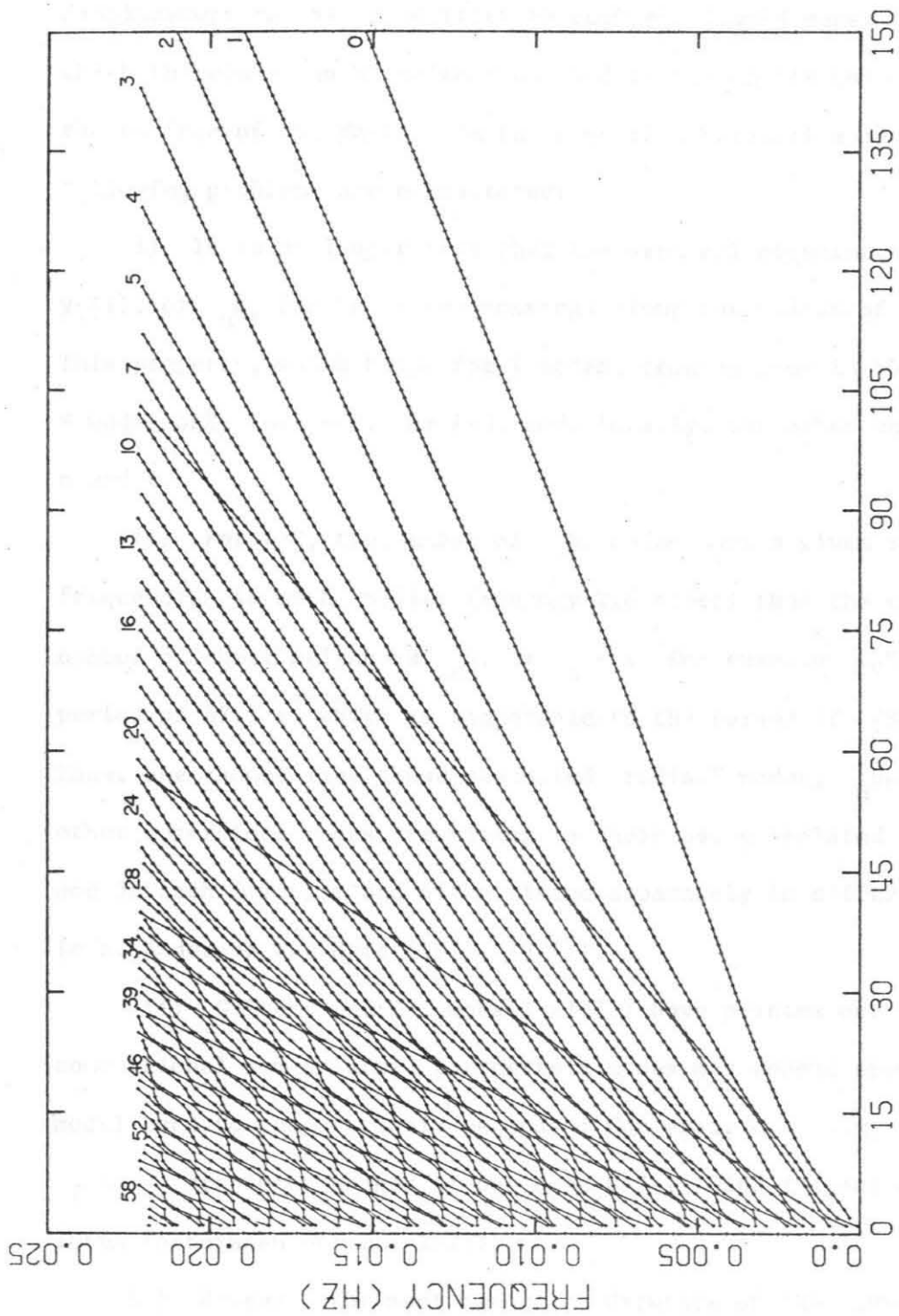

Figure 1.1. Frequency versus angular order plot of the spheroidal modes used in this study, as computed from model 1066A. Overtones are traced and labeled according to the conventional nomenclature. Radial modes ($\ell = 0$) are not included in overtone branches.

usually include the inner core torsional oscillations, for which no displacement can be transmitted through the liquid outer core, and which therefore can be neither excited in the mantle nor observed at the surface of the Earth. In the case of spheroidal modes the following problems are encountered:

i) It is no longer true that the vertical eigenfunction, $y_1(r)$, of ${}_nS_\ell$ has n zero-crossings along the radius of the Earth. This property, which holds for T modes, remains true in the case of S modes only for n=0, for ℓ=0, and, locally, for other values of n and ℓ.

ii) For ℓ=0, the number of ${}_nS_0$ modes over a given range of frequencies is much smaller (roughly 2.5 times) than the corresponding number of their neighbors ${}_nS_1$ or ${}_nS_2$: For example, ${}_{20}S_0$ has a period of 57.7 s, which is comparable to the period of ${}_{50}S_1$: 56.4 s. Thus, one cannot link those so-called "radial" modes, ${}_nS_0$, with the other spheroidal modes, resulting in their being isolated (e.g. Pekeris and Jarosch (1958)), and often listed separately in different tables (e.g. Anderson and Hart (1976, 1978)).

iii) Gilbert and Dziewonski (1975) have pointed out that the conventional nomenclature for certain modes may depend upon the Earth model used to compute their periods : For example, ${}_{26}S_1$ and ${}_{27}S_1$ are interchanged if one uses model 1066B instead of model 1066A (Anderssen et al., 1975).

iv) However, the most important drawback of the conventional nomenclature is the absence of continuity in the physical properties of the modes along overtone branches : Figure 1.1 is a plot of the

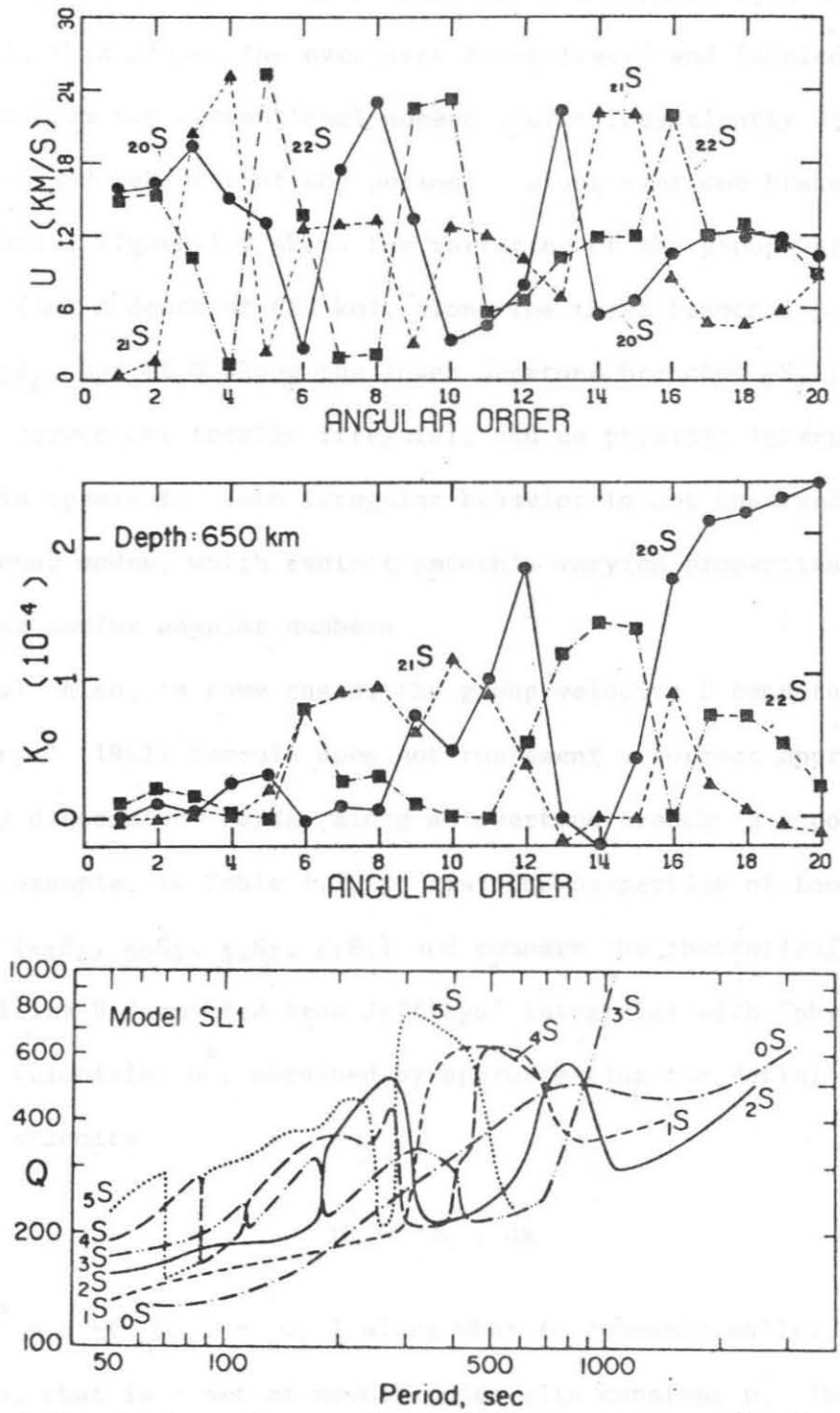

Figure 1.2. A plot of several physical properties of spheroidal modes along conventional overtone branches : group velocities U (top) and excitation coefficients K_0 (center) along $_{20}S_\ell$, $_{21}S_\ell$ and $_{22}S_\ell$, and Q (bottom) along the lower overtones $_0S_\ell$ to $_5S_\ell$. This last plot is taken from Anderson and Hart (1978).

eigenfrequencies of the spheroidal modes (computed from model 1066A) used in this study, the overtones being traced and labeled as they result from the conventional nomenclature: They clearly display a very rugged behavior of the periods T along overtone branches. Similarly, Figure 1.2 shows the variation of the group velocity U, and of K_0 (for a depth of 650 km), along the three branches ${}_{20}S_\ell$, ${}_{21}S_\ell$ and ${}_{22}S_\ell$, and of Q along the lower overtone branches ${}_0S_\ell$ to ${}_5S_\ell$. These curves are totally irregular, and no physical interpretation of them is apparent. Such irregular behavior is not observed for torsional modes, which exhibit smoothly varying properties at similar periods and/or angular numbers.

v) Also, in some cases, the group velocity U computed from Jeffreys' (1961) formula does not represent a correct approximation to the dispersion $d\omega/dk$ along an overtone branch n = constant. As an example, in Table 1.1, we list the properties of four adjacent modes (${}_{50}S_2$, ${}_{50}S_3$, ${}_{51}S_2$, ${}_{51}S_3$) and compare the theoretical group velocities U (computed from Jeffreys' integrals) with "physical" group velocities U^*, obtained by approximating the definition of group velocity :

$$U^* = d\omega \,/\, dk \qquad (1.4)$$

by $U^* = a \cdot ({}_n\omega_{\ell+1} - {}_n\omega_\ell)$ along what is commonly called an overtone branch, that is a set of normal modes with constant n. The agreement is seen to be very poor. Also, the other physical properties (such as Q, $y_3(a)$, K_0 .....) strongly vary along the overtone branches (n=50 or n=51). Again, this behavior is absent from torsional modes,

Table 1.1

An Example of Discrepancies between Dispersion Group Velocities U^* and Energy Integral Group Velocities U

Mode	T (s)	U (km/s)	Q_{SL2}	y_3
$_{50}S_2$	55.19	16.43	984	0.076
$_{50}S_3$	54.96	0.38	258	-7.98
$_{51}S_2$	54.98	0.43	260	-4.48
$_{51}S_3$	53.95	15.63	980	0.003

Dispersion group velocities U^* :

$_{50}S_2 - {}_{50}S_3$: 3.04 km/s $\qquad$ $_{51}S_2 - {}_{51}S_3$: 13.90 km/s

$_{50}S_3 - {}_{51}S_2$: 0.28 km/s $\qquad$ $_{50}S_2 - {}_{51}S_3$: 16.67 km/s.

for which the group velocity $U = J_1 / C J_0$ (in Jeffreys' (1961) notation) is always an excellent approximation to the dispersion $d\omega/dk$ along an overtone n = constant.

1.1.3 What should be called an overtone?

Going back to the example in Table 1.2, we achieve a much better agreement between U and U^* by computing U^* along "diagonals" ($_{50}S_2$-$_{51}S_3$ and $_{51}S_2$-$_{50}S_3$). As Jeffreys' calculation is, itself, based upon the physical concept of dispersion and uses equation (1.4) as a start, this suggests that the concept of an "overtone branch" as a set of modes sharing some physical property is, in the present case, better applied diagonally than along lines of constant n. Similarly, Brune (1964) has shown that the group velocity of a mode can be interpreted in terms of the spatial variation of the phase spectrum of body waves to which this mode contributes. His formalism, however, involved taking derivatives of the phase along overtones branches (I=constant in his notation), whose members may not contribute to the same continuous set of body waves in the classical nomenclature.

By doing so, we also regroup modes having comparable values of all physical properties, such as Q, and y_3 (see table 1.1). Also, Figure 1.3 shows a plot of the excitation coefficients N_0, K_0, K_1, K_2 as a function of depth for each of these four modes. It is evident that there exists a strong correlation between the eigenfunctions of $_{50}S_2$ and $_{51}S_3$, as well as between those of $_{50}S_3$ and $_{51}S_2$, rather than along the lines n=50 or n = 51. The modes with large K_0

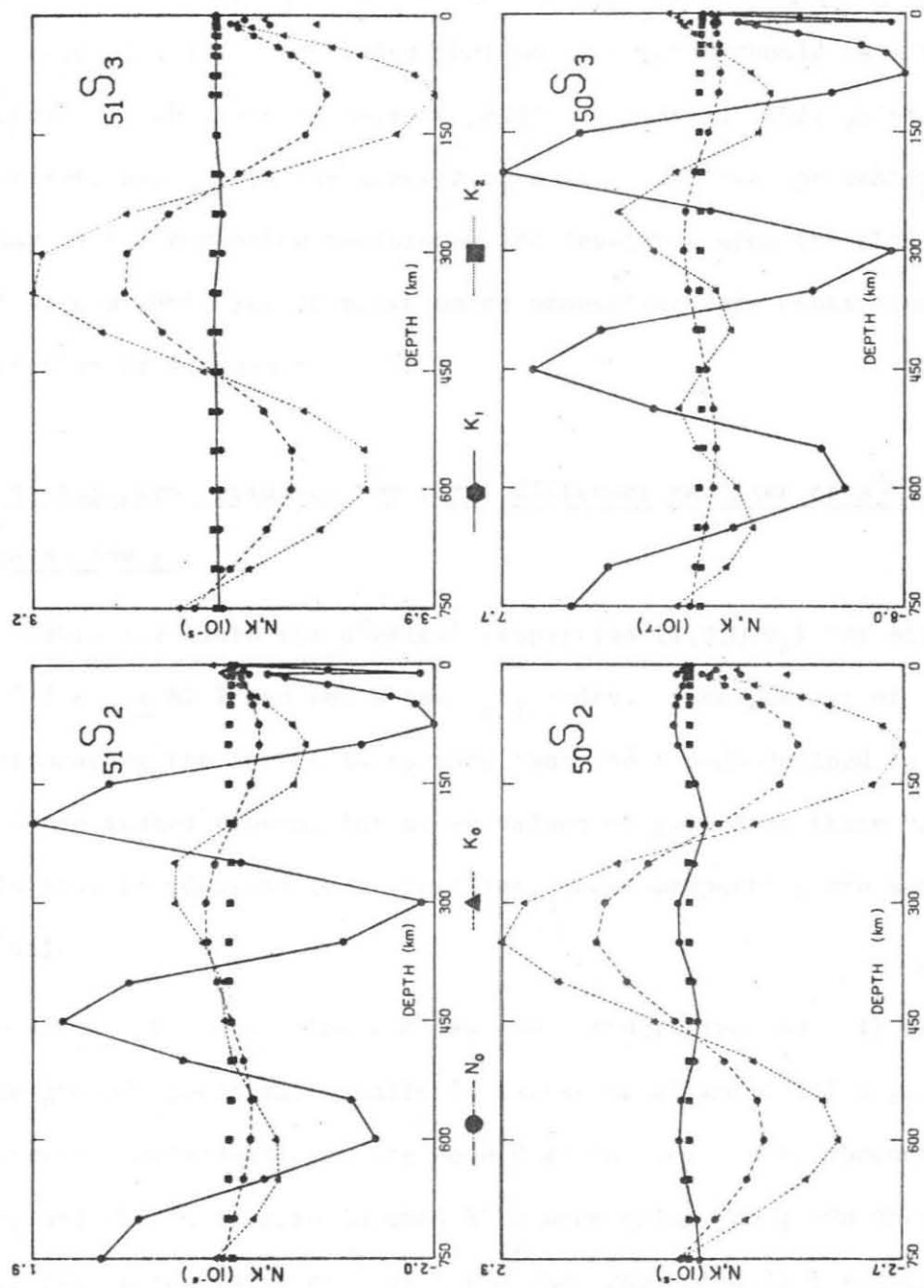

Figure 1.3. Excitation coefficients N_0, K_0, K_1, K_2 as a function of depth for the four adjacent modes $_{50,51}S_{2,3}$. For clarity, the functions are not all traced in the vicinity of the surface, where strong variations in elastic moduli give them an irregular behavior. Note the 'diagonal' correlation, between $_{50}S_2$ and $_{51}S_3$, $_{51}S_2$ and $_{50}S_3$.

and N_0 coefficients are those with larger group velocities, higher Q's and lower $|y_3|$. The other two modes exhibit large K_1's, have $|y_3|$ larger than 1, and share low group velocities and low Q's. From this evidence, it is concluded that mode branches should be allowed to cross, if they are to carry a physical meaning. This point is important, since both the concept of a wave, and the applicability of asymptotic expansion techniques are dependent upon the ability to deal with a whole set of modes whose properties vary continuously with wavenumber or frequency.

1.1.4 Empirical evidence for three different families of spheroidal modes at low ℓ.

Table 1.2 lists the physical properties (T,U,Q,y_3) for all modes ${}_nS_1$ ($7 \leq n \leq 62$) and for a few ${}_nS_5$ modes. (The purpose of incorporating the latter is to show that the trends defined by the ${}_nS_1$'s are indeed present for other values of ℓ.) From these values, it is easy to identify three families, whose properties are summarized in Table 1.3.

1st family : K modes. These modes are characterized by : i) very large group velocities, usually in excess of 25 km/s; ii) a value of Q extremely dependent upon the mean Q at the core-mantle boundary (CMB) and the inner core (around 8000 when using MM8 ; 300 when using SL2); iii) a low value of $|y_3|$ (on the order of 0.1) ; and iv) very low excitation coefficients for all depths down to 750 km. Items ii) and iv) clearly identify these modes as Inner Core modes (we use the letter K from the German "Kern") : The attenuation model

Table 1.2

Physical Properties of the Modes $_nS_1$ ($n \geq 7$) and of a few $_nS_5$

MODE	T (S)	U (KM/S)	Q MM8	Q SL2	Y3
7 S 1	449.2	6.82	378	336	5.964
8 S 1	348.3	14.03	1633	1055	0.224
9 S 1	312.3	0.67	356	304	-2.975
10 S 1	292.2	25.83	7961	289	0.160
11 S 1	271.3	15.18	1749	853	0.131
12 S 1	232.4	0.80	371	290	22.809
13 S 1	222.5	14.36	1475	934	-0.113
14 S 1	201.6	25.88	7746	296	-0.026
15 S 1	188.9	16.83	1729	816	0.040
16 S 1	186.6	0.69	333	264	26.257
17 S 1	163.4	15.55	1732	978	-0.142
18 S 1	156.1	1.18	351	275	8.275
19 S 1	154.6	27.32	7837	307	0.466
20 S 1	143.9	15.74	1900	1000	0.010
21 S 1	133.1	0.33	350	274	-8.145
22 S 1	127.8	14.99	1864	1063	0.109
23 S 1	125.9	28.07	9881	292	0.084
24 S 1	116.6	0.34	319	251	-65.163
25 S 1	115.5	14.22	1745	999	-0.043
26 S 1	106.3	27.41	8023	315	0.044
27 S 1	105.3	16.19	1782	831	0.078
28 S 1	103.9	0.46	323	251	-27.557
29 S 1	97.1	16.23	1643	970	-0.051
30 S 1	93.4	0.35	329	255	12.392
31 S 1	91.9	27.68	9120	299	0.011
32 S 1	90.2	17.38	1768	888	-0.022
33 S 1	85.0	0.42	329	255	-8.812
34 S 1	83.8	15.86	1692	1027	0.150
35 S 1	81.0	28.31	9936	304	0.028
36 S 1	78.4	14.69	1767	1017	-0.065
37 S 1	77.9	0.30	324	251	49.372
38 S 1	73.4	15.55	1852	1010	0.044
39 S 1	72.4	28.29	9878	297	0.117
40 S 1	71.9	0.24	324	250	-45.602

Table 1.2

(continued)

41	S	1	69.1	15.96	1700	992	-0.028
42	S	1	66.8	0.21	323	252	22.053
43	S	1	65.6	20.42	2269	572	-0.024
44	S	1	65.4	25.47	4041	379	-0.026
45	S	1	62.4	1.95	361	278	-2.987
46	S	1	62.2	14.90	1102	735	0.380
47	S	1	59.7	28.35	9674	297	-0.012
48	S	1	59.2	15.34	1597	943	-0.037
49	S	1	58.5	0.21	334	254	156.770
50	S	1	56.4	14.96	1677	1024	0.033
51	S	1	55.0	0.15	340	257	-41.330
52	S	1	54.9	28.55	9940	303	-0.127
53	S	1	53.9	15.16	1648	1007	-0.000
54	S	1	51.9	0.15	335	256	22.677
55	S	1	51.6	17.46	1778	962	-0.049
56	S	1	50.8	28.52	9775	297	-0.033
57	S	1	49.5	17.24	1653	992	-0.120
58	S	1	49.2	0.35	337	256	9.843
59	S	1	47.6	16.50	1710	966	-0.027
60	S	1	47.3	28.65	9595	302	-0.047
61	S	1	46.8	0.16	349	259	-267.085
62	S	1	45.7	15.03	1665	1033	0.030
31	S	5	82.7	23.96	5645	310	0.089
32	S	5	79.1	14.79	1737	921	0.018
33	S	5	77.6	0.77	328	253	-1.559
34	S	5	74.4	16.35	2051	667	0.028
35	S	5	73.4	24.47	5174	338	0.035
36	S	5	71.7	0.99	328	253	7.501
37	S	5	69.7	14.83	1632	968	-0.038
38	S	5	66.6	1.08	329	254	3.532
39	S	5	66.4	24.85	6362	307	0.062
40	S	5	66.0	15.90	1671	807	0.003

SL2 (Anderson and Hart, 1978) is characterized by a high-attenuation layer at the base of the mantle and in the inner core. It can also be proved that K modes are indeed the mostly unobserved "core" modes, as defined by Gilbert and Dziewonski (1975).

2nd family : C (Colatitudinal) modes. This is a family of highly attenuated modes, with low group velocities, and high values of $\left| y_3(a) \right|$. ${}_{51}S_2$ and ${}_{50}S_3$, studied in the previous section, belong to this family. Furthermore, Figure 1.2 shows, in the case of these two modes, that at all depths the excitation function K_1 remains very large, with K_0 still substantial, and about 10 times as large as K_2 . This property, illustrated in the case of this particular example, is indeed a common factor of the family. In view of the expressions for the coefficients K (Kanamori and Cipar, 1974), this is equivalent to the function $\left| y_1(r) \right|$ remaining small with respect to $\left| y_3(r) \right|$ at all depths. It is clear that the displacement in these modes is mainly colatitudinal, hence the "C".

3rd family : V (Vertical) modes. This family has intermediate group velocities (10 to 18 km/s for ${}_nS_1$), high values of Q in both models MM8 (1000-4000) and SL2 (700-2000), and very small values of $\left| y_3(a) \right|$. Furthermore, as shown on Figure 1.3, and confirmed by a further study, these modes have large values of N_0 and K_0, and very small K_1 and K_2. All of this suggests that the displacement in these modes is mainly radial or "vertical", hence the "V". These properties are shared by the radial modes ${}_nS_0$, which are in the same number (20 modes from 200 s. down to 45 s.), and have, by definition, no colatitudinal displacement or excitation functions K_1 and K_2. The radial modes

Table 1.3

Physical Properties of the Different Families of Modes at Low ℓ

Property	K	C	V
Group Velocity U (km/s)	20 to 30	0.3 to 4	9 to 17
Q	SL2 : 300 MM8 : 4000-9000	200 to 400	700 to 2000
y_3	Low (down to 10^{-3})	> 1 Up to 100	< 1 Down to 3×10^{-3}
Excitation Coefficients	All low	K_1 substantial K_0 comparable to K_1	K_1, K_2 low N_0, K_0 substantial

are thus part of the V family. At this point, we have defined empirically three different families of modes with low ℓ, clearly identified only for phase velocities larger than about 26 km/s. There have been isolated cases, when the individual properties of two modes may violate in some respect the general trends in their families. Table 1.4 gives two examples. We will see later that these are clear cases of coupling, due to a near coincidence in eigenfrequencies. The fundamental point is that, in this region of the (ω,ℓ) plane ($C > 26$ km/s), these are isolated occurrences, which do not represent any general physical trend.

Modes with larger values of ℓ.

For low values of the phase velocity ($C < 16$ km/s), Figure 1.1 shows that spheroidal modes are arranged along well-defined, regular, overtone branches. As in the case of torsional modes, the physical properties of the modes vary smoothly along those branches, and regularly from one branch to the next. We will call this family of modes "R" (Rayleigh) modes : The fundamental R modes do indeed generate classical Rayleigh waves, and it can be shown that higher overtones are similar to Rayleigh wave overtones, as described, for example, by Harkrider (1964, 1970).

At values of ℓ for which the phase velocity falls in the range 16-26 km/s, there is no such definite behavior. It would indeed be possible to try to define two groups of branches (as shown in the upper part of Figure 1.4) and associate them with V or C modes, or to allow large undulations along branches (as in the bottom of Figure

Table 1.4

Two Examples of Coupled Modes at low ℓ

Mode	Period s	U km/s	Q_{MM8}	Q_{SL2}	y_3
$_{20}S_3$	129.8	19.45	1858	458	0.18
$_{21}S_3$	127.7	20.41	2972	398	0.11
$_{15}S_4$	158.0	8.84	720	541	-0.28
$_{16}S_4$	152.3	7.55	494	390	0.39

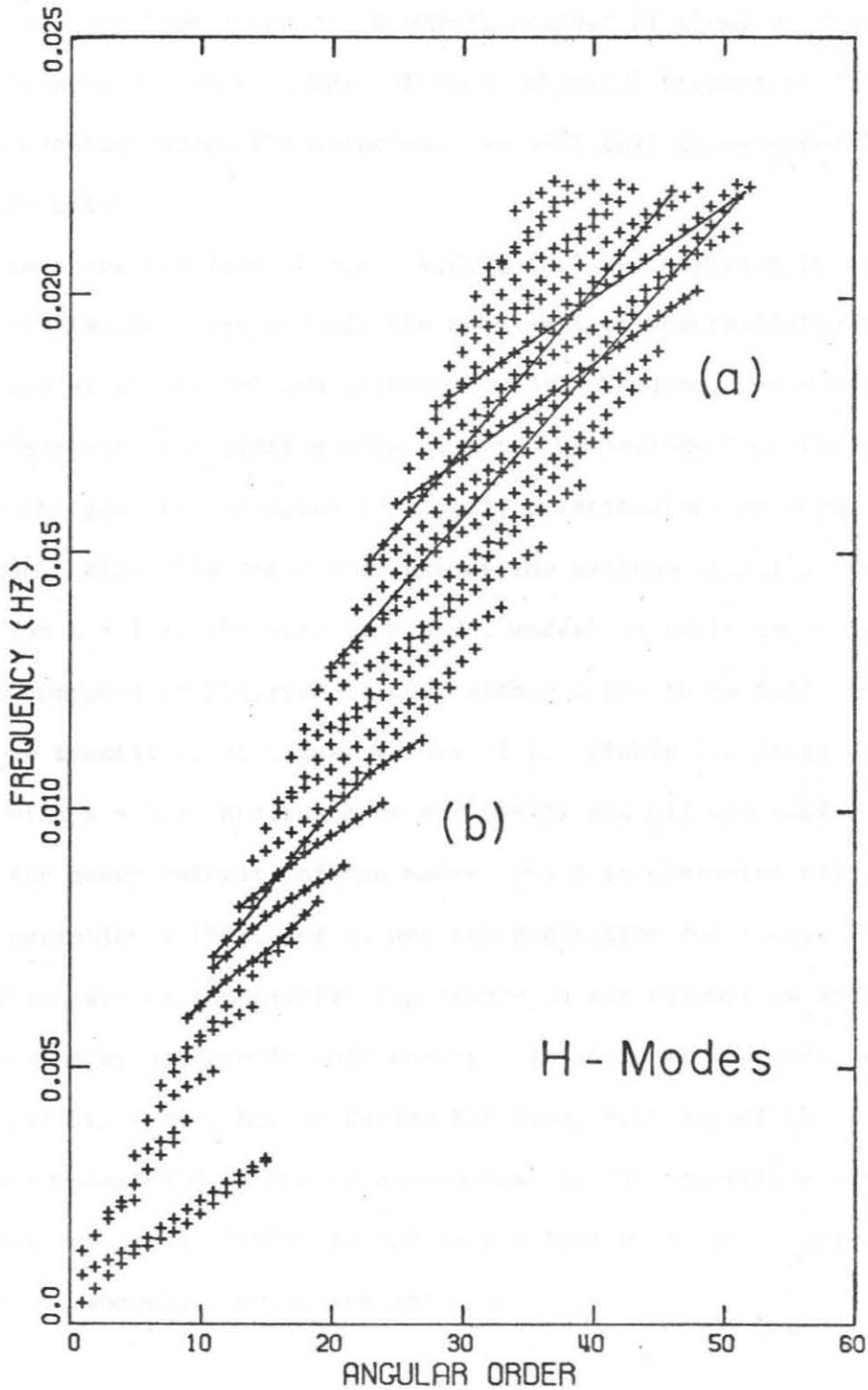

Figure 1.4. Frequency versus angular order plot of the H family of modes. In region (a), an attempt is made at neglecting coupling and treating the modes as part of the C and V families. In region (b), the opposite attempt is presented - incorporating them into the R family -.

1.4), and make them R modes. However, neither of these approaches is satisfactory, since in both of them, physical properties do not remain constant along the branches. We will call these modes "H" (Hybrid) modes.

The three families of modes K,C,V, isolated empirically at low ℓ in this section, are indeed, the ones defined theoretically by Anderssen et al. (1975) and Gilbert (1975). However, their theoretical investigations were limited primarily to the periods T of the modes, and to the general character (vertical, colatitudinal or core) of the solution. Also, they only made use of the extreme limiting case $\ell = 0$ (or $\ell = 1$ in the case of K and C modes) in their comparison with actual computed or observed values, although the three families can still be identified at higher values of ℓ. (Table 1.2 lists a few modes with $\ell = 5$.) Anderssen et al. (1975) and Gilbert (1975) did not study the group velocity of the modes, which is characteristic of their variation with ℓ, nor Q, nor the excitation functions. These properties are of fundamental importance in any attempt to synthetize seismograms by asymptotic mode theory. In the next section, we will show that it is possible to derive the group velocity of the families of low-ℓ modes (K,C,V) and to extend most of the properties derived by Anderssen et al. (1975) to non-zero values of ℓ, under very simple, if somewhat crude, assumptions.

1.2 A Theoretical Approach to the Various Properties of Spheroidal Modes of Low ℓ.

In order to show that most of the properties of the various families of modes can be derived simply, we shall consider here the normal modes of a homogeneous sphere (with only the possibility of a fluid core), and we shall neglect the influence of gravity.

The theoretical problem of the spheroidal eigenvibrations of a homogeneous sphere was studied by Love (1911) and Pekeris and Jarosch (1958). Takeuchi and Saito (1972) gave the complete solution for the eigenfunctions of a homogeneous sphere (pp. 243-244), where the exact (and rather elaborate) expressions of the solution can be found. Some of the theoretical results in the following section were given by Anderssen et al. (1975) and Gilbert (1975) for constant ℓ (mostly $\ell = 0$ and $\ell = 1$). Their extension to a variable ℓ allows a theoretical study of the group velocity of the modes.

Rather than start from the exact solutions and adapt the equations to our particular cases of interest, we will try to simplify the system of differential equations for spheroidal modes, before solving it, by use of physical arguments, thus keeping a stronger physical insight into the properties of the solutions. We start with Saito's (1967) system, and we assume that we can neglect the influence of gravity. The system then reduces to : $d\vec{y} / dr = C \vec{y}$, with $\vec{y}^{\,T} = (y_1, y_2, y_3, y_4)$, and :

$$
C = \begin{bmatrix}
-\frac{2\lambda}{\lambda+2\mu}\cdot\frac{1}{r} & \frac{1}{\lambda+2\mu} & \frac{L^2\ \lambda}{r\,(\lambda+2\mu)} & 0 \\
-\omega^2\rho+\frac{4\mu(3\lambda+2\mu)}{(\lambda+2\mu)\,r^2} & -\frac{4\mu}{\lambda+2\mu}\cdot\frac{1}{r} & -L^2\frac{2\mu(3\lambda+2\mu)}{(\lambda+2\mu)\,r^2} & \frac{L^2}{r} \\
-\frac{1}{r} & 0 & \frac{1}{r} & \frac{1}{\mu} \\
\frac{2\mu}{r^2}\cdot\frac{3\lambda+2\mu}{\lambda+2\mu} & -\frac{\lambda}{\lambda+2\mu}\cdot\frac{1}{r} & -\omega^2\rho-\frac{2\mu}{r^2}+4L^2\cdot\frac{\mu(\lambda+\mu)}{(\lambda+2\mu)\,r^2} & -\frac{3}{r}
\end{bmatrix} \qquad (1.5)
$$

Here again, $L^2 = \ell(\ell+1)$. For $\ell = 0$, this matrix has an entire quadrant of zeroes, which means that the system breaks down into two completely independent systems of order two : one involving y_1 and y_2, the other y_3 and y_4. We will now solve both of these simple systems, and look at the case of small, but nonzero L^2.

1.2.1 Solutions with mainly radial displacement ("V" modes).

For $\ell = 0$, the system is completely decoupled, and, as shown by Gilbert (1975), the solution for a homogeneous sphere compatible with the boundary conditions is a spherical Bessel function of order 1:

$$y_1 = j_1 (\omega r/\alpha). \qquad (1.6)$$

For high overtones :

$$_p\omega_0 \simeq p\pi\alpha/a . \quad (p \text{ integer}) \qquad (1.7)$$

The frequency spacing between the subsequent radial modes $_nS_0$ is therefore $\Delta f = \alpha/2a$. The average value of α in the Earth is 10.46 km/s (Jeffreys and Bullen, 1940). This yields $\Delta f = 8.21 \cdot 10^{-4}$ Hz, in excellent agreement with the average separation observed for $_nS_0$: $\Delta f = 8.27 \cdot 10^{-4}$ Hz. These results are similar to those of Anderssen et al. (1975).

For ℓ small, but nonzero, it is no longer possible to ignore y_3 and y_4 : The third column in matrix 1.5 will inevitably bring coupling between the vertical and horizontal motions. We will therefore simply assume that $|y_3| << 1$, and that the corresponding modes are still basically irrotational, that is:

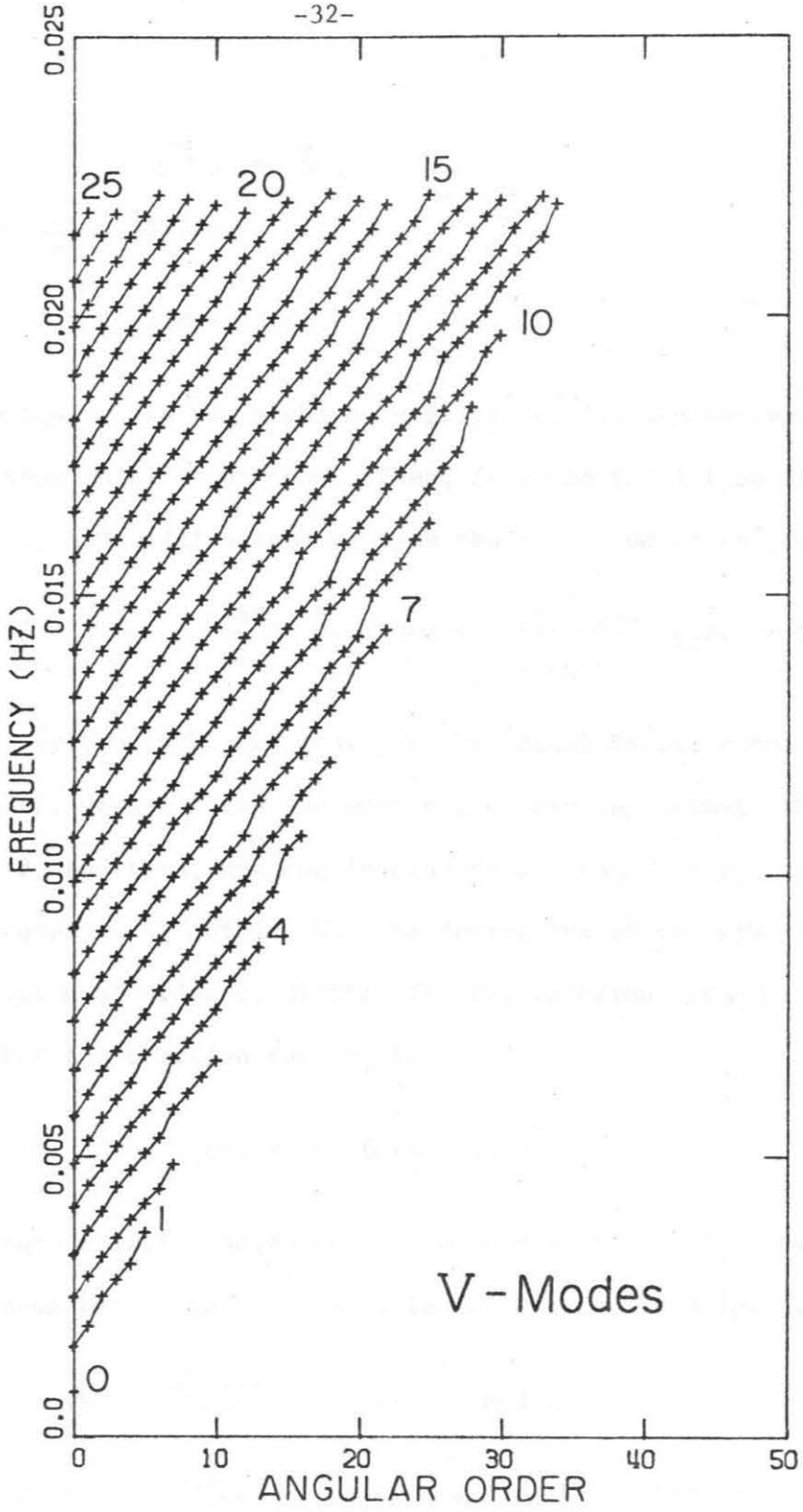

Figure 1.5. Frequency versus angular order plot of the V family of modes. Pseudo-overtones are traced and labeled according to the new proposed nomenclature. Note the easy integration of the radial modes into the family.

$$\overrightarrow{curl}\,\vec{u} = \vec{0} \,. \tag{1.8}$$

Using (1.5), this yields,

$$y_3' = dy_3/dr = -(y_3 - y_1)/r \simeq y_1/r \,. \tag{1.9}$$

This shows that while y_3 might be negligible, its derivative y_3' should be kept in all equations. Then, from the third line of (1.5), $y_4 = 2\mu\, y_1/r$, and eliminating y_2 from the first two lines yields:

$$y_1'' + \frac{2}{r}\, y_1' + \left[\frac{\omega^2}{\alpha^2} - \frac{L^2+2}{r^2}\right] y_1 + \left[\, 2 + \frac{2\mu(\lambda-2\mu)}{(\lambda+2\mu)^2}\,\right] y_3/r^2 = 0. \tag{1.10}$$

Given that $|y_3| << |y_1|$, and that for the actual Earth, either $\mu = 0$ (in the core), or $\mu = \lambda$ (in the mantle), we can approximate the last bracket by 2, and then, bearing in mind that $(r\, y_3)' = y_1$, we find that this equation is nothing but the derivative of the spherical Bessel equation of order ℓ, written for the function $(r\, y_3)$. We conclude that the solution for y_1 is :

$$y_1(r) = j_\ell'\,(\omega r/\alpha) \,. \tag{1.11}$$

Note that this solution holds for $\ell = 0$, since $j_0' = -\, j_1$. Using the well-known expressions (Abramowitz and Stegun, 1972 (p. 324)):

$$\begin{aligned} j_\nu\,(x) &= \sqrt{\pi/2x}\ \cdot J_{\nu+\frac{1}{2}}(x) \qquad \text{and :} \\ J_\nu\,(x) &\simeq \sqrt{2/\pi x}\ \cdot \cos\,(x - \nu\pi/2 - \pi/4) \qquad \text{for } x >> 1, \end{aligned} \tag{1.12}$$

we find that the boundary condition $y_2(a) = 0$ defining the angular eigenfrequencies of the V modes will rapidly require :

Table 1.5

Comparison of Theoretical and Observed Values of Frequency Spacing and Group Velocity in the three Families V, K, C

	V	K	C
Δf (Hz) computed	8.21×10^{-4}	1.43×10^{-3}	1.07×10^{-3}
Δf (Hz) observed			
$\ell = 0$	8.27×10^{-4}		
$\ell = 1$	8.29×10^{-4}	1.47×10^{-3}	1.07×10^{-3}
$\ell = 5$	8.32×10^{-4}	1.50×10^{-3}	1.06×10^{-3}
$\ell = 9$	8.41×10^{-4}	1.54×10^{-3}	1.05×10^{-3}
U^* (km/s) computed	15.7	28.6	0
U (km/s) observed	15.82	27.56	0.50
$\ell = 1$	15.82	27.56	0.50
$\ell = 5$	13.94	24.43	1.80
$\ell = 9$	13.74	23.01	3.31

$$ {}_p\omega_\ell = \frac{\alpha}{a} \pi \, [\, p + \ell/2 \,] \, . \qquad (1.13) $$

Here, p is a new "overtone" number inside the V family. We have thus derived the law of variation of the eigenfrequencies ${}_p\omega_\ell$ of the V modes, both with p and ℓ. This relation has two consequences :

a. The frequency spacing at a given ℓ should be independent of ℓ.

This is checked against a realistic Earth model in Table 1.5 : The frequency spacing varies less than 2% from $\ell = 0$ to $\ell = 9$, and stays within 3% of the value computed on the basis of our rather crude assumptions. This result was implicit from Gilbert's paper. However, the numerical values had only been checked against the theory by Anderssen et al. (1975) for $\ell = 0$ and $\ell = 1$.

b. The dispersion group velocity along a branch of V modes of constant p can be predicted.

According to (1.13), we have :

$$ d\omega / dk = a \; d\omega / d\ell \; = \alpha\pi/2 \, . \qquad (1.14) $$

The group velocity of a V branch should be $\pi/2$ times the average Earth's P-wave velocity. Again, taking the latter as 10.46 km/s, we obtain a figure of 16.43 km/s, in excellent agreement with the values of U characteristic of V modes. This agreement between U and $d\omega/dk$ along a V branch confirms that a branch of V modes with constant p is, indeed, a set of physically continuous modes. A further consequence is that the following relation holds :

$$ {}_{p+1}\omega_{\ell} \simeq {}_{\omega}\omega_{\ell+2} \qquad (1.15) $$

This fact is confirmed in Table 1.6 and in the general layout of V modes on Figure 1.5.

It is important to note that the radial modes ${}_pS_0$ completely share these properties, and can therefore be totally integrated into the V family.

The physical property limiting the field of separation between K, C and V modes in the (ω,ℓ) plane is the phase velocity C. Therefore, for high overtones, one expects the characteristic properties of the various families to hold even for relatively large values of ℓ, (ℓ = 10-20), for which the asymptotic expansion of the Legendre associated functions, as suggested by Kanamori and Stewart (1976), is valid and justifies the use of asymptotic theory. It is therefore fundamental to have established a theoretical proof of the validity of the group velocities U, computed from Jeffreys' formulas, as an accurate representation of the physical dispersion along a V branch.

1.2.2 Solutions with mainly colatitudinal displacements (C modes).

For $\ell = 0$, there can be no physical solution, since they would generate no displacement. However, this limiting case will be helpful when $L^2 \neq 0$. Assuming that $y_1 = y_2 = 0$, and following Gilbert (1975), one finds that the solution y_3 now involves both the Neumann and Bessel spherical functions of order 0. The solution for ω is rapidly Gilbert's equation (8) :

$$ {}_p\omega_0 = p\,\frac{\pi\,\beta}{a-r_c} \quad , \qquad (1.16) $$

Table 1.6

Example of the Law $_{p}\omega_{\ell+2} \simeq {}_{p+1}\omega_{\ell}$ for V and K Modes

Mode in Conventional Nomenclature	New	Period (s)	Error
$_{10}S_0$	$_{10}V_0$	110.4	0.3 %
$_{25}S_2$	$_{9}V_2$	110.8	0.9 %
$_{23}S_4$	$_{8}V_4$	111.8	1.1 %
$_{21}S_6$	$_{7}V_6$	113.0	2.8 %
$_{18}S_8$	$_{6}V_8$	116.2	
$_{38}S_{15}$	$_{14}V_{15}$	56.2	0.6 %
$_{36}S_{17}$	$_{13}V_{17}$	56.5	1.6 %
$_{34}S_{19}$	$_{12}V_{19}$	57.3	1.0 %
$_{32}S_{21}$	$_{11}V_{21}$	57.8	
$_{39}S_1$	$_{10}K_1$	72.4	0.4 %
$_{37}S_3$	$_{9}K_3$	72.7	1.0 %
$_{35}S_5$	$_{8}K_5$	73.4	2.3 %
$_{32}S_7$	$_{7}K_7$	75.1	2.0 %
$_{30}S_9$	$_{6}K_9$	76.6	

in total similarity to the torsional case. This yields $\Delta f = \beta/2\ (a-r_c) = 1.07 \cdot 10^{-3}$ Hz, for an average S-wave velocity of 6.18 km/s (Jeffreys and Bullen, 1940).

For ℓ nonzero, it is no longer possible to assume $y_1 = 0$. Similarly to our study of V modes, we will assume that $div\ \vec{u} = 0$, and that $|y_1| << |y_3|$. Then, we have, from (1.5) :

$$y_1' = L^2\ y_3 - 2\ y_1/r \simeq L^2\ y_3\ , \tag{1.17}$$

and :

$$y_3'' + \frac{2}{r}\ y_3' + [\ \frac{\omega^2\rho}{\mu} - \frac{L^2}{r^2}\ ]\ y_3 = 0\ . \tag{1.18}$$

Technically, this is a Bessel equation of order ℓ. However, since r is not allowed to become smaller than the radius of the core, r_c, then L^2/r^2 remains smaller than L^2/r_c^2. As long as we have

$$\omega^2 >> \frac{\beta^2}{r_c^2} \cdot L^2, \quad \text{or roughly} \quad C >> \beta\ a/r_c \simeq 12 \text{ km/s}, \tag{1.19}$$

this new term will be negligible, and the solution (whose boundary conditions are unchanged) will remain very similar to that for $\ell = 0$. Also, as r never becomes zero, the coupling coefficients of order L^2/r, in the matrix (1.5) will remain very small, and ensure that y_1 and y_2 are small. This is a fundamental difference which makes V and C modes behave differently. In other words, since the wave cannot propagate into the core, and as long as it has a high enough frequency, it cannot "feel" the curvature of the Earth; therefore, it is insensitive to the angular order number ℓ, which characterizes the variation with θ, and its eigenfrequencies are those of a plane wave between two fluid boundaries: This is what is expressed by

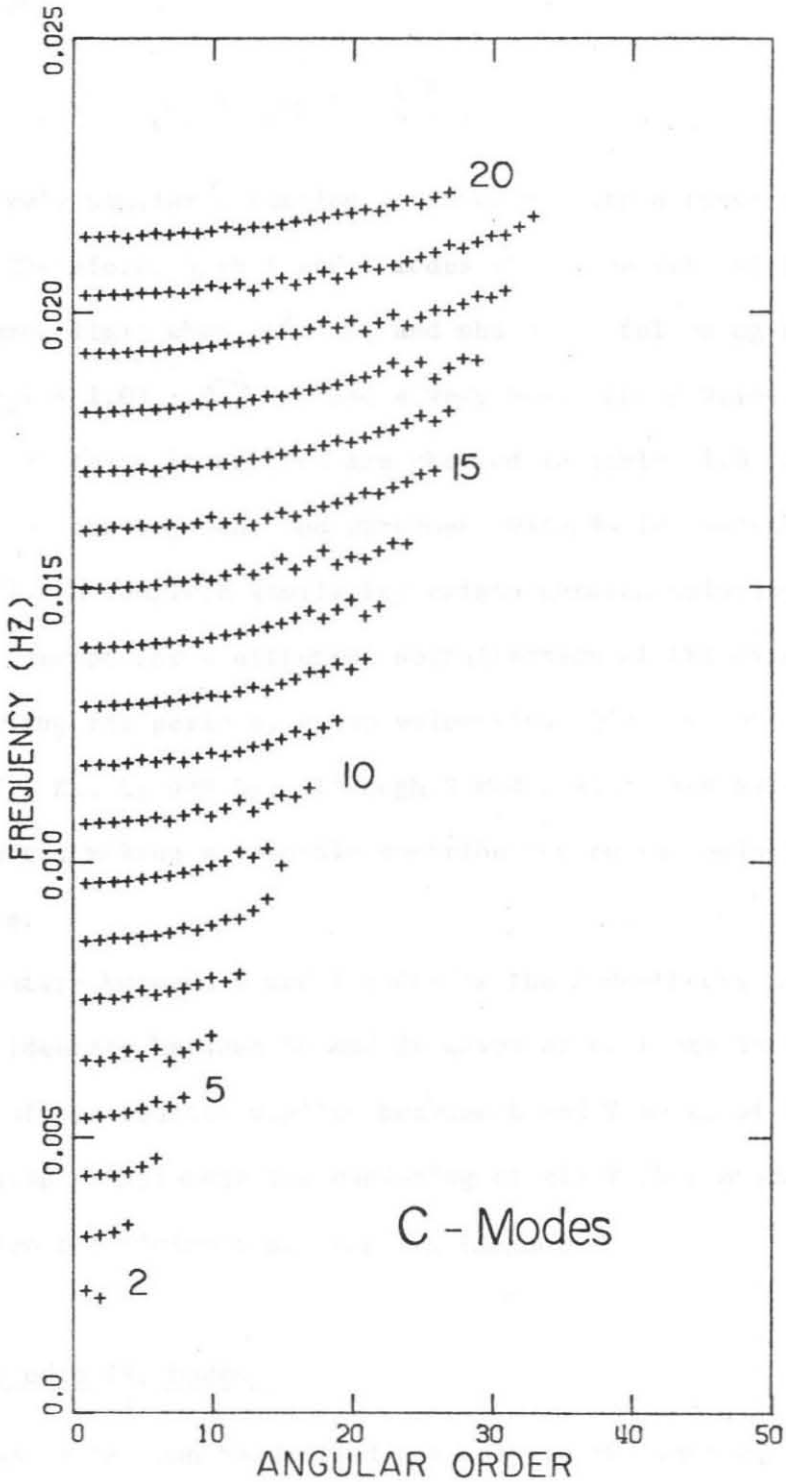

Figure 1.6. Frequency versus angular order plot of the C family of modes. Pseudo-overtones are labeled according to the new proposed nomenclature.

equation (1.20) :

$$p^{\omega}_{\ell} = p^{\omega}_{0} = \frac{p\pi\beta}{(a-r_c)} \quad . \tag{1.20}$$

An entirely similar situation would arise with a torsional system, and therefore, both T and C modes should be very similar to their common limit when $L^2 \to 0$, and share the following properties: $\Delta f = \beta/2(a-r_c) = 1.07 \cdot 10^{-3}$ Hz, and a very small group velocity at low ℓ. Both of these properties are checked in Table 1.5 and on Figure 1.6. As can be seen, the agreement extends for values of ℓ larger than 1. A complete similarity exists between solutions for C and T modes (except for a different normalization of the eigenfunctions), holding for periods, group velocities, Q's, and excitation functions, K_1, K_2, L_1 and L_2, although C modes also have substantial K_0 coefficients, making a possible contribution to the seismic displacements.

The identity between C and T modes is the mode-theory aspect of the trivial identity between SH and SV waves at vertical incidence. The absence of systematic coupling between C and V modes at high phase velocities simply expresses the vanishing of all P-SV transmission and reflection coefficients at zero incidence.

1.2.3 Inner core (K) modes.

Equation (1.18) can be applied not only to the mantle, but also to the solid inner core, although neglecting gravity certainly becomes a much poorer approximation. However, the interest in core modes is, at the present time, purely theoretical, as they are not significantly

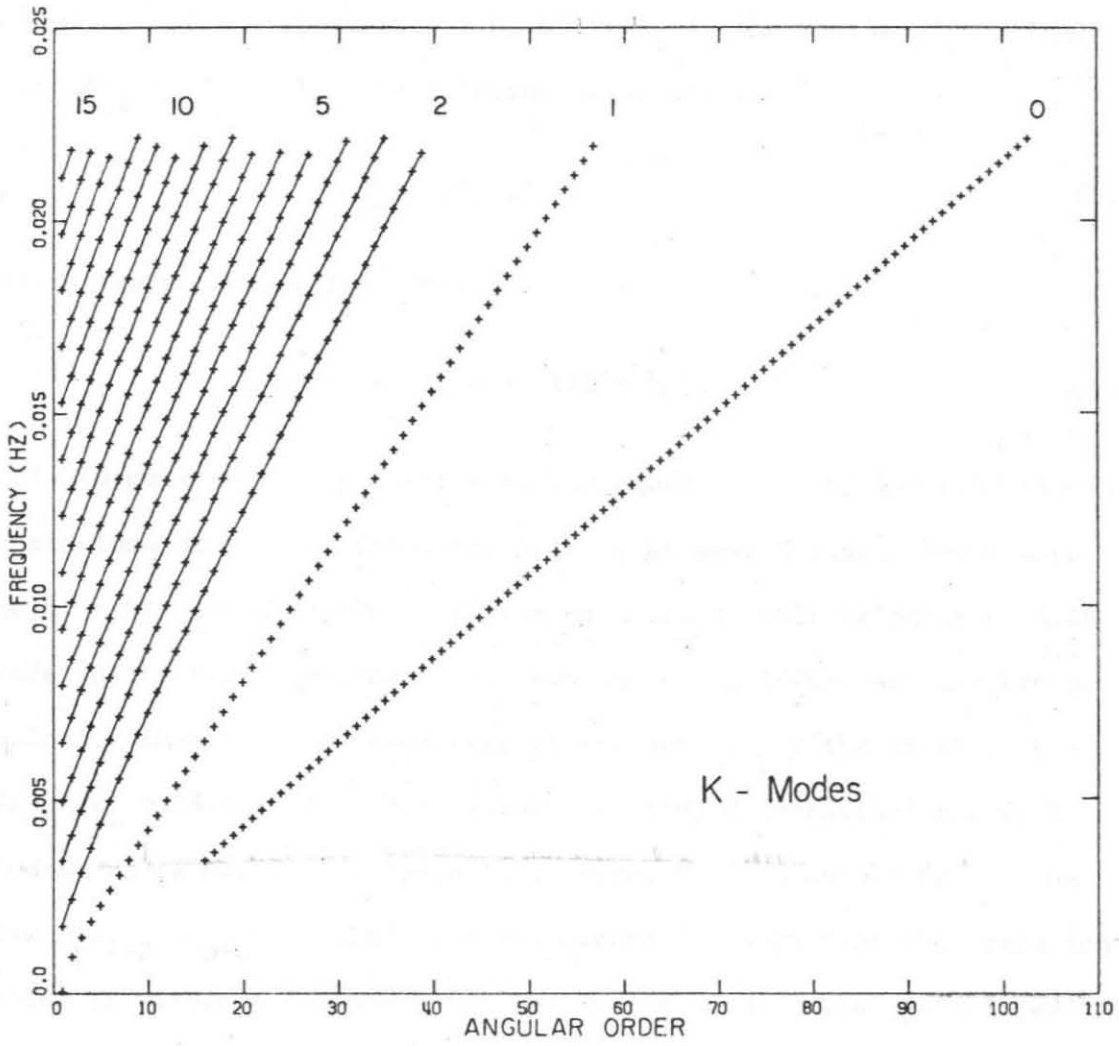

Figure 1.7. Frequency versus angular order plot of the K family of modes. Pseudo-overtones are traced and labeled according to the new proposed nomenclature.

excited by any realistic seismic source. Boundary conditions now require $y_3(0) = 0$; $y_4(r_i) = 0$, where r_i is the radius of the inner core (r_i = 1215 km). The solution is simply :

$$y_3 = j_\ell(\omega r/\beta) , \tag{1.21}$$

which leads to eigenfrequencies :

$${}_p\omega_\ell = \frac{\beta}{r_i} \pi [p + \ell/2 + \tfrac{1}{2}] . \tag{1.22}$$

This formula extends Gilbert's (1975) equation (9) by incorporating variations of ℓ. The frequency spacing between K modes should then be $\Delta f = \beta/2r_i = 1.43 \cdot 10^{-3}$ Hz, for an average shear velocity of 3.48 km/s inside the inner core (Anderson and Hart, 1976), and the group velocity theoretically predicted at the surface of the Earth : $U = \beta a \pi /2r_i$ = 28.6 km/s. These values are indeed characteristic of K modes, as is checked in Table 1.5. Also, K modes should follow the law ${}_p\omega_{\ell+2} \simeq {}_{p+1}\omega_\ell$; Table 1.6 and Figure 1.7 show that this relation holds to within a few percent. The low value of $y_3(a)$ associated with K modes is simply a consequence of the inability of the outer core to transmit transverse displacements: only the small vertical component y_1 can be transmitted through it to the mantle and surface of the Earth.

Although the displacement in them is similar ($|y_3| >> |y_1|$), equations (1.20) and (1.22) shows that C and K modes behave totally differently with varying ℓ, a fact which is not explicitly brought out in Gilbert's approach. When ℓ varies, K and V modes do indeed share a similar behavior, as their general layout shows on Figures

1.5 and 1.7. It can be said that <u>they</u> are the modes of a spherical body. As shown in Section 2.2, the mantle's C modes, insensitive to ℓ, behave like plane waves: they are the modes of a shell, at a wavelength large with respect to its inner radius.

In summary, by assuming that the original system is entirely decoupled at low ℓ, we have been able to derive most of the properties of the three families of modes, and their variation with ℓ. Note that the various assumptions which were made on $|y_3/y_1|$, $div\,\vec{u}$, etc... can be <u>a posteriori</u> checked to hold : It is possible to do so by using an exact solution, such as the one in Takeuchi and Saito (1972, p. 243), and assuming (in their notation) $\gamma = 0$; the upper sign in their equation (99) corresponds to V modes, the lower one to C modes.

1.2.4 Coupling at larger ℓ.

We will not discuss the large-ℓ limit of the differential system (1.5), since the theoretical study of surface waves has been quite extensive in the past decades. It can be shown very easily that, at large ℓ, (1.5) reduces to the classical equations governing surface waves (Takeuchi et al., 1962; Saito, 1967). However, we would learn nothing about overtones from the crude model we started with, since at high frequencies, when the Earth's curvature can be neglected, a homogeneous medium yields only the fundamental Rayleigh wave ${}_0S_\ell$.

On the other hand, it can be useful to examine the coupling between V and C modes as a function of ℓ as a particular case of coupling between two dynamical systems. This is an extremely frequent

phenomenon in physics, and in all fields (quantum mechanics, solid state physics, oscillatory dynamics, electrodynamics....), its basic effects (spreading out the eigenfrequencies and hybridizing the eigenfunctions) are essentially similar. Examples can be found in most textbooks (e.g. Rocard (1948), Kittel (1963)). In order to analyze the different forms of coupling occurring at various ranges of ℓ, let us think of the Earth as a physical system having two linear unperturbed dispersion relations : $\omega = \omega_c$ (C modes), and $\omega = \omega_0 + U.k$ (V modes), where k is the wavenumber around the surface of the Earth, U is the group velocity of the corresponding V modes. Although we have seen that the exact mathematical formulation of the problem is more intricate, the physical problem can be schematized by allowing the dispersion relation to become :

$$(\omega - \omega_c)\ (\omega - \omega_0 - U.k) = \varepsilon^2 \quad , \tag{1.23}$$

where ε is some measure of the intensity of coupling. As shown on Figure 1.8, the dispersion curves are hybridized into the two branches of a hyperbola:

$$\omega = \tfrac{1}{2}\,[\omega_0 + U.k + \omega_c] \pm \tfrac{1}{2}\sqrt{(\omega_0 + U.k - \omega_c)^2 + 4\,\varepsilon^2} \tag{1.24}$$

It is clear from Figure 1.8 that the range Δk of wavenumbers over which the hybridization takes place increases with ε, and it can be shown from equation (1.24) that

$$\Delta k = \frac{1}{\sqrt{A}}\ \frac{\varepsilon}{U} \quad , \tag{1.25}$$

where A is some measure of the maximum allowed perturbation of a branch.

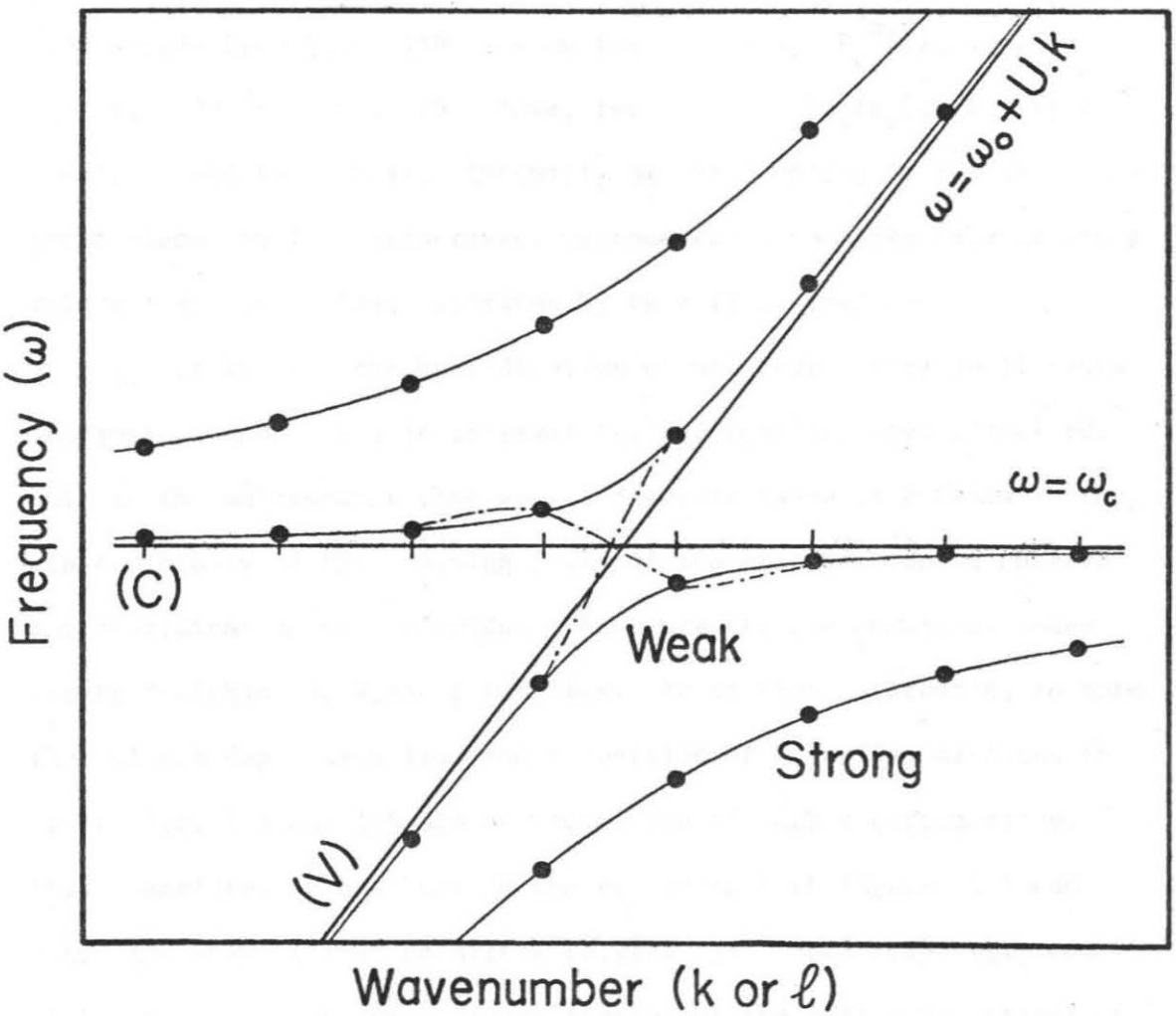

Figure 1.8. A simplified model of coupling between two families of modes. Units are arbitrary. Straight lines show the unperturbed dispersion curves. The hyperbolas represent hybridized dispersion curves for both weak and strong coupling. Dots identify individual modes for a model with discrete wavenumbers. Weak coupling is barely noticed, and results only in slightly irregular pseudo-overtone branches (dash-dot lines). Strong coupling, extending over several angular orders, generates hybridized branches.

Now, in the present case of the Earth, the coupling terms in equation (1.5) are proportional to L^2. However, the physical quantities directly comparable are the displacements u_r and u_θ. Expressions from Saito (1967) show that $u_r \propto y_1 \cdot P_\ell^m(\theta)$, while $u_\theta \propto y_3 \cdot dP_\ell^m(\theta)/d\theta$. Therefore, for $\ell >> 1$, $|u_\theta/u_r| \simeq (\ell + \frac{1}{2}) \cdot |y_3/y_1|$, and the physical intensity of the coupling is really proportional to ℓ. Furthermore, wavenumbers k can take only discrete values : $k = (\ell + \frac{1}{2})/a$, separated by $\delta k = 1/a$. Then :

i) at low ℓ, the hybridization occurs over a very small range Δk, smaller than the unit interval δk, and coupling goes unnoticed. Only in the unfavorable case when a discrete value of k falls in the close vicinity of the crossing point of two branches, do we observe any hybridization of the modes. These are the few anomalous modes observed within the V and C families. It is also interesting to note that slight departures from the properties of a family, as found in Tables 1.2, 1.4 and 1.6 are an indication of such a circumstance. This translates into a bump in the curves on both Figures 1.5 and 1.6. A similar situation arises between ${}_{10}S_2$ and ${}_{11}S_2$ (${}_3V_2$ and ${}_3K_2$), leading to the possible excitation of the latter by an earthquake, despite its nature as a core mode. The observation of this occurrence, by Dziewonski and Gilbert (1973) proved the existence of K modes, and demonstrated the solidity of the inner core.

ii) at intermediate ℓ, Δk is on the order of a few sampling units δk, and the two hybridized branches can be continuously identified: The properties of the modes along them vary continuously from one type of family to the other. However, the coupling range

Δk is still small enough that multiple coupling between more than two overtone branches does not take place : This is the general behavior of H modes.

iii) at large ℓ, $\Delta k >> \delta k$, the hyperbola degenerates into two parallel straight lines, and the modes are totally hybridized, over the whole spectrum (in fact coupling involves more than two branches at a time). This is of course the case of R modes, giving birth to a surface wave in which vertical and horizontal displacements are completely mixed (see Figure 1.9).

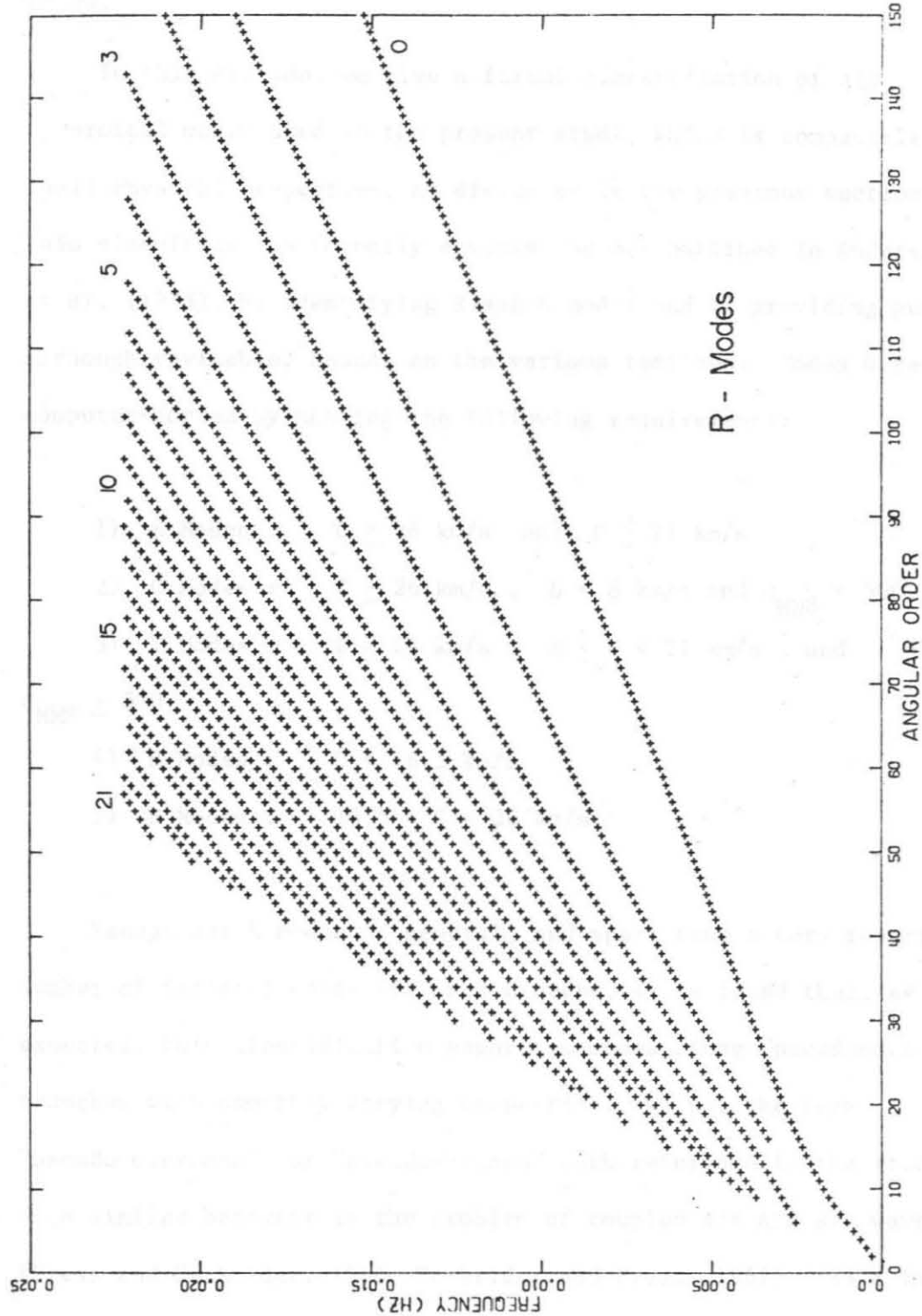

Figure 1.9. Frequency versus angular order plot of the R family of modes. Pseudo-overtones are labeled according to the new proposed nomenclature.

1.3. A Classification and Proposed New Nomenclature for Spheroidal Modes.

In this section, we give a formal classification of all spheroidal modes used in the present study, which is compatible with their physical properties, as discussed in the previous sections. This classification formally extends the one outlined in Anderssen et al. (1975), by identifying R and H modes and by providing general, although revisable, bounds on the various families. Modes were computer-sorted by meeting the following requirements:

1) K Modes : $C \geq 26$ km/s and $U \geq 21$ km/s

2) C Modes : $C \geq 26$ km/s , $U < 8$ km/s and $Q_{MM8} < 500$.

3) V Modes : $C \geq 26$ km/s , $8 \leq U < 21$ km/s , and $Q_{MM8} \geq 500$.

4) R Modes : $C < 16.5$ km/s

5) H Modes : $16.5 \leq C < 26$ km/s.

Except for H modes in general, and apart from a very restricted number of isolated cases of V and C modes, it is found that, as expected, this classification separates modes along "pseudo-overtone" branches with smoothly varying properties. We use the term "pseudo-overtone", or "pseudo-branch" with reference to the study of a similar behavior in the problem of coupled air and sea waves (Press and Harkrider, 1966; Harkrider and Press, 1967). In a few cases, in which coupling is important between V and C modes, both of the coupled modes would fall into a given family. A small violation

of the above requirements was then allowed to bring the slightly hybridized mode back into its original family. It was also decided to incorporate the two branches of Stoneley modes with phase velocities around 8.5 and 16 km/s into the K family, due to their low excitation coefficients. This helps define the pseudo-overtone branches of the R family. Due to the close coupling between the modes ${}_1S_\ell$ and ${}_2S_\ell$ ($\ell \leq 15$), these modes were included into the H family.

We now introduce a new nomenclature for spheroidal modes which identifies the family and pseudo-overtone branch to which a mode belongs. This nomenclature will use the five letters K, C, V, H, R, and two indices : p (pseudo-overtone index) and ℓ (angular order index). The following paragraphs discuss the assignment of the index p in the five families. Figures 1.4 to 1.7 and 1.9 are frequency vs. angular order plots of the various families. Extensive tables, giving the correspondence between the new nomenclature and the conventional one (taken as resulting from the use of model 1066A (Gilbert and Dziewonski, 1975)) have been prepared, and are available from the author on request.

1.3.1 ${}_pK_\ell$. Core and Stoneley modes. See Figure 1.7.

The two Stoneley branches at low phase velocity are labelled ${}_0K_\ell$ and ${}_1K_\ell$. Then, modes with given ℓ are sorted by increasing frequency. These modes are not excited by any realistic seismic source.

1.3.2 $_pC_\ell$. Colatitudinal modes. See Figure 1.6.

The various pseudo-overtone branches are labelled so as to realize the identity between $_pC_\ell$ and $_pT_\ell$ modes, as $\ell \to 0$. In this way, there does not exist a $_1C$ branch. This point should not appear as a drawback to the new nomenclature: it simply means that the corresponding modes are not part of the C family. In fact, they are H modes. Figure 1.6 shows that bumps do occur along C pseudobranches, bringing in negative apparent group velocities. This fact results from coupling with V modes, as discussed in section 1.2.4.

1.3.3 $_pV_\ell$ Vertical Modes. See Figure 1.5.

Similarly, the various pseudobranches are labelled so as to let $_pS_0$ and $_pV_0$ coincide. Again, except for $_0V_0$, there are no $_0V_\ell$ modes, and the maximum number for ℓ at a given p is itself a function of p. This fact simply means that the missing modes are part of the H family.

1.3.4 $_pR_\ell$ Rayleigh Modes. See Figure 1.9.

The only basic difference in nomenclature between $_pR_\ell$ and $_nS_\ell$ results from the removal of the Stoneley modes $_0K_\ell$.

1.3.5 $_pH_\ell$ Hybrid Modes. See Figure 1.4.

These modes, which correspond to intermediate coupling, lie at a crossing-point between two trends: the decoupled pseudo-branch of V and C modes, and the coupled surface wave trend of R modes. Note

that the distinction between H modes and V or C modes, or between H modes and R modes is extremely subjective and depends entirely on the amount of distortion one is willing to allow within the physical properties of V, C, or R modes, in other words, upon the allowance made for hybridization, a quantity similar to A in equation (1.25). Ideally, equation (1.5) shows that, except for $\ell = 0$, coupling between radial and colatitudinal displacements is never totally absent from any mode, and all modes could therefore be considered H modes. This is the basis for the conventional nomenclature, which, however, leads to a loss of most physical insight in the properties of spheroidal modes. We believe that the adopted values (16.5 and 26.5 km/s) for phase velocity bounds on H modes maintain a reasonable balance between the two tendencies. Note that the pseudo-overtone number, p, of no V, nor C nor R mode, is dependent on those bounds. Should the bounds change, a given mode might be moved out of his family, into another one, but it will retain its p index as long as it stays inside a given family. Given this evidence, and in order to achieve the same stability for H modes, it appears that the only reasonable nomenclature for H modes is to retain the conventional overtone number, that is to simply have ${}_nS_\ell$ relabeled ${}_nH_\ell$.

We can now check the effect of the new nomenclature on the five major drawbacks mentioned in section 1.2:

i) Once the values of p are used for both vertical ${}_pV_\ell$ and colatitudinal ${}_pC_\ell$ modes, and in the absence of occasional coupling, the eigenfunction (y_1 for V modes, y_3 for C modes) has p zero-crossings inside the Earth. In the case of the simple system

described in Section 1.2, this follows from the properties of the spherical Bessel functions. In the case of a radially heterogeneous Earth, this result comes from the Sturm-Liouville nature of the uncoupled differential system, either for V or C modes (Ince, 1956; p. 233).

ii) We have already shown that the radial modes ${}_nS_0$ are totally integrated in the V family, and that their apparent scarcity was an artifact of the conventional nomenclature.

iii) The physical nature and general properties of a mode can be immediately read from its name in the new proposed nomenclature. They will not depend on the model used for their computation. (Except, obviously, in the case of H modes). In the example chosen in Section 1.1.1 (${}_{26}S_1$ and ${}_{27}S_1$), one of the modes will remain a K mode, and will always be called ${}_7K_1$, the other one will stay a V mode, always called ${}_7V_1$, regardless of the influence on their relative periods of the Earth model being used in the computation.

iv) Figures 1.10 to 1.12 show the variations of some properties of V, C, K, and R modes along pseudo-overtone branches p = cst, and compare them to similar variations along conventional overtone branches, taken from Figure 1.2. A considerable improvement in the smoothness of these properties is achieved, which clearly permits interpolation along the pseudo-overtone branches.

v) The discussion in Section 1.1.3 has shown on a particular example that U was closely related to U^* along a p-branch better than along an n-branch. This is indeed a general trend, which can be checked all over the K, C, V and R families.

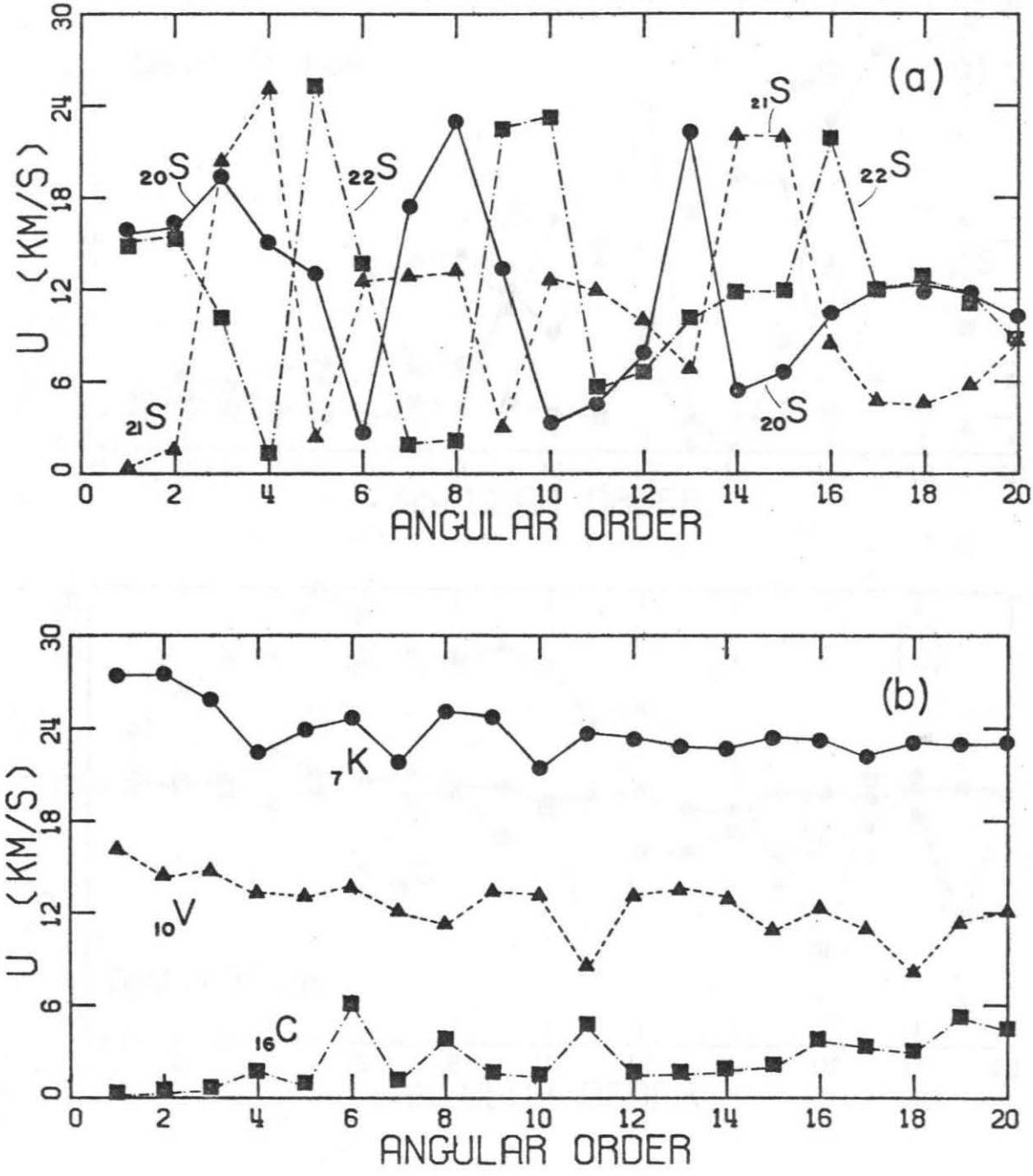

Figure 1.10. A comparison of the variation of the modes' group velocity along conventional overtones (top) and along pseudo-overtones of the new proposed nomenclature. The top figure is reproduced from Figure 1.2.

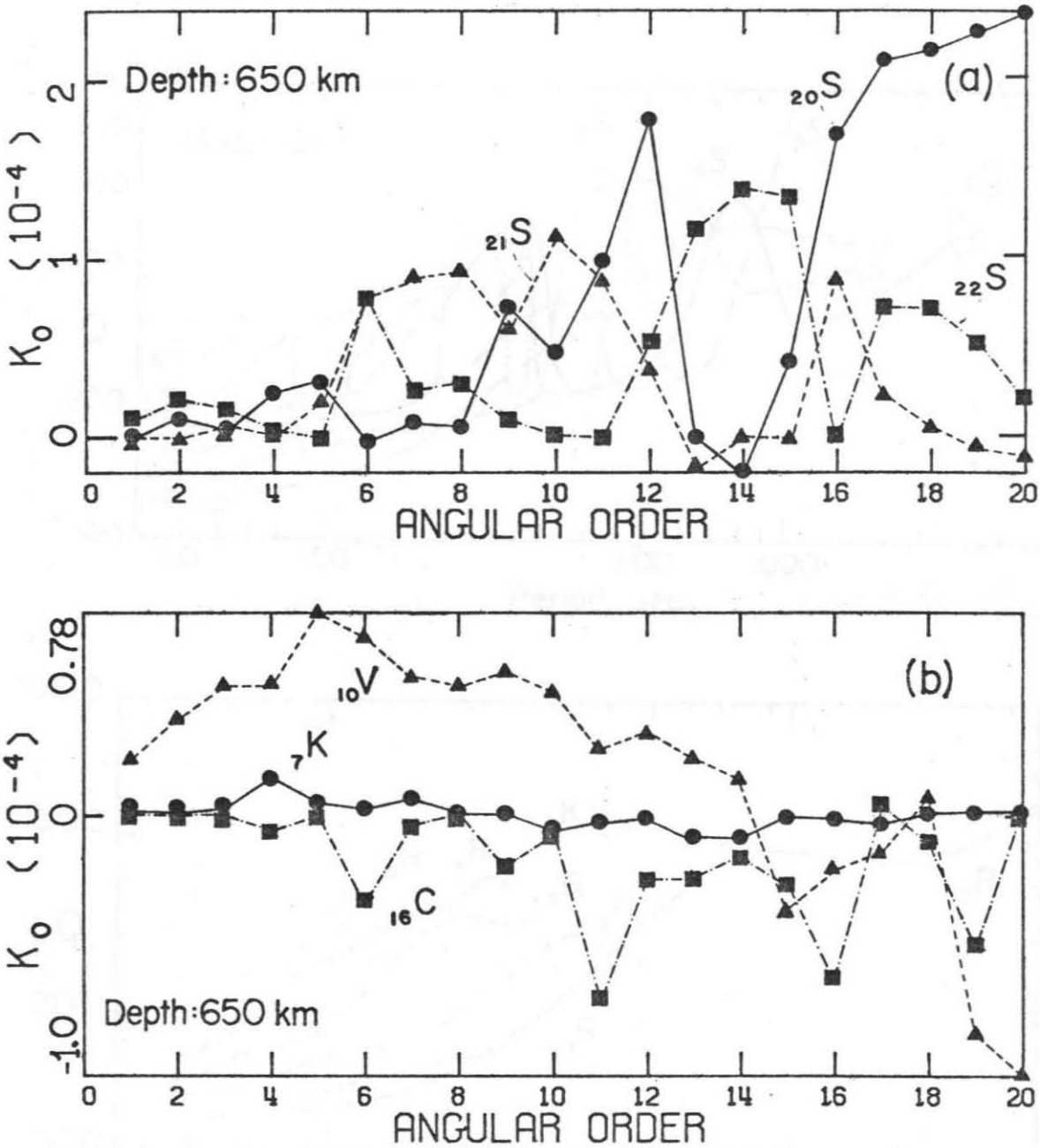

Figure 1.11. A comparison of the variation of the excitation (K_0 at a depth of 650 km) along conventional overtones (top) and pseudo-overtones of the new proposed nomenclature (bottom). The top figure is reproduced from Figure 1.2.

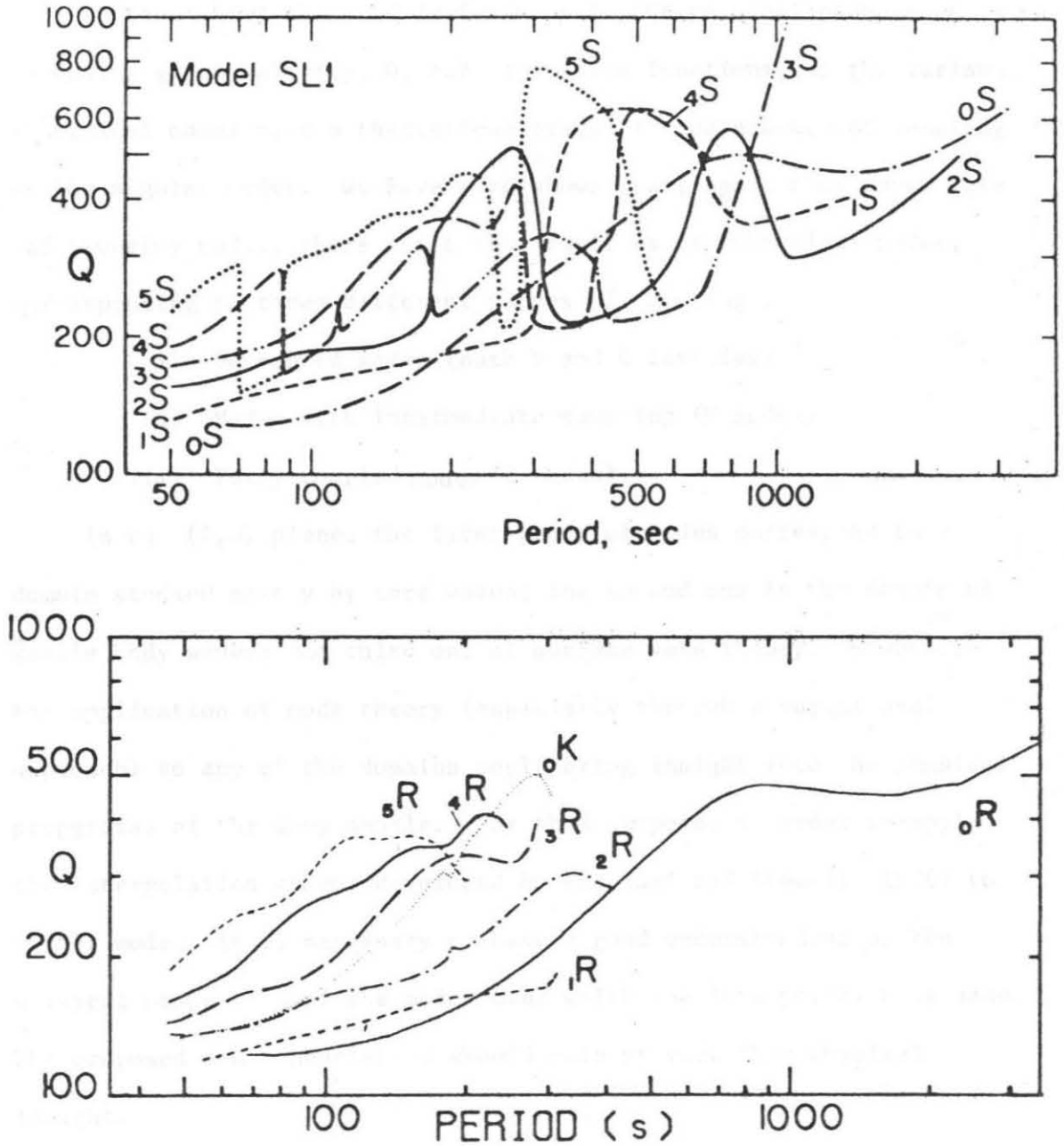

Figure 1.12. A comparison of the variation of the attenuation factor Q along conventional overtones (top) and pseudo-overtones of the new proposed nomenclature. The top figure is reproduced from Anderson and Hart (1978).

1.4 Conclusion

We have shown that the differences in the physical properties, including group velocity, Q, and excitation functions, of the various spheroidal modes have a theoretical origin in the absence of coupling at low angular order. We have also shown that, apart from Inner Core and Stoneley modes, there exist four families of spheroidal modes, corresponding to three different ranges of coupling :

i) Decoupled modes (both V and C families)

ii) Modes with intermediate coupling (H modes)

iii) Fully coupled modes (R modes).

In an (ℓ,ω) plane, the first group of modes correspond to a domain studied mostly by core waves; the second one is the domain of mantle body waves; the third one of surface wave theory. However, the application of mode theory (especially through a variational approach) to any of the domains could bring insight into the physical properties of the deep mantle. For this purpose, in order to apply the interpolation scheme developed by Kanamori and Stewart (1976) to higher modes, it is necessary to have a good understanding of the physical properties of the modes over which the interpolation is made. The proposed new nomenclature should help provide that physical insight.

CHAPTER 2

The Observability of Isotropic Seismic Sources: Application to the 1970 Colombian Earthquake

2.0 Introduction

The purpose of this chapter is to study the observability of isotropic components of the source mechanism of earthquakes having much larger deviatoric moments, in particular the 1970 Colombian event, which was the largest deep shock in the past twenty years. The mechanism of this earthquake has been the subject of considerable controversy since Dziewonski and Gilbert (1974) reported that the main earthquake source was preceded by a slow, isotropic precursor.

Isotropic components of earthquake source mechanisms, if observable, have important geophysical and petrological implications. Bridgman (1945) and Ringwood (1967) suggested a connection between petrological phase changes and deep earthquakes. Vaišnys and Pilbeam (1976) outlined a petrological model which predicts seismically observable phase changes, although Dennis and Walker (1965) had earlier suggested that these may be unobservably slow.

However, it has generally been assumed that earthquakes in the downgoing lithosphere do not have an isotropic component, principally on the basis of the very well-constrained fault plane solutions obtained when the source is assumed to be a shear dislocation (Sykes, 1968). The first solution for the P waves from an isotropic source ("center of dilation") in a homogeneous isotropic medium was given by Love (1944, p. 187). Isotropic sources were among the possibilities considered by Japanese seismologists studying focal mechanisms by using first motions; their early efforts are summarized by Matuzawa (1964). On the basis of strain records at Ñaña, Peru, Benioff (1964) suggested a volume change of 3% as part of a possible mechanism for a

deep Peruvian earthquake. Systematic efforts to use the amplitudes of seismic waves to search for a possible volume change in deep earthquakes were first made by Randall and Knopoff (1970), who reported both explosive and implosive components to seismic sources. The former could not be explained by the phase-change argument.

Mendiguren (1972, 1973) gave the first rigorous method for identifying free oscillation eigenperiods by using the excitation criterion. As part of his studies, Mendiguren found that for the deep Colombian earthquake (31 July 1970; h=651 km; 1.5°S, 72.6°W; m_b=7.1), the amplitude of fundamental modes between 150 and 1200 seconds were in agreement with a double-couple step function source. However, since the excitation of fundamental Rayleigh waves by a deep isotropic source is very inefficient, Mendiguren's results do not totally preclude the existence of an isotropic source. Later, Dziewonski and Gilbert (1974) and Gilbert and Dziewonski (1975) studied essentially the same WWSSN records as Mendiguren had studied earlier, but used almost all modes with periods longer than 80 seconds to invert for the moment tensor. They concluded that there had been a significant isotropic component to the source mechanism of the Colombian earthquake, and, further, that the isotropic source was precursory to the main source. There were several comments on this result (Geller, 1974; Hart and Kanamori, 1975; Mendiguren, 1976), and, in turn, several replies (e.g. Kennett and Simons, 1976), reflecting the important geophysical consequences of the proposed precursor.

In the present study, we first give a general discussion of the excitation of seismic waves by isotropic sources, and then discuss

the Colombian deep earthquake in detail. Since the primary questions regarding this event concern the nature of the source function at very long periods, we use an ultra-long period record (response peaked around 160 seconds) of the Colombian earthquake obtained at Pasadena. Synthetic seismograms obtained by normal mode summation are used to investigate the various proposed source mechanisms.

2.1 The Relative Excitation of the Earth's Normal Modes by Deviatoric and Isotropic Sources.

The excitation of the Earth's normal modes by seismic sources has been extensively studied. Following simple case studies in the early 1960's, Saito (1967) and later Takeuchi and Saito (1972) found general expressions for the excitation of any normal mode by any combination of point forces, including double-couples and dipoles without moment. Abe (1970) first applied Saito's results to the analysis of the free oscillations excited by the 1963 Kurile Islands earthquake. Kanamori and Cipar (1974) gave computationally convenient versions of Saito's expressions for a double-couple of arbitrary geometry. Other derivations of the excitation of normal modes were given by Gilbert (1970) and Gilbert and Dziewonski (1975), and also by Phinney and Burridge (1973).

The possibility of using an expansion of the Earth's motion on the complete set of its normal modes in order to construct synthetic seismograms was first applied by Y. Satô and his colleagues; their efforts are summarized in Landisman et al. (1970). In order to derive the optimal conditions under which isotropic sources can be observed, we will first study the relative amplitudes of the fundamental mode Rayleigh waves and of the P waves excited by dislocations with different source geometries and by isotropic sources, both deep and shallow. Although Douglas et al. (1971) and Gilbert (1973) did compare the amplitudes of P and Rayleigh waves for very shallow isotropic sources at high frequencies, they were primarily concerned with the m_b:M_s discriminant, and did not consider very long periods,

or sources significantly below the Earth's surface. It is well known that isotropic sources, especially at depth, are less efficient than deviatoric ones in exciting Rayleigh waves, but we will examine this phenomenon quantitatively.

2.1.1. Rayleigh Waves

In the notation of Kanamori and Cipar (1974), the amplitude of the vertical component of the spheroidal mode ${}_nS_\ell$ (overtone number n and angular order ℓ), excited by a double-couple is:

$$u_r(\vec{r},t) = y_1^S(r) \cos {}_n\omega_\ell t \; (K_0 \, s_R P_\ell^0 - K_1 \, q_R P_\ell^1 + K_2 \, p_R \, P_\ell^2) \qquad (2.1)$$

where the excitation coefficients K_0, K_1, K_2, depend only on the eigenfunctions at the depth of the source and on the kinetic energy of the mode; the source radiation pattern coefficients p_R, q_R, s_R depend only on the geometry of the source and the azimuth ϕ of the station; and P_ℓ^m is the associated Legendre function of azimuthal order m and angular order ℓ. It follows from the expressions for the source coefficients as a function of dip (δ) and slip (λ):

$$\begin{aligned} s_R &= \sin\lambda \sin\delta \cos\delta \\ q_R &= \sin\lambda \cos 2\delta \sin\phi + \cos\lambda \cos\delta \cos\phi \\ p_R &= \cos\lambda \sin\delta \sin 2\phi - \sin\lambda \cos\delta \sin\delta \cos 2\phi, \end{aligned} \qquad (2.2)$$

that K_1 is the excitation coefficient characteristic of a vertical dip-slip fault, and K_2 that of a vertical strike-slip. The coefficient

of K_0, s_R, is non-zero for any non-vertical fault having a dip-slip component. Expressions for K_0, K_1, K_2 are given by Kanamori and Cipar (1974):

$$K_0 = \frac{2\ell+1}{4\pi\, {}_n\omega_\ell^2 [I_1^S + L^2 I_2^S]\, r_s} \cdot \frac{2(3\lambda_s+2\mu_s)}{\lambda_s+2\mu_s} \cdot \{ y_1^S(r_s) - \frac{r_s}{3\lambda_s+2\mu_s} y_2^S(r_s) - \tfrac{1}{2} L^2 y_3^S(r_s)\}$$

$$K_1 = \frac{2\ell+1}{4\pi\, {}_n\omega_\ell^2 [I_1^S + L^2 I_2^S]\, \mu_s} \cdot y_4^S(r_s) \qquad (2.3)$$

$$K_2 = \frac{2\ell+1}{4\pi\, {}_n\omega_\ell^2 [I_1^S + L^2 I_2^S]\, r_s} \cdot y_3^S(r_s) \ , \qquad L^2 = \ell\,(\ell+1)$$

the notation used being that of Kanamori and Cipar (1974), except for the angular order (ℓ in the present study).

For an isotropic source (taken as positive in the case of an explosion), the vertical displacement is obtained from Takeuchi and Saito (1972):

$$u_r(\vec{r},t) = y_1^S(r) \cos {}_n\omega_\ell t \quad N_0 \cdot P_\ell^0 \ , \qquad (2.4)$$

with :

$$N_0 = \frac{2\ell+1}{4\pi\, {}_n\omega_\ell^2 [I_1^S + L^2 I_2^S]\, r_s} \cdot \frac{-4\mu_s}{\lambda_s+2\mu_s} \cdot \{ y_1^S(r_s) + \frac{r_s}{4\mu_s} y_2^S(r_s) - \tfrac{1}{2} L^2 y_3^S(r_s) \} . \qquad (2.5)$$

N_0 is proportional (Harkrider, 1964; Gilbert, 1970) to the radial factor of dilatation $D(r_s)$ where:

$$\varepsilon_{ii} = \varepsilon_{rr} + \varepsilon_{\theta\theta} + \varepsilon_{\phi\phi} = D(r)\ Y_\ell^m\ (\theta,\phi) \tag{2.6}$$

and can be rewritten in a simpler form:

$$N_0 = -\frac{2\ell + 1}{4\pi_n \omega_\ell^2\ (I_1^S + L^2\ I_2^S)}\ D(r_s) \tag{2.7}$$

For large values of ℓ (and for all ℓ at a distance $\theta = 90^o$) the Legendre functions P_ℓ^0, P_ℓ^1, P_ℓ^2 in (2.1) can be replaced by their asymptotic expansion:

$$P_\ell^m(\theta) = (-1)^m \ell^{m-\frac{1}{2}} (2/\pi\ \sin\theta)^{\frac{1}{2}}\ \cos\left[(\ell + \tfrac{1}{2})\ \theta + \frac{m\pi}{2} - \frac{\pi}{4}\right] . \tag{2.8}$$

The approximate relative excitation of a given mode by various types of seismic sources can therefore be studied through the four sets of numbers: $K_0/\sqrt{\ell}$, $N_0/\sqrt{\ell}$, $K_1\sqrt{\ell}$ and $K_2\ell^{3/2}$. Figure 2.1 shows the variation of these parameters for the fundamental spheroidal modes (Rayleigh waves) with angular order ℓ (or with period T) for three different source depths: shallow, intermediate and deep. The excitation coefficients N_0, K_0, K_1 and K_2 are computed using Gilbert and Dziewonski's model 1066A, and for a moment of 10^{27} dyn-cm. For the shallow source, the isotropic excitation $N_0/\sqrt{\ell}$ decreases slightly with increasing frequency relative to the deviatoric one, but remains basically constant. The situation is quite different for

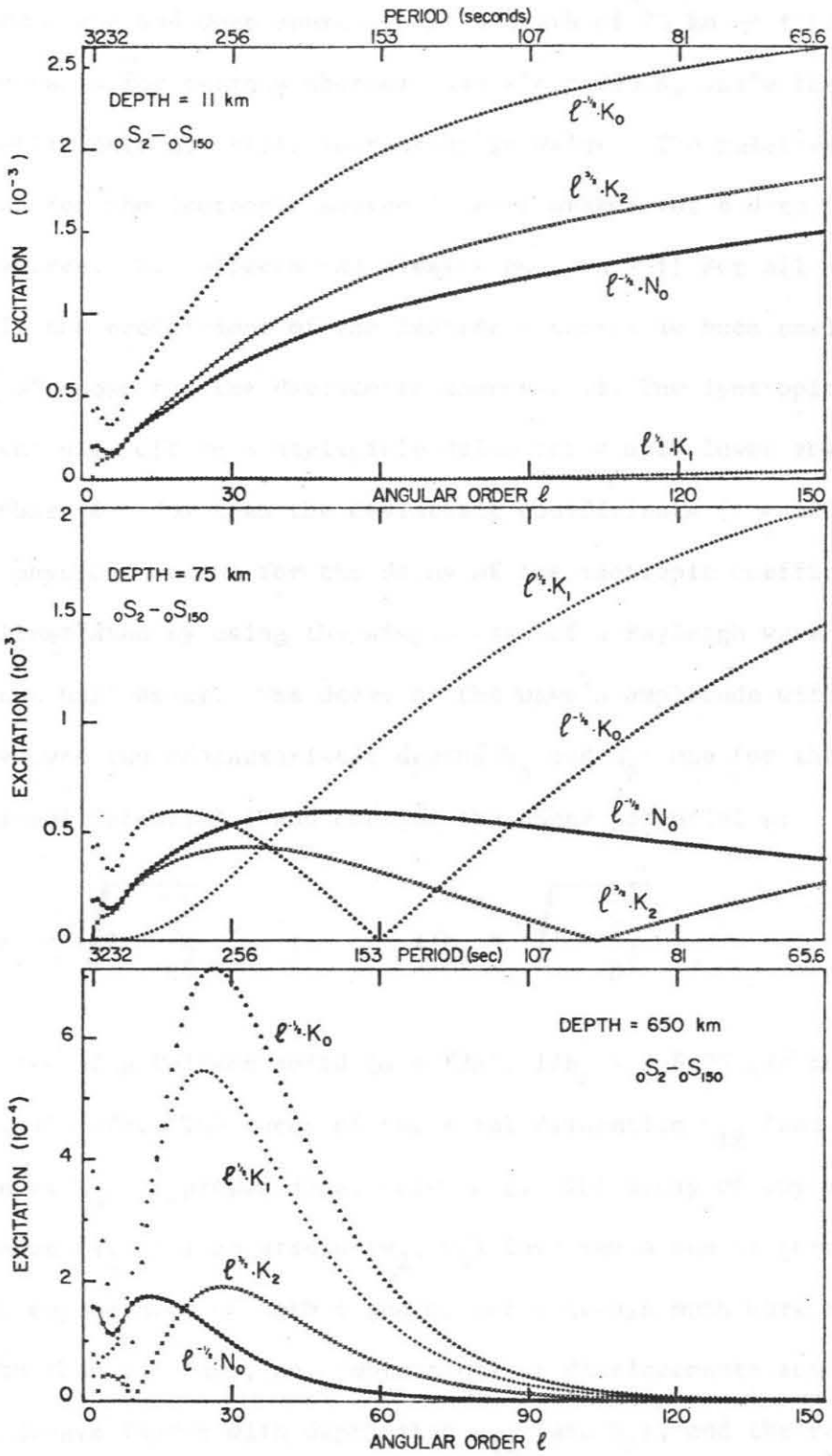

Figure 2.1. Values of the various excitation coefficients $\ell^{-1/2}N_0$, $\ell^{-2}K_0$, $\ell^{1/2}K_1$, $\ell^{1.5}K_2$ of spheroidal modes as a function of angular order (ℓ=2-150). A few values of the corresponding periods are shown. The source is shallow (top), intermediate (center) or deep (bottom).

the intermediate and deep sources. At a depth of 75 km we find that $N_0/\sqrt{\ell}$ decreases for periods shorter than about 200 s, while the other coefficients are still increasing in value. The relative excitation for the isotropic source is even weaker for a deep (h = 650 km) source. Two effects can clearly be seen. i) For all modes with $\ell > 15$ the coefficient of the isotropic source is much smaller than any of those for the deviatoric sources; ii) The isotropic coefficient dies off to a negligible value for a much lower angular order number ($\ell \simeq 70$) than the deviatoric coefficients ($\ell \simeq 120$).

The physical reason for the decay of the isotropic coefficient can be illustrated by using the simple case of a Rayleigh wave in a homogeneous half-space. The decay of the wave's amplitude with depth involves two characteristic depths h_ϕ and h_ψ: one for the compressional potential ϕ and one for the shear potential ψ:

$$1/h_\phi = \sqrt{1 - \frac{c^2}{\alpha^2}}\ \frac{\omega}{c} \quad ; \qquad 1/h_\psi = \sqrt{1 - \frac{c^2}{\beta^2}}\ \frac{\omega}{c} \tag{2.10}$$

For the case of a Poisson solid ($\alpha = \sqrt{3}\beta$), $1/h_\phi = 0.8475\ \omega/c$ and $1/h_\psi = 0.3933\ \omega/c$. The decay of the total dilatation ε_{ii} (and therefore of N_0) is proportional only to ϕ. The decay of any other displacement (y_1, y_3) or stress (y_2, y_4) involves a sum of terms with the depth dependences of both ϕ and ψ, but ϕ decays much more rapidly with depth than ψ. Thus, no combinations of displacements and stresses decays faster with depth than ε_{ii} (and N_0), and the ratio N_0/K_i will eventually behave as: $\exp[(1/h_\psi - 1/h_\phi)\,\omega\, z/c\,]$. At z = 650 km, this is on the order of 10^{-2} for T = 100 s and 10^{-8}

for T = 30 s. Although these figures are clearly only approximations for the case of a spherical, vertically heterogeneous, earth, this example provides physical insight into the relative efficiency of isotropic and dislocation sources. Jeffreys (1928) used a similar argument to show that deep sources will excite much smaller Rayleigh waves than shallow ones, although he did not distinguish between isotropic and deviatoric sources. Jeffreys' argument was later used by Stoneley (1931) to verify the existence of deep-focus earthquakes on the basis of their small Rayleigh wave amplitudes.

Figure 2.2 shows the relative Rayleigh wave excitation in the form of spectral radiation patterns. From Kanamori and Stewart (1976), the spectral amplitude of the vertical component of Rayleigh waves for a shear dislocation of unit moment is:

$$\left|U_r(\omega)\right| = \sqrt{\frac{\pi}{2\ell \sin\Delta}} \cdot \frac{a}{U} \cdot y_1^S(a) \cdot \left|s_R K_0 - \ell^2 p_R K_2 - i\ell q_R K_1\right| . \quad (2.11)$$

where ω is the angular frequency (in rd/s), a is the earth's radius, Δ is the epicentral distance, U is the group velocity and all other variables are defined above. The corresponding expressions for an explosion is

$$\left|U_r(\omega)\right| = \sqrt{\frac{\pi}{2\ell \sin\Delta}} \cdot \frac{a}{U} \cdot y_1^S(a) \cdot \left|N_0\right| . \quad (2.12)$$

Although this expression is derived from the asymptotic expansion of the Legendre functions, it is quite accurate, even at very long periods, away from the epicentral and antipodal areas. The spectral

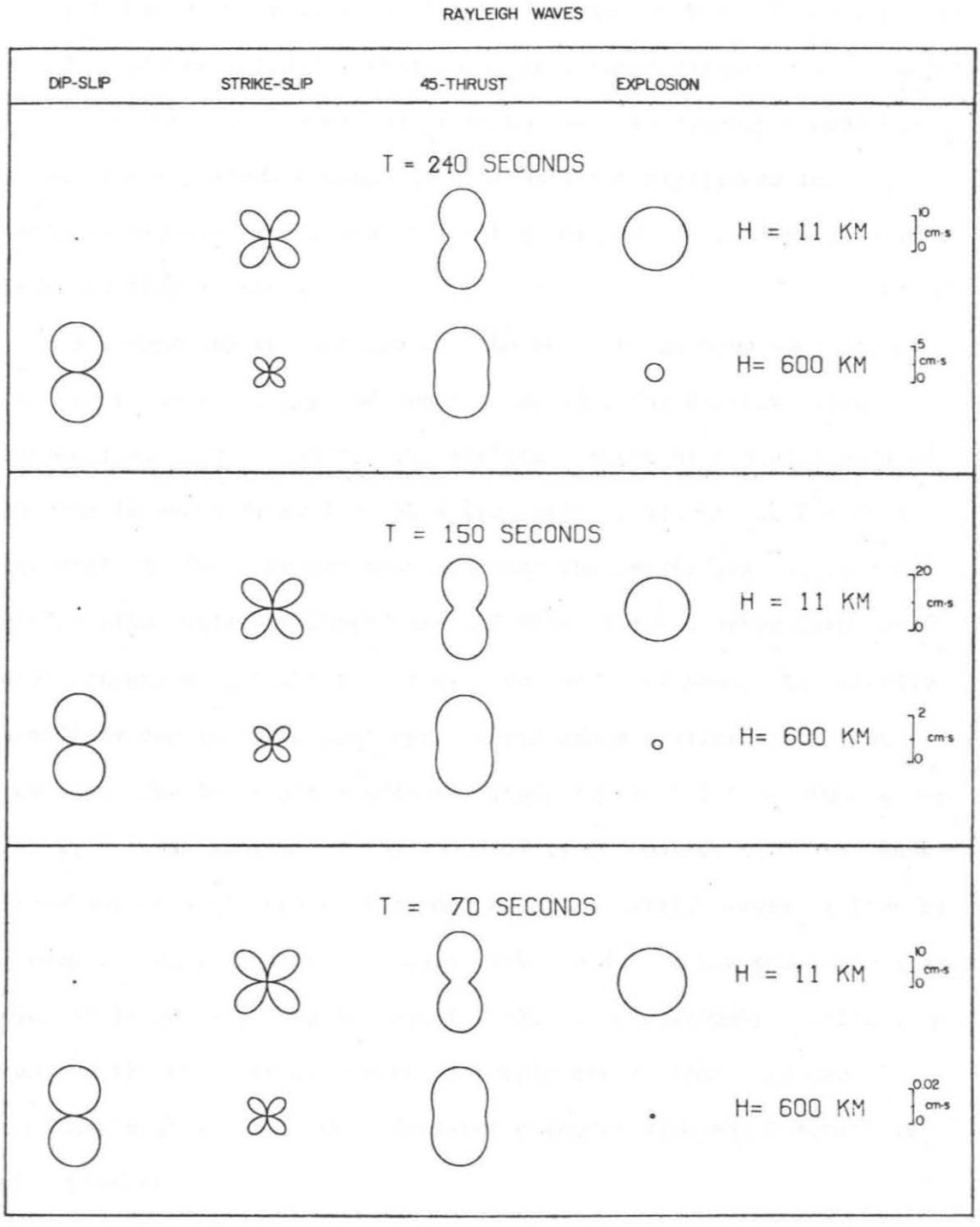

Figure 2.2. Radiation patterns of Rayleigh waves for both a surface event and a deep earthquake are compared for various source geometries at three different periods. The station distance is Δ=60° and a common moment rate of 10^{27} dyn.cm/s is assumed. The different scales are common to the four figures on a given line, but vary from line to line.

radiation patterns plotted on Figure 2.2 are for $\Delta = 60^{o}$ and a moment of 10^{27} dyne cm. For the shallow source, the radiation pattern amplitudes for three of the different mechanisms are roughly comparable at all three periods shown. In contrast, the amplitudes for the vertical dip-slip fault are negligible because the free surface is a node for this mechanism.

By comparing the spectra for the shallow and deep sources, we can study the frequency and depth dependence for Rayleigh wave excitation. For T = 240 s, the amplitude ratio of the shallow/deep sources is about 2; at T = 150 s the ratio is 10; and at T = 70 s the ratio is 500. We can also see that the amplitudes for the deep strike-slip fault are about one-half those for the other deep shear dislocations at all three periods. On the other hand, the relative amplitude for the deep isotropic source grows smaller at shorter periods. The isotropic source amplitude is about 5 times smaller at 240 s, 8 times smaller at 150 s and 17 times smaller at 70 s. Thus the absolute amplitude of fundamental mode Rayleigh waves excited by a deep isotropic source decreases very rapidly as the period decreases. Even at relatively long periods (70 s), it is extremely difficult to resolve the presence of a deep isotropic source from fundamental mode Rayleigh waves, when a deviatoric source with equal moment is also present.

2.1.2. Spheroidal Overtones

In the case of spheroidal overtones, the relative excitation efficiency of earthquakes and explosions depends primarily on the physical nature of the mode. Using the classification given in Chapter 1, 'V' modes, which contribute mainly to PcP and PKP, are found to be relatively sensitive to compressional sources, since N_0 is usually almost as large as K_0, while ℓK_1 and $\ell^2 K_2$ are consistently much smaller. In contrast, for 'C' modes, which contribute primarily to ScS_{SV}, the excitation efficiency of an explosion (N_0) is considerably smaller than that of a vertical dip-slip fault (ℓK_1). The intermediately coupled 'H' modes, which contribute mainly to P waves, show no definite trend for isotropic sources to be either more or less efficient. Therefore, it is much easier to use a body-wave approach to study the relative excitation by deviatoric and isotropic sources for the earliest part of the record.

2.1.3. P waves

Following Chung and Kanamori (1976) we write the displacement at the earth's surface generated by a source at depth h and distance Δ as:

$$U(t) = 2 \frac{g(\Delta,h)}{a} \frac{R_{\phi,h}}{4\pi \rho_h v_h^3} \dot{M}(t - \tau) . \qquad (2.13)$$

where g is the geometrical spreading factor

$$g(\Delta,h) = \left[\frac{\rho_h v_h}{\rho_o v_o} \frac{\sin i_h}{\sin \Delta} \frac{1}{\cos i_o} \left| \frac{di_h}{d\Delta} \right| \right]^{\frac{1}{2}} , \qquad (2.14)$$

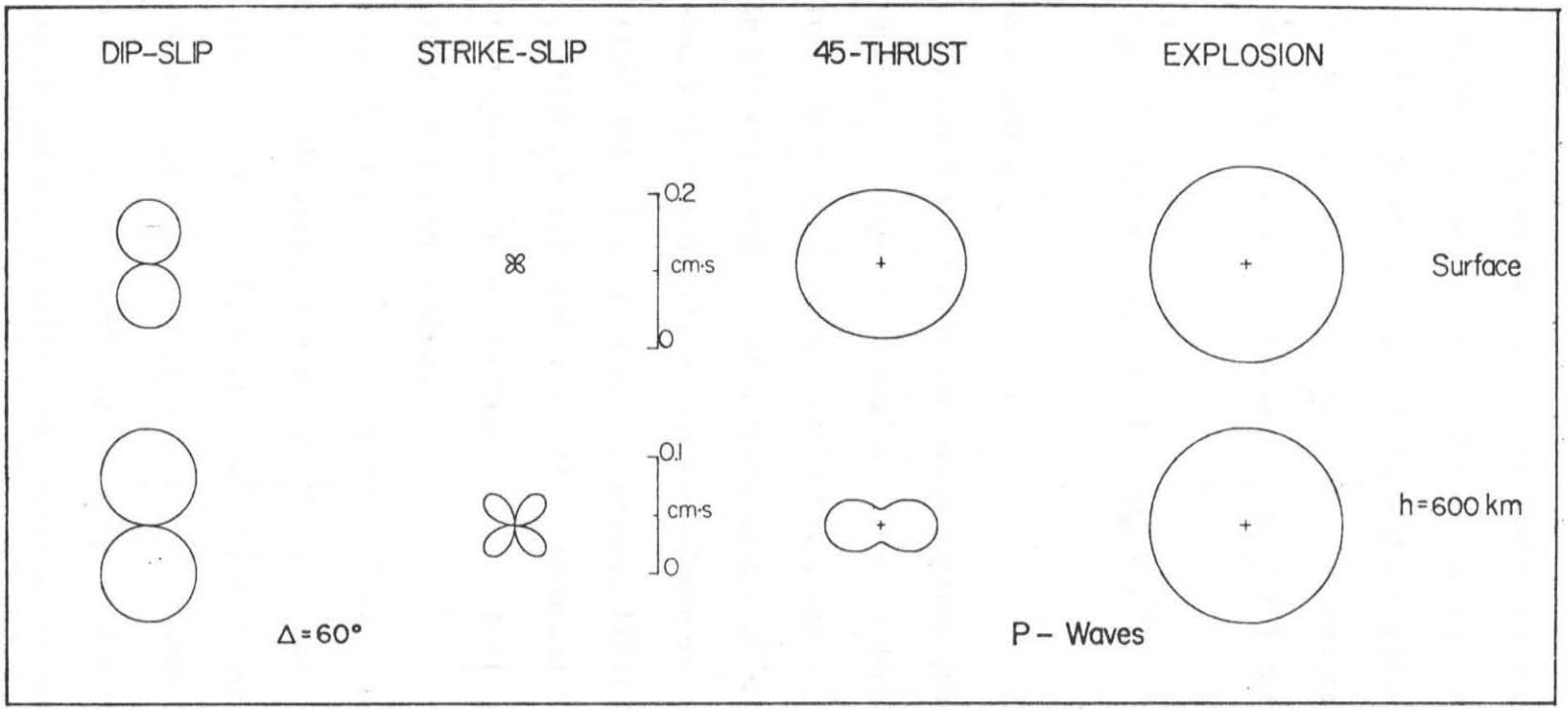

Figure 2.3. Spectral radiation patterns of P waves for both a surface event and a deep earthquake are compared for various source geometries. The dip-slip and strike-slip faults are both vertical, and the pure thrust dips at 45°. The station distance is Δ=60°, and a common step-function moment of 10^{27} dynes-cm is assumed.

a is the earth's radius, ρ_h, v_h and i_h are the density, velocity and take-off angle at the hypocenter, i_o is the incidence angle at the station, M is the moment time function of the source; $\tau = \int ds/v$ is the travel-time of the wave to the station, and the factor of 2 is an approximation to the effect of the free surface at the receiver. $R_{\phi,h}$ is the radiation pattern coefficient: $R_{\phi,h} = 1$ for an explosion and

$$R_{\phi,h} = s_R(3 \cos^2 i_h - 1) - q_R \sin 2i_h - p_R \sin^2 i_h \qquad (2.15)$$

for a pure double-couple.

Figure 2.3 compares the P-wave radiation pattern (the Fourier-transform of equation (2.13)) of an explosion, and 3 double-couple sources (vertical dip-slip, vertical strike-slip, and 45° dipping thrust) at both h=0 and h=600 km, at a distance $\Delta = 60^\circ$. A moment of 10^{27} dynes-cm, with step-function time dependence is used. Free surface reflections for the shallow source (Fukao, 1971; Langston and Helmberger, 1975) are not included. Also, equation (2.13) does not include various tunneling and diffraction phenomena, which may become important at very long periods.

The scale in Figure 2.3 is about a factor of two larger for the shallow sources. In all cases, the excitation of P waves by compressional and deviatoric sources is on the same order of magnitude, reflecting the small dependence of $U(\omega)$ on depth. These results for the excitation efficiency of P waves by the various sources are, to this level of approximation, totally independent of frequency. The spectral amplitudes for Rayleigh waves at periods from 240 s to

70 s (from Figure 2.2) are about 50 to 100 times greater than those for the P waves from the shallow source. For the deep sources however, the Rayleigh waves are 50 times bigger at T=240 s, but the P waves are 5 times bigger at T=70 s.

The relative efficiency of an explosion with respect to a double-couple remains about constant (and on the order of 1) with both depth and frequency for P waves, but decays very rapidly with increasing depth and frequency for Rayleigh waves. Thus, in order to resolve a possible isotropic component of the seismic moment tensor, an analysis of the body-wave part of the record is desirable. The body waves can be studied directly by using the initial P waves. However, the normal modes corresponding to P waves have low shear energy, and therefore high Q's. Thus, by waiting until modes with lower Q (higher shear energy) have been attenuated, one can study the high Q 'compressional' modes, which are roughly equivalent to P waves, and are most sensitive to an isotropic source (Dratler et al., 1971). Also, an investigation of surface waves at the longest possible periods (through the use of ultra long period records) is useful.

Figures 2.4 and 2.5 show synthetics starting 7 min after the origin time, and lasting 90 min, at a distance $\Delta = 90^{o}$ for four seismic sources at different depths, computed through summation of spheroidal modes. Fukao and Abe (1971) presented similar synthetics for torsional modes. The geometry of the sources and receiver is summarized in Table 2.1. Figure 2.4 uses the ultra-long period "33" instrument at Pasadena: The response of this seismometer is peaked around 160 s. Figure 2.5 uses the standard WWSSN "15-100" instrument,

Table 2.1

Geometric parameters of the three double-couple sources used in Figures 2.4 and 2.5

Parameter	Symbol	Dip-Slip	Strike-Slip	45-Thrust
Dip angle	δ	90°	90°	45°
Slip angle	λ	90°	0°	90°
Azimuth of station with respect to fault	ϕ	0°	45°	45°
Distance of station	Δ	90°	90°	90°
	p_R	0	1	0
	q_R	-1	0	0
	s_R	0	0	0.5

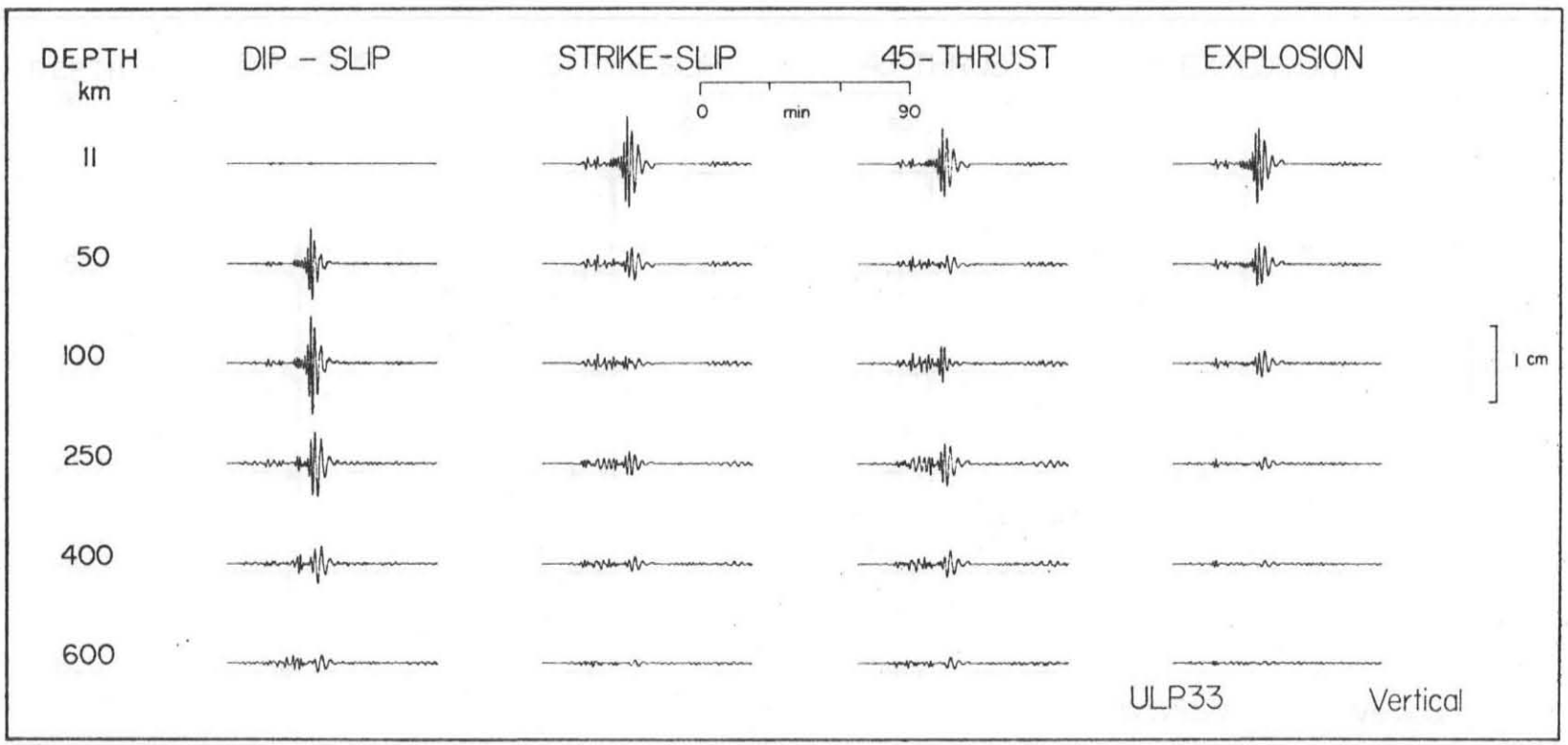

Figure 2.4. Vertical component synthetic seismograms for 4 different source geometries at 6 different depths. All seismograms begin 7 minutes after origin time and last 90 minutes. The station distance is $\Delta=90°$, the step-function moment 10^{27} dyn.cm, and the instrument used, the ULP33 in all cases.

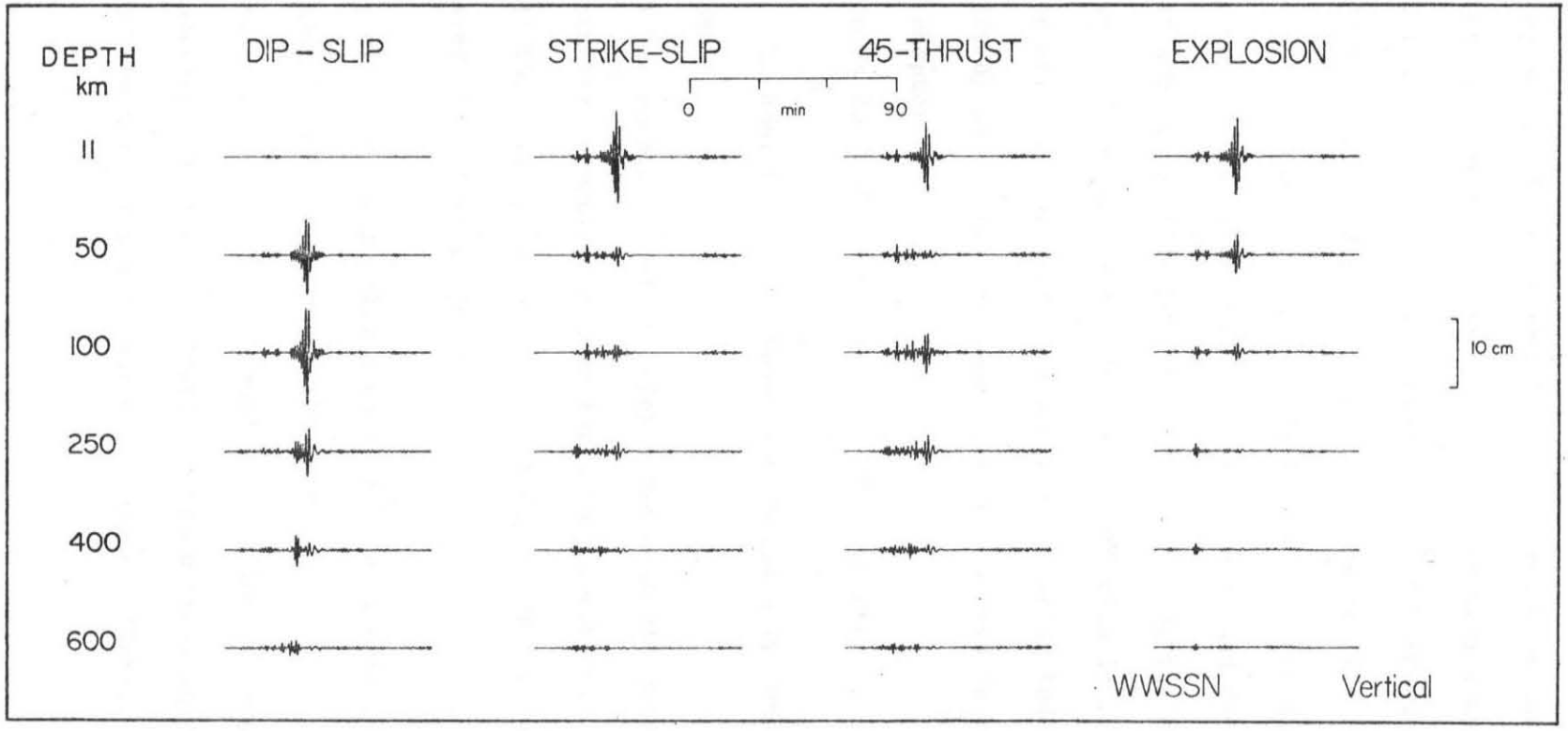

Figure 2.5. Vertical component synthetic seismograms for 4 different source geometries at 6 different depths. All seismograms begin 7 minutes after origin time, and last for 90 minutes. The station distance is Δ=90°, the step-function moment 10^{27} dyn.cm, and the instrument used, the WWSSN 15-100 in all cases.

whose response is peaked around 20 s. The response curves of these instruments are shown on Figure 2.6. The synthetics were obtained by summation of all spheroidal normal modes with frequencies less than 0.0125 Hz; all modes with higher frequencies ($T < 80$ s) were filtered out, to duplicate the conditions of Gilbert and Dziewonski's (1975) study. (The filter had zero phase shift and decayed linearly from unit amplitude at T=120 s to zero at T=80 s; the same low-pass filter is used for all of the data and synthetics in later sections.) The attenuation of the Earth was included by using Anderson and Hart's (1978) model SL2. The same Q model is used in later sections of this chapter.

Figures 2.4 and 2.5 demonstrate three points:

i) The amplitudes of P waves are essentially constant in all cases.

ii) The excitation of Rayleigh waves dies off more rapidly with depth for an explosion than for a double-couple.

iii) The Rayleigh-wave decay with depth for a given source is faster at shorter periods.

Similar, although not totally identical results were obtained for the colatitudinal (SV) component of the record.

Because of the larger isotropic excitation at long periods, we will concentrate in the next Section on an ultra-long period (ULP) record of the Colombian earthquake at Pasadena (PAS).

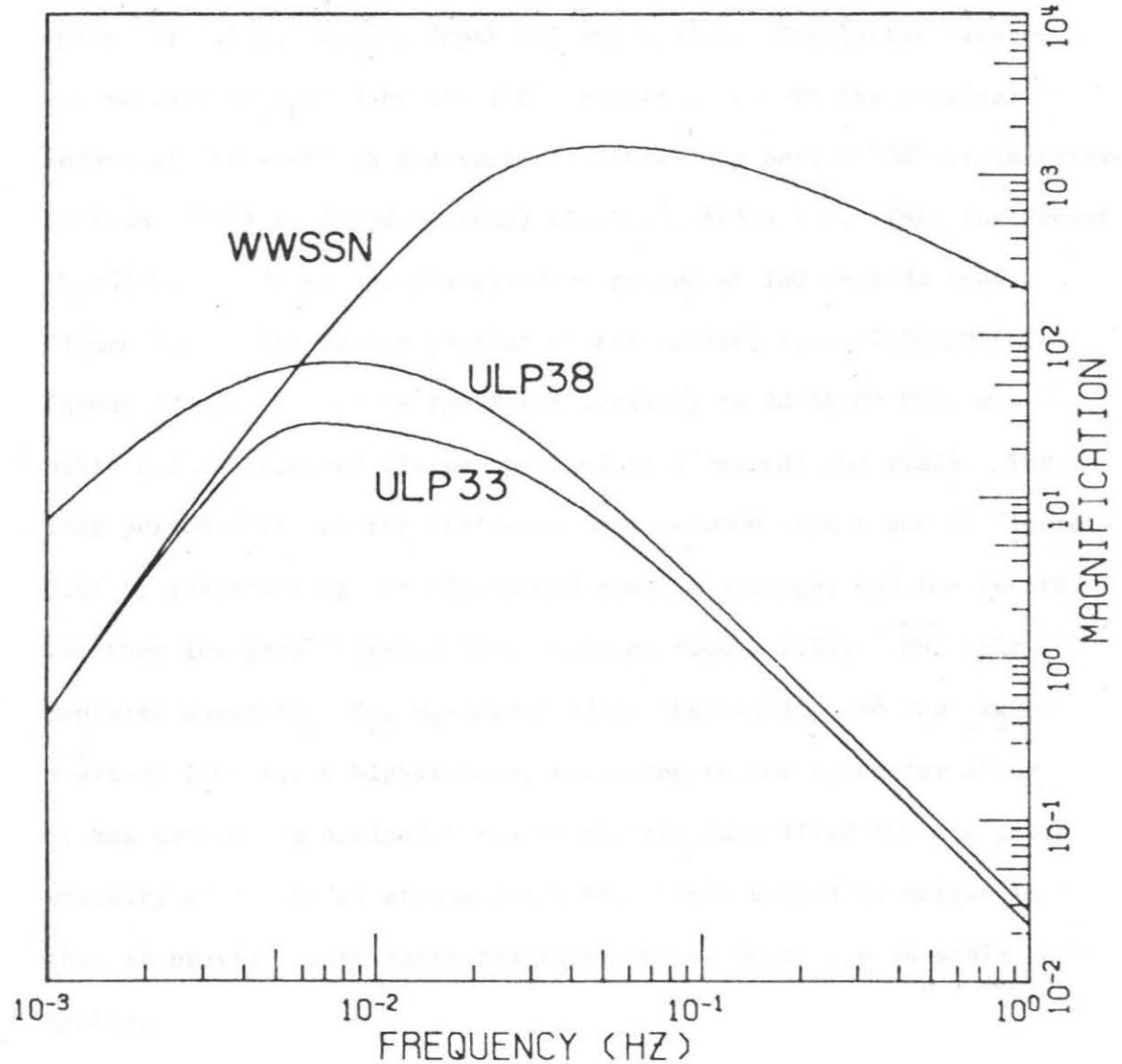

Figure 2.6. Response curves of the WWSSN 15-100, ultra-long period 'ULP33', and ultra-long period 'ULP38' Pasadena instruments.

2.2 Application to the 1970 Colombian Earthquake

The Colombian earthquake of July 31, 1970 is certainly the largest deep event to occur in recent times. Its hypocentral parameters, as determined by the USCGS are: Origin time 17:08:05.4 GMT; epicenter 1.5°S, 72.6°W; depth 651 km; m_b=7.1. The latter figure was revised to m_b=6.5 by the ISC. Figure 2.7 shows the original record of the event on the vertical ultra-long period "38" seismometer (Gilman, 1960) at Pasadena (PAS) (Δ=55.1°, ϕ=314.1°). This instrument (T_0=35 s; T_g=270 s) has its response peaked at 160 seconds (see Figure 2.6). The usable portion of the record, from 17:00:00 GMT (about 17 minutes before the first arrival) to 20:56:00 GMT, was digitized at 2-second (later smoothed to 5-second) intervals. The long period drift of the instrument was removed (top trace of Figure 2.9) by substracting the 600-second running average, and the record was then low-pass filtered (top trace of Figure 2.10). Multiple Rayleigh waves (R_1, R_2, R_3) are readily observable, and the $_1R_2$ overtone (the first higher mode, returning to the epicenter after it has passed the antipode) can be clearly identified (by its group velocity of 5.8 km/s) around 18:45 GMT. This record is unique in that it provides both early and later phases which are on-scale and usable.

The focal mechanism of the 1970 Colombian deep shock was initially studied by Mendiguren (1972) whose first-motion solution requires normal faulting. His solution was later used by Furumoto and Fukao (1976) to investigate the seismic moment of the earthquake through the use of synthetic surface waves. They obtained a value of

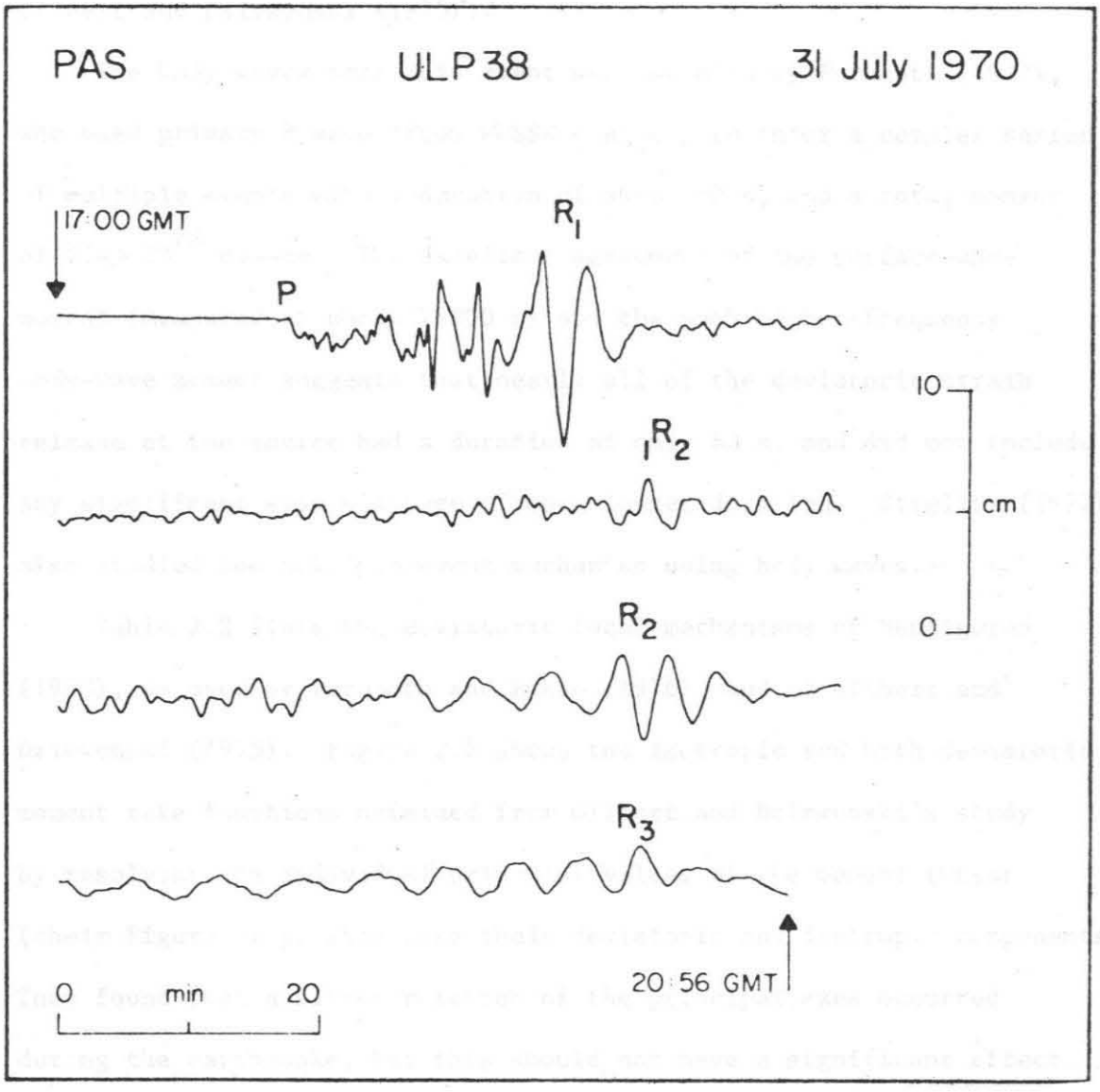

Figure 2.7. Original ultra-long period record of the Colombian earthquake at Pasadena. For clarity, the record has been plotted on four lines.

$M_o = 2.1 \times 10^{28}$ dyn-cm, and observed a slight rotation of the surface-wave radiation pattern with respect to the focal mechanism from the body-wave first motions. This rotation had also been reported by Gilbert and Dziewonski (1975).

The body waves from this event were studied by Furumoto (1977), who used primary P waves from WWSSN stations to infer a complex series of multiple events with a duration of about 60 s, and a total moment of 2.4×10^{28} dyn-cm. The excellent agreement of the surface-wave moment (measured at about T=200 s) and the much higher-frequency body-wave moment suggests that nearly all of the deviatoric strain release at the source had a duration of only 60 s, and did not include any significant slow slippage of much longer duration. Strelitz (1977) also studied the multiple event mechanism using body waves.

Table 2.2 lists the deviatoric focal mechanisms of Mendiguren (1973), as used by Furumoto and Fukao (1976), and of Gilbert and Dziewonski (1975). Figure 2.8 shows the isotropic and both deviatoric moment rate functions obtained from Gilbert and Dziewonski's study by resolving the individual principal values of the moment tensor (their Figure 27 p. 265) into their deviatoric and isotropic components. They found that a slight rotation of the principal axes occurred during the earthquake, but this should not have a significant effect at very long periods. In the present study, this rotation was neglected and the axes were treated as fixed in their average position.

It is possible to decompose the principal values of the moment tensor into an isotropic source and two mutually perpendicular

Table 2.2

Parameters of the deviatoric focal sources used in the synthetics

Source	Strike ϕ deg	Dip δ deg	Slip λ deg	Tensional axes ϕ , δ deg	Compressional axes ϕ , δ deg	Moment 10^{28}dyn-cm	Source function
Furumuto and Fukao (1976) / Mendiguren (1973)	148	58	-99	244,103	32,165	2.1	Step
Gilbert and Dziewonski (1975):							
D_1 : 1st deviatoric source	167	68	-87	255,112	82,157	See Figure 2.8	
D_2 : 2nd deviatoric source	298	76	-19	346, 93	255,112	See Figure 2.8	

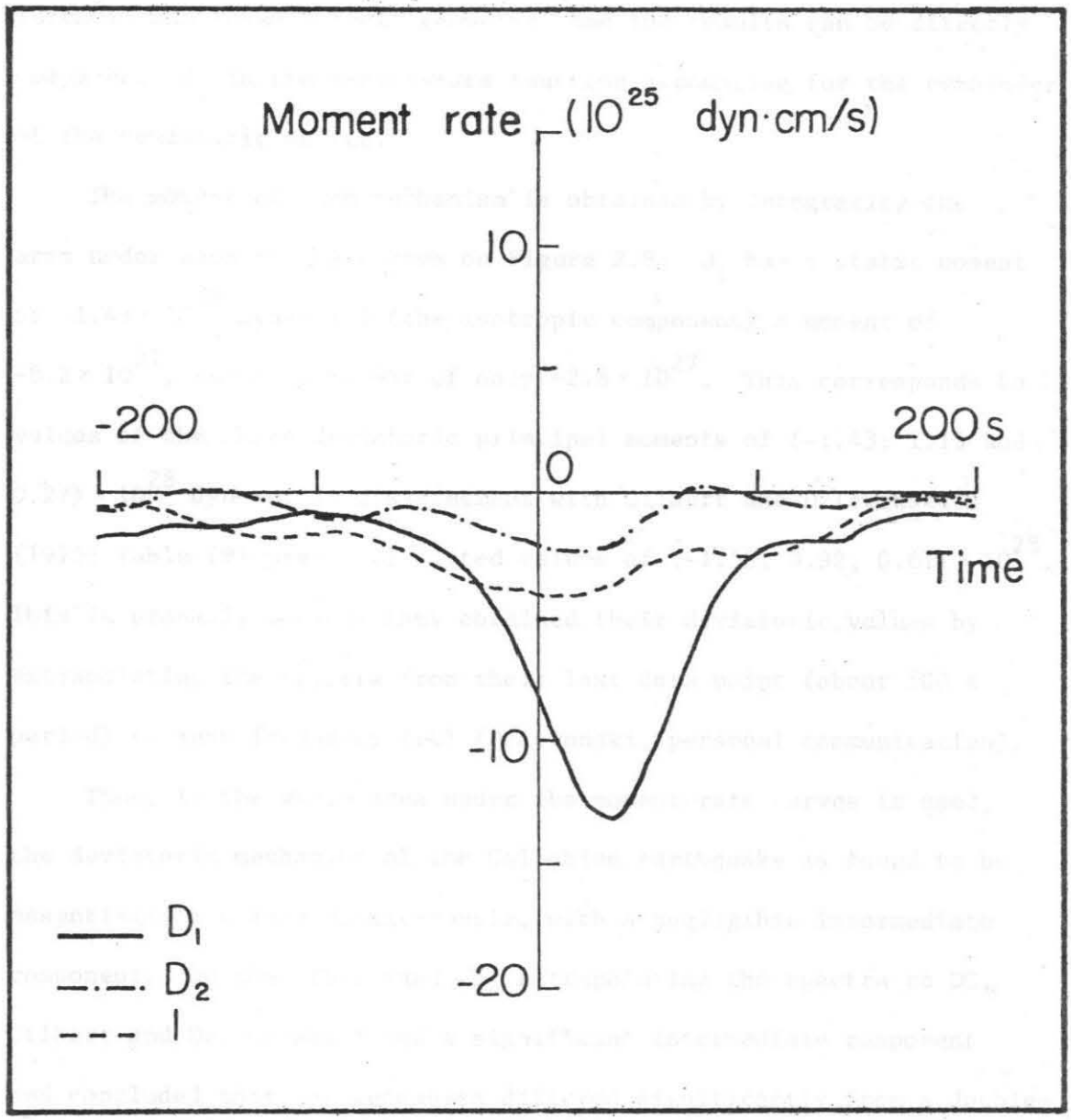

Figure 2.8. Moment rate function of both deviatoric (D_1,D_2) and of the isotropic (I) moment rate tensor components obtained by Gilbert and Dziewonski. Details of the geometry are listed in Table 2.2. D_1 is essentially equivalent to the double-couple sources of Mendiguren and Furumoto and Fukao.

double-couples, as shown on Figure 2.8; this way, the double-couple moment-rate function D_1 is essentially that for Mendiguren's and Furumoto and Fukao's fault geometry, and the results can be directly compared. D_2 is the moment-rate function accounting for the remainder of the deviatoric source.

The moment of each mechanism is obtained by integrating the area under each of the curves on Figure 2.8: D_1 has a static moment of -1.43×10^{28} dyn-cm; I (the isotropic component) a moment of -8.2×10^{27}; and D_2 a moment of only -2.8×10^{27}. This corresponds to values of the three deviatoric principal moments of (-1.43, 1.15 and 0.27) $\times 10^{28}$ dyn-cm, in disagreement with Gilbert and Dziewonski's (1975; Table (9) page 266) listed values of (-1.53, 0.92, 0.61) $\times 10^{28}$. This is probably because they obtained their deviatoric values by extrapolating the spectra from their last data point (about 500 s period) to zero frequency (DC) (Dziewonski, personal communication).

Thus, if the whole area under the moment-rate curves is used, the deviatoric mechanism of the Colombian earthquake is found to be essentially a unique double-couple, with a negligible intermediate component. On the other hand, by extrapolating the spectra to DC, Gilbert and Dziewonski found a significant intermediate component and concluded that the mechanism differed significantly from a double-couple.

Synthetic seismograms were then computed for the various source models, using the mode summation technique. Figure 2.9 shows a comparison of the observed trace (detrended by subtracting the running average) (a) with these synthetics. The synthetic for Furumoto and

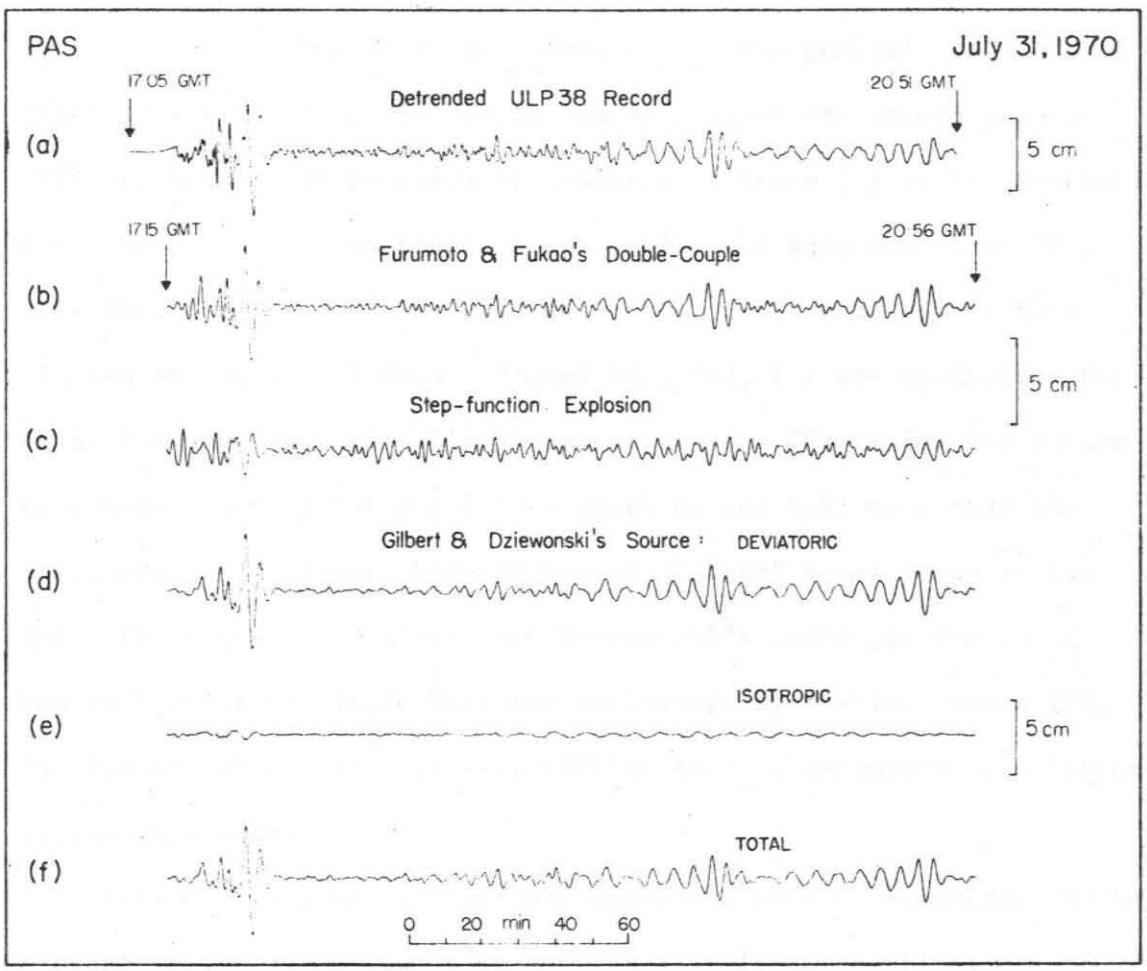

Figure 2.9. (a) Detrended trace of the ULP38 record at Pasadena. (b) Synthetic for Furumoto and Fukao's source, using a step-function moment of 2.1×10^{28} dyn.cm. (c) Synthetic for an isotropic step-function source of the same moment as (b), drawn on the same scale. (d) Synthetic for Gilbert and Dziewonski's deviatoric source. (e)Synthetic for Gilbert and Dziewonski's isotropic source. (f) Synthetic for Gilbert and Dziewonski's entire source. (d), (e) and (f) are on the same scale.

Fukao's (1976) step function double-couple (with a moment of 2.1×10^{28} dyn-cm) -shown in trace (b)- is in excellent agreement with the data. In addition to the agreement of the wave shapes and dispersion of the fundamental Rayleigh waves R_1, R_2, R_3, and of the second arrival of the first Rayleigh overtone ${}_1R_2$, the general amplitude of the high frequency content of the later part of the record agrees with the data. For purposes of comparison, trace (c) is the synthetic for a step-function isotropic source, with the same moment as (b). Note that the P - to - Rayleigh ratio for (c) is much higher than allowed by the actual data. Traces (d), (e), (f) are synthetics for Gilbert and Dziewonski's (1975) source. Trace (d) is for the entire deviatoric part of their solution (both D_1 and D_2); note that the amplitude of the later, high-frequency, "noise" seems somewhat too low. Trace (e), for Gilbert and Dziewonski's isotropic source I, has much lower amplitude than the deviatoric synthetic. Trace (f), the sum of (d) and (e), is very similar to (d), because of the latter's larger amplitude.

The influence of an isotropic component on the seismogram can be systematically investigated by constructing linear combinations of synthetics (b) and (c) (and (d) and (e)), with various ratios between isotropic and deviatoric moments. The results are shown in Figures 2.10 (Furumoto and Fukao's source) and 2.11 (Gilbert and Dziewonski's source). In each of these figures, the upper trace is the original data, low-pass filtered at 80 seconds, since Gilbert and Dziewonski (1975; p. 216) have indicated that their solution loses significance at higher frequencies; however this filter hardly changes the

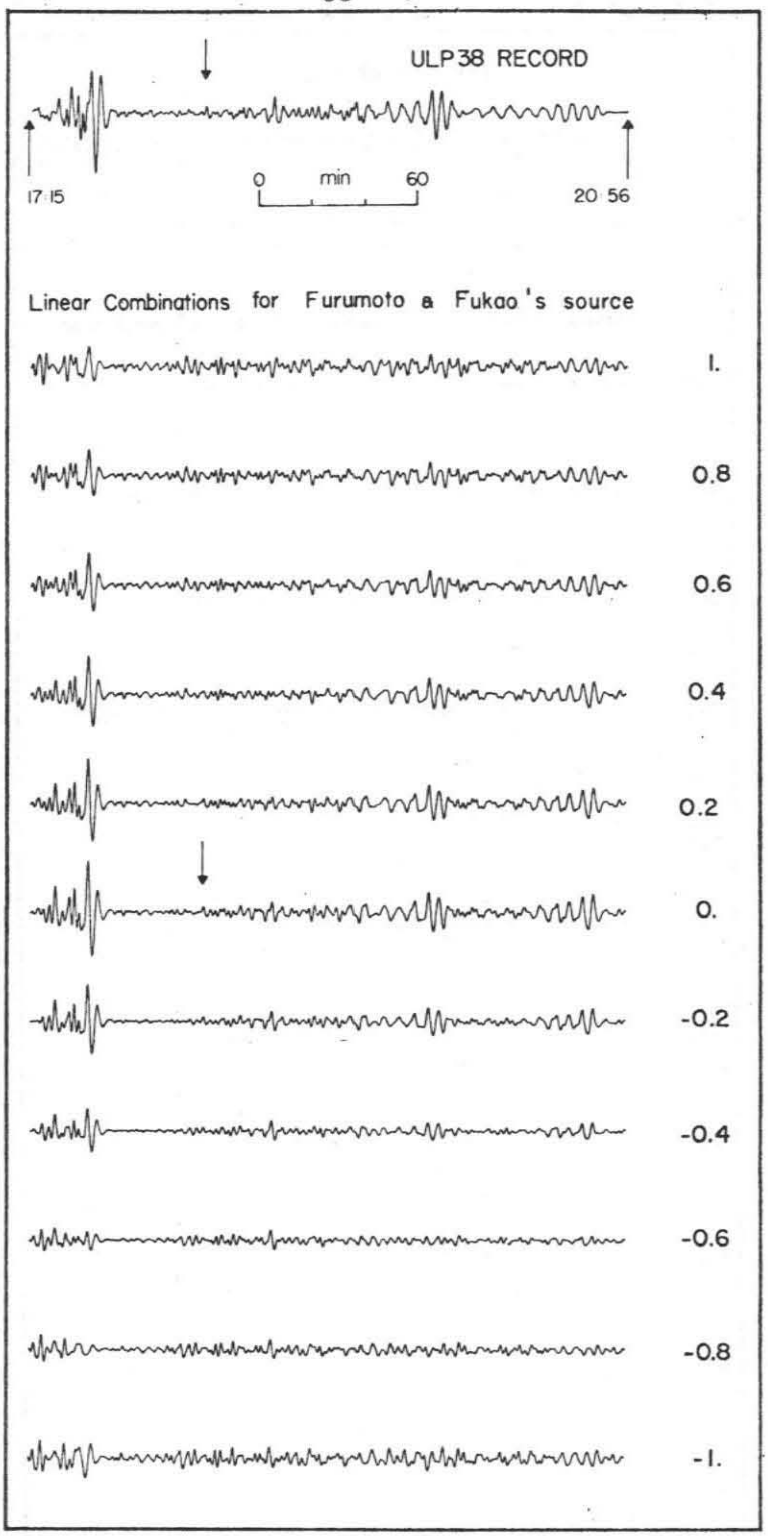

Figure 2.10. Top: Original trace at PAS, filtered at $T \geq 80$ s. Bottom : Synthetics for seismic sources ranging from pure implosion (+1) to pure explosion (-1), obtained by linearly combining (b) and (c) on Figure 2.9. The number at right is F (see text). The arrow points to the phase $_2R_2$. The scale is common to all 11 traces, and the total moment is kept a constant.

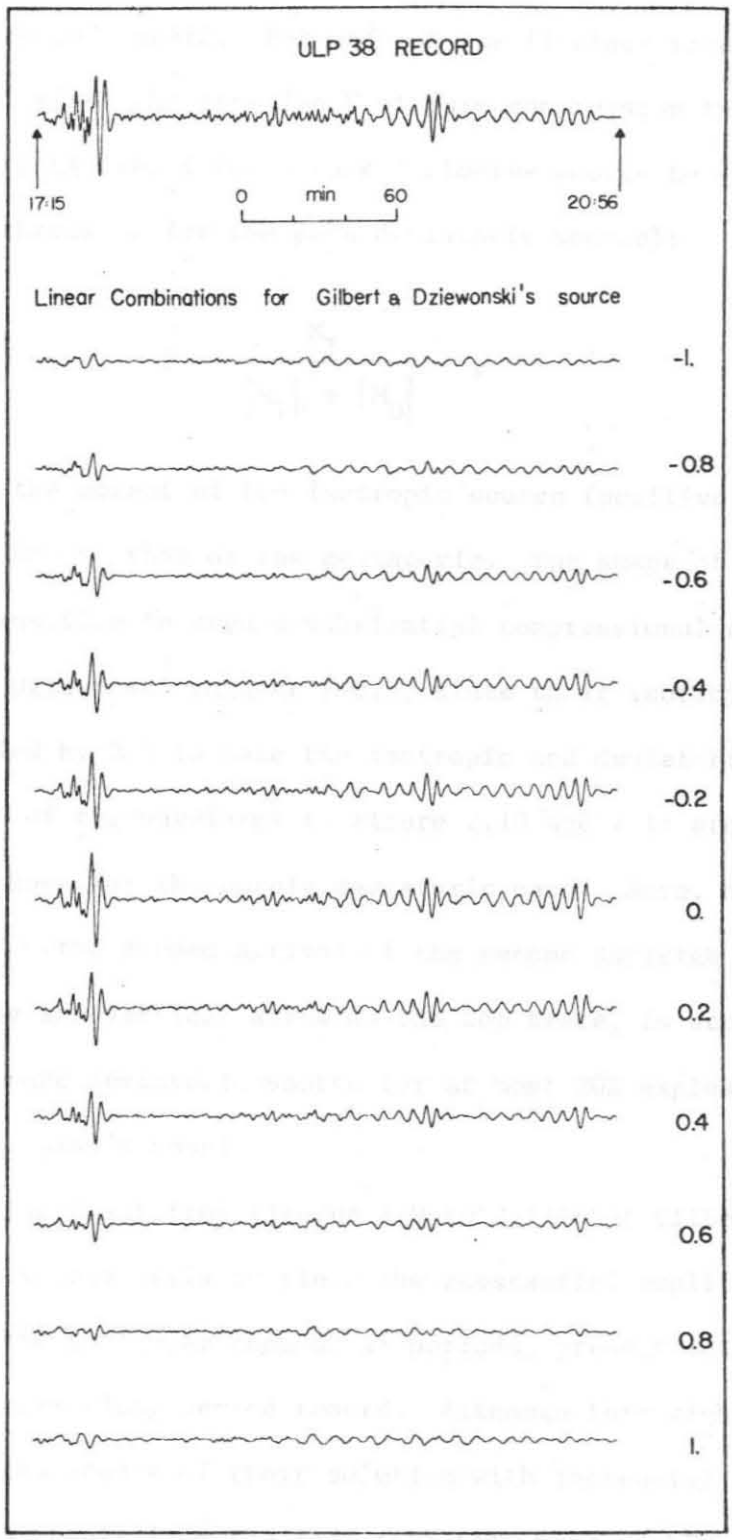

Figure 2.11. Top: Original trace at PAS, filtered at T > 80 s. Bottom : Synthetics for seismic sources ranging from pure explosion (-1) to pure implosion (+1), obtained by linearly combining (d) and (e) on Figure 2.9. The number at right is the fraction F (see text). The scale is common to all 11 traces, and the total moment is kept a constant.

ultra-long period record. For each of the 11 other traces, the number at the right gives the fraction F of pure compression included in the source (ranging from 1 for a pure implosive source to -1 for a pure explosion, through 0 for the pure deviatoric source):

$$F = \frac{M_I}{|M_I| + |M_D|} \quad , \tag{2.16}$$

where M_I is the moment of the isotropic source (positive for an implosion), and M_D that of the deviatoric. The shape of the signals is very insensitive to even a substantial compressional component. Gilbert and Dziewonski suggest F=0.3, since their isotropic source was multiplied by 3.3 to make the isotropic and deviatoric moments equal. Most of the waveforms in Figure 2.10 and 2.11 are very similar to those for the purely deviatoric case. Note, however, that the phase ${}_2R_2$ (the second arrival of the second Rayleigh wave overtone), identified by the vertical arrow on the top trace, is accurately fit only by the pure deviatoric source (or at most 20% explosion), using Furumoto and Fukao's model.

It is also clear from Figures 2.9 to 2.11 that Gilbert and Dziewonski's source fails to yield the substantial amplitudes at the shortest (although longer than 80 s) periods, present in the first half of the ultra-long period reocrd. Although this might reflect a loss of significance of their solution with increasing frequency, it might also result from the fact that they were unable to use the first one or two hours of data (generally off-scale on most WWSSN instruments). Since the omission of the first hour of data attenuates

the high-frequency part of the spectrum, a correction for Q is required. Gilbert and Dziewonski used the Q model MM8 (Anderson et al. 1965), which was designed to fit the Q's of the fundamental torsional and spheroidal modes, but not overtone data. Any departure of the actual Q from this model would have a strong effect on the higher frequency content of the spectrum, especially for overtones such as the ${}_1R_2$ and ${}_2R_2$ phases.

The theoretical inadequacy of Rayleigh waves to resolve an isotropic component of the moment tensor is further confirmed by a systematic cross-correlation of the observed trace (Figure 2.9a) with linear combinations of traces (b,c) (or (d,e)), windowed between 17:27:00 and 17:48:20 (R_1) and between 19:20:00 and 20:02:40 (R_2). The results are shown in Figure 2.12.

As we discussed above, the isotropic source does not excite Rayleigh waves efficiently; if the isotropic source were to be resolved by use of a single record, the P waves should be used. A visual comparison of the synthetics suggests that there is very little change in the body-wave traces for $-0.4 \leq F \leq 0.4$. Therefore, it seems very unlikely that an isotropic source of the size ($F = 0.3$) given by Gilbert and Dziewonski could actually be resolved from the data at a single station. Note also that, in general, the synthetics in Figure 2.11 (Gilbert and Dziewonski's sources) seem significantly lacking in high frequencies, while the frequency content of the synthetics calculated using Furumoto and Fukao's step function source seem much better in this regard.

These results, strongly suggesting that an isotropic component

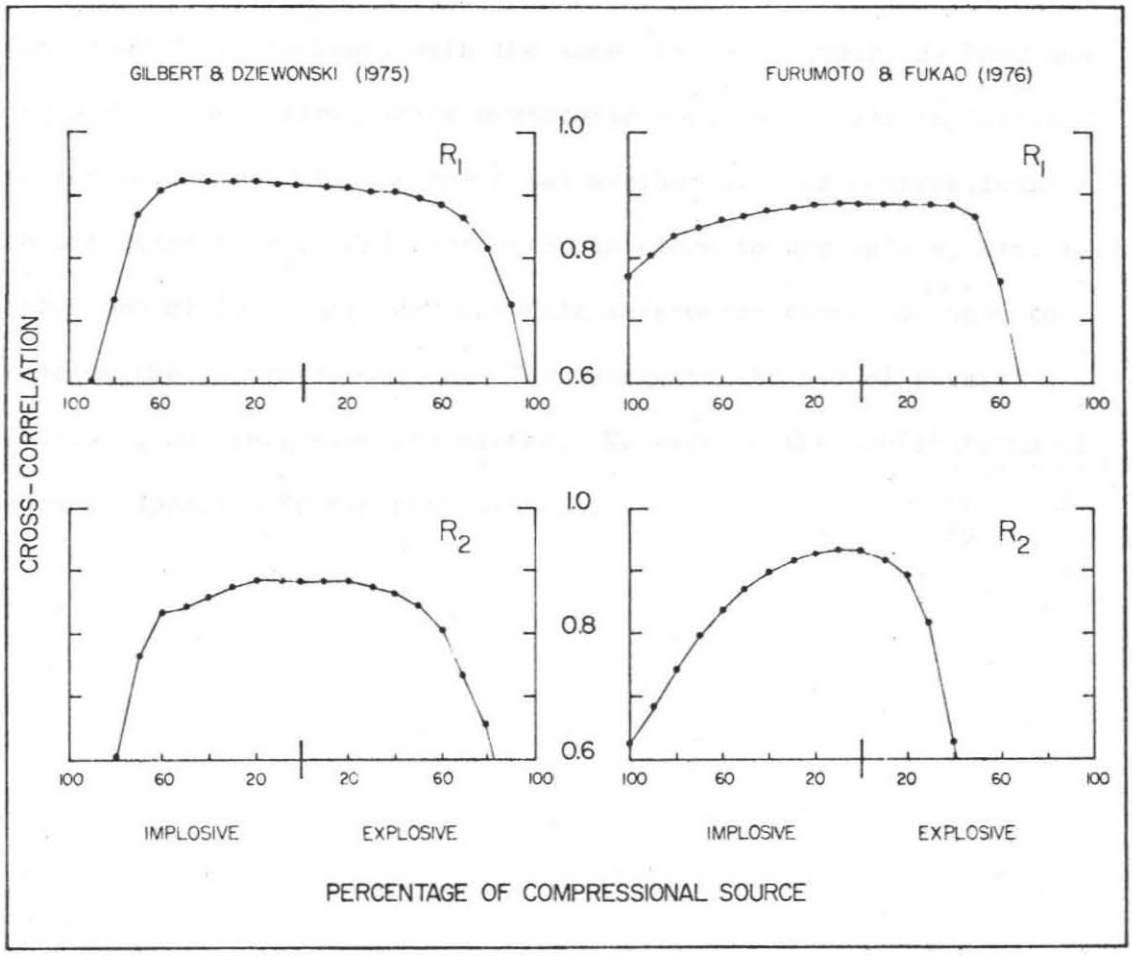

Figure 2.12. Variation of the cross-correlation between observed signal and synthetic, as a function of the amount of compressional source allowed in the synthetic. The traces on the left are for Gilbert and Dziewonski's model, the ones on the right for Furumoto and Fukao's. The windows R_1 and R_2 are described in the text. Values of the cross-correlation lower than 0.6 are not plotted.

cannot be resolved from a single high-quality record, are in agreement with the suggestion by Gilbert and Dziewonski (1975), that a stacking and inversion procedure should be used to search for the isotropic source. Figure 2.13 shows a synthetic obtained for a standard long-period WWSSN instrument, with the same station geometry as PAS, and for Gilbert and Dziewonski's deviatoric sources (a) and implosive source (b). Trace (c) is the total synthetic. The compressional contribution to the WWSSN synthetic is close to negligible, especially after one or two hours, and a single seismogram cannot be used to resolve the isotropic source. This suggests the use of several stations, and inversion procedures. We examine the implications of such an approach in the next section.

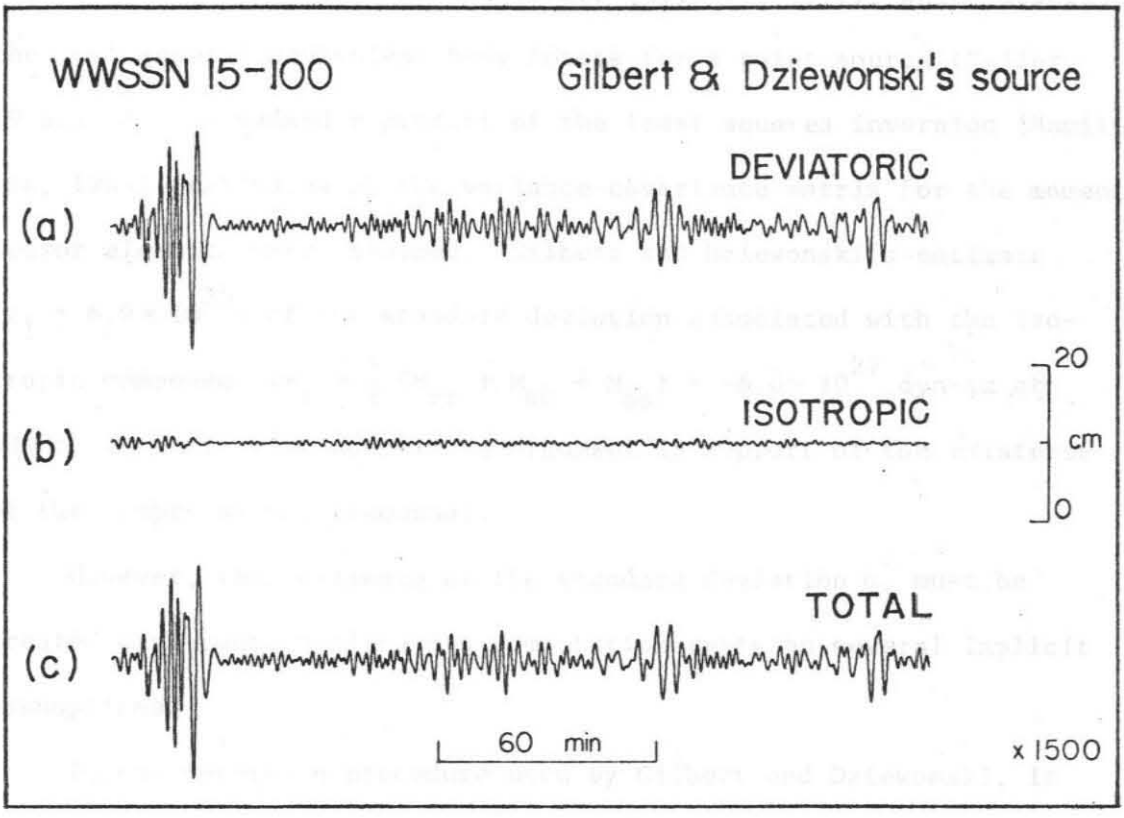

Figure 2.13. Synthetic seismograms obtained for Gilbert and Dziewonski's source, assuming a WWSSN instrument. (a) Deviatoric sources D_1 and D_2 only. (b) Isotropic source (I) only. (c) Full source. This type of record was used in Gilbert and Dziewonski's inversion. The geometry of the station is that of Pasadena.

2.3 Problems Associated with Least-Squares Inversion

2.3.1 Outline

The source mechanism determined by Gilbert and Dziewonski (1975) for the Colombian earthquake was obtained through a least-squares inversion for the source moment tensor (Gilbert, 1970), which describes the most general equivalent body forces for a point source (Geller, 1976). As a standard byproduct of the least squares inversion (Hamilton, 1964), estimates of the variance-covariance matrix for the moment tensor elements were obtained. Gilbert and Dziewonski's estimate ($\sigma_I = 6.9 \times 10^{26}$) of the standard deviation associated with the isotropic component ($M_I = \frac{1}{3}(M_{rr} + M_{\theta\theta} + M_{\phi\phi}) = -6.0 \times 10^{27}$ dyn-cm at 400 s) is their most compelling argument in support of the existence of the compressional precursor.

However, this estimate of the standard deviation σ_I must be treated with caution since its computation rests on several implicit assumptions.

In the inversion procedure used by Gilbert and Dziewonski, it is tacitly understood that the Earth model is known exactly, and errors in it are ignored. It is well known that under such circumstances, estimates of variances can be unrealistically low: a classic example is the case of earthquakes in central California, which presumably occurred on the San Andreas Fault, but were consistently located on a plane 1 km to the west of the fault. This error occurred because the flat-layered model used to locate earthquakes did not reflect the actual, laterally heterogeneous, earth structure (Healy and Peake, 1975). Another well-known case is the way that measurements

of fundamental physical constants, such as the speed of light, or Avogadro's number, have frequently changed by several standard deviations over previous measurements, as systematic biases were eliminated (Particle Data Group, 1971; 1976).

In the present case, the following are possible causes of systematic errors in the moment tensor inversion:

(i) Most gross earth models are in reasonably good agreement at long periods. However, none of these models fit the observed great-circle group velocities very well, suggesting that further improvement may be needed. Also, the effects of lateral heterogeneity are not included, despite significant fluctuation of phases velocities along great-circles (Toksöz and Anderson, 1966; Kanamori, 1970; Okal, 1977).

(ii) The observed spectral data must be corrected for the effects of Q. Any errors in the Q model, which, especially for overtones, is very poorly constrained, probably cause systematic errors in the resulting moment tensor.

(iii) Although there exist very accurate calibration procedures using random telegraph signals (e.g. Moore and Farrell, 1970), the WWSSN calibration is performed by exciting the instrument with a step-function. This causes large uncertainties in the calibration at long periods, where the instrument response is small and decays as T^{-3}. Systematic errors at long periods could also be caused by a poor knowledge of the phase response.

A comparison of individual values reported for the moment of the Colombian earthquake is made in Table 2.3. The existing scatter

Table 2.3

Moment Values for the Colombian Earthquake

Reference	Moment (dyn-cm)
Mendiguren (1972)	11.6×10^{27}
Furumoto and Fukao (1976)	2.1×10^{28}
Furumoto (1977)	2.4×10^{28}
Gilbert and Dziewonski (1975)*	15.3×10^{27}

*Moment value for the main deviatoric component D_1, essentially on the same plane as Mendiguren's source.

($(1.80 \pm 0.56) \times 10^{28}$ dyn-cm) in these values, obtained through different, although careful, studies of WWSSN data, suggests that the above-listed causes of error may indeed strongly affect the results of the least-squares inversion performed by Gilbert and Dziewonski (1975).

Finally, Gilbert and Dziewonski neglected the covariances between individual moment components in computing the standard deviation associated with the isotropic component M_I. We will show that these non-zero terms have a significant contribution.

In the following paragraph, we carry out a numerical experiment, investigating in detail the various causes of systematic error.

2.3.2 Numerical Experiment

In this section, we use Gilbert and Dziewonski's method to invert some fictitious "data" obtained by calculating theoretical spectra, which we allow to be perturbed, relative to the model used in the inversion, in order to study the possible effects of such unknown parameters as lateral heterogeneity or uncertain instrument response.

We use the matched filter technique of Gilbert and Buland (1976), more elegant than, but essentially equivalent to, the one used by Gilbert and Dziewonski. Gilbert and Buland give a general scheme for inverting to find the moment tensor as a function of frequency, by considering the excitation of the earth's normal modes. Inversion methods for moment tensor determination from body waves have also been developed by Stump (1976) and Strelitz (1978); methods for surface waves have been given by Mendiguren (1977) and Aki and Patton

(1977).

The procedure outlined by Gilbert and Buland works as follows: assuming we observe the spectrum $\vec{U}(\omega_j)$ at several (say N_s) stations, we can write the spectrum as:

$$\vec{U}(\omega_j) = H(\omega_j)\,\vec{f}(\omega_j), \tag{2.17}$$

where $\vec{U}$ is a (complex) N_s-element column vector, H is a $N_s \times 6$ (complex) matrix describing the earth's transfer function (assumed to be known exactly in the inversion), and $\vec{f}^T = (M_{rr}, M_{\theta\theta}, M_{\phi\phi}, M_{r\theta}, M_{r\phi}, M_{\theta\phi})$ is the unknown moment-rate tensor. For greater stability we assume that $\vec{f}$ is constant within a frequency band of K distinct frequencies, and get a generalized version of equation (2.17),

$$\vec{U} = H\vec{f}, \tag{2.18}$$

which we solve by standard least squares techniques:

$$\vec{f} = (H^T H)^{-1} H^T \vec{U}. \tag{2.19}$$

In practice, Gilbert and Buland break up $\vec{f}$, $\vec{U}$ and H into their real and imaginary parts and solve for each separately (Gilbert, 1977; personal communication). In that case, $\vec{f}$ has 12 elements, $\vec{U}$ has $2KN_s$, and H is a $2KN_s \times 12$ matrix.

From standard least-squares theory, the variance-covariance matrix is given by:

$$V = (H^T H)^{-1} \sigma^2, \tag{2.20}$$

where σ^2 is the variance of an individual observation. Usually σ^2 is unknown, and it is standard practice, which was followed by Gilbert and Dziewonski, to estimate σ^2 from the residuals. One defines

$$\vec{R} = \vec{U} - H\vec{f} \tag{2.21}$$

and then

$$\sigma^2 = \frac{\vec{R}^T \vec{R}}{2K N_s - 12} \tag{2.22}$$

is an unbiased estimate of the variance, which can be used in (2.20).

Our numerical experiment is carried out in the following way: From an assumed moment tensor $\vec{f}_o$, taken as identical to Mendiguren's solution (see Table 2.3), we compute an observed spectrum $\vec{U}$, allowing for some perturbation, say H_p, of the Earth model H. We then invert $\vec{U}$ assuming an unperturbed model, the result being

$$\vec{f} = (H^T H)^{-1} H^T H_p \vec{f}_o \ . \tag{2.23}$$

The difference between $\vec{f}$ and $\vec{f}_o$ represents the effect of neglecting the departure of the actual Earth (H_p) from the model used in the inversion (H). The details of the computation of the elements of the matrix H can be found in Okal and Geller (1978a), and will not be repeated.

We use a fictitious network of 10 stations, evenly spaced in azimuth from 0^o to 360^o, at a common epicentral distance of 60^o from a deep (h = 650 km) event. Both vertical and azimuthal components are used in the spectrum $\vec{U}$. It was found (Okal and Geller 1978a) that the additional information in the azimuthal component reduces the

error on the corresponding components ($M_{\theta\theta}$ and $M_{\phi\phi}$) of M, without affecting its trace M_I, thereby increasing σ_I^2 with respect to $\sigma^2(M_{\theta\theta})$ or $\sigma^2(M_{\phi\phi})$.

a. Unperturbed Model

As a first step, we investigate the standard deviation, for a perfectly known earth model. Table 2.4 shows the matrix V (see equation (2.20)), for the real components of the moment tensor, sampled around $\omega = 0.023$ (actually for ω = 0.021, 0.022,....., 0.025) rad/s (T = 273 s), with a maximum variance, σ^2_{max}, normalized to 1. All of the covariance terms are zero, except for those relating $M_{\theta\theta}$, $M_{\phi\phi}$ and M_{rr}. These must be included in finding the relative standard variance of the isotropic moment:

$$\sigma_I^2 = \frac{1}{9}\left[\sigma^2(M_{rr}) + \sigma^2(M_{\theta\theta}) + \sigma^2(M_{\phi\phi}) + 2\,\mathrm{cov}(M_{rr}, M_{\theta\theta}) + 2\,\mathrm{cov}(M_{\theta\theta}, M_{\phi\phi}) + 2\,\mathrm{cov}(M_{\phi\phi}, M_{rr})\right]. \tag{2.24}$$

Evaluating this expression for the values in Table 2.4 (with a maximum variance $\sigma^2_{max} = 1$), we get $\sigma_I^2 = 0.597$. If the covariance terms were omitted from (2.24) (as apparently done by Gilbert and Dziewonski), we would get the lower value σ_I^2 (incomplete) = 0.289, which yields a standard deviation about $\sqrt{2}$ times too small. This may partly explain the favorable standard deviation claimed by Gilbert and Dziewonski (1975).

Table 2.4

Variance-Covariance Matrix V at $\omega = 0.023$ rad/s

	M_{rr}	$M_{\theta\theta}$	$M_{\phi\phi}$	$M_{r\theta}$	$M_{r\phi}$	$M_{\theta\phi}$
M_{rr}	0.598	0.505	0.505	0	0	0
$M_{\theta\theta}$	0.505	1.000	0.377	0	0	0
$M_{\phi\phi}$	0.505	0.377	1.000	0	0	0
$M_{r\theta}$	0	0	0	1.000	0	0
$M_{r\phi}$	0	0	0	0	1.000	0
$M_{\theta\phi}$	0	0	0	0	0	1.000

b. Lateral Heterogeneity

In order to investigate the effect of lateral heterogeneity on the inversion procedure, the matrix H was perturbed to allow for a fluctuation of the phase velocities (or equivalently of the modes' frequencies) along the great-circles through the ten sampling stations. As a first order approximation, it can be assumed that the eigenfunctions (or equivalently the excitation coefficients N_0, K_0, K_1, K_2, L_1, L_2) remain unchanged (Geller and Stein, 1978). A maximum variation of 1.5%, corresponding to the reported observed lateral heterogeneity in surface wave phase velocities (see for example Part II of this thesis) was allowed. Overtones were allowed a less pronounced fluctuation, in order to model the disappearance of lateral heterogeneity with depth (Okal, 1977). Several focal mechanisms were studied, and among simple mechanisms, it was found that a 45°-dipping thrust (or normal) fault was most sensitive to the presence of lateral heterogeneity. Results for the mechanism of the 1970 Colombian deep shock as proposed by Mendiguren (1973) ($\delta = 58^{\circ}$; $\lambda = -99^{\circ}$) are shown on Figure 2.14. The real and imaginary parts of the moment rate tensor M, as resulting from the inversion are shown as + symbols in the frequency domain, superimposed on the actual components M_o. The standard deviation estimate (σ_I (incomplete) in the isotropic component) is shown in the third column. Finally, the fourth column shows the time-domain variation of the components of the moment-rate tensor. Although the solution keeps fairly intact the δ-function character of the main components of M, a totally artificial isotropic component is obtained, whose amplitude can reach 40% or more of the

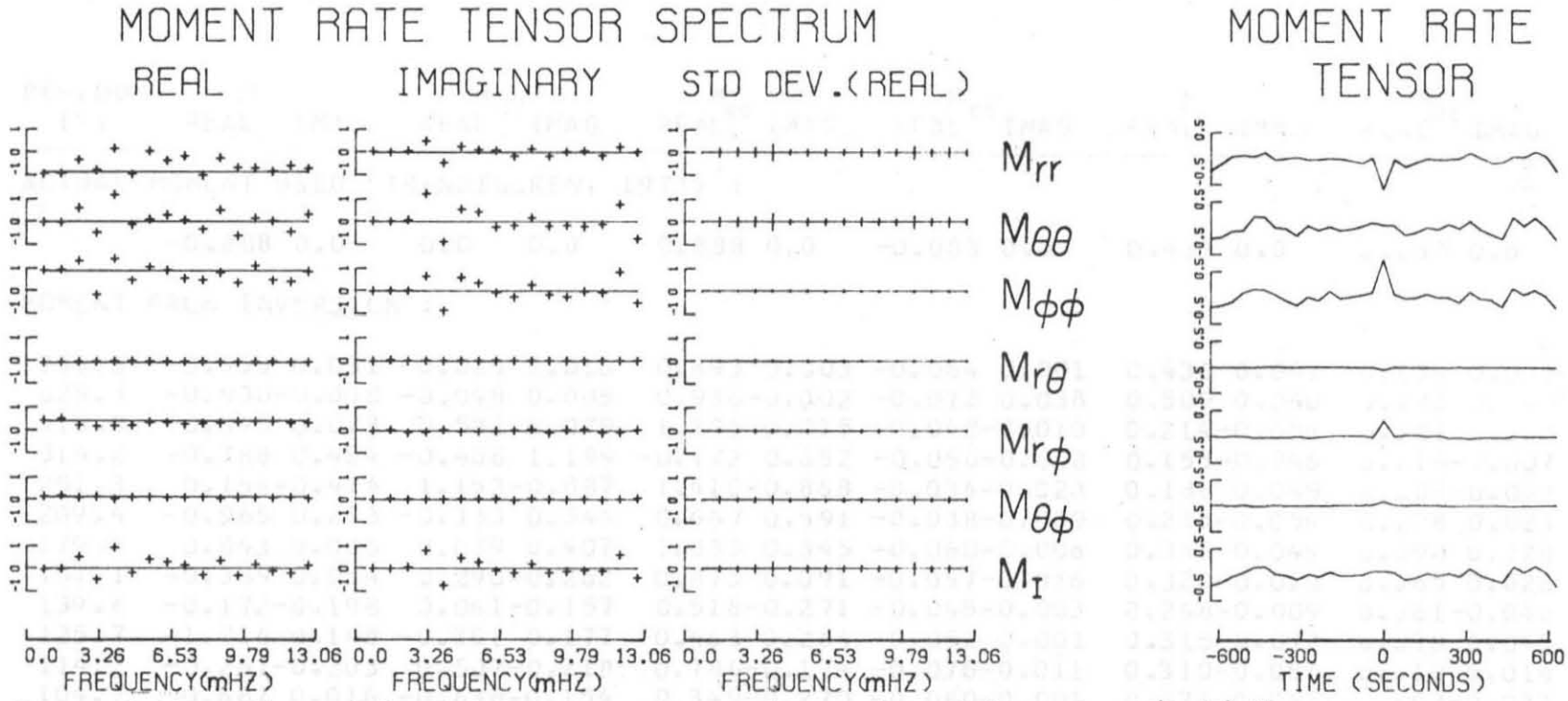

Figure 2.14. Effect of lateral heterogeneity on the results of inversion. (Left) The moment rate spectrum tensor components (+) are compared with the actual components used in the source (full lines). M_I is the isotropic component [(1/3) Tr(M)]. The standard deviations are also shown. (Right) Time-domain variation of the various components.

TABLE 2.5

RESULTS OF INVERSION IN THE PRESENCE OF LATERAL HETEROGENEITY

PERIOD (S)	M_{rr} REAL	M_{rr} IMAG	$M_{\theta\theta}$ REAL	$M_{\theta\theta}$ IMAG	$M_{\phi\phi}$ REAL	$M_{\phi\phi}$ IMAG	$M_{r\theta}$ REAL	$M_{r\theta}$ IMAG	$M_{r\phi}$ REAL	$M_{r\phi}$ IMAG	$M_{\theta\phi}$ REAL	$M_{\theta\phi}$ IMAG
ACTUAL MOMENT USED (MENDIGUREN, 1973) :												
	-0.888	0.0	0.0	0.0	0.888	0.0	-0.083	0.0	0.433	0.0	0.133	0.0
MOMENT FROM INVERSION :												
1256.6	-0.953	0.031	-0.029	0.016	0.893	0.003	-0.084	0.001	0.436	0.003	0.134	0.000
628.3	-0.930	-0.008	-0.048	0.005	0.936	-0.002	-0.072	0.038	0.509	0.040	0.180	0.048
418.9	-0.345	0.073	0.582	0.079	1.295	0.015	-0.048	-0.010	0.214	-0.086	0.081	0.000
314.2	-0.788	0.484	-0.488	1.199	-0.172	0.652	-0.050	-0.008	0.155	-0.046	0.116	-0.007
251.3	0.154	-0.474	1.153	-0.887	1.410	-0.868	-0.034	-0.020	0.186	0.049	0.008	-0.002
209.4	-0.965	0.253	-0.133	0.544	0.467	0.591	-0.038	-0.009	0.215	-0.054	0.108	0.023
179.5	0.043	0.085	0.089	0.407	1.035	0.345	-0.060	-0.006	0.346	-0.045	0.090	0.028
157.1	-0.389	0.054	0.290	-0.262	0.875	-0.091	-0.057	-0.016	0.320	-0.010	0.065	0.026
139.6	-0.172	-0.198	0.061	-0.157	0.518	-0.271	-0.045	-0.003	0.248	-0.009	0.081	-0.040
125.7	-1.016	0.148	-0.351	0.177	0.463	0.264	-0.052	0.001	0.315	0.072	0.098	0.045
114.2	-0.261	-0.203	0.507	-0.218	0.786	-0.174	-0.076	-0.011	0.310	-0.087	0.018	0.014
104.7	-0.687	0.016	-0.638	-0.154	0.349	-0.270	-0.080	-0.001	0.371	0.042	0.102	-0.022
96.7	-0.712	0.033	0.149	-0.240	1.088	-0.021	-0.060	-0.014	0.380	0.047	0.075	-0.004
89.8	-0.848	-0.175	-0.010	-0.124	0.466	-0.087	-0.065	-0.011	0.388	-0.099	0.046	-0.012
83.8	-0.599	0.224	-0.473	0.760	0.378	0.826	-0.070	-0.010	0.307	-0.074	0.089	0.027
78.5	-0.745	0.002	0.315	-0.740	0.828	-0.535	-0.077	-0.008	0.332	0.041	0.037	0.041

TABLE 2.5
(CONTINUED)

ISOTROPIC MOMENT (1/3)*TR(M)

PERIOD (S)	M_I REAL	IMAG	σ_I INCOMPLETE	COMPLETE
1256.6	-0.029	0.017	0.0132	0.0175
628.3	-0.014	-0.002	0.1576	0.1360
418.9	0.510	0.056	0.0987	0.1213
314.2	-0.483	0.778	0.1172	0.1754
251.3	0.905	-0.743	0.1910	0.3091
209.4	-0.210	0.463	0.0819	0.1177
179.5	0.389	0.279	0.0947	0.1544
157.1	0.259	-0.099	0.0847	0.1369
139.6	0.135	-0.209	0.0881	0.1410
125.7	-0.301	0.196	0.1086	0.1420
114.2	0.344	-0.199	0.0909	0.1398
104.7	-0.325	-0.136	0.0939	0.1501
96.7	0.175	-0.076	0.1579	0.2648
89.8	-0.130	-0.129	0.0876	0.1372
83.8	-0.231	0.604	0.1108	0.1589
78.5	0.133	-0.424	0.0768	0.1069

deviatoric moment. Individual values are listed in Table 2.5.

The static value of M_I has no significance since the mode inversion procedure cannot be extended to zero-frequency. In the present experiment, M(0) was arbitrarily set equal to $M(\omega_1)$, ω_1 being the first non-zero sampling frequency, (ω_1 = 0.005 rad/s) (see Table 2.5). A similar approach, used by Gilbert and Dziewonski (Dziewonski, 1977 personal communication) is to extrapolate the value of M around 500 s. In any case, lateral heterogeneity cannot be expected to play a substantial role at very long periods, and the important result from this experiment remains the large artificial isotropic component resulting from the inversion at periods of 300 s or below, in any case much larger than the standard variations obtained by Gilbert and Dziewonski through the incomplete procedure, making use only of the first line in (2.24) (see Table 2.5).

c. Instrument Responses

A similar investigation was made of the effect of deviation from the instruments' standard magnification. The matrix H was kept unperturbed, except for a random fluctuation of ± 20% in the amplitude of the spectra. Figure 2.15 shows that such a perturbation has only a very small influence on the results of the inversion.

d. Uncertainties in Q

Little is known on the values of Q for higher modes and some recent studies (Nakanishi, 1977; Okal, unpublished results) have shown that previous estimates of Q for fundamental Rayleigh-wave might be regionally inaccurate. In order to investigate the effect of such

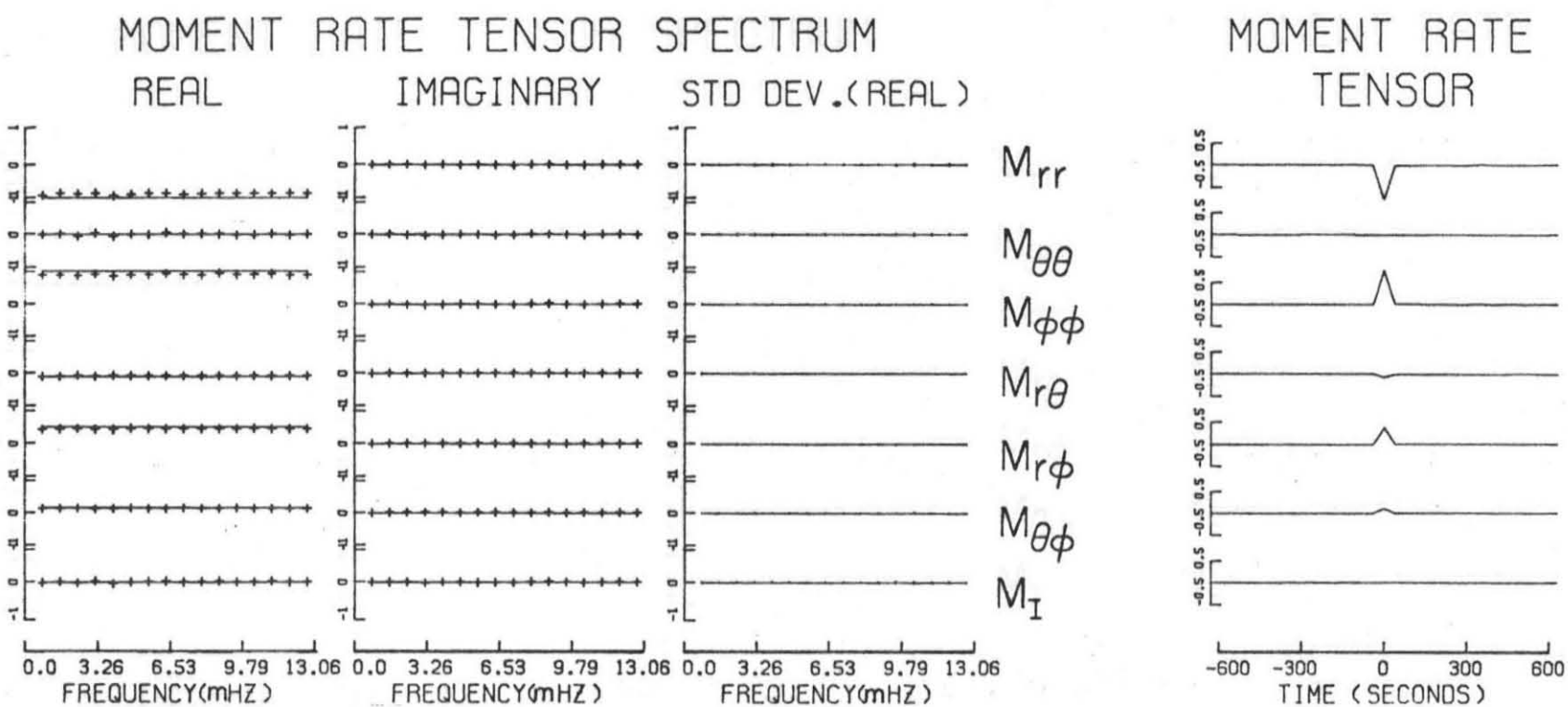

Figure 2.15. Effect of random fluctuation in instruments' responses on the result of inversion. Details as in Figure 2.14.

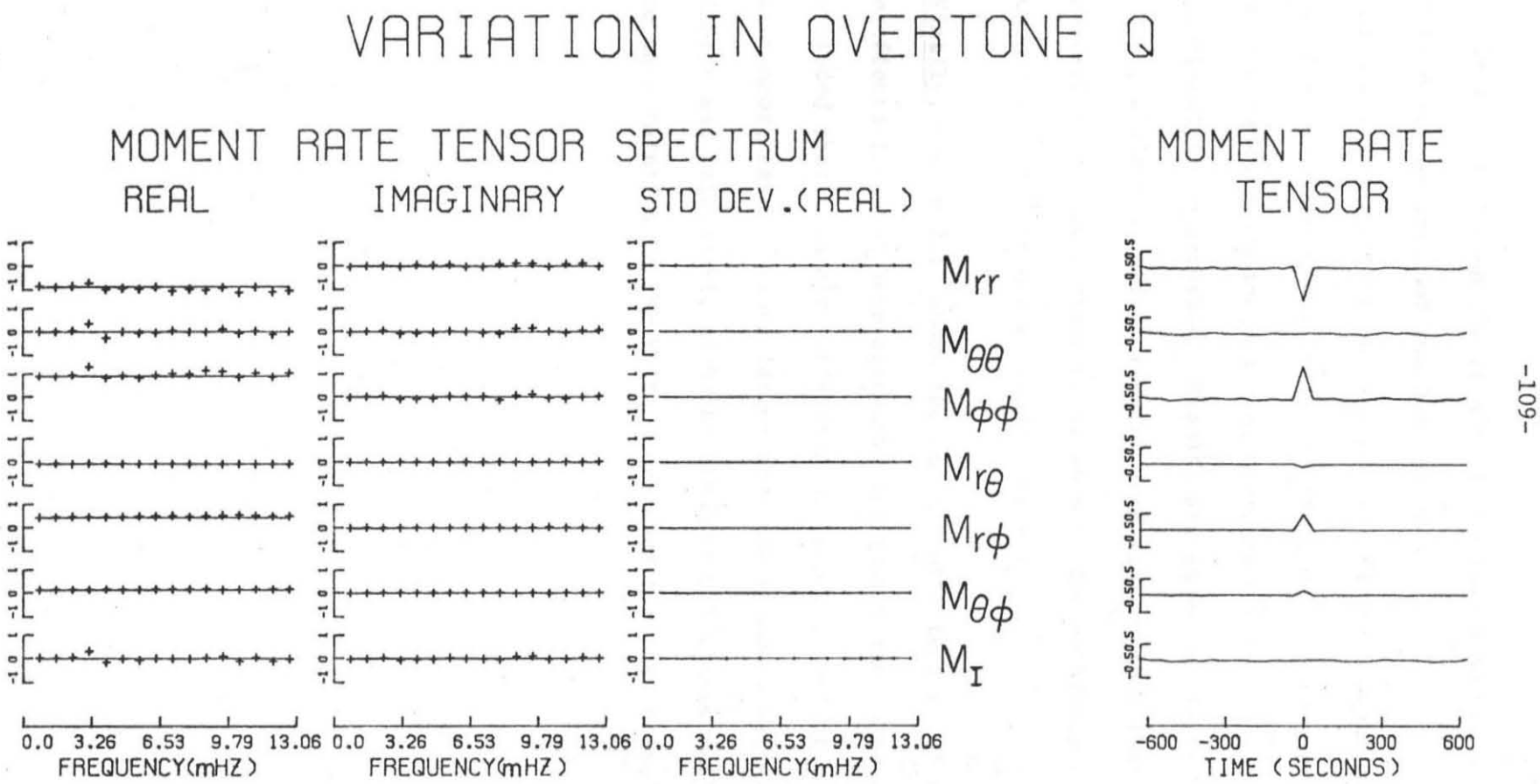

Figure 2.16. Effect of variation in overtone attenuation on the results of inversion. Details as in Figure 2.14.

errors in the model H on the result of the inversion, we allowed a simplified perturbation of the Q model used.

As a first approximation, Nakanishi's (1977) suggestion that lateral variations in Q may be substantial, was not retained. It was decided to artificially increase the overtone Q's by 30% while keeping the fundamentals unperturbed. Results are shown on Figure 2.16 and show that, while this effect remains much smaller than that of lateral heterogeneity, it may further contribute to the departure of the computed solution $\vec{f}$ from the actual source $\vec{f}_0$.

e. Finally, Figure 2.17 shows the results of a test run including all three effects (lateral heterogeneity, instrument response, Q). It is concluded that a purely artificial isotropic component of the moment tensor, several times larger than the standard variation claimed by Gilbert and Dziewonski, might be the result of a systematic error, due to uncertainties in the Earth model used for the inversion.

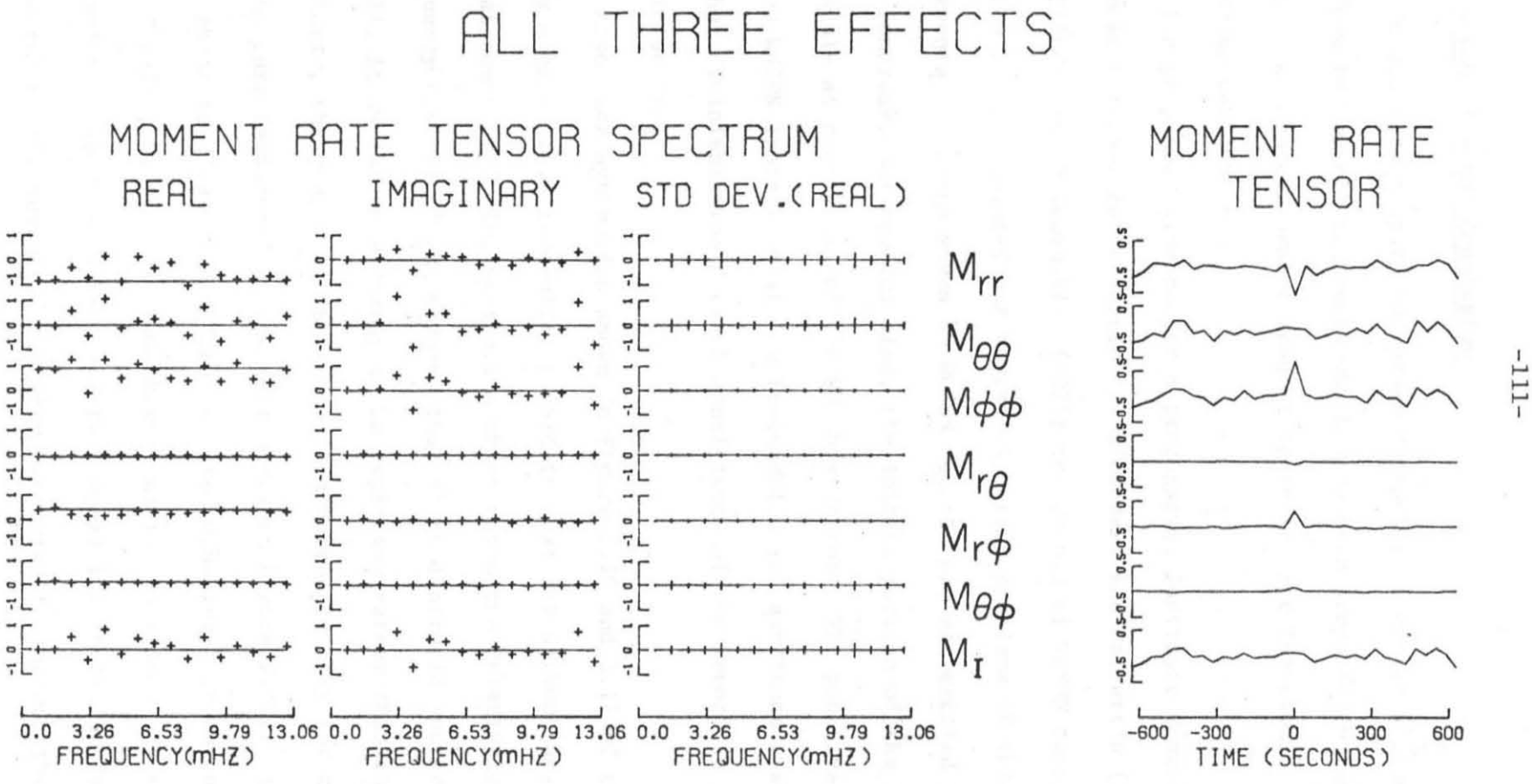

Figure 2.17. Cumulative effect of lateral heterogeneity, random fluctuation in instruments' responses, and variation in overtone attenuation on the results of inversion. Details as in Figure 2.14.

2.4 Discussion and Conclusion

In order to compare the present results to previous studies, we will now review all arguments which have been proposed in favor of, or against, a compressional component in the source function of the Colombian earthquake.

The proposed evidence for a precursive, isotropic component of the moment tensor rests mainly on Dziewonski and Gilbert's (1974) and Gilbert and Dziewonski's (1975) inversions of WWSSN records. Section 2.1 has pointed out several inherent problems of this method: Fundamental Rayleigh waves on WWSSN records are not excited efficiently by a compressional source; also, the initial portion of the record is off-scale at nearly all of the WWSSN stations. The poor response of the WWSSN instrument at low frequencies (ω^3 amplitude response) further diminishes the overall sensitivity of the record to an isotropic source.

Also, the synthetics shown in Figure 2.10 and 2.11 of the present study suggest that the entire record is best fit without any compressional component. The synthetics which match the relatively large frequency content of ${}_1R_2$ suggest that if an isotropic source is present at all, it is far more likely to be explosive rather than implosive. Similarly, the phase ${}_2R_2$ is synthetized correctly only for the case of the pure deviatoric source (see arrow on Figure 2.10). (However this phase is close to the limit of the noise level in our signal.)

Finally, Section 2.3 has shown that the extremely low standard variation claimed by Gilbert and Dziewonski for their isotropic component of the moment, (even when corrected to include the

covariance terms in equation (2.24)) fails to take into account systematic sources of error such as the presence of lateral heterogeneity, which, alone, can result in an artificial isotropic moment as large as 40% of the deviatoric one at certain frequencies. This destroys the statistical significance of their result.

A further report supporting the existence of the compressional precursor was presented by Kennett and Simons (1976), on the basis of the strain record at Ñaña, Peru. Although Hart and Kanamori (1975) used this record as evidence against the existence of the precursor, Kennett and Simons reported a significant correlation between this record (once detrended) and synthetics which included the precursor. However, the Ñaña record is extremely noisy, and their conclusion seems uncertain. Furthermore, in order to reconcile their conclusion with the total absence of any visible precursors on the WWSSN stations in South America, Kennett and Simons had to propose an ω^{-4} dependence of the isotropic displacement. They stated that "This would eliminate all chance of detecting this precursor using conventional long-period seismographs". It seems likely that the ω^{-4} frequency dependence would then preclude the detection of the precursive implosion from the entire records on WWSSN seismographs, including the surface waves used by Gilbert and Dziewonski in their 1975 inversion.

Luh and Dziewonski (1975) were able to obtain fairly good agreement between 75 observed and synthetic seismograms at WWSSN stations by using Gilbert and Dziewonski's source functions. However, they do not discuss the sensitivity of their fits to the presence of the isotropic component.

Mendiguren (1972, 1973), Furumoto and Fukao (1976) and more recently Furumoto (1977) all have been able to achieve excellent fits to the data without precursive or isotropic components in the moment rate tensor, using data almost entirely from WWSSN records. Although Furumoto's study was concentrated at periods less than 60 s, i.e. outside Gilbert and Dziewonski's working interval in frequency, it is interesting to note that no good correlation exists between primary P-wave traces at San Juan, Puerto Rico (SJG) and Natal, Brazil (NAT) (Furumoto, 1977 Figure 7), two stations nodal for the deviatoric source. Since an isotropic source would be most evident at these nodal stations and would tend to produce correlated waveforms, the poor fit suggests an absence of any compressional source at periods shorter than 100 s.

Gilbert and Dziewonski (1975) noted the very different time functions of the deviatoric and isotropic components of the moment rate tensor. They noted that the deviatoric components of the moment tensor were coseismic, and that only the isotropic source was precursory. A somewhat different conclusion can be reached from Figure 2.8, in which we present the time functions for particular combinations of the principal components of the moment rate tensor given by Gilbert and Dziewonski (1975, Figure 27). In Figure 2.8, I, the isotropic moment rate function, is the average of the three principal components. D_1 is the moment rate function for a double couple on a fault plane which is essentially the same as that inferred by Furumoto and Fukao (1976). Finally, D_2 is the moment rate function for a double couple on essentially the plane defined by the T and null axes of Furumoto

and Fukao's source.

A remarkable difference between the overall time constants of I, D_1 and D_2 emerges from Figure 2.8. D_1 has a time constant of about 100 s, but since Gilbert and Dziewonski did not consider data at periods below 80 s, this time function is essentially equivalent to the step-like time function which Mendiguren (1973) and Furumoto and Fukao (1976) also found for the double couple on this fault plane. On the other hand, both I and D_2 have very long rise times of about 300 s. Moreover, <u>both</u> I and D_2 appear to be precursory, in contrast to D_1 which is clearly coseismic, and not precursory.

Since these results were derived from WWSSN instruments which have very poor ultra long period response (Figure 2.6), it is very tempting to conclude that i) the source function D_1, which corresponds to the fault plane found by other investigators, is correct and confirmed by the study in Section 2.2. ii) the very large time for I and D_2 suggests that the energy for these source functions is concentrated at long periods (about 300 s), for which the response of the WWSSN instrument is extremely poor.

We therefore suggest that I and D_2 are probably the result of noisy data at very long periods, and of systematic errors, as illustrated by the numerical experiment in Section 2.3.

CHAPTER 3

Shear Wave Velocity at the Base of the Mantle From Profiles of Diffracted SH Waves.

3.0 Introduction

The seismic properties of the deepest parts of the mantle, in the vicinity of the core-mantle boundary (CMB) have been the subject of extensive, and at times controversial, studies. Individual observations of a decrease in S wave velocity near the CMB (Cleary, 1969; Bolt et al., 1970) and of an associated low-Q zone (Mikumo and Kurita, 1968) have been reported. Some data obtained from free oscillation Q studies (Anderson and Hart, 1978) have supported these reports, although gross earth models (Gilbert and Dziewonski, 1975; Anderson and Hart, 1976) have usually failed to yield a low shear velocity zone at the base of the mantle. Furthermore, recent data on the Q of ${}_0S_2$ (Stein and Geller, 1978) argue against such a low Q zone and leave this question unresolved. Also, an increase in S-wave velocity above the CMB has been proposed by Mitchell and Helmberger (1973) on the basis of ScS to S amplitude ratios.

The seismic properties just above the CMB have significant geophysical implications. A low-Q, low S-velocity zone might be related to efficient heat transfer across the boundary, and possibly, also, to a difference in chemical content in the deepest shells of the mantle. In turn, the composition of the deepest mantle bears directly on our understanding of the differentiation process in the Earth and other planets (Jacobs, 1975).

Most of the seismic evidence for a low S-wave velocity zone at the base of the mantle comes from the study of SH waves diffracted along the CMB into the shadow zone for direct S waves, as sketched on Figure 3.1. We will call this phase Sd. Cleary et al. (1967),

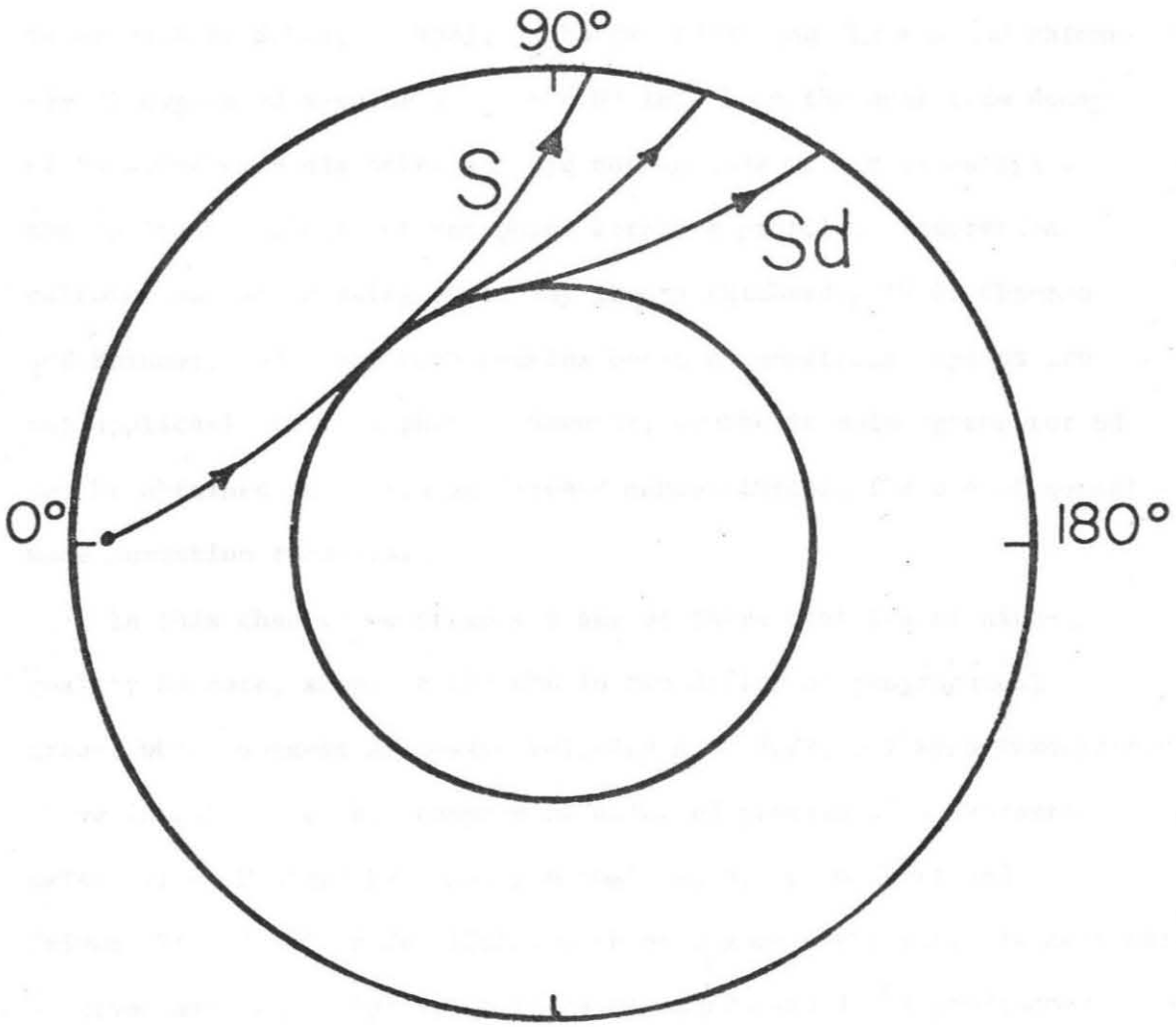

Figure 3.1. A sketch of the phase Sd, used in this Chapter. It is diffracted along the core-mantle boundary and emerges in the shadow zone. The relative sizes of the mantle and core are real.

Cleary (1969), Bolt et al. (1970) and Hales and Roberts (1970) reported values obtained from Sd studies of, respectively, 7.06, 6.8, 6.99 and 6.78 km/s for the S-wave velocity at the base of the base of the mantle, β_c, as opposed to Jeffreys' 7.30, Anderson and Hart's 7.23, or Gilbert and Dziewonski's 7.25. Mondt (1977), using the techniques of Scholte (1956), Richards (1970) and Chapman and Phinney (1972) suggested a value of β_c = 8.03 km/s from the amplitude decay of Sd waves with distance, but did not include Q, nor investigate the apparent velocity of the phase across a profile. Theoretical calculations of Sd using exact ray theory (Richards, 1970; Chapman and Phinney, 1972) are very complex because geometrical optics are not applicable to this phase. However, synthetic seismograms for Sd can be obtained in a straightforward manner through the use of normal mode summation techniques.

In this chapter we present a set of three profiles of high-quality Sd data, sampling the CMB in two different geographical areas, which suggest an S-wave velocity $\beta_c = 7.22 \pm 0.1$ km/s immediately above the CMB. We then compare an observed profile with synthetic seismograms obtained by summing normal modes, for Gilbert and Dziewonski's (1975) model 1066A, with very good agreement. In contrast, observed amplitudes for Sd at large distances ($\Delta > 120^o$) are inconsistent with models including a small but finite (β = 0.73 - 2 km/s) rigidity in the core, in a layer extending 25 km or more below the CMB.

The existence of Sd was mentioned by Gutenberg and Richter (1935), but the first reported data are found in Lehmann (1953). Cleary et al.

(1967) first measured the apparent slowness of the phase. Their value ($p = 8.61$ s/deg) corresponds to $\beta_c = 7.06$ km/s for a radius of the core $r_c = 3485$ km. Later, Cleary (1969) proposed $\beta_c = 6.8$ km/s. However, both of these studies used a single station (Canberra, Australia) and several earthquakes at various azimuths. Errors in the earthquakes' hypocentral parameters can cause large uncertainties in the final results. The opposite experiment (using a single event recorded along a profile of stations at the same azimuth) has the advantage of eliminating epicentral errors, and of providing a fairly uniform waveshape. Bolt et al. (1970) used such a profile of diffracted SH waves for the (shallow) August 31, 1968 Dasht-e-Bayāz (Iran) earthquake, and obtained $\beta_c = 6.99 \pm 0.1$ km/s. However, Sd picks for a shallow event are complicated by the presence of much surface structure. Also, the focal mechanism of the 1968 event (strike-slip on a nearly vertical fault; (see Niazi, 1969)) was quite unfavorable to excitation of Sd, especially at the particular azimuths used by Bolt et al. In this study, we use high-quality Sd profiles for three deep earthquakes (Tonga, 1967 and 1969; Japan Sea, 1973). Using deep earthquakes eliminates possible problems caused by later phases. Also, the focal mechanism excites Sd efficiently for the 1967 Tonga and 1973 Japan Sea events (for which accurate focal mechanisms have been published). The mechanism is apparently favorable for the 1969 Tonga event.

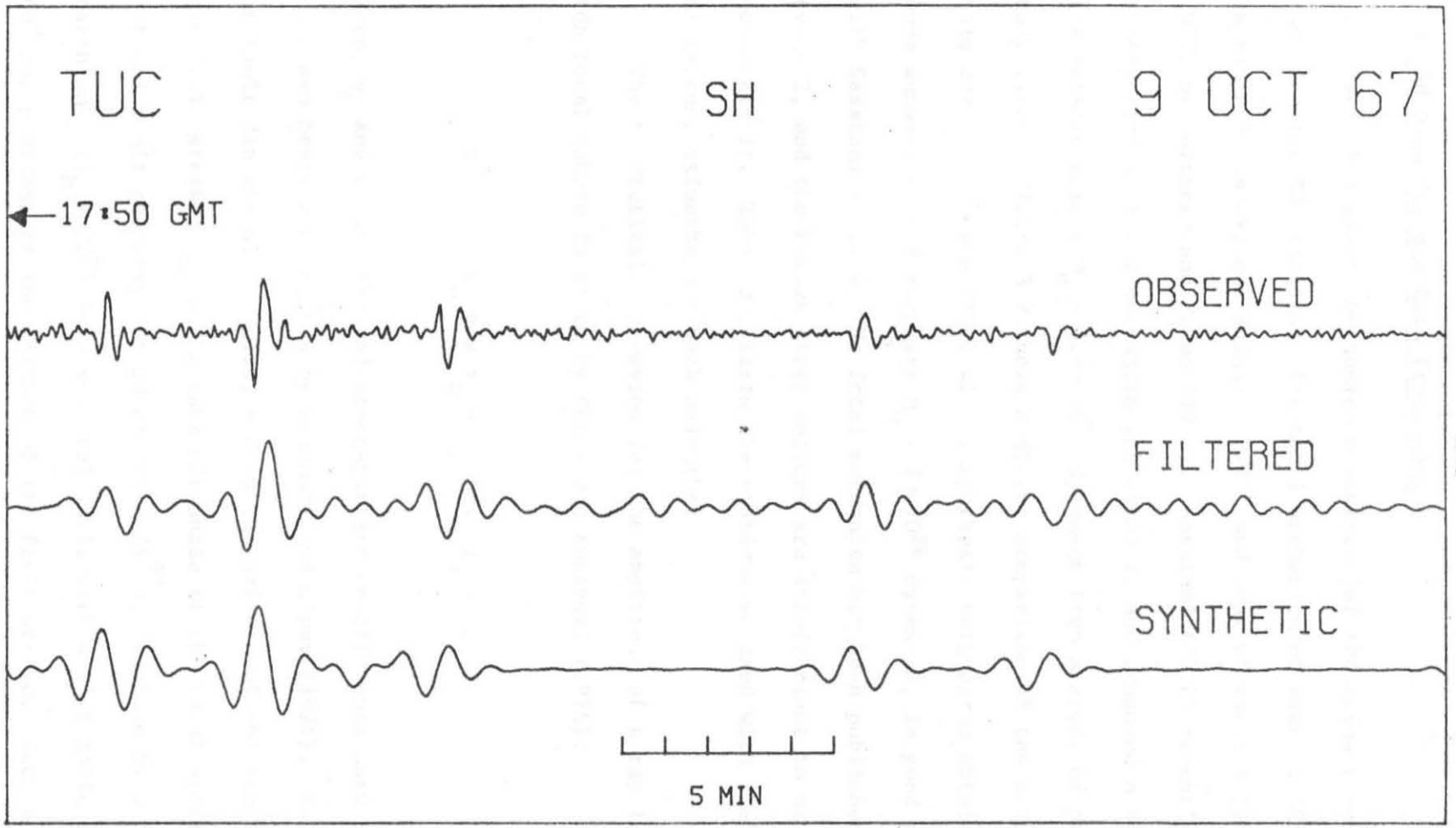

Figure 3.2. A comparison of the observed trace at Tucson for event 1, with a synthetic obtained by mode summation. The center trace represents the data, filtered to remove all periods less than 45 s. The same filter is used in the synthetic.

3.1 Sd Data Set and Data Processing

Table 3.1 gives the source parameters of the three events we used for the Sd profiles. The focal mechanism of event 1 (9 Oct 1967) is given by Isacks and Molnar (1971), and that of event 3 (29 Sep 1973) by Furumoto and Fukao (1976). Sasatani (1976) recently published a very similar focal mechanism for event 1, and proposed a value of its seismic moment $M_o = 5.7 \times 10^{26}$ dynes-cm from a study of primary body waves. Figure 3.2 shows a direct comparison of the record of this event at Tucson (TUC) with a synthetic seismogram obtained by mode summation, and suggests $M_o = 7 \times 10^{26}$ dynes-cm, in good agreement with Sasatani's value. No focal mechanism has been published for event 2, and the P-wave first motions are insufficient to properly constrain it. Table 3.2 lists the stations we used with their distances, azimuths and back azimuths.

The theoretical expression for the amplitude of a ray leaving the focal sphere is given by Chung and Kanamori (1976):

$$R^{SH} = - q_L \cos i_h - p_L \sin i_h \,. \qquad (3.1)$$

Here, q_L and p_L are the radiation-pattern coefficients used in normal mode synthesis and defined by Kanamori and Cipar (1974). They depend on fault dip and slip angles, and on the azimuth of the station from the fault strike; i_h is the take-off angle at the focal sphere. The optimal fault geometry for Sd profiles (R^{SH}=1) excited by a deep earthquake ($i_h = 30^o$) is a vertical fault with a slip angle of about 60^o and stations at the azimuth of the fault strike. Such a mechanism

Table 3.1

Seismic Events used in the Study of Sd

Number	Area	Date	Epicenter	Depth km	Origin Time GMT	Focal Mechanism Strike	Dip	Slip	Reference
1	Tonga Islands	9 Oct 67	21.1°S 179.3°W	605	17:21:46.0	54°	85°	-83°	a,b
2	Tonga Islands	10 Feb 69	22.7°S 178.8°E	635	22:58:03.3	Unconstrained at present			
3	Japan Sea	29 Sep 73	41.9°N 130.9°E	575	00:44:00.8	186°	83°	90°	c

References (a) Isacks and Molnar (1971) (b) Sasatani (1976) (c) Furumoto and Fukao (1976)

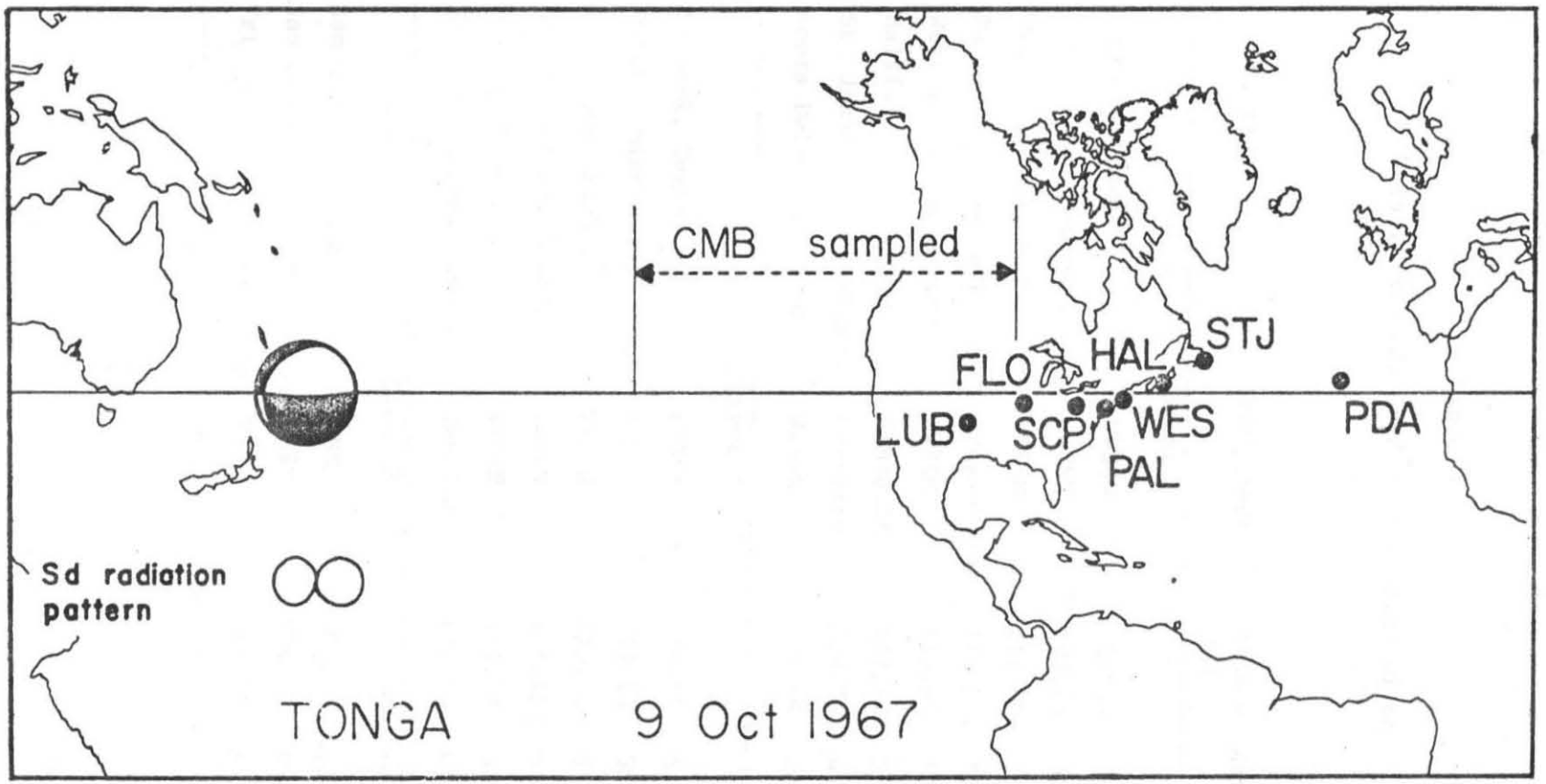

Figure 3.3. Map of the profile used for event 1. This is a Mercator projection whose baseline is the mean great circle linking the epicenter and stations. Also shown are the earthquake focal mechanism (shaded area compressional), the theoretical radiation pattern for Sd, and the portion of core-mantle boundary sampled by the profile.

Table 3.2

Seismic Records used in the Study of Sd

Code	Station	Instrument	Distance (°)	Azimuth (°)	Back Azimuth (°)
		Event 1			
LUB	Lubbock, Texas	WWSSN	91.64	54.7	245.9
FLO	Florissant, Missouri	WWSSN	102.18	53.2	252.9
SCP	State College, Penna.	WWSSN	112.00	53.5	260.9
PAL	Palisades, New York	Press-Ewing	115.00	53.7	263.4
WES	Weston, Massachusetts	WWSSN	117.06	52.4	265.7
HAL	Halifax, Nova Scotia	Canadian	122.72	50.0	272.3
STJ	St. John's, Newfoundland	Canadian	129.83	45.3	282.9
PDA	Ponta Delgada, Azores	WWSSN	151.86	48.6	299.3
		Event 2			
LUB	Lubbock, Texas	WWSSN	94.06	55.5	245.6
OXF	Oxford, Mississippi	WWSSN	104.04	58.4	252.2
AAM	Ann Arbor, Michigan	WWSSN	110.44	51.8	257.7
SCP	State College, Penna.	WWSSN	114.42	54.3	260.6
WES	Weston, Massachusetts	WWSSN	119.49	53.3	265.5
STJ	St. John's, Newfoundland	Canadian	132.27	45.9	283.1
		Event 3			
BEC	Hamilton, Bermuda	WWSSN	104.56	13.5	348.1
SJG	San Juan, Puerto Rico	WWSSN	118.12	18.4	345.7
TRN	Trinidad, Trinidad & Tobago	WWSSN	126.37	15.0	348.6

causes a large amount of shear energy to be radiated downward; the Sd amplitude, to first order, can be considered as depending on the value of R^{SH} for grazing incidence on the CMB. Such large amplitudes of downgoing S waves also lead to excellent multiple ScS phases. The three earthquakes used here were previously used in multiple ScS studies (Okal and Anderson, 1975; Yoshida and Tsujiura, 1975; Sipkin and Jordan, 1976). Also, the 1967 Tonga event was used in a recent SKS study (Kind and Müller, 1977). The radiation pattern factors for the two events whose mechanisms are known are $R^{SH} = 0.901$ (event 1) and $R^{SH} = 0.811$ (event 3) at the azimuths of our profiles. Thus, the quality of the data is considerably better than in previous studies (For the Dasht-e-Bayāz event recorded at American stations, $R^{SH} = 0.08$).

Records were rotated into SH polarization whenever the station's back azimuth was more than 10 degrees away from natural polarization. Records at Canadian stations and PAL were equalized to the amplitude and phase response of the WWSSN instrument. We will concentrate on event 1, because of the excellent quality of the data, and the well-determined focal mechanism; however, all of our results are confirmed by events 2 and 3.

Figure 3.3 shows the profile for events 1 and 2. The data for event 1 are shown on Figure 3.4. Sd has a very sharp onset at all stations up to STJ. The identification of Sd at PDA is more difficult on the unfiltered record, because of the smaller signal and larger noise level of this island station, but Sd is clear on the filtered record (Figure 3.5). The phase sSd is also present on all records.

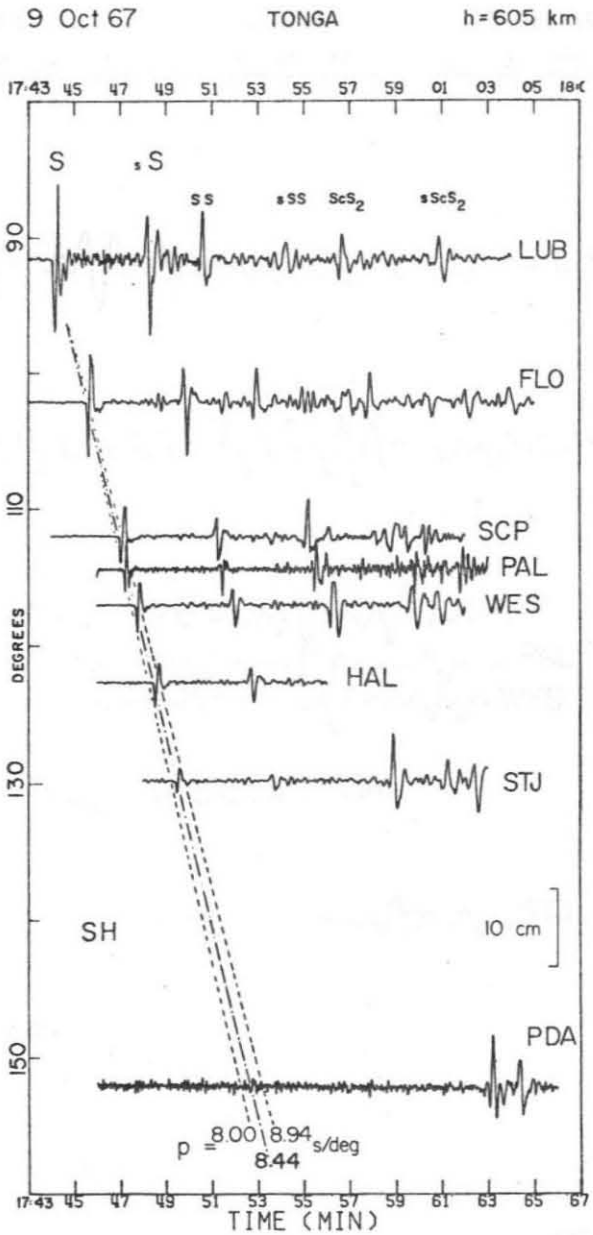

Figure 3.4. Observed data profile for event 1. The seismograms have been equalized to a standard magnification of 1500, and rotated into SH polarization. The oblique lines show the result of alignment of the sharp onsets with a straight edge (p_o = 8.44 s/deg), and lines of constant slowness corresponding to velocities of 6.8 and 7.6 km/s at the core-mantle boundary.

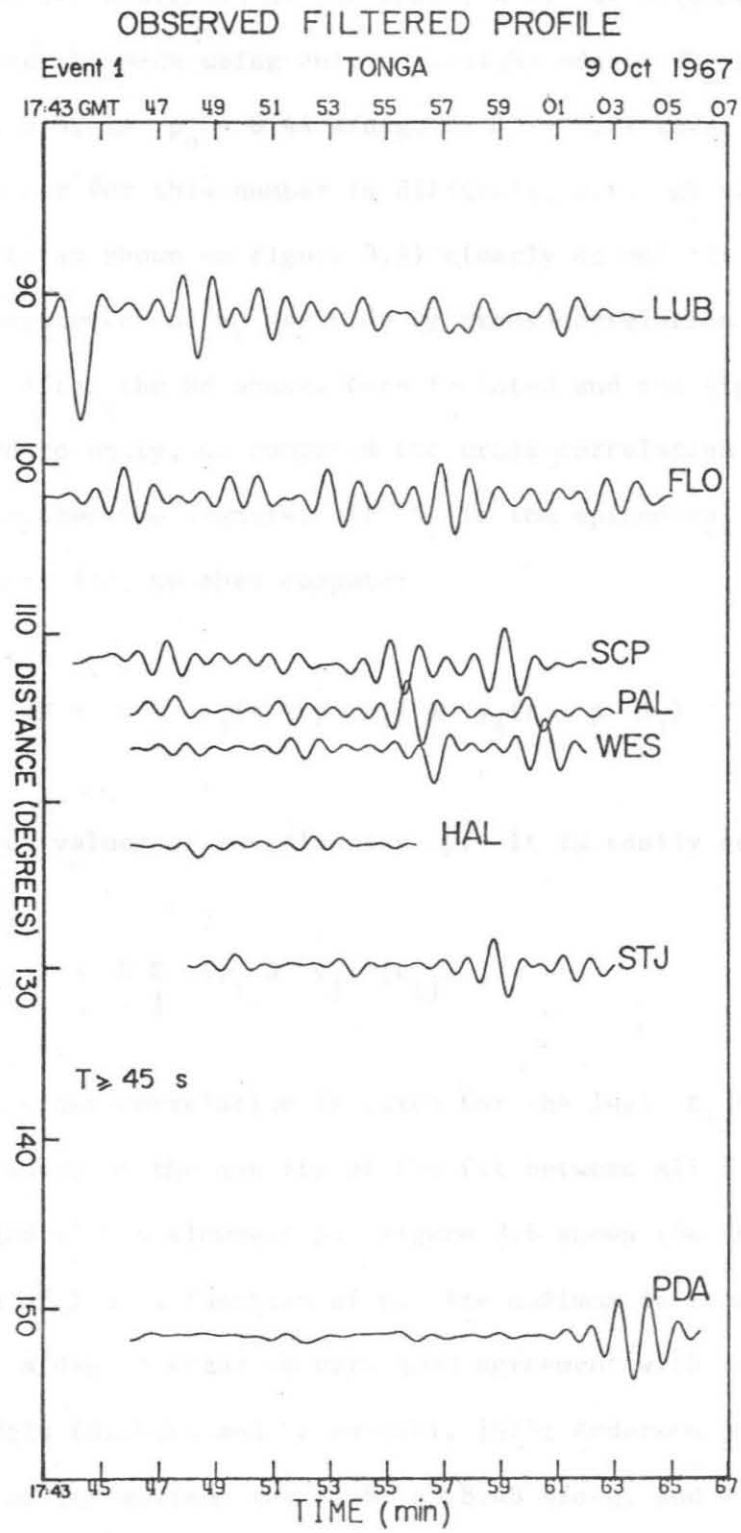

Figure 3.5. Observed profile for event 1 (from Figure 3.4), filtered at $T \geq 45$ s. Note that Sd and sSd are detected all the way to PDA.

Given the sharpness of the onset, a visual alignment of the first arrivals can be made using only a straight edge. The result, shown on Figure 3.4, is $p_o = 8.44$ s/deg, or $\beta_c = 7.21$ km/s. Estimating the error bar for this number is difficult, although values of 6.8 and 7.6 km/s (also shown on Figure 3.4) clearly do not fit the data. A second measurement of β_c was made by cross-correlation of the various records. After the Sd phases were isolated and the signal energy normalized to unity, we computed the cross-correlation functions $y_i \oplus y_j$ between the signals. If Δ_i is the epicentral distance of the i-th station, we then compute:

$$F = \sum_i \sum_j y_i(t - p \cdot \Delta_i) \oplus y_j(t - p \cdot \Delta_j) \qquad (3.2)$$

for various values of the slowness p. It is easily seen that:

$$F = \sum_i \sum_j (y_i \oplus y_j)(t_{ij}) , \qquad (3.3)$$

where the cross-correlation is taken for the lag: $t_{ij} = p \cdot (\Delta_i - \Delta_j)$. F is a measure of the quality of the fit between all 8 traces when time-lagged with a slowness p. Figure 3.6 shows the (smoothed) variation of F as a function of p. Its maximum is reached for $p_o = 8.41$ s/deg, a value in very good agreement with recent gross earth models (Gilbert and Dziewonski, 1975; Anderson and Hart, 1976). F is 95% of its maximum for $8.38 < p < 8.48$ s/deg, and 90% for $8.37 < p < 8.53$ s/deg.

In principle, the theoretical shape of the diffracted pulse

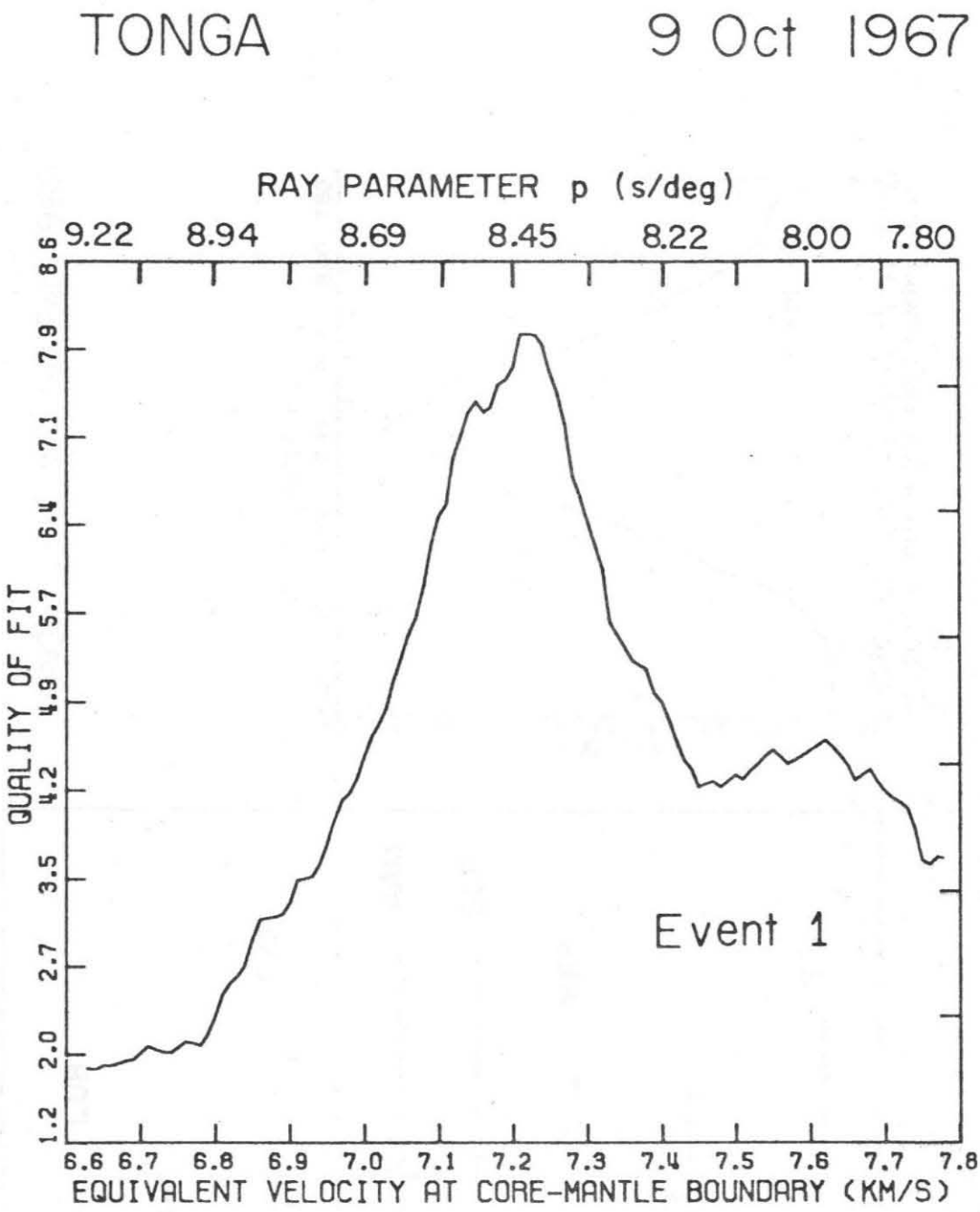

Figure 3.6. Variation of the cross-correlation function F as a function of slowness p (or equivalent shear velocity at the CMB), for event 1.

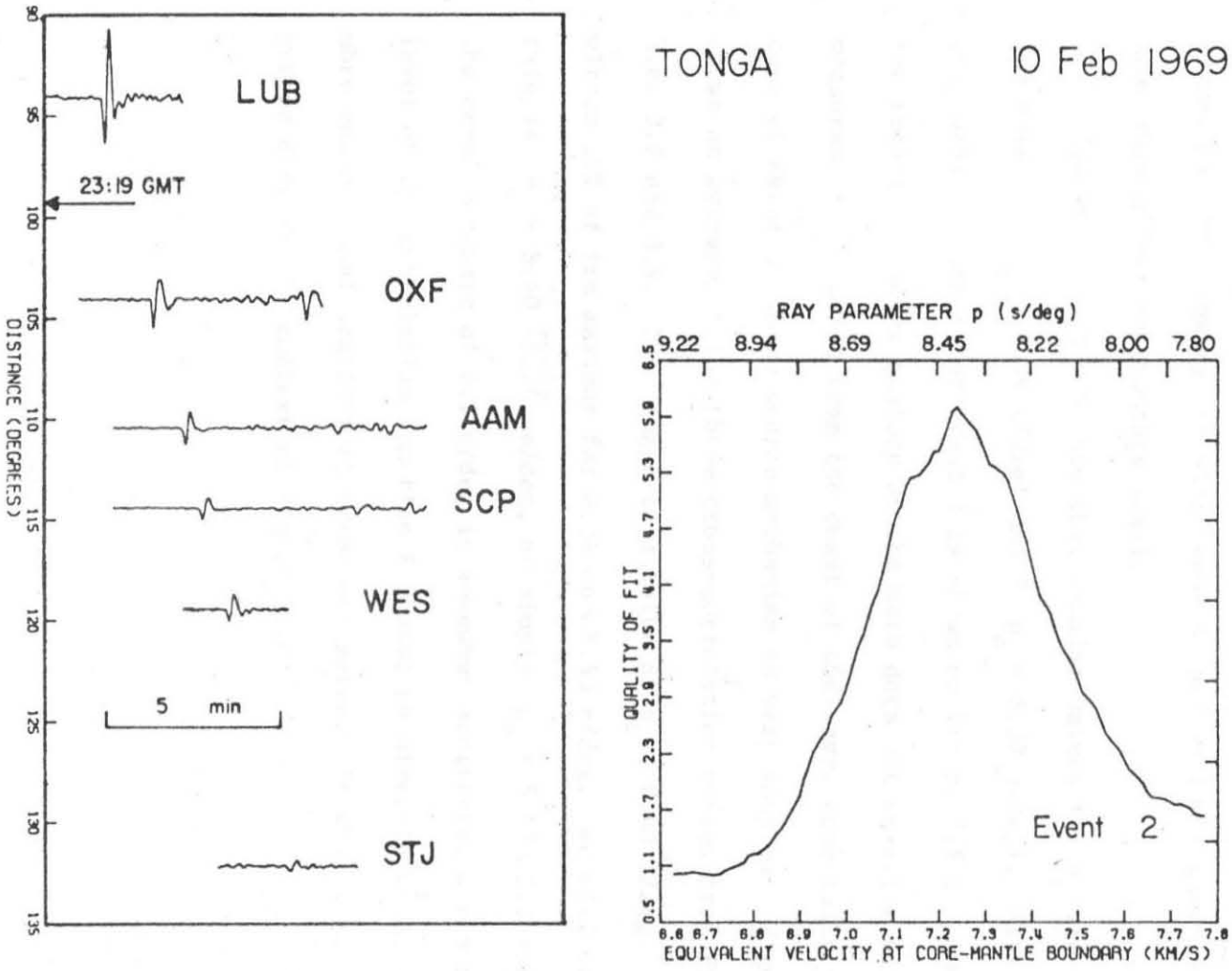

Figure 3.7. Experimental profile and variation of the cross-correlation function F for event 2.

should change with distance (Chapman and Phinney, 1972), possibly leading to a bias in the cross-correlation. However, the amount of distortion should be minimal for SH waves. Also, the excellent agreement in our study between the values of p_o obtained at high frequency (by aligning the sharp onsets) and at low frequency shows that this effect is probably small.

Figures 3.7 and 3.9 show that similar values for p_o are obtained for events 2 (p_o = 8.39 s/deg) and 3 (p_o = 8.37 s/deg). (The geographical layout for event 3 is shown on Figure 3.8). However, the relatively lower quality of the data does not permit a direct measurement of $dT/d\Delta$ from the onset of the wave, especially in the case of event 3, whose source mechanism is very complex. Figure 3.10 shows an average of the three cross-correlation curves from Figures 3.6, 3.7 and 3.9. This suggests a value of p_o = 8.40 s/deg. F is within 90% of its maximum for $8.34 < p < 8.53$ s/deg. We will write this as $p_o = 8.40^{+0.13}_{-0.06}$ s/deg, or simply $p_o = 8.43 \pm 0.1$ s/deg. The error estimate of 0.1 s/deg is somewhat arbitrary, since the 90% level of the correlation function F cannot be directly related to more conventional statistical error estimates. It should be interpreted only in the context of Figure 3.10.

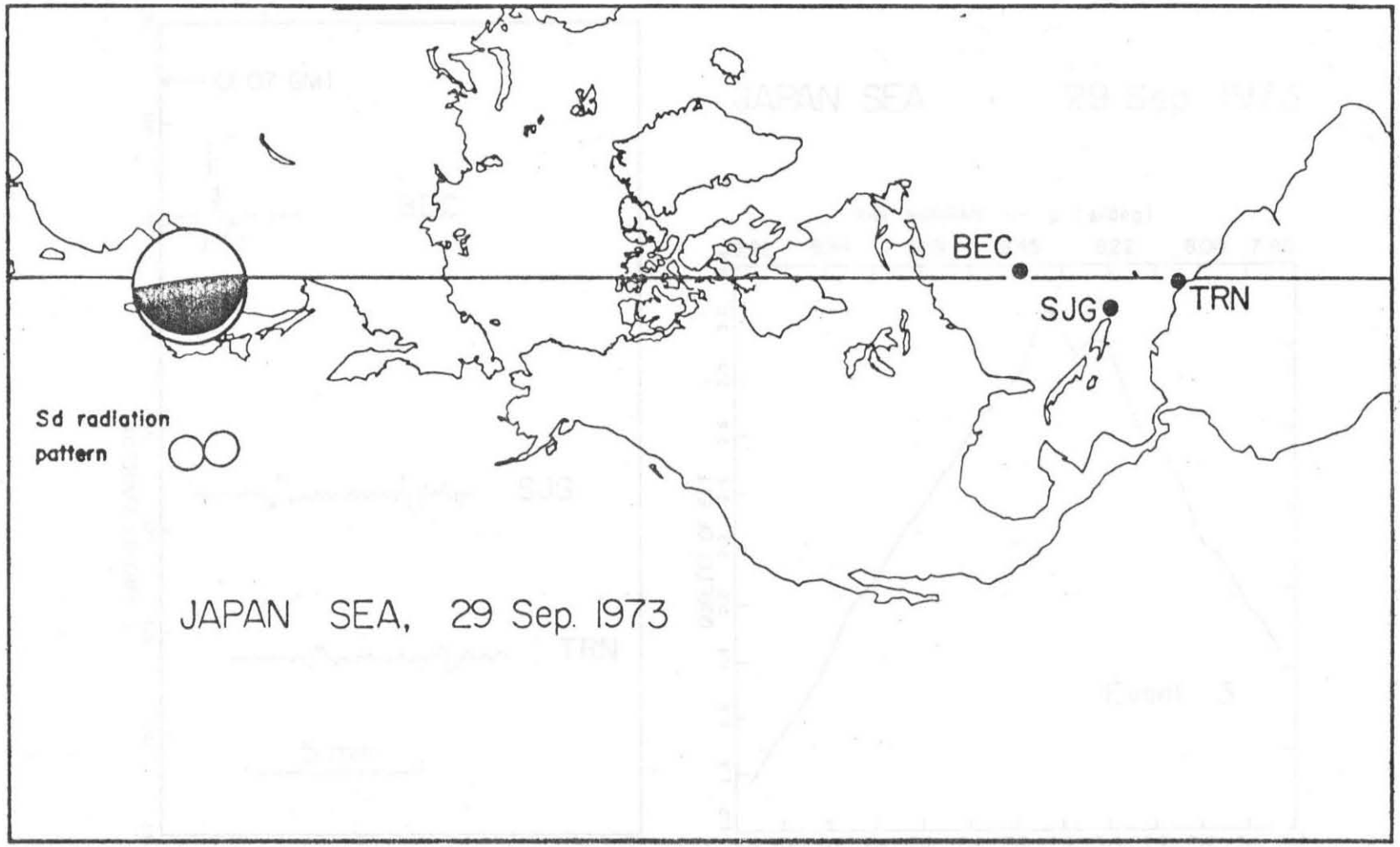

Figure 3.8. Map of the profile used for event 3. This is a Mercator projection whose baseline is the mean great circle linking epicenter and stations. Also shown are the focal mechanism of the earthquake (shaded area compressional) and its theoretical radiation pattern for Sd.

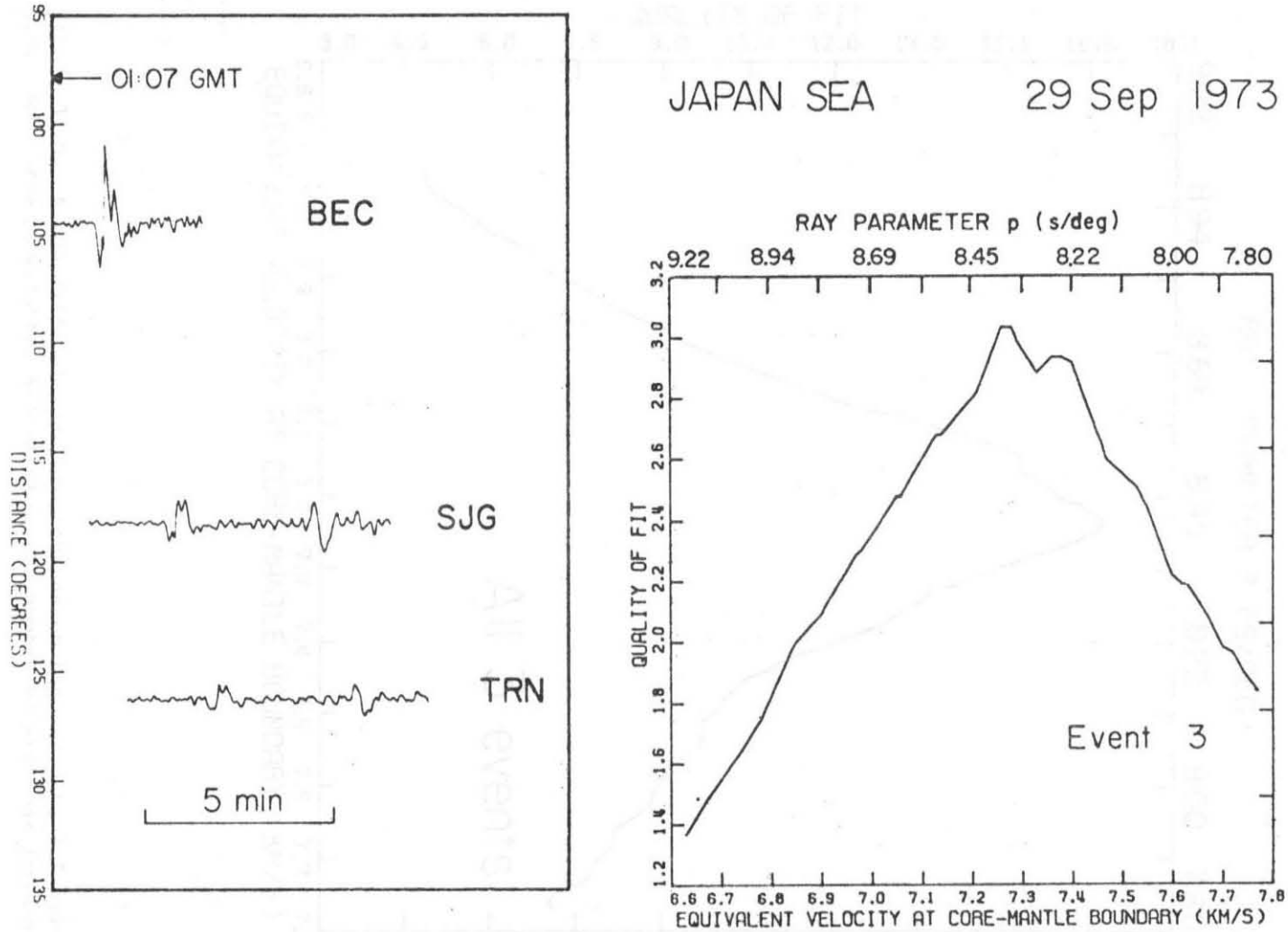

Figure 3.9. Experimental profile and variation of the cross-correlation function F for event 3.

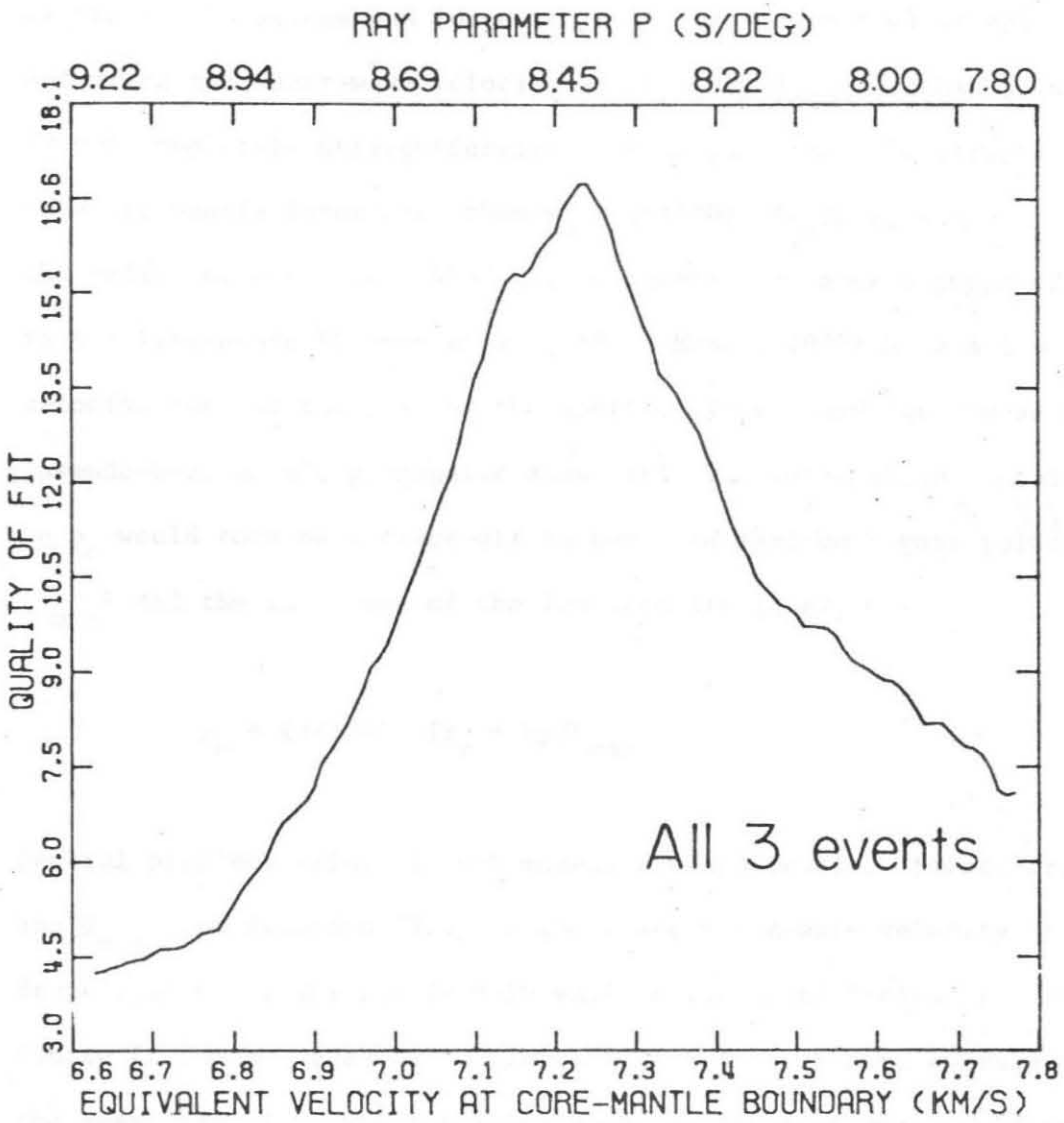

Figure 3.10. A composite of the three curves on Figures 3.6, 3.7 and 3.9. Each curve is weighted according to the number of stations involved.

3.2 Interpretation

In the previous section, the slowness of Sd across three profiles of stations was found to be $dT/d\Delta = p_o = 8.43$ s/deg. Inferring the shear-wave velocity at the CMB, β_c, from this slowness is not completely straightforward. If Sd is actually diffracted along the core-mantle interface, then $p_o = (\pi/180) \cdot (r_c/\beta_c)$, where r_c is the radius of the core (3485 km). However, some models proposed in the literature (Cleary et al., 1969; Mondt, 1977) have a low-velocity zone at the base of the mantle. This could lead to an SH "pseudo-head wave", propagated above it. The information contained in p_o would then be a trade-off between the maximum S wave velocity (β_{max}) and the thickness of the low-velocity layer, h:

$$p_o = (\pi/180) \cdot (r_c + h)/\beta_{max} \quad . \tag{3.4}$$

Several problems arise if such models are applicable. First, treating β_{max} from equation (3.4) as the exact shear-wave velocity at the deepest point of the ray is only valid at infinite frequency. At a finite frequency, the wave slowness will represent some average of the shear velocity over a thickness on the order of one wavelength. The value of p_o resulting from the cross-correlation should then be frequency-dependent for a model with a velocity gradient. The excellent agreement between the high-frequency values of p_o from the first arrivals (8.44 s/deg) and the broad-band values from cross-correlation (8.43 ± 0.1 s/deg) suggests that there is no appreciable frequency dependence of p_o. To further investigate the possible

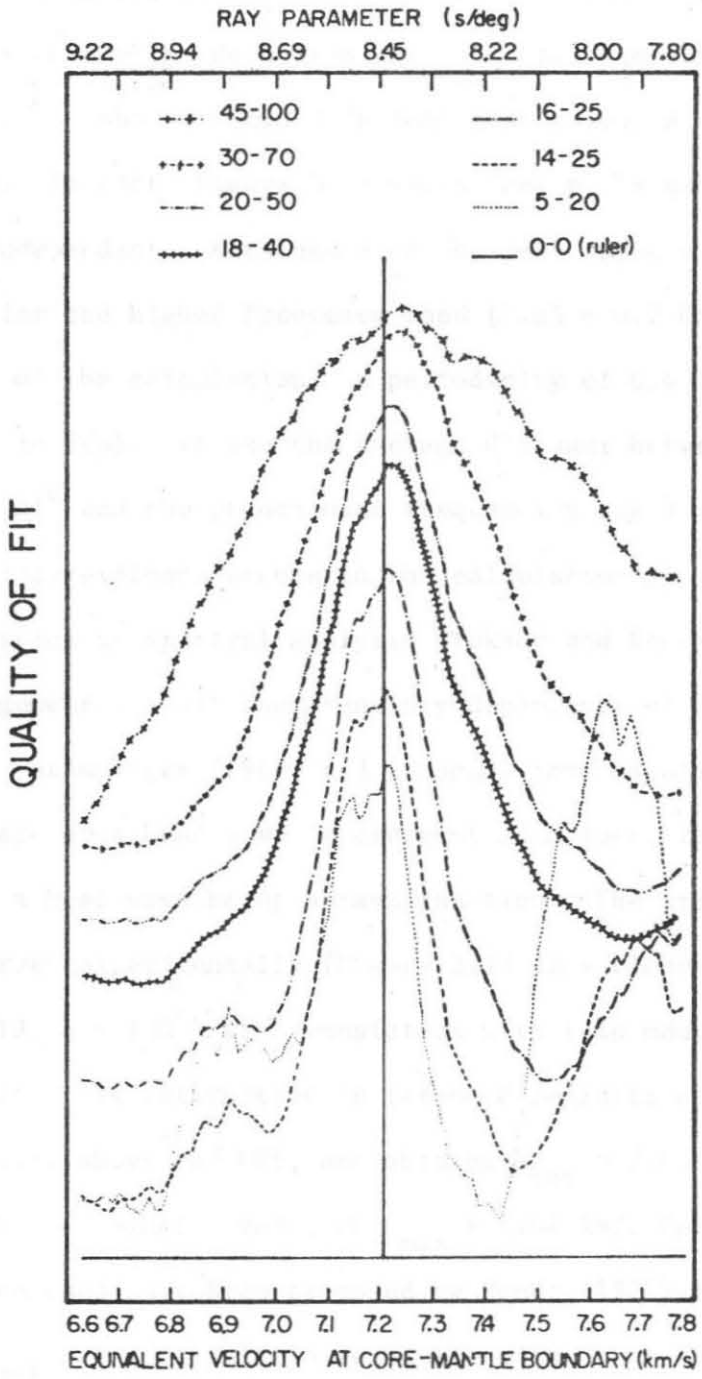

Figure 3.11. Variation of the cross-correlation function F with slowness and frequency, for event 1. The ranges of the band-pass filters used are shown (in s) at the top of the figure. The full line is the result of aligning the sharp onsets. The vertical scale is arbitrary, and the curves have been shifted along it to improve clarity.

frequency dependence, we ran the cross-correlation program after band-pass filtering the data from event 1. An observable frequency dependence of p_o should yield different peak values at different frequencies. In fact, Figure 3.11 shows that p_o is essentially frequency-independent. Although a second peak appears around p = 7.95 s/deg for the higher frequency band (0.05 - 0.2 Hz), this is an artifact of the calculation: a periodicity of 0.4 to 0.5 s/deg is expected in F(p), because the average distance between couples of stations is 21^o and the predominant frequencies are 0.10 - 0.125 Hz. (A similar indeterminacy occurs in the calculation of surface-wave phase velocities by spectral analysis (Toksöz and Ben-Menahem, 1963)). A second argument against the frequency dependence of p_o comes from ray theory. Helmberger (1968, and personal communication) has shown that the shape of a head wave is emergent in nature, the step-function response of a head wave being a ramp function. The profile of sharp onsets observed experimentally (Figure 3.12 is a close-up of the record at STJ, $\Delta = 130^o$) is inconsistent with this model).

Also, if p_o is interpreted in terms of refraction along a high-velocity layer, above the CMB, one obtains β_{max} = 7.44 km/s for a 100 km-thick low-velocity zone, or β_{max} = 7.64 km/s for 200 km. (These thicknesses have been proposed by Mondt (1977).) These high values of β_{max} are difficult to reconcile with other seismological data (vertical ScS travel-time, free oscillation periods, etc.) and would also have to be explained on geochemical grounds. Finally, section 3.3 will show that synthetic seismograms obtained by mode summation are incompatible with β_c = 6.8 km/s and suggest a very small

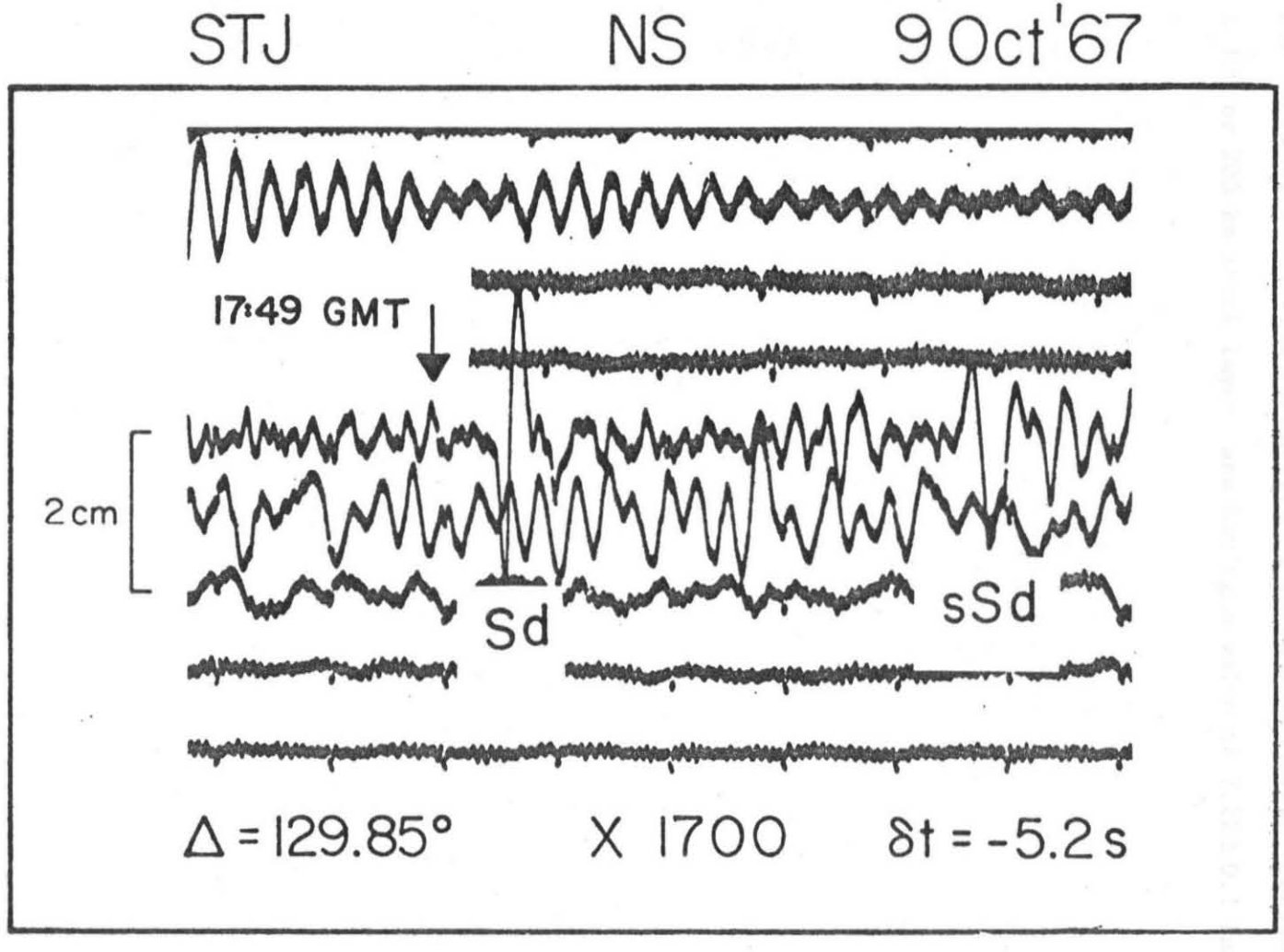

Figure 3.12. A close-up of the phase Sd at STJ (Δ = 129.85°) for event 1. Note the sharp onset of the phase, which cannot be reconciled with the behavior of a head-type wave.

extent to any possible low-velocity zone.

We therefore consider that possible frequency-dependence of p_o can be ruled out. β is considered as being essentially constant over a 100 or 200 km thick layer, and having a value of 7.22 ± 0.1 km/s.

3.3 Synthetics of Sd

We will investigate the velocity structure at the CMB by studying the decay of the Sd amplitudes along the profile of event 1. At periods greater than 45 s, to which our present synthetics are restricted, it is not possible to resolve the Q structure near the CMB, since the effect of Q on Sd amplitudes is very small. Records filtered at $T \geq 45$ s therefore provide a tool to investigate the purely elastic decay of Sd with distance, involving only propagation effects, and no attenuation. As an alternative to the full wave theory approach to this problem, we calculate synthetic seismograms by summing all the normal toroidal modes of the Earth, following the procedure described by Kanamori and Cipar (1974), but including all overtone branches. We first use a set of normal modes computed from model 1066A (Gilbert and Dziewonski, 1975) and no attenuation. All 2021 modes with periods greater than 45 seconds are included. A zero-phase low-pass filter with linear amplitude response between 1/45 Hz and 1/70 Hz is used to compensate for the sharp cut-off at 45 s period in the synthetics. A similar filter is also applied to the data. Results are shown in Figure 3.13, and compared to the filtered trace reproduced from Figure 3.5. The agreement between them is very good.

This figure shows that the synthesis of long-period body waves by summation of normal modes is practical and convenient for phases such as Sd, which violate geometrical optics. This point was first demonstrated by Yasuo Satô and his colleagues (e.g. Landisman et al. (1970)).

Furthermore, it was observed that the modes with phase velocities

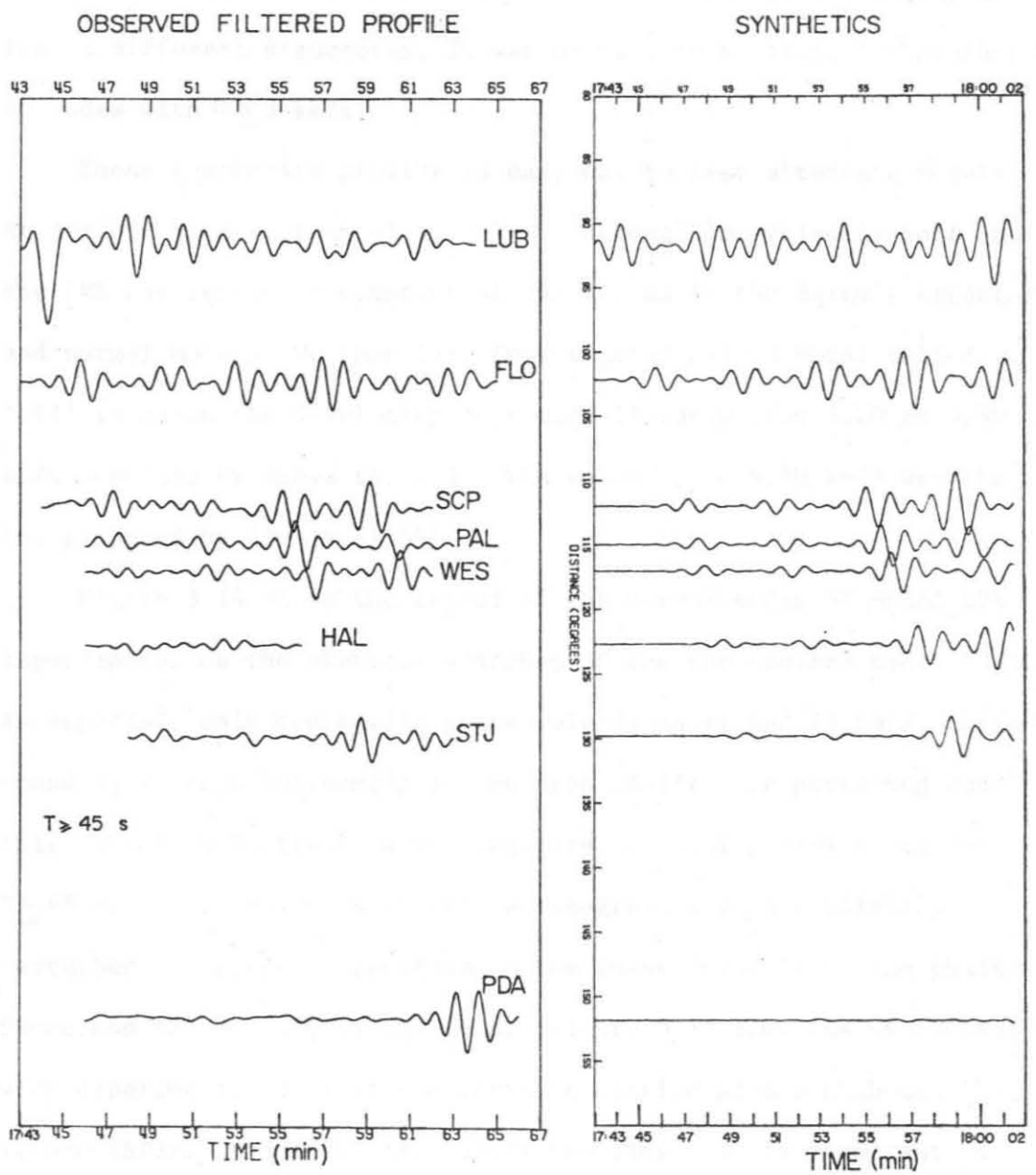

Figure 3.13. A comparison of the observed filtered profile for event 1 (left; reproduced from Figure 3.5), with a synthetic profile (right) obtained by mode summation, using model 1066A.

smaller than 9 km/s contribute very little to any synthetic of Sd. This should be expected since these modes correspond to rays bottomming at least 1250 km above the CMB, and have an important contribution only to the later mantle phases, such as SS. In testing models corresponding to different structures, it was decided to restrict the synthetics to modes with $C \geq 9$ km/s.

These synthetics provide an easy way to test alternate models. At periods greater than 45 s, only a "strong" low-velocity zone above the CMB can result in substantial variations in the Earth's structure and normal modes. We therefore investigated only a model called 'LVZ' in which the S-velocity decreases linearly from 7.20 to 6.80 km/s over 200 km above the CMB. The value $\beta_c = 6.80$ km/s was the one proposed by Cleary (1969).

Figure 3.14 shows the layout of the normal modes of model LVZ superimposed on the overtone branches of the unperturbed model 1066A. As expected, only modes with phase velocities around 13 km/s, corresponding to rays bottomming in the deep mantle, are perturbed and this deviation increases with frequency, remaining very small for $T \geq 45$ s. As a result, synthetic seismograms are only slightly perturbed. However, a decrease in the phase velocity of the phase Sd across the profile is observed. Figure 3.15 compares synthetics with experimental data at the farthest station with a high-quality record (STJ). Model LVZ is clearly too slow. It is important to note that the time difference between the peaks of Sd for models 1066A and LVZ (about 17 s) reflects almost exactly the difference in geometrical travel time along 32^{o} of CMB:

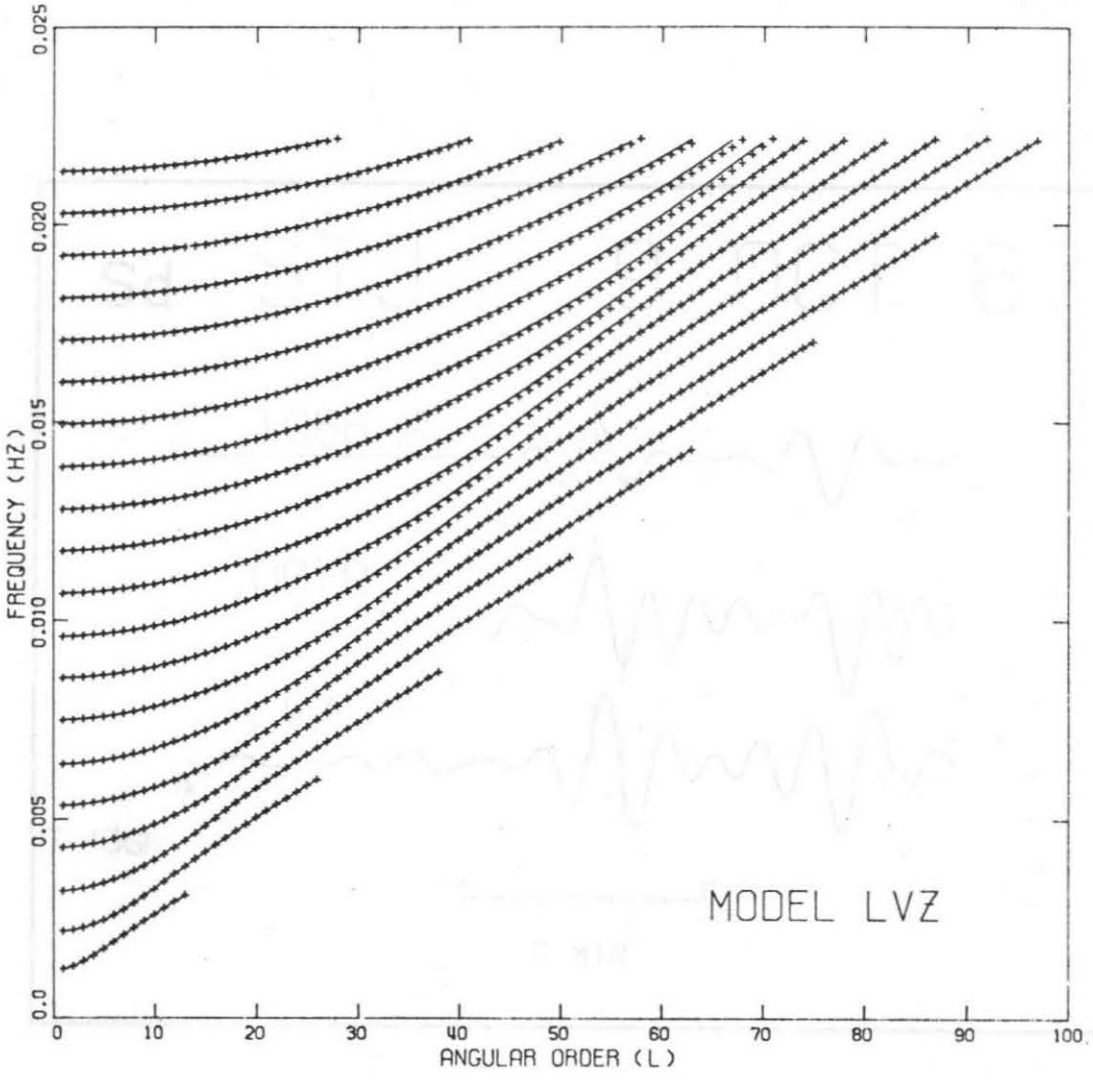

Figure 3.14. Frequency versus angular order plot of the modes with phase velocity greater than 9 km/s, and period greater than 45 s, for model LVZ, including a low-velocity zone at the base of the mantle. The + signs are the individual modes for model LVZ, the full lines the regular overtones for the unperturbed model 1066A.

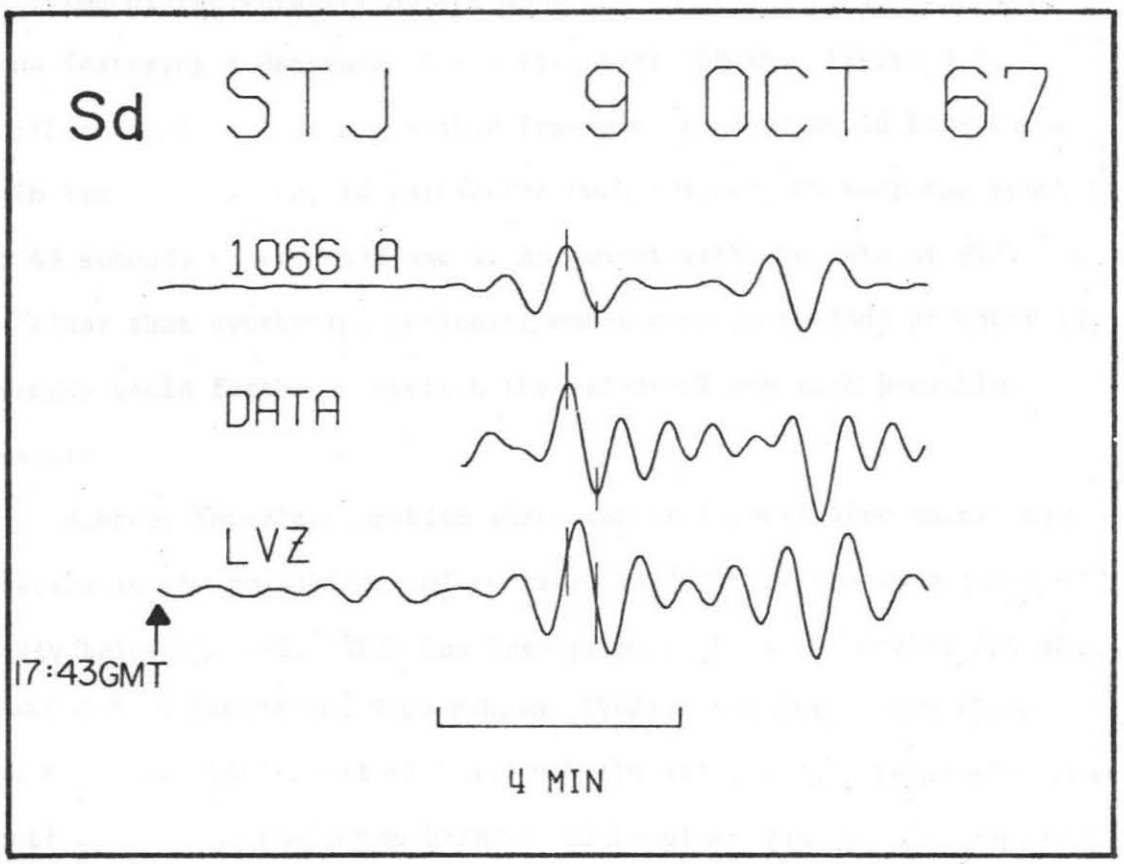

Figure 3.15. A comparison of the filtered observed data at STJ (center) with synthetics computed for both the unperturbed model 1066A (top) and model LVZ (bottom). The vertical ticks, all aligned on the same two lines, show the better agreement of the data with 1066A, rather than LVZ. The separation in time of the peaks of the 1066A and LVZ synthetics is approximately 17 s.

$$\delta t = \frac{32}{180}\pi \; r_c \left(\frac{1}{6.8} - \frac{1}{7.25} \right) = 18 \text{ s.} \qquad (3.5)$$

This confirms the validity of interpreting the apparent slowness of the wave across the profile along the rules of geometrical optics in terms of the velocity at the CMB, β_c, and rules out a low-velocity zone featuring a decrease of 0.4 km/s over 200 km. Figure 3.15 further suggests that a possible low-velocity zone would have to be much less pronounced, in particular much thinner, to keep the synthetic at 45 seconds unperturbed and in agreement with the data at STJ. It is clear that synthetics including modes down to periods of about 15 seconds would further constrain the extent of any such possible feature.

Another important problem which can be investigated using synthetics is the possibility of non-zero rigidity of the core immediately below the CMB. This has been proposed from the amplitudes of S and ScS (Balakina and Vvedenskaya, 1962), of multiple ScS (Sato and Espinosa (1967), and of P and PcP (Ibrahim, 1971). Ibrahim's arguments were criticized by Buchbinder and Poupinet (1973), who proposed instead a thin (4 km) liquid layer of light (ρ = 6 g/cm^3) material separating mantle and core. Such a liquid layer clearly does not affect Sd and, therefore we have not investigated this model. On the other hand, Anderson and Kovach (1964) proposed a maximum rigidity $\mu < 2 \times 10^{10}$ dynes/cm^2 (or $\beta < 0.5$ km/s) on the basis of the relative amplitude decay of multiple ScS. A finite rigidity (on the order of $0.5 - 2 \times 10^{11}$ dynes/cm^2) of the core would have to be reconciled

Table 3.3

Parameters of Models with a Rigid Layer at the Top of the Core

Model	Rigidity (dyn/cm^2)	Shear-wave Velocity (km/s)	Thickness (km)
βC1	4.0×10^{11}	2.00	50
βC2	4.0×10^{11}	2.00	200
βC3	1.0×10^{11}	1.00	35
βC4	5.3×10^{10}	0.73	25

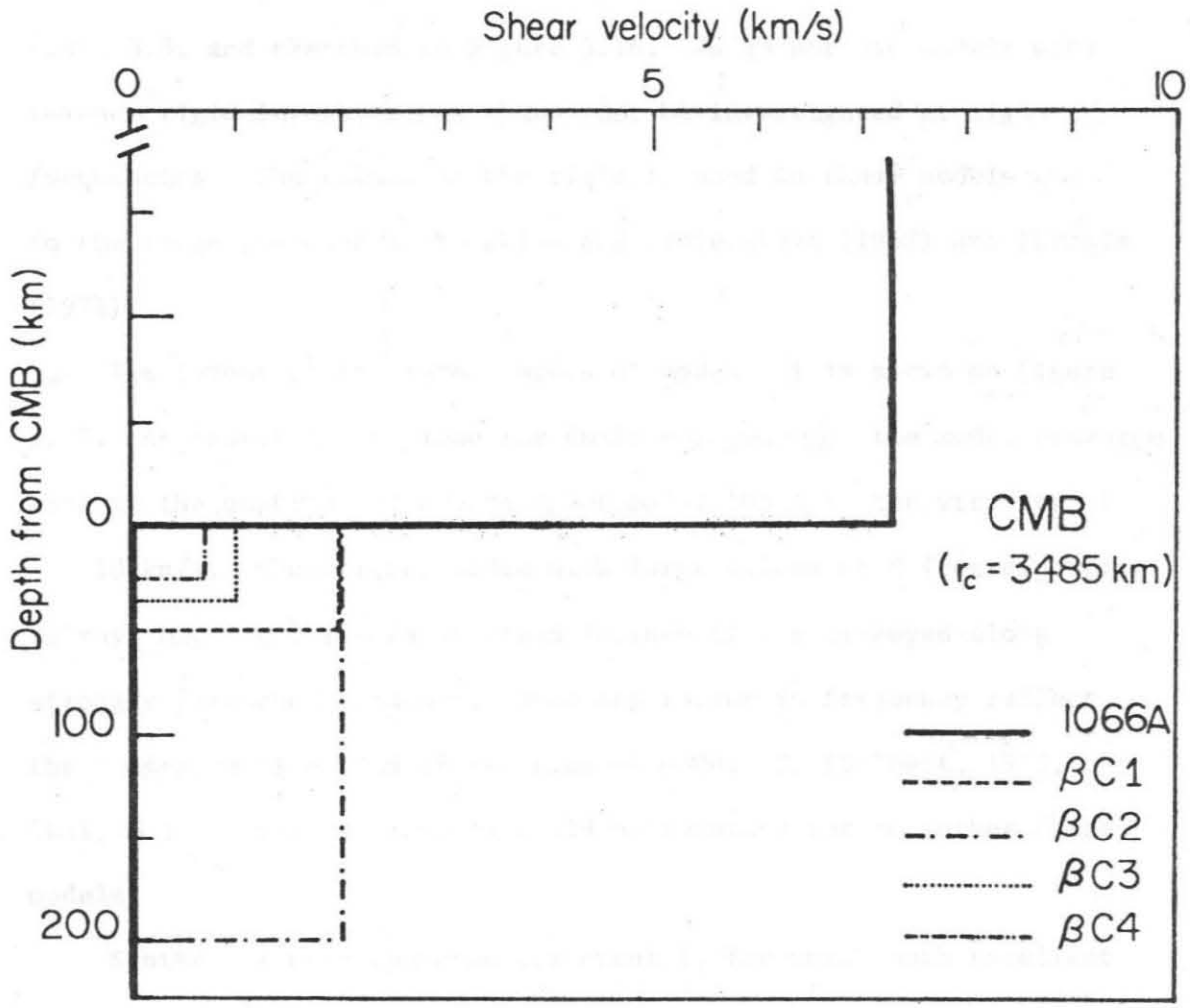

Figure 3.16. Sketches of the models used in the investigation of the possible rigidity of the upper part of the core. All models are identical to 1066A in the mantle and below a depth of 200 km, measured from the core-mantle boundary.

with a large amount of apparently contradictory seismic data (vertical ScS time; free oscillation eigenperiods, etc...). We chose to investigate if the existence of a layer of slightly rigid material just below the CMB is compatible with Sd amplitudes.

For this purpose, we use four models, which are described in Table 3.3, and sketched in Figure 3.16. We do not use models with thinner rigid layers, since these must be investigated at higher frequencies. The values of the rigidity used in these models are in the range proposed by Balakina and Vvedenskaya (1962) and Ibrahim (1971).

The layout of the normal modes of model βC1 is shown on Figure 3.17. As expected from mode-ray duality arguments the modes converge back to the unperturbed overtones of model 1066A in the vicinity of $C = 10$ km/s. However, the modes with large values of C (corresponding to rays hitting the core at steep incidence) are arranged along strongly perturbed branches, whose separation in frequency reflect the longer vertical ScS travel time of model βC1 (Gilbert, 1975; Okal, 1978a). Similar layouts would be obtained for the other three models.

Synthetics were computed for event 1, for which both excellent data and an accurate focal mechanism are available. Figure 3.18 compares the various synthetics with the data. In all four models, Sd disappears as a distinct seismic phase around 115^{o}: in models βC1 and βC2, the phase simply vanishes, while in models βC3 and βC4, which have lower rigidities, the corresponding energy is smeared out, perhaps as a result of interference phenomena in the rigid layer.

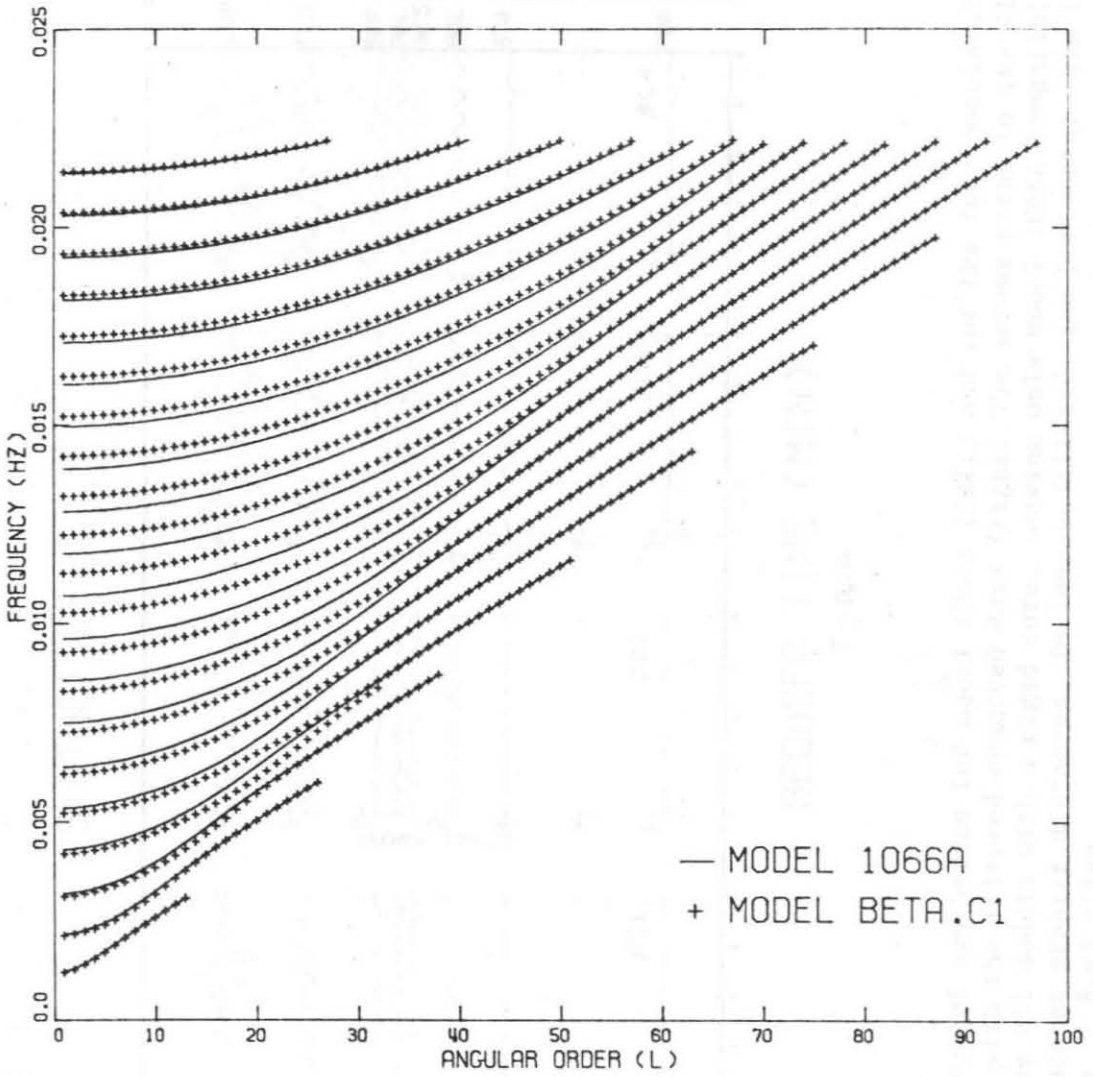

Figure 3.17. Frequency versus angular order plot of the modes with phase velocity greater than 9 km/s, and period greater than 45s, for model βC1. The + signs are the individual modes for model βC1, the full lines the regular overtones for the unperturbed model 1066A.

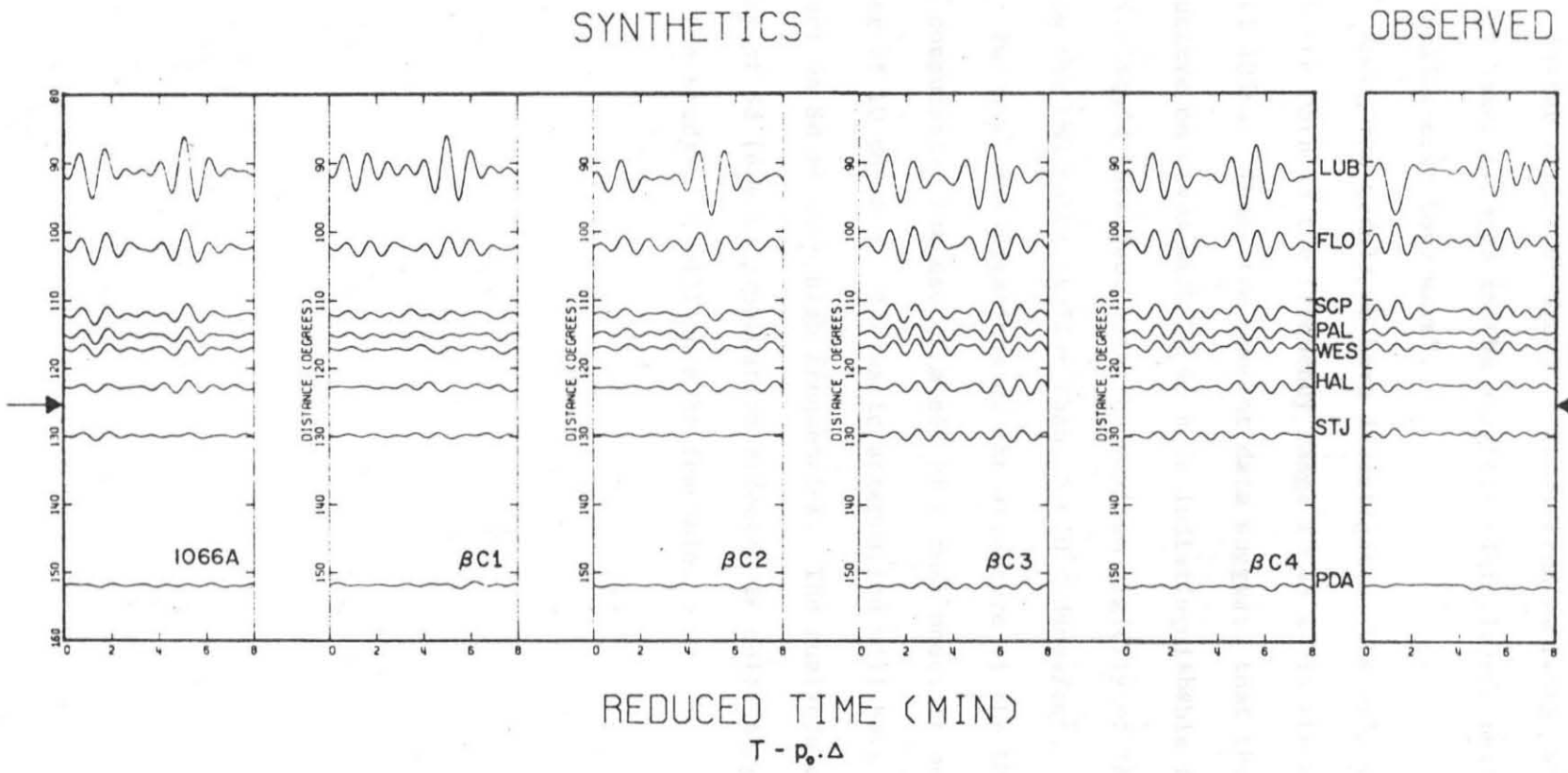

Figure 3.18. Comparison of synthetics for model 1066A (left) and for the four models with rigidity in the core (center), with the filtered observed data (right).The arrows point to the distance 125°, where Sd disappears for all models with a rigid core, leaving only model 1066A compatible with the observation of the phase at greater distances. To improve clarity, the horizontal axis is scaled in reduced time, using p_o = 8.43 s/deg.

This faster amplitude decay is considered as being caused by seismic energy being trapped in the slightly rigid layer, perhaps as a kind of "upside-down Love wave".

Among the models we have investigated, the only one compatible with the data in the frequency range $T \geq 45$ s is the conventional model 1066A. Thus, the present data suggest that the effect of CMB structure on waves with $T \geq 45$ s is indistinguishable from a simple solid-liquid interface with the maximum rigidity of the "liquid" below the CMB being smaller than 5×10^{10} dynes/cm^2.

Further investigations of the structure of the CMB will require the computation and use of a set of normal modes at periods on the order of 10 to 20 s. Anelastic attenuation will have an important effect on Sd at such high frequencies. The analysis of the elastic decay of Sd (due to propagation effects) is quite straightforward, and the study of Q will then be feasible.

3.4 Conclusion

By studying several profiles of SH waves diffracted around the core (Sd), their average slowness is found to be $p_o = 8.4 \pm 0.1$ s/deg. When this value is interpreted as being due to the S velocity just above the core-mantle boundary (β_c), it implies $\beta_c = 7.22 \pm 0.1$ km/s, in contrast to previous models requiring a low S velocity zone just above the CMB.

Synthetic seismograms computed by summing normal modes may be used to study the effect of different CMB velocity structures on Sd waveshapes. They confirm the absence of a low-velocity zone affecting waves with $T \geq 45$ s and show that certain models with non-zero S velocity below the CMB are inadmissible.

II. SEISMIC INVESTIGATIONS OF UPPER-MANTLE LATERAL HETEROGENEITY

INTRODUCTION

Over the past 15 years, the theory of plate tectonics has given a new dimension to our knowledge of the structure of the Earth and of the mechanisms by which it evolves. J. Tuzo Wilson (1976) recently summarized in the following terms the breadth of this theory:

> "The acceptance of continental drift has transformed the earth sciences from a group of rather unimaginative studies based upon pedestrian interpretations of natural phenomena into a unified science that holds the promise of great intellectual and practical advances."

One of the basic premises of plate tectonics is that relatively thin plates are moving about over a partially molten asthenosphere (Anderson, 1962; Anderson and Sammis, 1970). Parameters of this very simple model can be adjusted to allow for lateral heterogeneity, notably for structural differences between oceans and continents, and for intrinsic heterogeneities inside the oceanic plates.

Seismic evidence for structural differences between continents and oceans was reported by Gutenberg, as early as 1924. Systematic regionalization of seismic data (Anderson and Toksöz, 1963; Dziewonski, 1970; Kanamori, 1970) have indicated that the oceanic lithosphere is faster than the continental one but that the oceanic asthenosphere, being probably both thicker and structurally slower, is globally slower than the continental one (if any). Furthermore, because of the distribution of seismic stations and epicenters, most studies of the structure of the Earth have a strong continental bias. Free oscillation results (Jordan and Anderson, 1974; Gilbert and Dziewonski, 1975; Anderson and Hart, 1976) have suggested that the average Earth has slower seismic velocities than determined from body-wave solutions.

Recent studies (Liu et al. 1976; Kanamori and Anderson, 1977) have shown that a substantial part of this discrepancy between body- and surface-wave results is due to neglecting the effect of attenuation in surface-wave studies. On the other hand, it has been proposed (Jordan 1975 a,b) to explain this apparent continent versus ocean heterogeneity through models extending structural differences to much greater depths (possibly as deep as 650 km), and involving complex circulation and differentiation of material in the mantle. In view of the limited depth resolution of surface waves (from which most of the information regarding oceanic upper-mantle structure was obtained), it appears necessary to test the basic plate tectonics premise through independent means. One such possibility is offered by the study of multiply reflected ScS phases, presented in Chapter 1.

Lateral heterogeneity within the oceanic plate has been extensively studied under many aspects: bathymetry (e.g. Tréhu et al., 1976), heat flow (e.g. Parsons and Sclater, 1977), gravity (e.g. Kono and Yoshii, 1975), analysis of volcanic patterns (Vogt, 1974 a, b), and, of course, seismic properties (e.g. Hart and Press, 1973; Kausel et al., 1974, Forsyth, 1975, Yoshii, 1975). Most of the data is consistent with a general thickening of the oceanic lithospheric plate with age, as described, for example, by Leeds et al. (1974). An exact knowledge of the structural properties of the oceanic plates is then a major asset in investigating lateral variations in the deep structure of the mantle, particularly under continents, whose smaller size restricts the data available for direct investigations. The use of very long period Rayleigh waves (T = 200

to 300 s) makes possible a sampling of the mantle to a depth of about 600 km. Such an investigation of the lateral heterogeneity of the mantle in the light of intrinsic oceanic inhomogeneities is the subject of Chapter 2.

In both cases, it is concluded that the simple plate tectonics model with only shallow lateral heterogeneity is sufficient to adequately model all observed seismic lateral variations.

The results in Chapter 1 have been published as Okal and Anderson (1975), those in Chapter 2 as Okal (1977) and Okal (1978b).

CHAPTER 1

Lateral Heterogeneities in the Upper Mantle From Multiple ScS Travel-Time Residuals.

1.0 Introduction

In this chapter, multiply reflected ScS travel-times are used in an investigation of the lateral heterogeneity of the upper mantle. Several arguments can be made in favor of using shear rather than compressional waves: First, as they travel slower, the relative residuals are expected to be larger, and therefore, more accurate for shear waves than for compressional ones. Second, it is usually assumed that the low velocity zone, which was suggested by Gutenberg (1926, 1948), then identified by Dorman et al. (1960) under oceans, and later studied under North America by York and Helmberger (1973), represents a partially molten asthenosphere (Green, 1972) involving high attenuation (Helmberger, 1973) and a higher Poisson ratio. This last point is consistent with experimental observations of upper mantle shear structure (Helmberger and Engen, 1974), and contributes to making S wave travel-times even more sensitive to lateral variations in the properties of the low velocity zone. Finally, SH waves (and at, a steep incidence, because of favorable reflection coefficients, SV-polarized shear waves), stay trapped between atmosphere and liquid core and can sample the mantle through multiple reflections more efficiently than their PcP counterparts, whose energy leaks into the core and whose multiples are not regularly observed.

Regional studies of S wave travel-time residuals have been carried out, notably by Ibrahim and Nuttli (1967), Hales and Roberts (1970) and Sengupta and Julian (1974). A global investigation of lateral variations in shear wave travel-times was made by Sipkin

and Jordan (1975), who studied lateral inhomogeneities of the upper mantle by use of the phase ScS for a number of deep events. They found a difference of 5 seconds between oceans (slow) and continents (fast), and argued that continental and oceanic mantle must differ to at least 400 km and possibly as deep as 600 km. However, in their study, oceanic data rest entirely on the use of only 4 stations, which they presume represent normal ocean: Kipapa, Hawaii (KIP); Rarotonga, Cook Islands (RAR); Afiamalu, Western Samoa (AFI) and Bermuda (BEC). All of these are on volcanic islands whose activity is in no case older than 30 million years. It is questionable, indeed, whether any island station can be taken as standing on typical oceanic lithosphere. In order to investigate travel-time anomalies in areas where no stations are available, we study travel-time residuals for multiply-reflected ScS waves. The surface-reflection points of many of these phases are at places which cannot be studied by use of direct phases, such as S or ScS, notably under oceans. Figure 1.1 is a sketch of the ray path of these phases across the mantle.

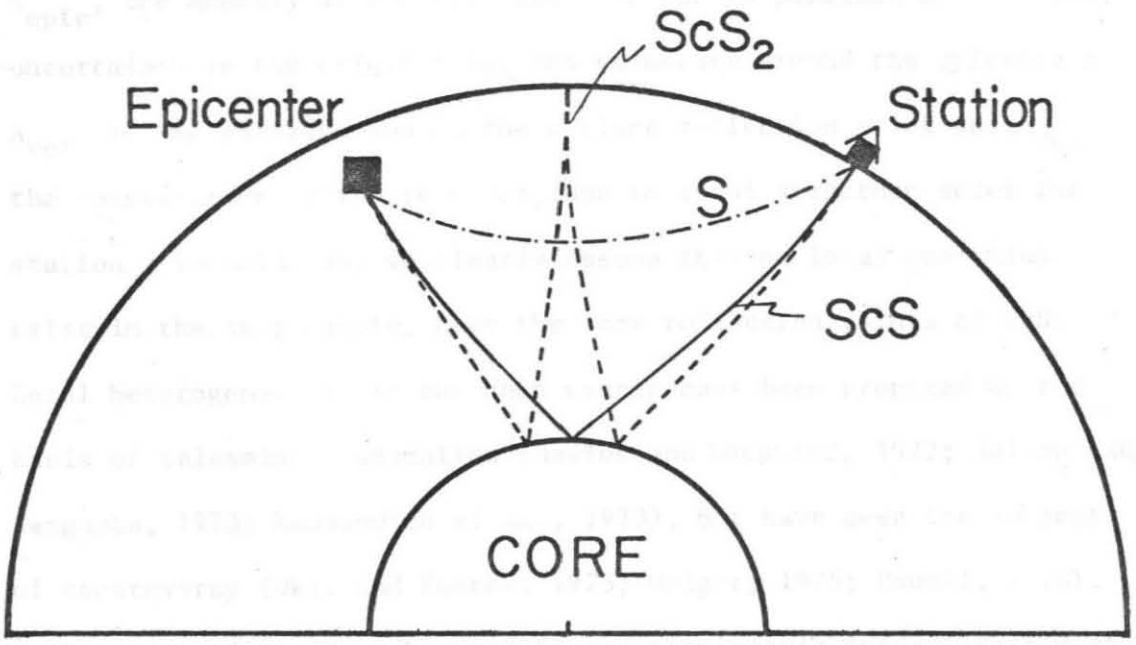

Figure 1.1. Sketch of the ray paths of S, ScS and ScS_2 through the mantle from a deep earthquake. (For clarity, the size of the core has been reduced.)

1.1 Outline of the Method

The residual δ (observed minus Jeffreys-Bullen (JB) times), say for ScS_2, may be written:

$$\delta_{ScS_2} = A_{epic} + A_{refl} + A_{rec} \,. \qquad (1.1)$$

A_{epic}, the anomaly at the epicenter, is due to possible mislocation, uncertainty in the origin time, and structure around the epicenter; A_{refl} is the contribution at the surface reflection point and A_{rec} the contribution at the receiver, due to local structure under the station. In doing so, we clearly assume that no local anomalies exist in the deep mantle, near the core reflection points of ScS. Local heterogeneities in the deep mantle have been proposed on the basis of teleseismic anomalies (Davies and Sheppard, 1972; Julian and Sengupta, 1973; Kanasewich et al., 1973), but have been the subject of controversy (Okal and Kuster, 1975; Wright, 1975; Powell, 1976). Both seismic data (Doornbos, 1975) and gravimetric interpretation of satellite navigation data (Lambeck, 1976) suggest that the scale of possible lateral heterogeneities in the lower mantle is probably very small. No feature extending over a characteristic length the size of a continent has ever been reported. Although such models cannot be excluded by the present analysis, our goal is to explain the travel-time anomalies by simple models restricting them to the upper mantle.

Because of the quasi-vertical incidence of any ScS path, the anomalies A_{epic} and A_{rec} are approximately the same for ScS or any

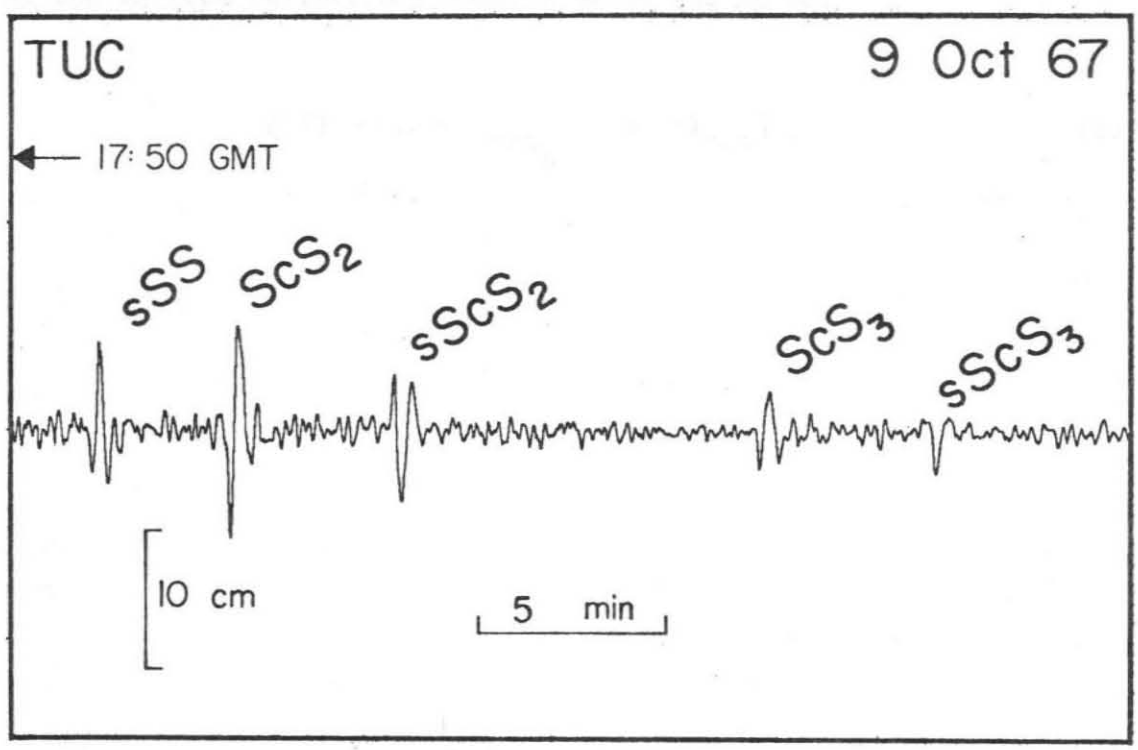

Figure 1.2. Example of a typical record of multiply-reflected ScS phases.

ScS_n. Therefore, the difference in time residuals $\delta_{ScS_2} - \delta_{ScS}$ clearly represents A_{refl}, which, in turn, because of the steep incidence of any ScS_n, is approximately equal to twice the one-way anomaly to a vertical S, due to upper mantle structure under the reflection point. In the case of a higher order ScS_n, such anomalies at the various reflections would clearly add up to:

$$(1/2) \cdot [(o-c)_{ScS_n} - (o-c)_{ScS}] \, . \qquad (1.2)$$

1.2 Data Set and Data Processing

For the present study, we used long-period records from ten deep earthquakes, listed on Table 1.1. Figure 1.2 shows a typical trace of ScS_2 and ScS_3, together with the surface-reflected $sScS_2$ and $sScS_3$. We chose not to use these surface-reflected phases, which, for the most part, travel upwards in the slab in the vicinity of the source: A slight change in the ray parameter can result in a substantial difference in the paths travelled (Toksöz et al. 1971), and in an important term $A_{epic}(sScS_n) - A_{epic}(sScS_m)$. At distances larger than 70^o, the phase S was used rather than ScS and the time anomalies involved were $(o-c)_{ScS_2} - (o-c)_S$. It will be shown that this does not introduce any systematic bias in the results.

Records were digitized and cross-correlated to obtain $o_{ScS_2} - o_{ScS}$. Computed values, obtained from Jeffreys and Bullen's (1940) Tables were corrected for ellipticity, using Bullen's (1938) tables for ScS. A further correction was needed to take into account the topographical elevation at the surface-reflecting point, for which a surface velocity of 3.36 km/s was used. The (two-way) correction is then 0.595 second per km of altitude, or, in the case of a sea-bottom reflection, -1.07 second per 1000 fathoms of depth.

We estimate that the resulting one way residuals are accurate to ±0.5 second.

All of the cross-correlated phases were time-lagged and plotted superimposed. A quality index was assigned, depending on the fit of the superposition, varying from 3 (excellent) to 0 (bad). All data with quality indices 0 and 1 were eliminated. Figure 1.3 shows a

Table 1.1

Seismic Events used in the Multiple ScS Study

	Event	Date	Origin Time GMT	Epicenter °N	Epicenter °E	Depth km	m_b
1	Fiji-Tonga	9 Oct 67	17:21:46.2	-21.10 ;	-179.26	605	6.2
2	Argentina	8 Dec 62	21:27:20.0	-25.78 ;	-63.13	582	*
3	Fiji-Tonga	10 Feb 69	22:58:03.3	-22.75 ;	178.76	635	6.0
4	Argentina	9 Sep 67	10:06:44.5	-27.62 ;	-63.15	577	5.9
5	Okhotsk Sea	29 Jan 71	21:58:03.2	51.69 ;	150.97	515	6.0
6	Okhotsk Sea	30 Aug 70	17:46:08.9	52.36 ;	151.64	643	6.5
7	Banda Sea	18 Oct 64	12:32:24.9	-7.17 ;	123.86	585	5.8
8	Peru-Brazil	15 Feb 67	16:11:11.8	-9.05 ;	-71.34	598	6.1
9	Banda Sea	11 Feb 69	22:16:11.5 ;	-6.76 ;	126.74	425	6.0
10	Peru-Brazil	3 Nov 65	01:39:03.2	-9.04 ;	-71.32	587	5.9

(*) No body-wave magnitude reported. $M_{[PAL]}$ = 6 3/4 .

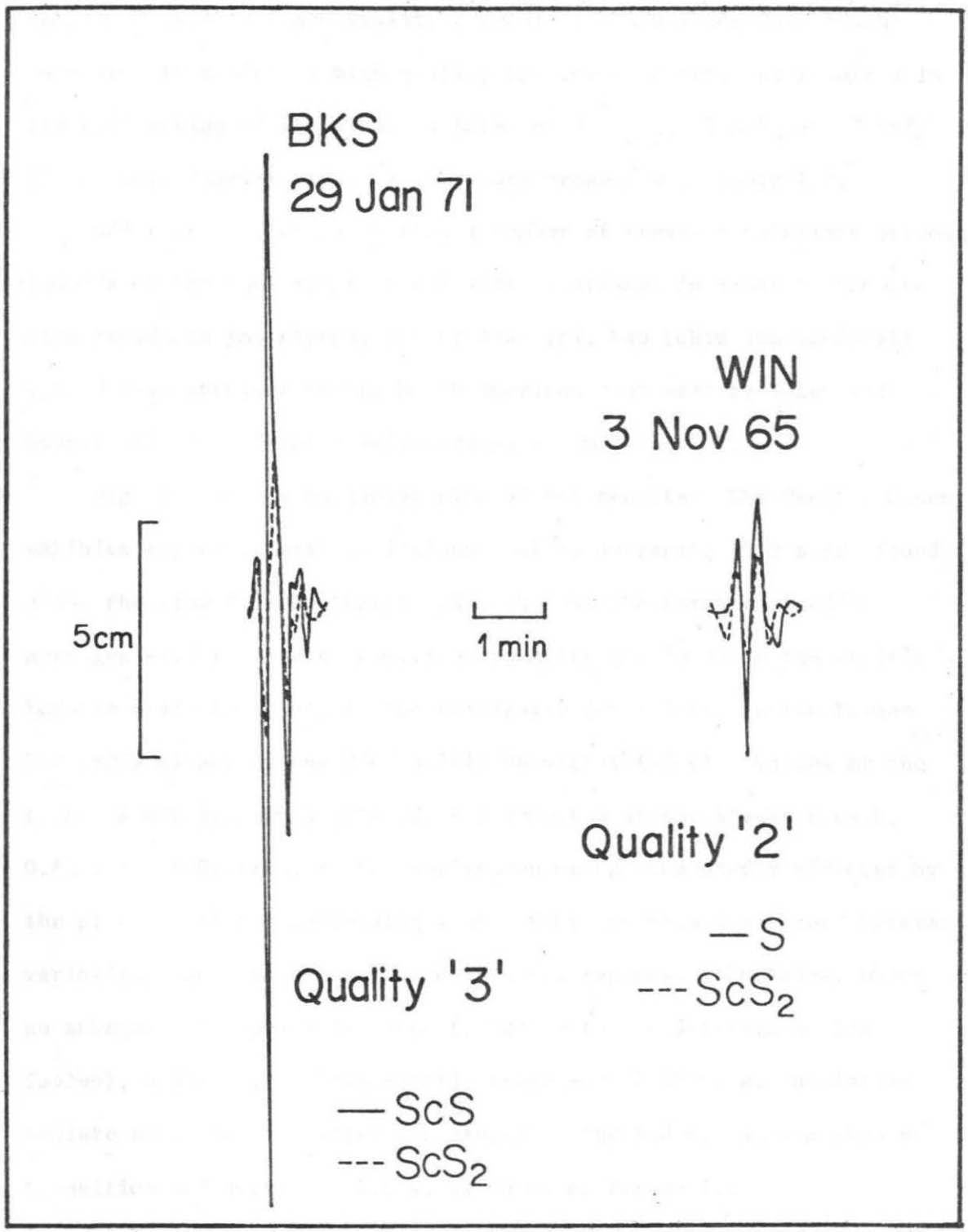

Figure 1.3. Samples of 'Quality 3' and 'Quality 2' pairs of cross-correlated phases. Distances are 59.6° for Berkeley (BKS) and 85.2° for Windhoek (WIN).

sample of quality 3 and quality 2 records. This check was thought necessary to achieve a high quality for the data set. It resulted in the elimination of 24 pairs. A total of 77 ScS_2, 15 ScS_3 and 2 ScS_4 phases were finally used. Results are presented in Table 1.2.

Additionally, we calculated a number of cross-correlations between records of the same event at different stations, in order to compare some residuals (at Kipapa, Poona, Akureyri, Kap Tobin and Windhoek) with delays obtained on the North American continent by Hales and Roberts (1970). These results are given in Table 1.3.

Figure 1.4 is a worldwide plot of our results: The Pacific Ocean exhibits strong lateral variations: values averaging +0.9 s are found along the line Fiji-Southwest U.S., whereas the Northern Pacific averages -1.2 s. Strong positive anomalies are found in the Artic's Eurasia Basin (+2.3 s), in the Philippine Sea ($\sim$3 s), in the Tasman Sea (+3.9 s) and at the Mid-Pacific Mountains ($\sim$5 s). Values at the trenches are largely scattered, (-1.1 ± 0.6 s at the Alaska trench, 0.4 ± 2 s off Guatemala), the reflection being undoubtedly affected by the presence of the descending slab. South America also shows lateral variations, and can be separated into two regions: the Andes, where no substantial anomaly is found (relative to the Jeffreys-Bullen Tables), and the Brazilian shield, averaging -2.15 ± 1 s. An intermediate zone, located along the slopes of the Andes, makes a smooth transition and averages -1.2 s, as shown on Figure 1.5.

It is not possible to account for these data with Sipkin and Jordan's (1975) hypothesis of a simple continent vs. ocean difference. Their model of a 5 s delay of oceanic travel-time would lead to a

Table 1.2

Two-way Residuals obtained in this Study

Event, station and phases used			Quality index	$o_2 - o_1$ (s)	Ellipticity correction (s)	Altitude correction (s)	Two-way residual (s)
1	AFI	2-1	2	936.5	1.0	-1.1	4.4
1	MUN	2-1	2	827.5	0.3	0.3	2.1
1	TAU	2-1	2	892.5	0.1	-1.0	7.8
1	ALQ	2-1*	3	753.5	3.1	-3.0	0.6
1	TUC	2-1*	3	771.5	3.2	-2.9	3.9
1	LUB	2-1*	3	745.5	3.1	-2.9	-1.9
1	ALQ	3-2	2^-	845.5	1.0	-2.4	2.9
1	FLO	3-2	3	822.0	0.9	-2.1	0.8
1	COL	3-1*	2	1593.0	1.3	-6.6	0.6
1	ALQ	4-2	3	1734.5	3.3	-5.1	7.8
2	BHP	2-1	2	878.5	3.3	0.1	-2.1
2	BEC	2-1	3	824.0	1.4	0.4	-3.5
2	ARE	2-1	3	933.5	0.8	2.2	0.4
2	CAR	2-1	2	881.0	1.3	0	-4.1
2	LPB	2-1	2	936.0	0.8	2.5	0.8
2	COR	2-1*	2	756.5	1.3	-2.0	4.8
2	LPA	2-1	2	929.5	0.3	0	-2.9
2	FLO	2-1	2	794.5	1.4	1.1	-4.3
2	LPA	3-1	2^-	1865.0	0.7	0	-3.1
2	CAR	3-1	2	1798.5	2.5	0.1	-5.7
2	LPB	3-1	2	1872.0	1.7	2.2	0.9
2	DUG	2-1*	2^+	783.0	1.3	-1.5	-0.9
2	WES	2-1*	2	840.0	1.3	0	-7.1
3	KIP	2-1	2	851.0	1.4	-3.6	5.0
3	ALQ	2-1*	3	750.5	1.3	-2.9	2.8

Table 1.2
(continued)

3	TUC	2-1*	2	759.0	1.4	-2.9	-0.2
3	SHK	2-1*	3	825.0	1.4	-2.6	3.2
3	LUB	2-1*	3	741.0	1.4	-2.9	-1.1
3	TUC	3-2	3	847.5	1.0	-2.8	2.7
3	ALQ	4-2	3	1723.0	2.0	-4.7	4.3
4	NNA	2-1	3	921.0	0.9	0.5	0.9
4	ARE	2-1	3	933.5	0.8	2.2	2.0
4	SPA	2-1	2	809.5	-1.6	-2.4	0.3
4	TUC	2-1	2^-	783.0	1.4	-1.4	0.7
4	GEO	2-1	3	796.0	1.4	0	-5.9
4	SJG	2-1	2^-	857.0	1.3	0	-3.6
4	TRN	2-1	2	875.0	1.3	0	-4.6
4	OXF	2-1	2^+	800.5	1.4	1.8	-5.3
4	QUI	2-1	2	900.5	1.1	2.6	0.2
4	ARE	3-1	2^-	1869.0	1.6	1.1	0.1
4	NNA	3-1	3	1854.0	1.8	-2.9	-0.2
4	DUG	2-1*	2^-	775.0	1.3	-1.6	-3.3
5	DAV	2-1	2	854.0	0.4	-2.3	6.0
5	DUG	2-1	3	807.0	-1.5	0	-3.6
5	PMG	2-1	2	815.5	0.9	-1.6	-1.8
5	MAT	2-1	2^-	921.5	-0.6	0	-0.9
5	MAN	2-1	2	869.5	0.1	0	5.5
5	COL	2-1	2^-	890.5	-1.8	0	0.9
5	CHG	2-1	2	843.0	-0.2	0	1.5
5	COR	2-1	2	831.0	-1.5	0	-2.8
5	AKU	2-1	2	813.0	-2.7	-2.2	4.5

Table 1.2
(continued)

5	BKS	2-1	3	815.0	-1.3	-2.2	-3.1
5	NDI	2-1	2^-	822.0	-0.8	0.9	-3.4
5	LON	2-1	3	834.0	-1.6	0	-1.3
5	AFI	2-1	2^-	797.0	1.0	-1.6	10.0
5	TAU	2-1*	2	737.5	1.5	-2.2	-5.8
5	MUN	2-1*	2^-	752.0	1.4	-3.5	-2.5
5	AAM	2-1*	2	810.0	-2.2	0.9	2.2
5	MAN	3-1	2^-	1783.5	0.2	1.6	12.1
5	MAT	3-1	2	1852.0	-1.2	0	-2.0
5	DAV	3-1	2^-	1758.5	0.6	-3.8	7.6
6	LON	2-1	3	834.5	-1.6	0	-1.5
6	COR	2-1	2^+	833.0	-1.5	0	-1.5
6	KIP	2-1	2^+	841.5	-0.3	-3.3	-3.1
6	RAB	2-1	3	825.5	0.7	-3.3	-1.0
6	HNR	2-1	2	813.0	0.9	-3.3	1.3
6	FLO	2-1	2^+	783.0	-1.9	0.2	2.1
6	MUN	2-1*	3^-	747.5	1.4	-3.5	-3.5
6	ADE	2-1*	2^+	755.0	1.4	-2.2	-2.0
6	FLO	3-1	2	1811.0	-3.6	0	0.8
7	WEL	2-1	2	831.0	0.5	0.1	1.0
7	SBA	2-1	2	779.5	-0.5	-2.9	1.3
8	ALQ	2-1	3	835.0	1.1	0.4	0
8	LPB	2-1	2	935.0	1.2	0.1	0.1
8	MNT	2-1	2	834.5	1.0	0	0.5
8	JCT	2-1	2	857.5	1.2	0	3.5
8	AAM	2-1	2^-	842.0	1.0	-1.1	1.6

Table 1.2
(continued)

8	WES	2-1	3	843.0	1.0	-2.3	0.6
8	TUC	2-1	2	831.5	1.2	-1.6	0.7
8	WIN	2-1*	2	790.5	0.8	0	23.6
8	SDB	2-1*	2^-	768.0	1.0	-3.2	-3.9
8	GDH	2-1*	2	788.0	0.4	-3.0	2.0
8	CMC	2-1*	3^-	775.0	0.6	0	0.3
9	AFI	2-1	3	814.5	1.1	-1.2	-4.6
10	WIN	2-1*	2	790.0	0.8	0	22.9
10	SDB	2-1*	2^-	767.5	1.0	-3.2	-4.6

(*) Asterisk indicates the use of S in lieu of ScS at distances greater than 70°.

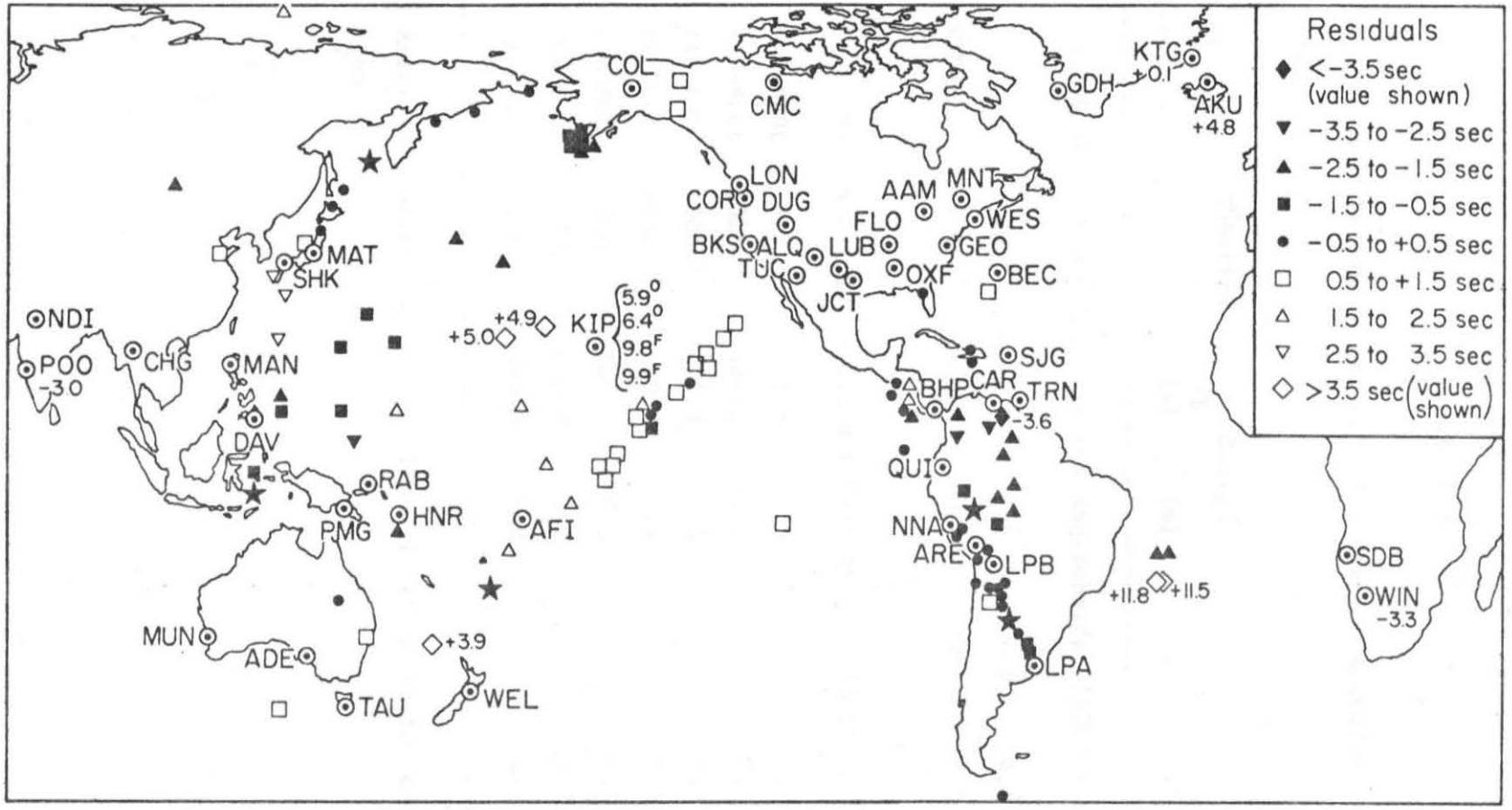

Figure 1.4. Map of the world showing one-way S anomalies as described in legend. Values larger than 3.5 s in absolute value are shown in full. Stars each identify two events. Stations not shown are SBA (Scott Base) and SPA (South Pole). Numbers adjoining stations are anomalies derived directly from S or ScS (see Table 1.4). At KIP, O and F identify data respectively from the Okhotsk and Fiji areas.

Table 1.3

Direct Determination of a Few Station Anomalies

Event and stations used	Observed (s)	Ellipticity JB (s)	Ellipticity (s)	Topography (s)	o - c (s)	Station residual (s)
A. Base : ALQ = 1.1 s (Hales and Roberts, 1970) (ScS_2)						
1 COL-ALQ	10.0	2.8	2.1	-0.2	9.1	COL 2.1
8 WIN-ALQ	184.5	163.4	0.1	-0.4	21.4	WIN -3.3
B. Base : COL = 2.1 s (from above) (ScS)						
1 KIP-*COL	312.5	321.8	-1.5		7.8	KIP 9.9
3 KIP-*COL	315.0	324.2	-1.5		7.7	KIP 9.8
6 KIP-COL	-108.5	-102.9	1.3		4.3	KIP 6.4
5 KIP-COL	-104.5	-99.3	1.4		3.8	KIP 5.9
5 KTG-COL	158.0	160.3	-0.3		-2.0	KTG 0.1
5 POO-COL	230.5	233.9	1.7		-5.1	POO -3.0
5 AKU-COL	196.5	194.6	-0.2		2.1	AKU 4.2

(*) Asterisk denotes use of S in lieu of ScS at distances greater than 70°.

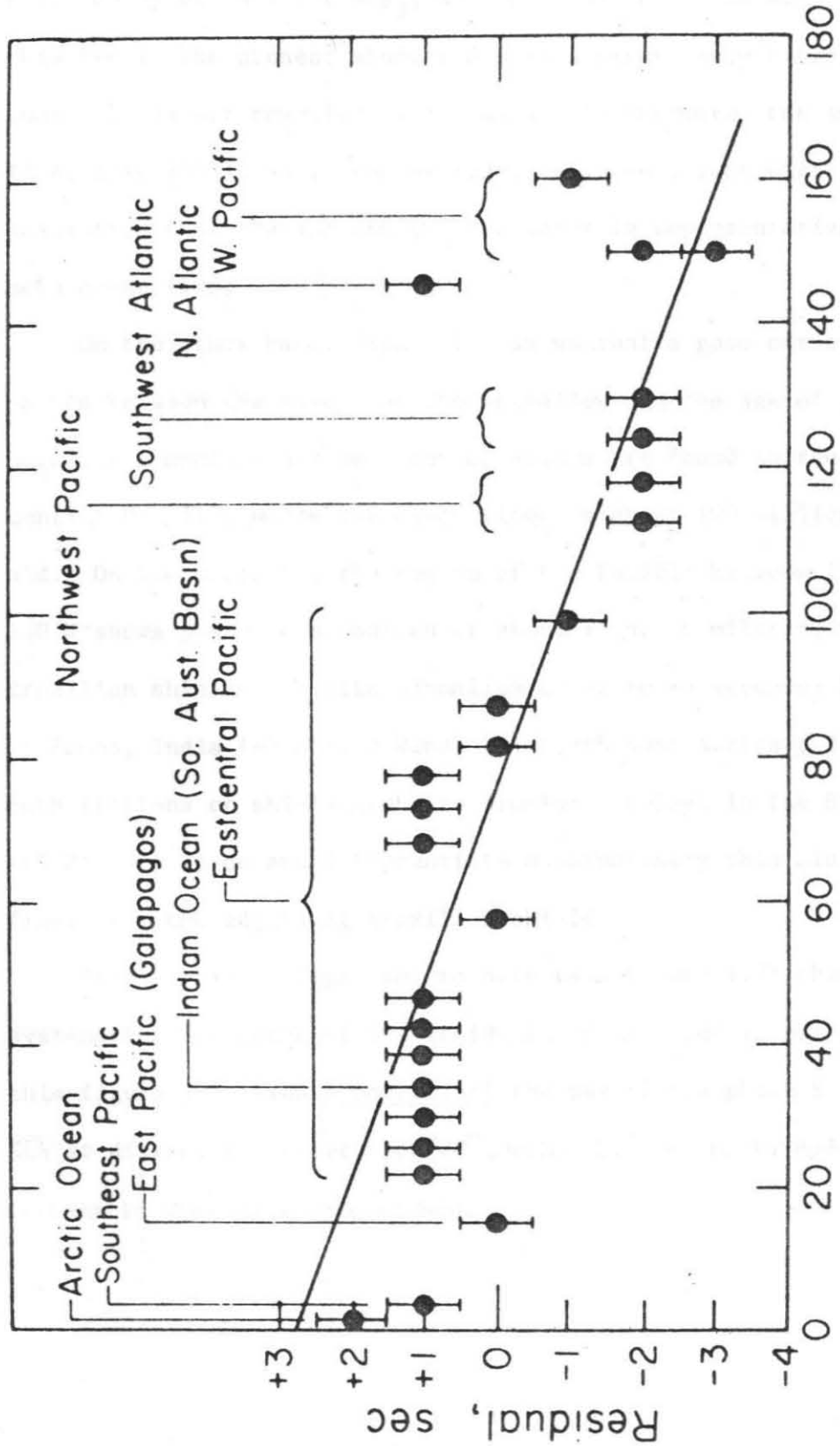

Figure 1.5. Variation of one-way residuals with the age of the oceanic plate.

total delay of 20 s for ScS_3, and 30 s for ScS_4. No such values are obtained in the present study and such a discrepancy between ocean and continent is not revealed by our data. Furthermore, the small anomaly +1 s, only 250 km away from Bermuda, is inconsistent with their assumption that station BEC ($\sim$3.5 s late) is representative of the mean ocean floor.

On the other hand, Figure 1.6 shows that a good correlation exists between the values of the anomalies and the age of the plate: negative anomalies on the order of -1.5 s are found in the North-central Pacific, where the ocean floor is about 100 million years old. On the opposite, the region of the Pacific between 125 and 150°W shows positive anomalies of about +1 s. Similarly, the Brazilian shields exhibits anomalies of -2 to -3 seconds; ScS delays at Poona, India (-3 s) and Windhoek, South West Africa (-3.3 s), both stations on shield are also similar. Delays in the Brazil Basin (-2.05 ± 0.5 s) do not differentiate substantially this old oceanic floor from the adjoining Brazilian shield.

Finally, it is important to note (see Figure 1.7) that no systematic dependence of the residuals on distance is present. Also, this figure justifies a posteriori the use of the phase S in lieu of ScS at distances greater than 70°, which is seen to introduce no systematic biasing in the method.

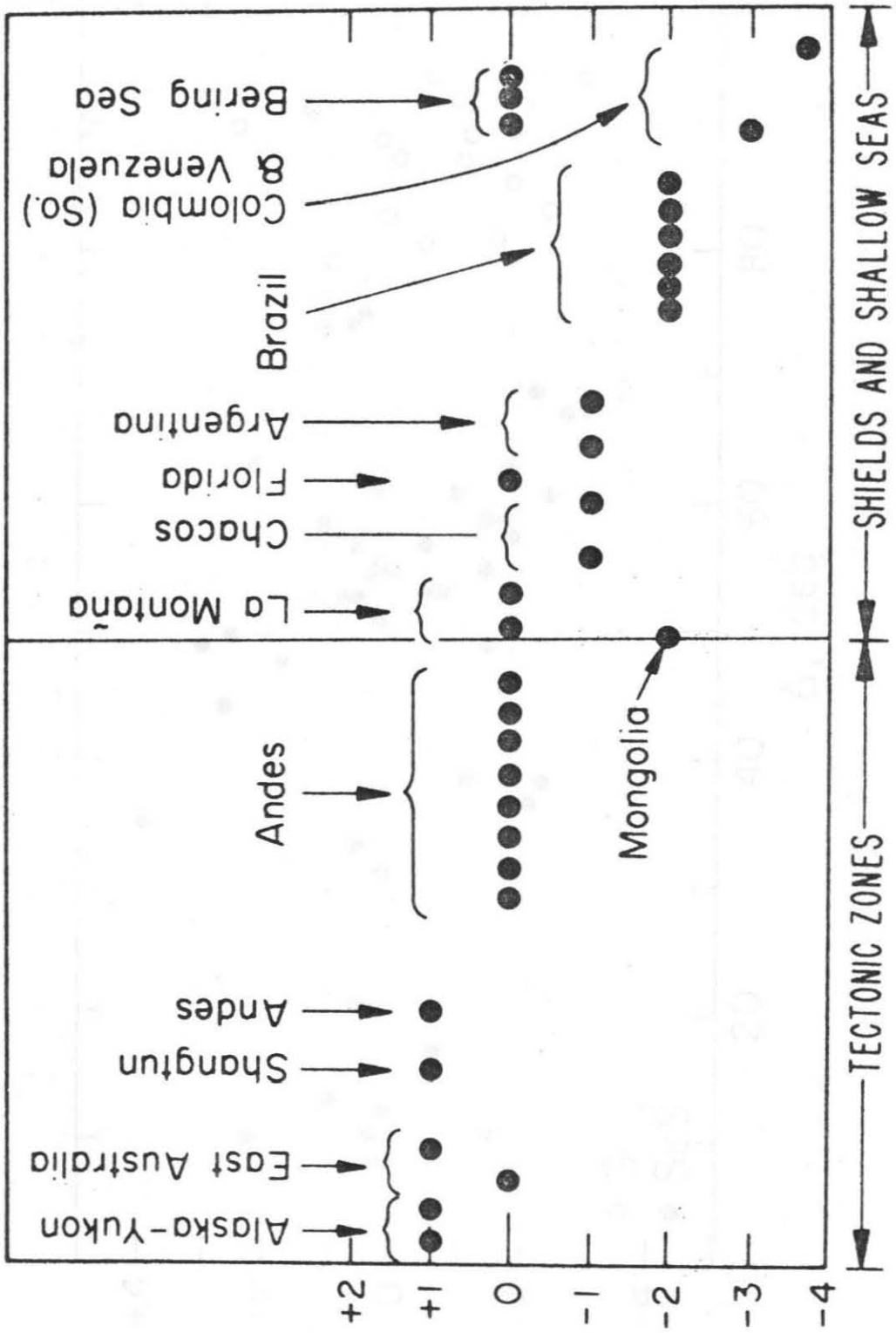

Figure 1.6. Variation of one-way continental and shallow sea ScS residual with tectonic structure.

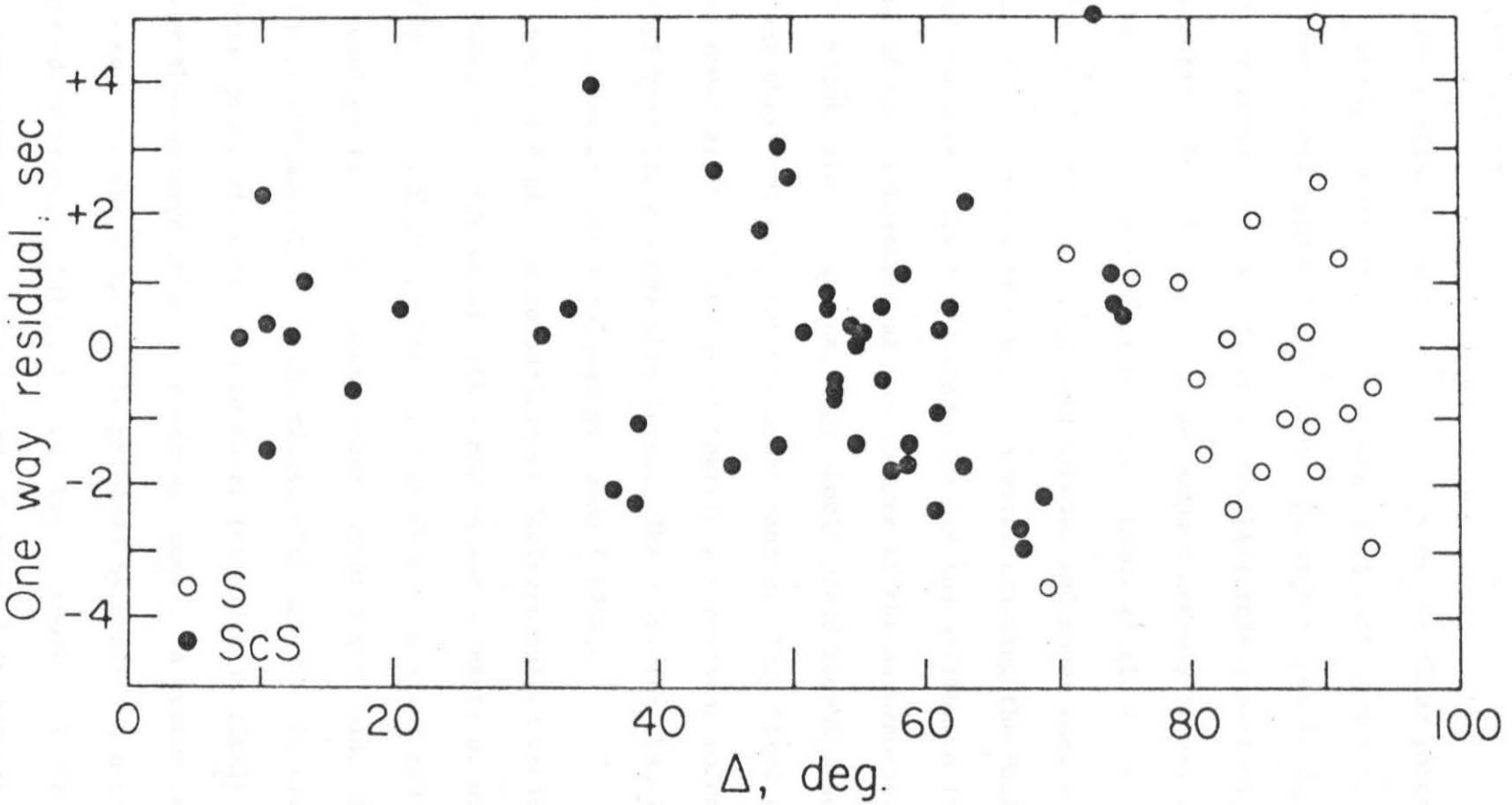

Figure 1.7. Plot of one-way ScS residuals as a function of distance between epicenter and stations. Note that no definite trend is present. Also note that the substitution of S for ScS at larger distances does not introduce any systematic bias.

1.3 Discussion

The similarity in travel-time between the older parts of the ocean and old continental shield argues against deep structural differences and suggests that both regions have poorly-developed low-velocity zones. It is worthwhile checking this important result with other data. For this purpose, we compute one-way travel-times above 180 km, for a variety of structures. Leeds et al. (1974) and Kausel et al. (1974) determined oceanic crustal and upper mantle structure as a function of age from Rayleigh waves crossing the Pacific. They found phase velocity increasing with age and attributed it to thickening of the lithosphere at the expense of the asthenosphere. Although their models are not unique, they should yield roughly the right average shear velocity for the upper mantle. They fixed the base of their model at 180 km and it is therefore convenient to compare average velocities above this level. The model for the oldest part of the ocean was later revised by Leeds (1975).

Table 1.4 gives a comparison of Jeffreys-Bullen residuals for the resulting Leeds et al. (LKK) models and a number of other models. Residuals for LKK in the Pacific vary from -2.1 s for 150 million years old crust to +1.3 s, for young crust, about 5 m.y. old. A value of +1.9 s is extrapolated for the ridge, although this is clearly a minimum value, since the mantle under the ridge is likely to be slower than assumed in any theoretical model. A better estimate (+3.6 sec) for the ridge can be obtained by modifying a structure proposed by Francis (1969), for the region south of Iceland. Alternate estimates of +2.5 to 5.2 s are obtained from measured P-delays

Table 1.4

Jeffreys-Bullen S Residuals for the Upper 180 km in a Variety of Models

Model	Region	Reference	Residual (s)	
			Computed	Observed
LKK (150 m.y.)	Pacific Ocean	f	-2.1	-2.3
LKK (100 m.y.)	Pacific Ocean	a	-1.2	-1.6
LKK (70 m.y.)	Pacific Ocean	a	0.0	+0.9 (50 m.y.)
LKK (10 m.y.)	Pacific Ocean	a	+1.3	
CANSD	Canadian Shield	b	-1.3	-2.0 (Brazil)
C2	Gross Earth	c	-0.7	
CIT11A	Gross Earth	d	-0.6	
SHR14	North America	e	-0.2	

References :

a Leeds et al. (1974)
b Brune and Dorman (1963)
c Anderson and Hart (1976)
d Anderson and Toksöz (1963)
e Helmberger and Engen (1974)
f Leeds (1975).

in Iceland. These values are roughly consistent with those found in this study for AKU (+4.8 s) by direct measure of S and ScS delays. A value of +4.4 sec was also reported along the mid-Atlantic ridge by Girardin and Poupinet (1974). The value obtained from Leeds et al.'s structure for 100 m.y. old lithosphere (-1.6 s) agrees almost exactly with the value (-1.5 s) found here for the oceanic region of this age in the Northcentral Pacific.

The variation of shear velocity with depth in the published models (Jordan and Anderson, 1974; Anderson and Hart, 1976) considered by Sipkin and Jordan (1975) also gives support to the idea that variations in the ScS residuals are due primarily to variations in the upper mantle. For example, the spread of one-way vertical S travel-time for a variety of models, is 2.0 s to 50 km, increasing to 3.0 s to 200 km. Differences between models remain between 1.6 to 3.2 s down to 700 km, indicating that most of the variation is above 200 km. The present conclusions may be compared with those of Tryggvason (1961) who used a particularly favorable geometry of events to study both oceanic and continental structure. He concluded that at a depth less than 400 km, possibly at 140 km, the difference between oceanic and continental structure had disappeared. Our results also compare favorably with those of Hart and Press (1973) who used S_n velocities across the Atlantic to investigate the cooling of the lithosphere away from the ridges. They found a large similarity between continents and old oceanic floor.

Since the present study was originally published in August, 1975, the problem of continent versus ocean heterogeneities has continued

receiving much attention. A similar study by Sipkin and Jordan (1976) has yielded comparable results concerning the variation of S-wave residuals with tectonic age across oceans. However, these authors fail to observe a similarity between shields and the oldest ocean floors, with minimum residuals in the oceans on the order of -1 s. According to Sipkin and Jordan (1976), it is then necessary to extend lateral heterogeneities between oceans and continents to depths greater than 400 km to account for these data (Jordan, 1975 a, b). We believe that the present data, whose quality was strictly constrained by deleting all pairs with poor quality indices, represent a more homogeneous set than Sipkin and Jordan's. The records at Trieste, Italy of event 5 (29 Jan 1971) presented by Sipkin and Jordan (1976) on their Figure 15 (p. 6317), for example, would have been given a quality index of 1^- at the most. Records of such poor quality have not been used in the present study.

Consequently, we think that present reliable multiple-ScS travel-time data do not warrant substantial structural differences between continents and oceans at depths greater than 200 km. This is also in agreement with a study by Lambeck (1976) who used expansions of the Earth's gravity field to study lateral density anomalies in the Upper Mantle. Although this method becomes less sensitive at greater depths, it suggests no long-wavelength correlations between possible seismic and gravity anomalies.

Butler (1977) pointed out that travel-time differences obtained by cross-correlation (as in the present study) may be systematically biased toward longer values, due to the effect of the attenuation

operator Q. For two waves with different travel-times, such as ScS and ScS_2, theoretical wave shapes will be different, resulting in a value of $o_{ScS_2} - o_{ScS}$ increased by roughly a few seconds. The magnitude of this effect is dependent on the value of Q .

Estimates of Q_β for ScS waves in the mantle vary widely. Anderson and Kovach (1964) and Kovach and Anderson (1964) proposed $Q_\beta = 600$, on the basis of South American data, in agreement with Press's (1956) value of 500. Jordan and Sipkin (1977) proposed $Q_\beta = 156 \pm 13$, using a stacking of Western Pacific data. Best et al. (1974) proposed a value of $Q_\beta = 300$ for a vertical path under the Hawaii Islands. Sato and Espinosa (1967) obtained $Q_\beta = 580$ for a path linking South and North America. Yoshida and Tsujiura (1975) used multiple ScS phases recorded in Japan from the Japan Sea deep earthquake of 1973 to propose $Q_\beta = 290$, but their results are rather scattered. Estimates obtained by other methods include $Q_\beta = 380$ (Choudhury and Dorel, 1972) under the Tasman Sea and Southeastern Indian Ocean and $Q_\beta = 230$ (Kanamori, 1967) under Central America, both obtained from the comparison of spectral contents of ScS and ScP.

An attempt was made at using the present data set to solve for Q_β in the mantle. However, the values obtained were too scattered to warrant publication. The problem of body-wave attenuation in the mantle remains open, and Q_β is only definitely constrained to the range 100 to 500.

Figure 1.8 shows a pair of ScS phases for event 2 at BEC. When compared to Butler's (1977) synthetic seismograms, the excellent correlation between the two waveshapes argues in favor of very little

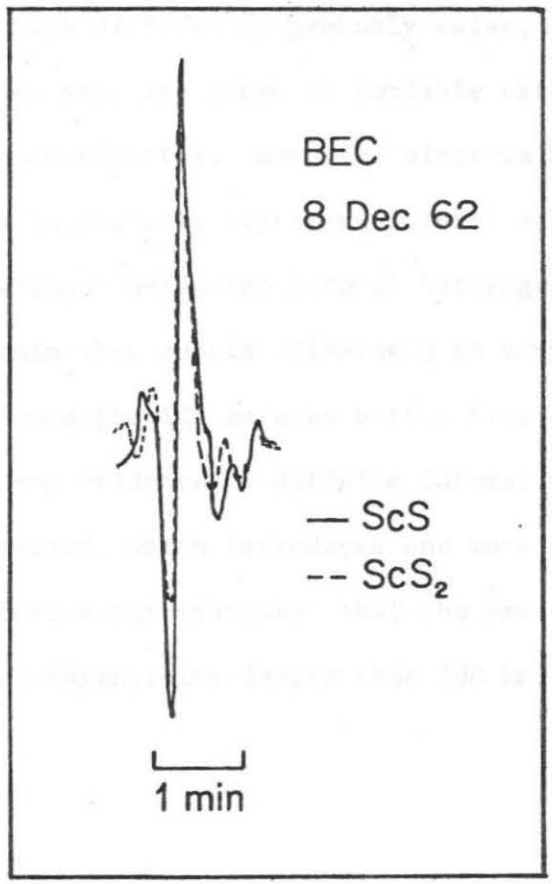

Figure 1.8. Cross-correlated records of event 2 at Bermuda. Note the quasi-identical waveshapes, arguing against any major effect of the attenuation operator Q. The epicentral distance is 57.8°.

attenuation and a large value of Q_β, in agreement with Sato and Espinosa's (1967) proposed $Q_\beta = 580$ over a closely related path.

In any case, the effect of attenuation in biasing $o_{ScS_2} - o_{ScS}$ is almost completely independent of distance, since this value is always on the order of 700 to 900 seconds. Any bias in the regional differences reported would therefore have to come from a regional difference in Q. Such differences probably exist, (owing notably to the existence of low velocity zones of variable extent under the oceans and certain continents). However, since we have shown that our earlier models (implicitly rejecting lateral variations of Q) can fit our data without extending lateral heterogeneities below 200 km, it is certain than models allowing Q to vary only above a depth of 200 km should provide an even better fit. Therefore, in the absence of any evidence of definite lateral variations of Q_β, Butler's suggestion, which introduces one more parameter previously constrained, reinforces our statement that the present data does not warrant lateral heterogeneities deeper than 200 km.

1.4 Mantle Hotspots Under Hawaii and Trindade: Evidence from S Delays

As shown in Tables 1.2 and 1.3 and on Figure 1.4, strong positive anomalies are found for rays propagating in the top section of proposed mantle hotspots: ScS at Kipapa, Hawaii, is delayed 6 s from the Sea of Okhotsk, and 9.8 s from the Fiji-Tonga area. ScS_2 recorded at Windhoek from two deep Peruvian earthquakes of almost identical epicenter both show a one-way anomaly of +11.5 s at their reflecting point, located at the island of Trindade, in the Brazil Basin of the South Atlantic Ocean. Rays from these events to Sá da Bandeira, Angola, which miss the island and reflect in the Brazil Basin itself, have an anomaly (-2 s) which agrees with the values predicted by model LKK for this age of oceanic lithoshere.

Seismic observations of deep mantle anomalies below the Hawaiian hotspot, and their interpretation in the frame of Wilson's (1963, 1965) and Morgan's (1971) proposed theories, have been the subject of some controversy: while Kanasewich et al. (1973) have reported teleseismic anomalies for rays bottomming in the deepest part of the proposed upwelling column, Okal and Kuster (1975), using records of Aleutian events in French Polynesia, have failed to confirm these results. Studies by Capon (1974), Noponen (1974), Berteussen (1976) and Vermeulen and Doornbos (1977) have shown that most teleseismic slowness and azimuth anomalies at large networks could in fact be explained by local geology under the receiving arrays. Powell (1975, 1976) similarly confirmed the crucial importance of local geology, although some of her results still suggest the possibility of identifying teleseismic anomalies.

The present study suggests that the top part of the upwelling column has to be made of slow material, even if the total vertical travel-time agrees with the Jeffreys-Bullen Tables (Best et al., 1974). This requires a vertical heterogeneity in the column, with a higher velocity at the bottom, although this higher velocity should be spread over a large vertical extent, so as not to be detected by teleseismic array studies. A possible model involving chemical differences was proposed by Anderson (1975) and a recent experiment across the Yellowstone area (Hadley et al., 1976) yielded results which could be consistent with this general frame. Finally, the anisotropy observed at Kipapa (6 seconds from the Sea of Okhotsk, 9.8 seconds from Fiji Islands) could result from the horizontal distance (300 km) between Kipapa (located on Oahu) and the presumed hotspot column, under the island of Hawaii.

The volcanism of the island of Trindade, in the South Atlantic Ocean, was studied by Cordani (1968), who used the K-Ar method to infer ages between 1.50 and 2.90 million years b.p. These results were later confirmed by Valencio and Mendía (1974), who obtained ages ranging from 1.2 ± 1.0 to 6.4 ± 3.5 m.y.b.p. Oversby (1971) and Baker (1973) have shown that this young island is unique among Atlantic islands in its degree of undersaturation, suggesting origin from a hydrous mantle. This is consistent with a greater degree of partial melting and large S delays. The large contrast between S anomalies at Trindade ($+11.5$ s) and in the nearby Brazil basin (-2.0 s) constrains this partially molten region to a restricted geographical area (see Figure

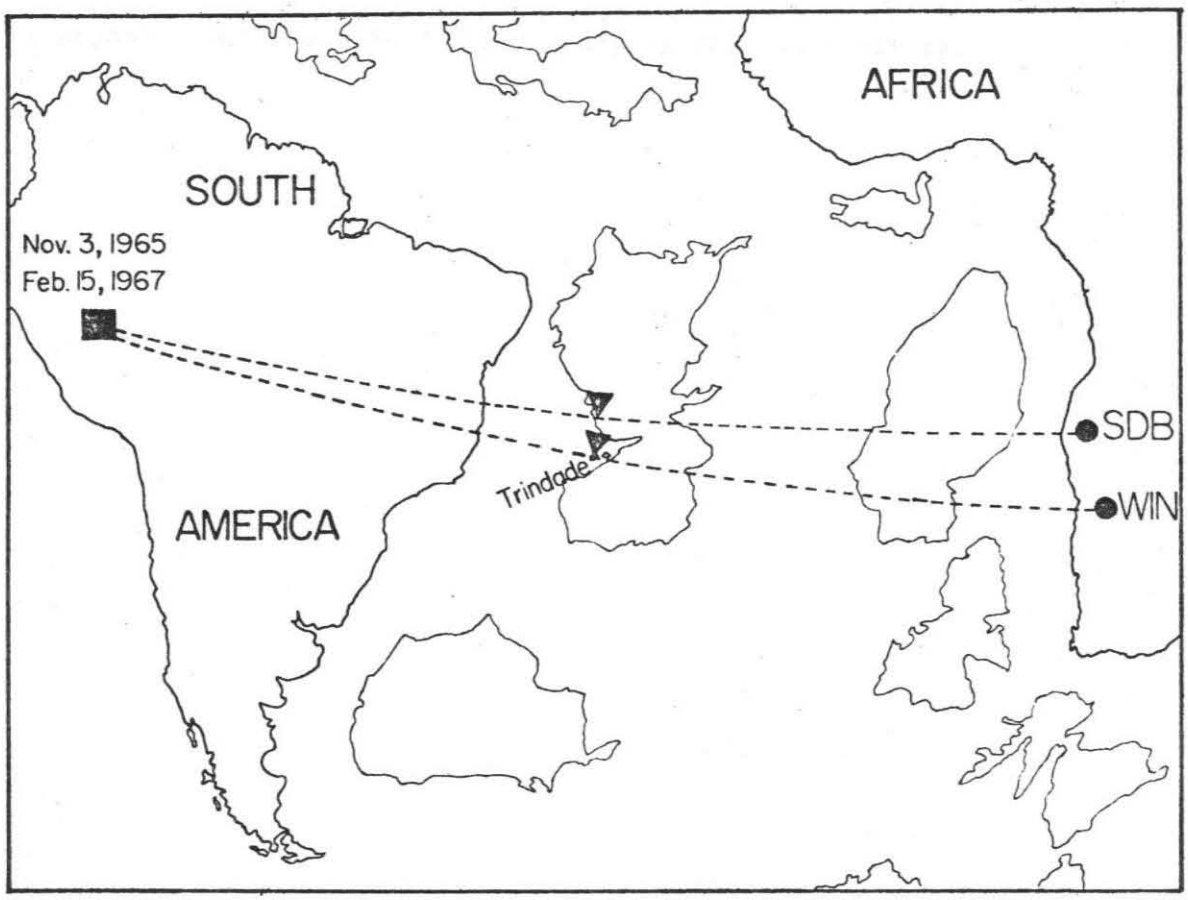

Figure 1.9. Map of the South Atlantic showing the rays from the Peru-Brazil events to the Southern African stations. The thin traces are the 5000 m isobaths, delineating the deep oceanic basins. The two triangles mark the surface reflection points of ScS_2. The Islands of Trindade and Martin Vaz are shown.

1.9), and strongly advocates for the existence of a hotspot under Trindade, or its immediate neighborhood, as proposed in the model by Minster et al. (1974). The implementation of a seismic station on the island, contemplated in the early stages of the WWSSN project, and now scheduled for the end of 1978 (Mendiguren, 1978; personal communication), could help in further studying this possibility.

1.5 Conclusion

Lateral variations of S travel-time residuals as reported in this chapter occur over distances too short to let them be associated with structures 400 km or deeper. Rather, they seem to correlate fairly well with the general pattern of plate tectonics. Delays, in general, decrease with the age of the plate and are largest for oceanic islands and recently active continental areas. The older oceanic lithosphere has residuals similar to continental shields. The residuals are generally consistent with variations in the upper 200 km found by independent means. The responsible structures should primarily be sought in the lithosphere and asthenosphere. The following chapter will present the results of a study of very long period Rayleigh waves, aimed at gathering additional information on upper mantle lateral heterogeneities.

CHAPTER 2

The Effect of Intrinsic Oceanic Upper-Mantle Heterogeneity on Regionalization of Long-Period Rayleigh-Wave Phase Velocities.

2.0 Introduction

In a series of recent papers, Jordan (1975 a,b) and Sipkin & Jordan (1975, 1976) have proposed that lateral heterogeneities between oceans and continents extend to depths of 400 km, and possibly 600 km. Their conclusion is based on the study of ScS travel times, and on the discrepancy between models inverted from body- and surface-wave data. On the other hand, the results in Chapter 1, obtained from a different set of ScS data, suggest that the travel-time differences between oceans and continents can be accounted for by the upper 180 km of crust and mantle. Furthermore, it has recently been shown (Liu, Anderson & Kanamori 1976; Anderson et al. 1977; Hart, Anderson & Kanamori 1976, 1977) that the discrepancy between inversions of body- and surface-wave data was due to anelasticity in the mantle. In view of these controversies, it is important to investigate whether or not a definite continent-ocean lateral heterogeneity is present in surface-wave phase velocities, at periods on the order of 200 to 300 s, whose values are substantially dependent on seismic velocities down to 600 km. Models recently derived from regionalization of surface-wave phase velocities (Toksöz & Anderson 1966; Dziewonski 1970; Kanamori 1970) generally exhibit continent-ocean lateral heterogeneities. Furthermore, Kanamori's results show a fairly large scatter in the differences between Rayleigh-wave phase velocities for oceans and shields, at 200-300 s.

However, at shorter periods, recent investigations of oceanic surface-wave phase velocities (Leeds et al. 1974; Kausel et al. 1974; Leeds 1975) have yielded a model of the evolution of the oceanic

lithosphere, which is basically consistent with theoretical models derived from plate tectonics (Parker & Oldenburg 1973). This model shows that considerable lateral heterogeneities exist within the oceanic plates. This effect might be responsible for the scatter in Kanamori's results, which were obtained on the assumption of a uniform oceanic phase velocity, but from data sampling all ages of the oceanic lithosphere. This warrants a reassessment of continental phase velocities obtained from the pure-pathing method, as described by Toksöz & Anderson (1966), Dziewonski (1970) and Kanamori (1970). The object of the present chapter is to carry out such a regionalization of Rayleigh-wave phase velocities, taking into account their variation with age across oceanic plates. In a detailed study of surface waves in the East Pacific, Forsyth (1975) recently confirmed the dependence of the velocities with the age of the plate, and also claimed that Love- and Rayleigh-wave data are inconsistent unless anisotropy is introduced in the upper mantle. However, in view of the very limited set of data available at long periods, and of the many different models which can explain the observed anisotropy, we decided not to take anisotropy into account in the present study.

In Section 2.1, we build up a table of theoretical Rayleigh-wave oceanic phase velocities, for several values of the age of the lithosphere, by assuming that the ocean below 180 km is similar to the gross earth model C2, as described by Anderson & Hart (1976). We then use a few 'pure-age' paths, in a two-station computation, to check the overall agreement of this model with local data. In Section 2.2, we then carry out a regionalization of dispersion curves,

solving for pure-path continental values, and allowing for a variation of oceanic velocities with age, in accordance with the results from the first section. Again, we make sure that the results agree with direct experimental values obtained from two pure continental paths by the two-station method. In Section 2.3, we discuss the results and compare them with the two models proposed by Jordan (1975a) for continental and oceanic structure (with substantial differences down to 650 km). We prove the latter's incompatibility with the data. We also discuss Dziewonski's (1971) shield models with respect to the recent vertical shear-wave data obtained from ScS studies.

2.1 Rayleigh-Wave Phase Velocities From an Oceanic Model of Aging Lithosphere

Studies of Rayleigh-wave phase velocities at shorter periods ($T \leq 150$ s) have led Leeds and co-workers (Kausel et al. 1974; Leeds et al. 1974; Leeds 1975) to a seismic model of the evolution of the lithospheric plate with age in the Pacific Ocean. In the present study, we will assume that lateral heterogeneity under the ocean is confined to the upper 180 km, and that the remaining part of the mantle is identical to the average earth model C2. This way, we define eight different oceanic models (hereafter 'Ocean 1'—'Ocean 8'), corresponding to the eight regions defined in Leeds et al. (1974) (respectively 150, 120, 100, 70, 50, 30, 15 and 5 Myr old), after the three older regions have been corrected in accordance with Leeds' later paper (1975). We compute theoretical phase velocities at five standardized periods (T = 292.57, 256.00, 227.55, 204.80 and 186.18 s), which are harmonics of the main fundamental 2048-s window, which will be used in all Fast-Fourier transform analyses in the present paper. Results are shown in Table 2.1, and on Figure 2.1. Differences in velocities between younger and older oceans are on the order of 1.5 to 2%, which is at least as large as the continental-oceanic differences reported in previous studies (Kanamori 1970; Dziewonski 1970).

Before proceeding any further, it is necessary to check these results against experimental values. The use of waves with periods in the range 200 to 300 seconds restricts the choice of the data to a fairly small number of events, in which energy is present at such

Table 2.1

Theoretical Rayleigh-Wave Phase Velocities for Oceanic Models

Ocean 1 - Ocean 8

Model	Age	Velocity (km/s) at Period (s)				
	m.y.	292.57	256.00	227.55	204.80	186.18
Ocean 1	150	5.260	4.989	4.788	4.642	4.535
Ocean 2	120	5.249	4.976	4.771	4.619	4.506
Ocean 3	100	5.242	4.968	4.761	4.607	4.492
Ocean 4	70	5.237	4.963	4.756	4.601	4.485
Ocean 5	50	5.234	4.960	4.753	4.599	4.482
Ocean 6	30	5.227	4.953	4.746	4.592	4.475
Ocean 7	15	5.208	4.934	4.728	4.575	4.458
Ocean 8	5	5.184	4.909	4.703	4.549	4.433

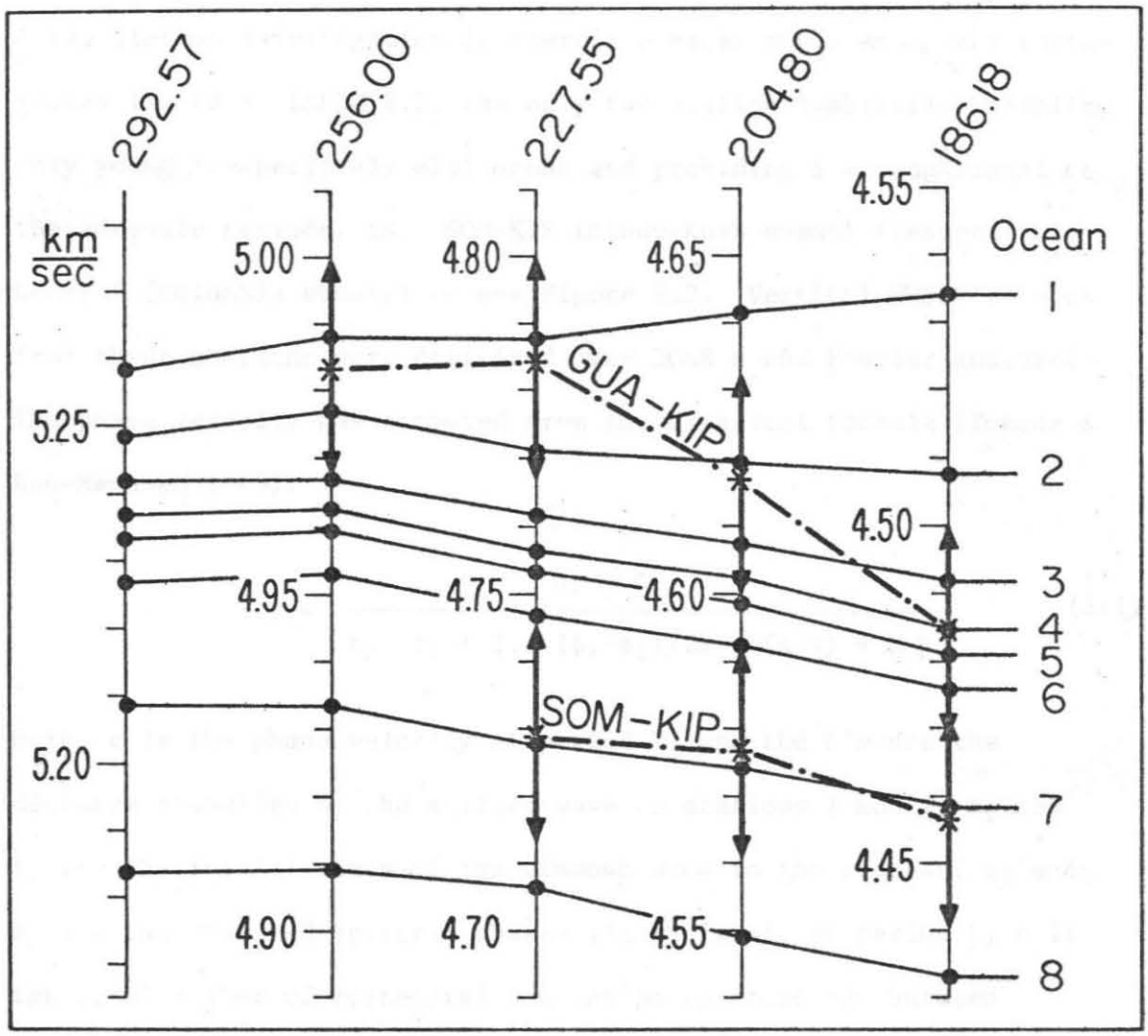

Figure 2.1. Theoretical Rayleigh-wave phase velocities for models 'Ocean 1' to 'Ocean 8'. Different baselines are used at the five standard periods to eliminate the mean average dispersion. Superimposed are experimental data (*) from the 'pure-age' paths KIP-SOM and KIP-GUA. The vertical arrows centered on them are error bars.

periods. These are listed in Table 2.2. Furthermore, these are large earthquakes, for which, most of the time, no rupture mechanism accurate enough to allow the use of a one-station method, is available. A two-station investigation is therefore necessary. Among the earthquakes listed in Table 2.2, the only two-station combination sampling only young (respectively old) ocean and providing a strong signal at the adequate periods, is: SOM-KIP (Hindu-Kush event) (respectively: GUA-KIP (Colombia event)) — see Figure 2.2. Vertical WWSSN records from these stations were digitized over 2048 s and Fourier analyzed. The phase velocity was computed from the classical formula (Toksöz & Ben-Menahem 1963):

$$c = \frac{\Delta_2 - \Delta_1}{t_2 - t_1 + T.\,[\,(\phi_2-\phi_1)/2\pi + (n/4) + N\,]} \qquad (2.1)$$

Here, c is the phase velocity at period T, and the Δ's are the distance travelled by the surface wave to stations 1 and 2, t_1 and t_2 are the initial times of the windows used in the process, ϕ_1 and ϕ_2 are the observed spectral phases (in radians), at period T, n is the total number of epicentral and antipodal crossings between stations 1 and 2, and N is a suitable integer. The accuracy of the data is on the order of twice the digitizing unit (2s) in time, or 0.01 km/s for c. Results are shown in Table 2.3. Most of the SOM-KIP trace samples the Chile rise separating the Antarctica and Nazca plates (region 8), then the East Pacific Rise (regions 7 and 8), and finally young lithosphere (mostly regions 6 and 5). The average would then be expected to resemble models 'Ocean 6' or 'Ocean 7'. On the other

Table 2.2

Coordinates and Magnitudes of Earthquakes used in Chapter 2

Number	Name	Epicenter (°N ; °E)	Date	M_w (*)
1	Rat Island	51.3 ; 178.6	4 Feb 65	8.7
2	Alaska	61.1 ; -147.6	28 Mar 64	9.2
3	Kurile	44.8 ; 149.5	13 Oct 63	8.5
4	Niigata	38.7 ; 139.2	16 Jun 64	7.6
5	Hindu-Kush	36.4 ; 70.7	14 Mar 65	[7.5]
6	Mindanao	6.5 ; 126.2	2 Dec 72	[7.4]
7	Mongolia	45.2 ; 99.2	4 Dec 57	8.1
8	Assam	28.4 ; 96.7	15 Aug 50	8.6
9	Moluccas	-2.4 ; 126.0	24 Jan 65	[7½]
10	Chile	-38.0 ; -73.5	22 May 60	9.5
11	Colombia	-1.5 ; -72.6	31 Jul 70	(2×10^{28})
12	Auckland Isl.	-49.1 ; 164.2	12 Sep 64	[7]
13	Kamchatka	52.6 ; 160.3	4 Nov 52	9.0
14	Peru-Brazil	-13.8 ; -69.3	15 Aug 63	(7×10^{27})
15	Indonesia	-11.1 ; 118.4	19 Aug 77	8.6

(*) M_w as defined in Kanamori (1977b). For smaller events, only M_s is given, in brackets. For deep events, only the seismic moment, M_o is given, in parentheses.

Table 2.3

Experimental Oceanic Phase Velocities from the Two-Station Method

Event	Path	Velocity (km/s) at Period (s)				
		292.57	256.00	227.55	204.80	186.18
11	GUA-KIP	*	4.983	4.784	4.618	4.484
5	SOM-KIP	*	*	4.729	4.577	4.455

(*) No substantial energy in the record at these periods.

hand, the GUA-KIP path samples the older parts of the Pacific Ocean (even possibly older than 150 Myr) (regions 1, 2, 3), and should then resemble models 'Ocean 1' or 'Ocean 2'. As can be seen from Tables 2.1, 2.3 and Figure 2.1, the results agree with these expectations. Thus, these experimental data give evidence that lateral heterogeneity within the Pacific plate is important at periods of 200-300 s, and is fairly well accounted for by models 'Ocean 1'-'Ocean 8'. This suggests that there is no need to extend the oceanic lateral heterogeneity below 180 km. This indeed, is what most theories of plate tectonics predict, and also agrees with our ScS results (Okal and Anderson, 1975; and Chapter 1): We were able to account for variations in multiple-ScS travel-time residuals across oceanic lithosphere by models whose heterogeneity was confined to the upper 180 km of the Earth. This result also allows us to assume from now on in this study that oceanic Rayleigh-wave phase velocities and their variation with the age of the plate are known.

2.2 Continental Velocities: Regionalization of Rayleigh-Wave Phase Velocities Allowing for Lateral Heterogeneity in the Oceanic Lithosphere.

Unfortunately, at the time when this study was made, it was not possible to isolate data to be processed by the two-station method over a pure shield path. Apart from the general distribution of stations and of the events listed in Table 2.2, one additional reason may be the smaller size of the continents, relative to the oceans, which makes both the numerator and the denominator in equation (2.1) smaller, yielding very inaccurate values of c. Consequently, regionalization of great-circle phase velocities was then necessary to obtain pure-path values of Rayleigh-wave phase velocities at periods larger than 180 s. Later, however, the August 19, 1977 Indonesian earthquake provided pure-shield data across the Canadian shield. In the present section, we carry out such a regionalization, allowing for the observed lateral heterogeneity in the oceanic lithosphere. We then use the recent Indonesian data as an independent check of our results.

DATA SET

The data used in this section includes both new data and data taken from previously published studies, which were interpolated to our standard periods. Table 2.4 lists the new data set, obtained from records analyzed in the present study. Records of the Kamchatka earthquake at Pasadena, were from the north-south component of the high-gain strain instrument. All other records were from vertical long-period WWSSN instruments. In the case of the Rat Island

Table 2.4

Experimental Rayleigh-Wave Phase Velocities for Great-Circle Paths Obtained in the Present Study

Event, station and phases used			Velocity (km/s) at Period (s)				
			292.57	256.00	227.55	204.80	186.18
1	HLW	R5 - R9	5.235	4.952	4.753	4.603	*
1	SOM	R4 - R6	5.237	4.953	4.754	4.602	4.482
1	CTA	R5 - R9	*	4.972	4.771	4.621	*
2	SPA	R3 - R5	5.246	4.966	4.764	4.612	4.497
2	AFI	R5 - R7	5.234	4.945	4.750	4.604	4.498
2	RAB	R5 - R7	*	4.984	4.772	4.617	4.499
2	GUA	R5 - R7	*	4.967	4.761	4.615	4.504
3	GUA	R5 - R7	5.221	4.929	4.687	4.550	4.461
4	GIE	R2 - R4	5.242	4.967	4.766	4.602	4.490
13	PAS	R2 - R4	5.227	4.959	4.757	4.616	4.488

(*) No substantial energy in the records at these periods.

Table 2.5

Additional Data taken from the Literature

Event, station and reference			Velocity (km/s) at Period (s)				
			292.57	256.00	227.55	204.80	186.18
2	PAS	b†	5.231	4.954	4.746	*	*
3	MDS	c	5.243	4.962	4.760	4.604	4.487
3	AAE	d†	5.234	4.952	4.750	4.598	4.488
3	ADE	d†	5.246	4.975	4.774	4.613	4.499
3	AFI	d†	5.239	4.963	4.763	4.616	4.508
3	HNR	d†	5.240	4.972	4.767	4.612	4.500
3	SHI	d†	5.223	4.952	4.742	4.595	*
3	TOL	d†	5.238	4.969	4.766	4.615	4.501
7	PAS	e†	*	4.954	4.746	4.592	4.485
8	PAS	e†	5.232	4.955	4.745	4.598	4.489
9	PAS	f†	5.246	4.952	4.751	4.604	4.492
10	PAS	g†	5.240	4.960	4.754	4.596	4.476
12	PAS	f†	5.238	4.956	4.746	4.592	4.479
14	GDH	h	5.223	4.955	4.754	4.607	4.491
14	NUR	h	5.232	4.959	4.754	4.604	4.491
14	MAL	h	5.239	4.967	4.763	4.611	4.497
14	AFI	h	5.241	4.964	4.757	4.604	4.491
14	ALQ	h	5.231	4.961	4.755	4.602	4.485
14	AAM	h	5.232	4.960	4.759	4.611	4.497

(*) No data reported at these periods.

(†) Data used in Kanamori's (1970) solution.

a This study

b Toksöz and Anderson (1966)

c Abe et al. (1970)

d Kanamori (1970)

e Toksöz and Ben-Menahem (1963)

f Ben-Menahem (1965)

g Anderson et al. (1965)

h Dziewonski (1970).

earthquake (event 1), a strong aftershock interferes with most of the records of R_7. Therefore, R_9 is used together with R_5 at stations CTA and HLW. Table 2.5 similarly lists the additional data obtained from the literature.

REGIONALIZATION

Regionalization of the Earth was carried out by partitioning its surface into 248 cells: a 15-degree grid, both in latitude in longitude, was used, with special adjustments made in the polar regions. The areas of the various cells are not all equal, but the present partitioning of the Earth was found to be most convenient for rapid computer regionalization of great-circle paths. Only four different oceanic regions were considered. They are labelled A, B, C and D: A includes regions older than 135 Myr, and model A is taken as identical to 'Ocean 1'. B ranges from 135 to 80 Myr, and model B is an average of models 'Ocean 2 and 3'. C ranges from 80 to 30 Myr, and model C is an average of models 'Ocean 3, 4, 5 and 6'. D ranges from 30 Myr to 0, with model D averaging models 'Ocean 6, 7 and 8'. An attempt was initially made, using a much finer grid, to resolve all eight regions defined in Leeds' study. However, considering the wavelengths used in the present study (all larger than 830 km), this was found unnecessary. The grid is shown on Figure 2.2.

Continents were divided into shields (region S) and Phanerozoic mountainous areas (region M). Trenches and marginal seas were kept as a separate entity (region T). Ages of the oceanic lithosphere were taken from the *Map of the Age of the Oceans* published by the

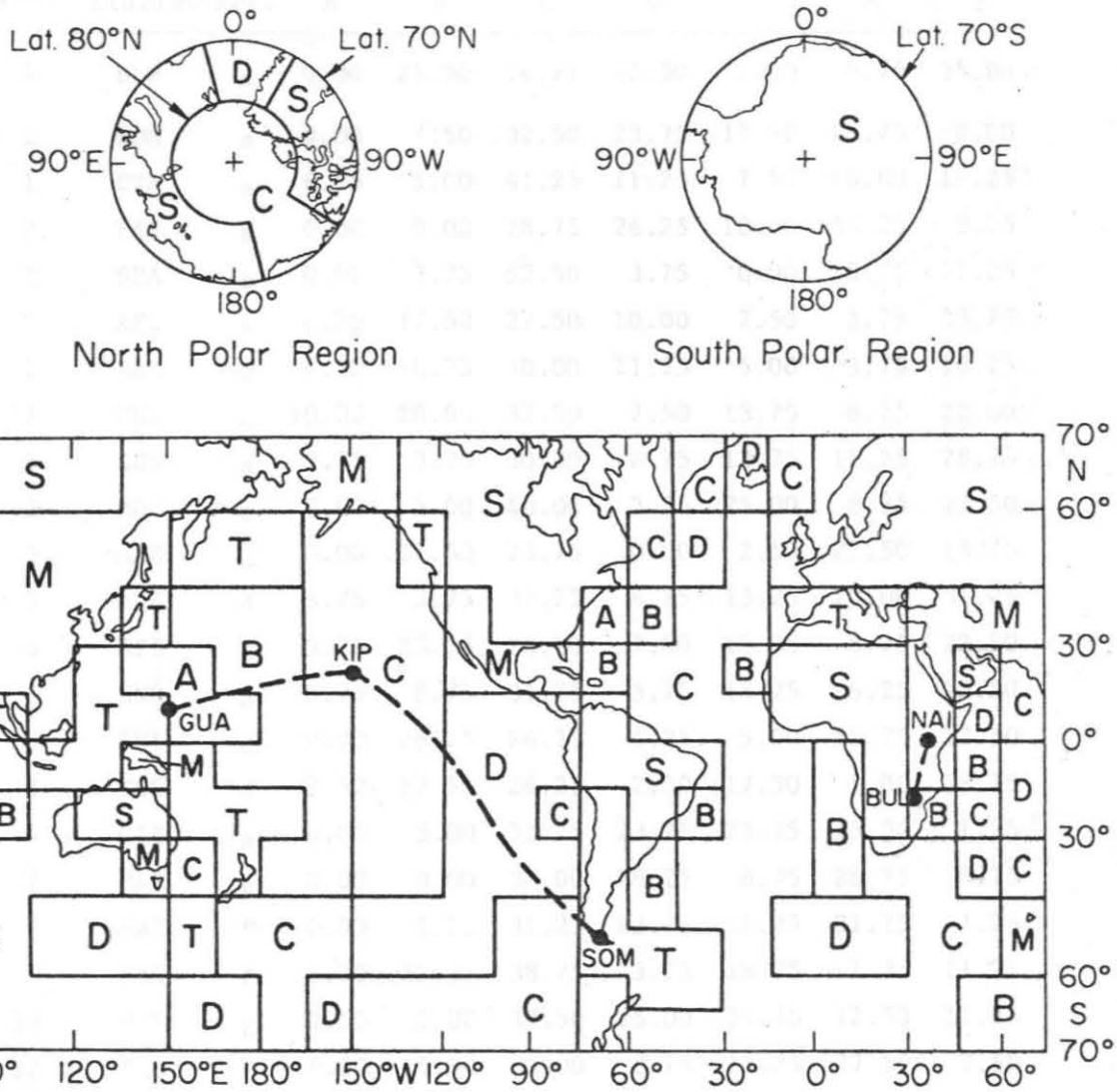

Figure 2.2. Map of the regionalization grid of the Earth used in Section 2.2. Labels A, B, C, D, M, S, T are explained in text. Also shown are the paths used for the two-station experiments : GUA-KIP, KIP-SOM and BUL-NAI.

Table 2.6

Percentage of Great Circle Paths Lying in Each of the Seven Regions

Event	Station	Ref.	A	B	C	D	T	M	S
1	HLW	a	0.00	25.00	16.25	10.00	5.00	8.75	35.00
1	SOM	a	0.00	7.50	32.50	23.75	17.50	18.75	0.00
1	CTA	a	8.75	5.00	41.25	11.25	7.50	10.00	16.25
2	PAS	b	0.00	0.00	28.75	26.25	10.00	26.25	8.75
2	SPA	a	0.00	3.75	52.50	3.75	0.00	18.75	21.25
2	AFI	a	0.00	17.50	27.50	10.00	7.50	3.75	33.75
2	RAB	a	7.50	16.25	40.00	11.25	5.00	3.75	16.25
2	GUA	a	10.00	10.00	32.50	7.50	13.75	6.25	20.00
3	GUA	a	3.75	3.75	30.00	8.75	13.75	11.25	28.75
3	MDS	c	0.00	5.00	40.00	3.75	25.00	8.75	17.50
3	AAE	d	0.00	27.50	23.75	10.00	2.50	22.50	13.75
3	ADE	d	3.75	3.75	31.25	6.25	13.75	10.00	31.25
3	AFI	d	3.75	23.75	20.00	7.50	13.75	8.75	22.50
3	HNR	d	8.75	8.75	31.25	3.75	18.75	6.25	22.50
3	SHI	d	0.00	26.25	26.25	6.25	5.00	18.75	17.50
3	TOL	d	7.50	12.50	26.25	2.50	17.50	5.00	28.75
4	GIE	a	0.00	5.00	31.25	23.75	23.75	15.00	1.25
7	PAS	e	0.00	0.00	30.00	26.25	8.75	26.25	8.75
8	PAS	e	0.00	1.25	31.25	23.75	11.25	31.25	1.25
9	PAS	f	5.00	21.25	38.75	3.75	18.75	1.25	11.25
10	PAS	g	2.50	0.00	37.50	25.00	11.25	12.50	11.25
12	PAS	f	0.00	15.00	30.00	8.75	11.25	27.50	7.50
13	PAS	a	1.25	8.75	30.00	23.75	20.00	16.25	0.00
14	GDH	h	3.75	5.00	23.75	3.75	16.25	16.25	31.25
14	NUR	h	1.25	1.25	31.25	12.50	28.75	7.50	17.50
14	MAL	h	7.50	17.50	31.25	7.50	21.25	5.00	10.00
14	AFI	h	1.25	12.50	21.25	8.75	12.50	11.25	32.50
14	ALQ	h	0.00	6.25	32.50	15.00	8.75	12.50	25.00
14	AAM	h	0.00	11.25	17.50	3.75	15.00	20.00	32.50

References : see Table 2.5.

Geological Society of America (1974). A computer program was written, which samples any great-circle path at 500-km intervals, and computes the percentage of its length falling into the seven different regions. The results are listed in Table 2.6.

SOLVING FOR CONTINENTAL VELOCITIES

At each of the five standardized periods (T), we solve the system of equations

$$\sum_j x_{ij}/v_j(T) = 1/c_i(T) \qquad (2.2)$$

for v_S, v_M and v_T, using a least-square technique. Here j = A,B,C,D, T,M,S is the index of the region; i is the index of the path; x_{ij} is the fraction of path i lying in region j, and $c_i(T)$ is the observed phase velocity at period T along great-circle i. Rather than solving for all seven v_j's, we fix v_A, v_B, v_C, and v_D to their known values obtained in Section 2.1, listed in Table 2.7, and solve only for v_S, v_M, v_T. This has the effect of reducing the number of unknowns, in view of the relatively small amount of data available. In so doing, we are ignoring the phase delays introduced along the path by heterogeneities elsewhere in the Earth, as discussed by Madariaga & Aki (1972). We are then seeking to explain the differences between Kanamori's and Dziewonski's models merely in terms of pure-path phase velocities.

Another objection to the use of equations (2.2) was Dahlen's (1975) suggestion that deep lateral heterogeneities in the mantle could cause variations as large as 0.2 % in the apparent great-circle

Table 2.7

Phase Velocities used in Models A, B, C, D
when solving for Models T, M, S

Model	Velocity (km/s) at Period (s)				
	292.57	256.00	227.55	204.80	186.18
A	5.259	4.989	4.788	4.642	4.535
B	5.246	4.972	4.766	4.613	4.499
C	5.236	4.961	4.754	4.600	4.483
D	5.206	4.932	4.726	4.572	4.455

Table 2.8

Solution for Rayleigh-Wave Phase Velocities in Regions T, M, S

Region	Phase Velocity (km/s) at Period (s)				
	292.57	256.00	227.55	204.80	186.18
T	5.279	4.989	4.804	4.644	4.522
M	5.202	4.941	4.712	4.575	4.466
S	5.223	4.948	4.742	4.598	4.499

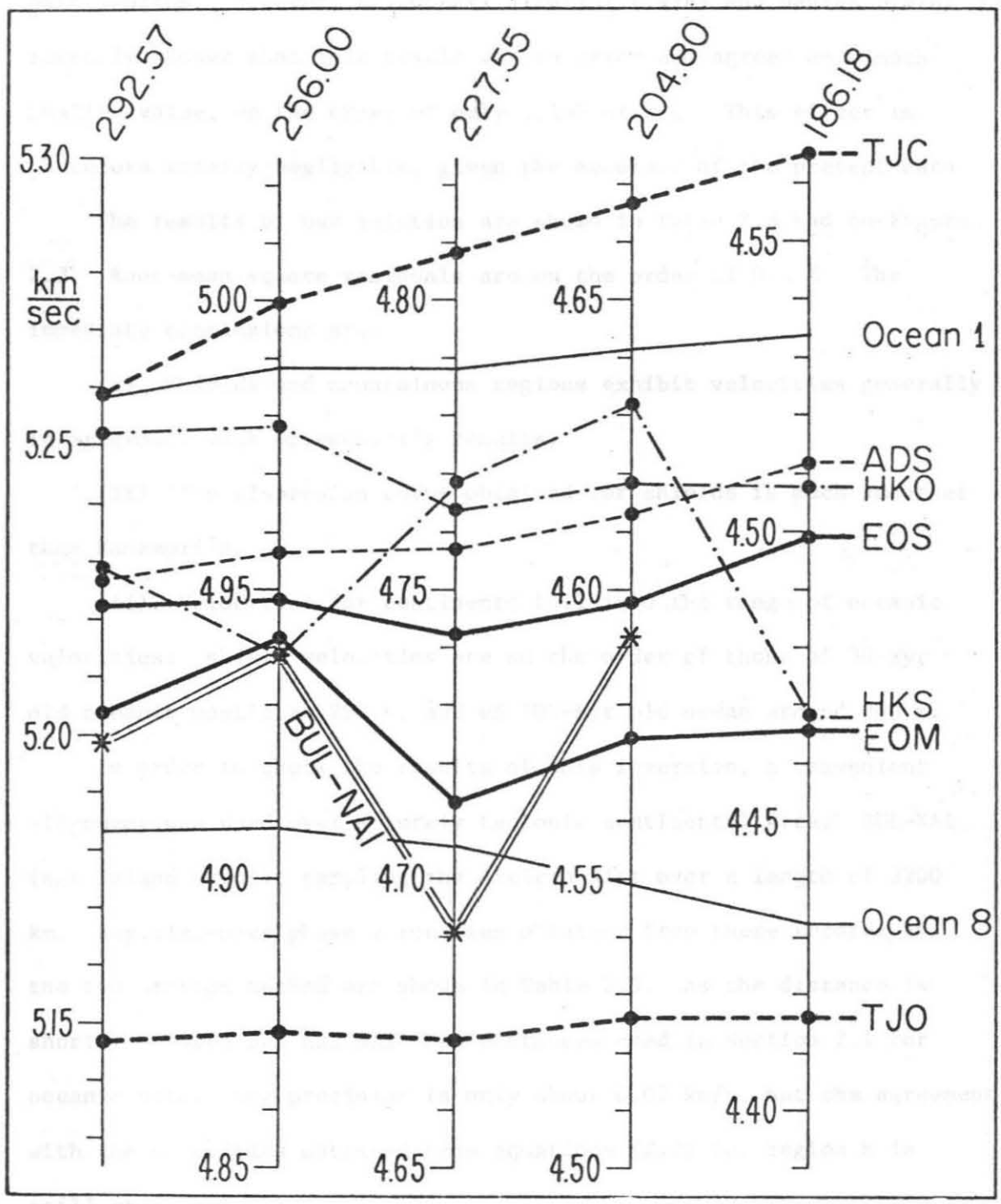

Figure 2.3. Regionalized phase velocities obtained for shields (EOS) and mountainous areas (EOM) in the present study, as compared to ADS (Dziewonski's shield values), HKS and HKO (Kanamori's shield and ocean values) and TJO and TJC (Jordan's oceanic and continental models, uncorrected for Q).Also shown are models 'Ocean 1' and 'Ocean 8', giving the range of variation of oceanic velocities, and experimental data from the 'pure' path BUL-NAI, obtained by the two-station method.

path lengths. However, Dziewonski & Sailor (1976) and Dahlen (1976) recently showed that this result was in error and agreed on a much smaller value, on the order of only 1/150 of 1 %. This effect is therefore totally negligible, given the accuracy of the present data.

The results of our solution are shown in Table 2.8 and on Figure 2.3. Root-mean square residuals are on the order of 0.5 %. The immediate conclusions are:

(i) Shields and mountainous regions exhibit velocities generally in agreement with Dziewonski's results.

(ii) The dispersion curve obtained for shields is much smoother than Kanamori's.

iii) Velocities for continents fall into the range of oceanic velocities: shield velocities are on the order of those of 30-Myr old oceanic mantle at 292 s, and of 100-Myr old ocean around 200 s.

In order to check the results of this inversion, a convenient alignment was used over a purely tectonic continental area: BUL-NAI (Rat Island event), sampling the African Rift over a length of 3200 km. Rayleigh-wave phase velocities obtained from these records by the two-station method are shown in Table 2.9. As the distance is shorter between BUL and NAI than distances used in Section 2.1 for oceanic paths, the precision is only about 0.02 km/s, but the agreement with the velocities obtained from equations (2.2) for region M is still excellent.

After the original study reported in this Section was completed and published, the Indonesian earthquake of August 19, 1977 made possible a direct independent check of the shield velocities obtained

Table 2.9

Experimental Continental Rayleigh-Wave Phase Velocities from the Two-Station Method

Event	Path	Velocity (km/s) at Period (s)				
		292.57	256.00	227.55	204.80	186.18
1	BUL - NAI	5.199	4.940	4.690	4.591	*

(*) No substantial energy in the records at these periods.

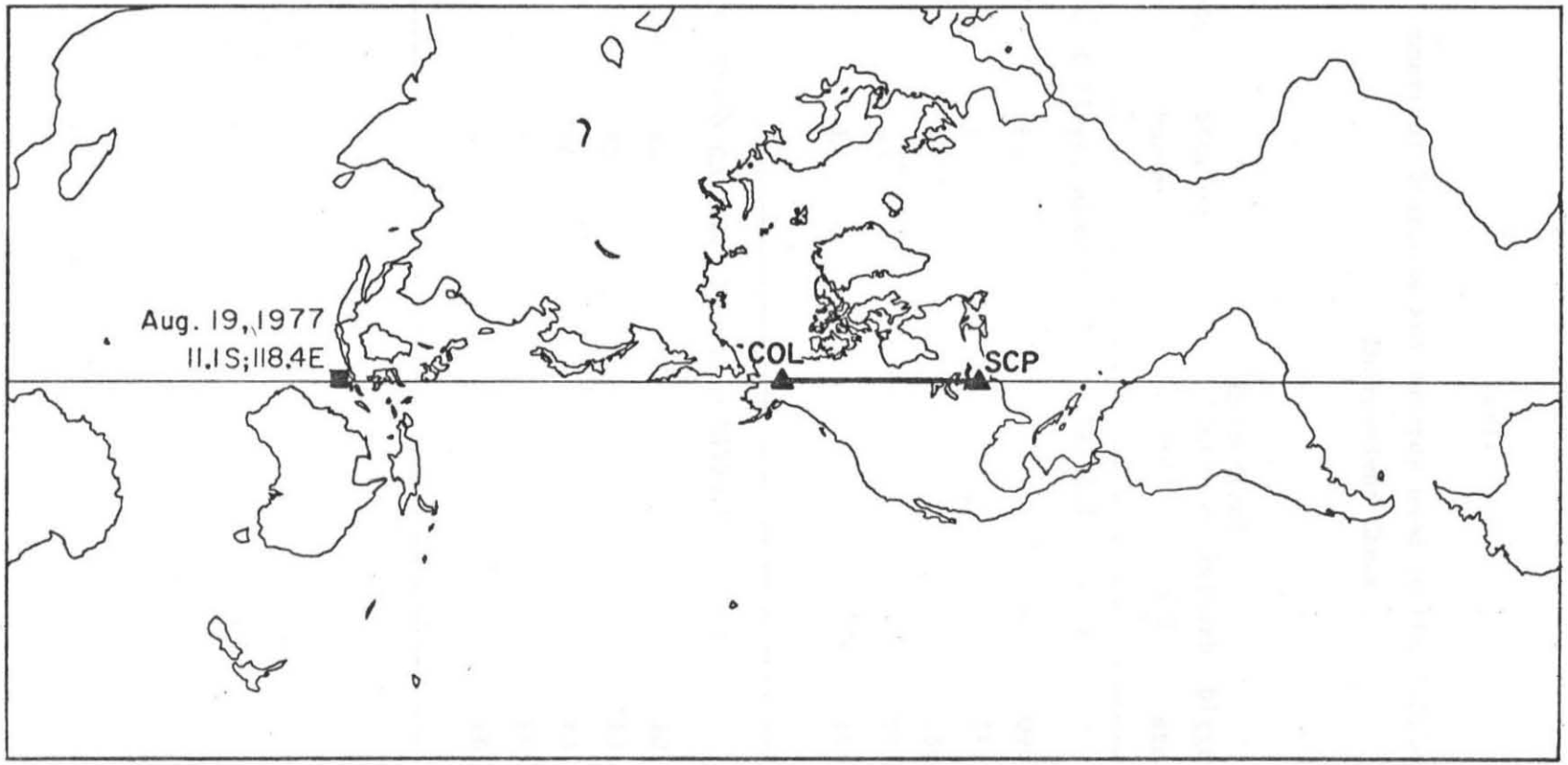

Figure 2.4. Map of the world showing the epicenter (black square) and stations used in the Sumba independent check. This Mercator projection uses the great circle through epicenter and stations as a baseline, in order to minimize distortion along the path under study.

Table 2.10

Summary of Stations and Records used in the Indonesian Event Independent Check

Code	Station / Phase	Epicentral Distance (km)	Azimuth (°)	Digitizing window starts	ends
COL	College, Alaska	11298.1	25.7		
	R3			09:56	10:16
	R4			11:08	11:33
	R5			13:00	13:25
	R6			14:06	14:42
	R7			16:11	16:35
SCP	State College, Penna.	16353.7	23.1		
	R4			10:42	11:11
	R5			13:17	13:46
	R6			13:46	14:22
	R7			16:24	16:54
	R8			16:54	17:26

at very long periods from our inversion. This very large event was assigned an M_s of 8.0 at Pasadena, and Stewart (1978) estimated its moment to be larger than 1×10^{29} dyn-cm. It created strong Rayleigh waves at COL and SCP, these two stations being separated by only 2.6° in azimuth. Figure 2.4 shows the geographical layout of the great circle linking the two stations and the epicenter. Table 2.10 gives the details of the seismic phases used in this study. A clock correction of -500 ms was applied to the records at SCP. The calibration pulses were digitized, filtered at $T \geq 150$ s, and checked to be identical at both stations.

Seismograms were digitized at 2 s intervals and Fourier analyzed at the five standard periods. For the wavetrains used (R_4 to R_8), spectral amplitudes are usually peaked between 200 and 300 s. We eliminated all spectral components whose amplitude was less than one-half the maximum spectral amplitude in the corresponding record. These components appear as asterisks (*) in Tables 2.11 and 2.12. The phase velocities were then computed using equation (2.1). This is believed to be the first direct two-station measurement of Rayleigh wave velocities over shield at ultra-long periods.

Results are listed in Table 2.11 and plotted on Figure 2.5. The error inherent to the method is on the order of twice the digitizing unit (2 s) in the time domain, or 0.02 km/s for c. This figure is larger than for the oceanic case reported in Section 2.1, because of the shorter path between the two stations. The corresponding error bars are shown as arrows on Figure 2.5. Figure 2.5 shows that these experimental values are in good agreement with the dispersion

Table 2.11

Shield Values of Rayleigh-Wave Phase Velocities obtained by the Two-Station Method between COL and SCP

Phases used	Velocity (km/s) at Period (s)				
	292.57	256.00	227.55	204.80	186.18
R 4	*	*	*	*	4.496
R 5	*	5.005	4.777	4.649	*
R 6	5.226	4.983	4.726	4.561	4.546
R 7	*	4.906	4.779	*	*
Mean	5.226	4.965	4.761	4.605	4.521
Standard deviation		0.042	0.024	0.044	0.025

(*) No substantial energy in the records at these periods.

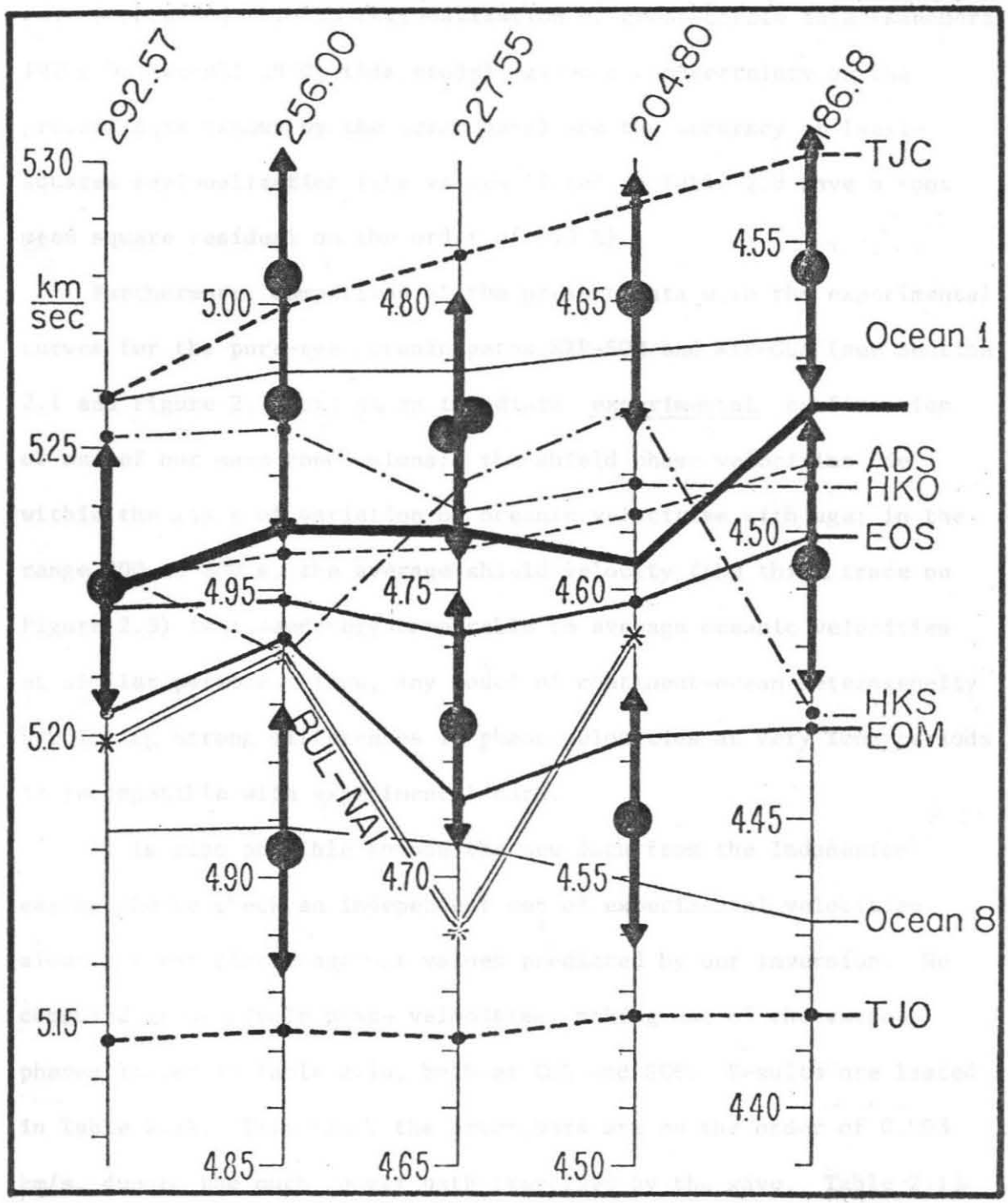

Figure 2.5. Experimental Rayleigh wave phase velocities obtained over the pure shield path COL-SCP. The big dots are the individual data points (from Table 2.12), with the vertical arrows showing the error bars. The thick trace across the figure is the resulting average experimental shield velocity. Other curves are described in Figure 2.3.

curves obtained through regionalization of great-circle data (Kanamori 1970; Dziewonski 1970; this study), given the uncertainty on the present data (shown by the error bars) and the accuracy of least-squares regionalization (the values listed in Table 2.8 have a root mean square residual on the order of 0.5 %).

Furthermore, comparison of the present data with the experimental curves for the pure-age oceanic paths KIP-SOM and KIP-GUA (see Section 2.1 and Figure 2.1) brings an immediate experimental confirmation of one of our main conclusions: the shield phase velocities lie within the range of variation of oceanic velocities with age; in the range 200 to 300 s, the average shield velocity (the thick trace on Figure 2.5) is indeed very comparable to average oceanic velocities at similar periods. Thus, any model of continent-ocean heterogeneity predicting strong differences in phase velocities at very long periods is incompatible with experimental data.

It is also possible to use the new data from the Indonesian earthquake to check an independent set of experimental velocities along a great-circle against values predicted by our inversion. We computed great circle phase velocities, making use of the various phases listed in Table 2.10, both at COL and SCP. Results are listed in Table 2.12. This time, the error bars are on the order of 0.003 km/s, due to the much longer path travelled by the wave. Table 2.13 gives the theoretical values obtained from the models derived in the inversion (and listed in Tables 2.7 and 2.8). Because of the slight difference in azimuth between COL and SCP, the two great circles through these stations are not exactly identically regionalized into

Table 2.12

Experimental Phase Velocities along the Great Circles Sumba-COL and Sumba-SCP

Records used	Velocity (km/s) at Period (s)				
	292.57	256.00	227.55	204.80	186.18
COL R3 - R5	5.227	4.953	4.756	4.600	*
COL R5 - R7	5.234	4.968	4.764	4.607	*
COL R4 - R6	*	*	4.735	4.652	4.514
SCP R4 - R6	5.256	*	4.775	4.631	4.507
SCP R5 - R7	*	4.955	4.764	*	*
SCP R6 - R8	5.251	4.964	4.770	4.620	*
Mean	5.242	4.960	4.760	4.622	4.511

(*) No substantial energy in the records at these periods.

Table 2.13

Theoretical Values obtained along the Great Circles Sumba - COL and Sumba - SCP using Models derived in the Inversion

Great Circle	Velocity (km/s) at Period (s)				
	292.57	256.00	227.55	204.80	186.18
Sumba - COL	5.242	4.965	4.761	4.609	4.494
Sumba - SCP	5.241	4.964	4.760	4.608	4.494

seven standard regions, and the theoretical values are very slightly different. Nevertheless, the agreement between the average values measured over the great circles and those expected from these models is excellent and fits well within the standard error accompanying the results of inversion.

Such a direct computational test by independent data is a very desirable confirmation of any model obtained by an inversion technique: In addition to providing a least-squares fit to the 29 records used in the inversion, models T (trench areas), M (mountainous areas), and S (shields) correctly predict the dispersion along this new great-circle path.

Another independent check recently came in a study by Aki and Patton (1978, personal communication), who used Rayleigh waves from a number of Central Asian earthquakes to investigate the Siberian shield and the adjoining mountainous areas, through the one-station method. Although their study involves mainly shorter periods (< 200 s), they report basic agreement with the high-frequency end of the present results.

2.3 Discussion

Before discussing the results of the previous section with respect to Dziewonski's and Kanamori's, it is worth noting the velocities obtained for the trench areas (region T). These are definitely larger than the corresponding average oceanic values. Again, for lack of data over sufficiently long paths, we were unable to check this observation by the two-station method. However, it is worth noting that a surface wave at 200 to 300 s, travelling over the area with a wavelength of 800 to 1500 km, will sample both the adjoining lithosphere, which is the oldest and fastest part of the ocean, and, at depth, the downgoing slab. The latter has been shown, both experimentally (Utsu 1967; Katsumata 1970; Isacks & Molnar 1971) and theoretically (Toksöz et al. 1971) to be an area of higher seismic velocities. It may be that these effects dominate the low-velocity areas of partial melting which accompany the slab.

We first want to compare our results with Dziewonski's and Kanamori's. Our shield and mountain velocities basically agree with Dziewonski's, and they exhibit a behavior somewhat different from those of Kanamori (see Figure 2.3). As both data sets were used in the present inversion, these discrepancies require an explanation. Table 2.6 shows that Kanamori's paths sample more ocean than Dziewonski's (56 % of the paths versus 47 %). More importantly, the distribution of these oceanic paths among regions A, B, C, D is far from constant: for example, the Kurile—AFI great-circle path falls 27.5 % into the fast regions A and B, and 27.5 % into the slow regions C and D. Meanwhile Alaska—PAS falls 0 % into A and B, and 55 % into

C and D. Similarly, Mongolia--PAS falls 0% into A and B, and 56.2% into C and D. Conversely, Dziewonski's paths are much more similar to each other. In terms of the solution of the least-squares system under the assumption of only one oceanic velocity at each period, Kanamori's paths will be more unstable than Dziewonski's. We think that the larger diversity of the oceanic paths in Kanamori's data was responsible for the apparent scattering of his shield velocities, and for the discrepancy which exists between his results and Dziewonski's, especially around 180 s.

This can be checked by solving equations (2.2), using only the data used in Kanamori (1970) as identified in Table 2.5 by a dagger (†). The results of this test are listed in Table 2.14. Although the obtained shield values are somewhat higher than those from both this study and Dziewonski's, their trend is much less dispersive than Kanamori's (1970) solution. Values obtained for the mountainous areas are also in good agreement with those from both the present inversion - Table 2.8 - and the two-station investigation - Table 2.9 -.

Having investigated a range of oceanic models and confirmed Dziewonski's shield values in view of intrinsic oceanic heterogeneity, we will now discuss the phase velocities obtained from the two models proposed by Jordan (1975a), for continental and oceanic mantles. These two models differ to depths on the order of 650 km. Theoretical values computed from Jordan's oceanic and continental models are listed in Table 2.15. At this point, it should be noted that nowhere in the present study has the effect of anelasticity - as pointed out by

Table 2.14

Solution for Rayleigh-Wave Phase Velocities using only data used by Kanamori (1970) († in Table 2.5)

Region	Velocity (km/s) at Period (s)				
	292.57	256.00	227.55	204.80	186.18
M	5.213	4.954	4.724	4.571	4.488
S	5.223	4.978	4.780	4.629	4.527

Liu et al. (1976) - been taken into account in the computation of surface-wave velocities. However, both Leeds' models and model C2 were obtained from inversions of surface-wave data, which did not take this effect into account. Therefore direct comparison is possible, since the Q correction would have the same effect on both experimental and theoretical velocities. On the other hand, Jordan's models are primarily body-wave models, obtained to match discrepancies reported from travel-time analyses. Therefore, a correction for the frequency dependence of elastic moduli caused by Q should be included before comparing Jordan's models to values obtained from surface-wave data. Hart et al. (1977) recently reported that, at the periods involved (180 to 300 s), the Q correction for spheroidal modes is on the order of 1%, which means that phase velocities derived uncorrected from surface-wave data are about 0.05 km/s slow. Conversely, the correction to be applied to phase velocities derived from body-wave models, such as Jordan's, in order to compare them to velocities from the present study, is on the order of -0.05 km/s. As shown in Table 2.15 and Figure 2.3, this correction makes Jordan's continental model basically consistent with experimental shield data, as obtained from this study, or Dziewonski's. However, a similar correction will move the oceanic values (curve 'TJO' on Figure 2.3) still further away from the experimental data from any part of the ocean. Although in Jordan's own words, the two models which he describes are only tentative, the important point is the difference between them, which he reports to be warranted by body-wave data. Such a difference at a substantial depth (on the order of 600 km) will

Table 2.15

Theoretical Rayleigh-Wave Phase Velocities for Jordan's Oceanic and Continental Models

Model	Velocity (km/s) at Period (s)				
	292.57	256.00	227.55	204.80	186.18
Oceanic model	5.148	4.874	4.673	4.526	4.417
Continental model	5.259	5.000	4.808	4.667	4.561

always lead to large continent-ocean surface-wave phase-velocity differences, regardless of the global average value.

In a recent paper, Sipkin & Jordan (1976) state that the 'base-line discrepancy' between continents and oceans can be explained in terms of a different value of Q under oceans and continents. The maximum possible lateral variation in Q would consist of a perfectly elastic oceanic mantle ($Q = \infty$) and of an anelastic continental mantle. (In fact, Kanamori (1970) reports no such definite behavior in the attenuation of surface waves, and this model is just unrealistic.) Even so, using this hypothetical model to correct continental velocities, and keep oceanic ones uncorrected, Figure 2.3 shows that we are left with an average difference between them of 0.07 km/s, and we are unable to reconcile the two models with the experimental data. Therefore, we conclude that the models of Jordan and Sipkin & Jordan are incompatible with the present available Rayleigh-wave phase velocity data in the range 200 to 300 s.

Finally, we want to discuss the models which were derived by Dziewonski (1971) from his sets of oceanic and shield velocities, with respect to the data available at shorter periods and from body-wave studies. We have first computed Rayleigh-wave phase velocities for Dziewonski's (1971) shield models S1 and S2, at periods of 60 and 100 s. Results are reported in Table 2.16. Models S1 and S2 are totally compatible with the experimental data reported by Brune & Dorman (1963) over Canadian shield, and by Noponen (1966) for Finnish shield. The models also agree with Kanamori & Abe's (1968) recomputation of theoretical phase velocities from model CANSD, allowing for

Table 2.16

Theoretical (T) and Experimental (E) Rayleigh-Wave Phase Velocities at Shorter Periods

Model	Reference		Velocity (km/s) at 60 s	100 s
S1	Dziewonski (1971)	(T)	4.151	4.208
S2	Dziewonski (1971)	(T)	4.161	4.191
CANSD	Kanamori and Abe (1968)	(T)	4.161	4.230
Continental	Jordan (1975a)	(T)	4.129	4.221
CANSD	Brune and Dorman (1963)	(E)	4.155	4.202
Finnish	Noponen (1966)	(E)	4.18	*

(*) No data reported at this period.

the curvature of the Earth, and for gravity at T> 70 s. Jordan's (1975a) continental model yields phase velocities substantially lower at 60 s, higher at 100 s, thereby exhibiting a dispersion between 60 and 100 s not in agreement with either of the experimental sets of shield data.

Although the term 'shield' is used in various studies with a somewhat variable meaning - as pointed out by Dziewonski (1971) - it is noteworthy to confirm the basic compatibility of Dziewonski's models S1 and S2 with data at shorter period.

Our results on multiple ScS travel-times (see Chapter 1), as well as Sipkin and Jordan's (1976) ask for travel-time residuals for shield on the order of -2 s, with respect to the Jeffreys-Bullen tables. Okal & Anderson (1975) also report a +1 s residual for average (50 - 70 Myr old) ocean. We have computed residuals with respect to Jeffreys-Bullen for the top 620 km of Dziewonski's models O1 (+1.9 s), S1 (1.0 s) and S2 (-1.0 s). As explained earlier in this paper, a correction for Q should be applied to these values, obtained from surface-wave models, before comparing them with body-wave data, such as the one derived from the Jeffreys-Bullen tables. This correction is on the order of -1.1 s (Hart et al. 1977). We end up with the following residuals: O1: +0.8 s; S1: -0.1 s; S2: -2.1 s.

Therefore, we conclude that Dziewonski's shield model S2 reconciles (a) body-wave travel-time residuals; (b) short-period Rayleigh-wave data; and (c) long-period surface-wave data. Model S1 (which has no low-velocity zone) provides an excellent fit to (b) and (c), but stays somewhat slow in terms of body waves. Although a more accurate

description of the oceanic mantle is given by Leeds' various models, Dziewonski's model O1 is compatible with both average oceanic body-wave data, and with long-period surface-wave data. Thus, it is possible, through models O1 and S2, which differ insignificantly (less than 0.7%) below 240 km, to fully account for all presently available seismic data individualizing continents and oceans. These data do not warrant strong lateral heterogeneities (on the order of 0.13 km/s or 2.7% in Jordan's models), between oceans and continents at depths greater than 250 km.

2.4 Conclusion

Our results can be summarized as follows:

(i) Oceanic models at depths shallower than 180 km, developed from the study of short-period Rayleigh-wave phase velocities, combined with the average model C2 at greater depths, correctly predict longer period (200 to 300 s) oceanic phase velocities, and their variations with the age of the plate, which can be as high as 2.5%.

(ii) Such intrinsic oceanic inhomogeneities may create scatter in the dispersion curves, if not taken into account when regionalizing great-circle data for 'pure-path' phase velocities. When these heterogeneities are taken into account, continental velocities are found to be in agreement with Dziewonski's values, obtained from paths sampling the oceanic lithosphere fairly regularly.

(iii) Rayleigh-wave phase velocities for continental areas (both shields and mountainous regions) fall within the range of oceanic models, and the difference between average oceanic and continental velocities is on the same order of magnitude as the variation within the oceanic plate due to its age. This is incompatible with Jordan's models of strong, deep lateral heterogeneities between oceans and continents. Recent data from the Indonesian event give a direct *experimental* confirmation of this result.

(iv) Dziewonski's (1971) shield model S2 reconciles all presently available experimental data for shields (body-wave, short- and long-period surface wave) without any substantial structural difference below 240 km with the average oceanic model O1.

REFERENCES

Abe, K., Determination of Seismic Moment and Energy from the Earth's Free Oscillations, Phys. Earth Plan. Inter., 4, 49-61, 1970.

Abe, K., Y. Satô and J. Frez, Free Oscillations of the Earth Excited by the Kurile Islands Earthquake (1963), Bull. Earthq. Res. Inst. Univ. Tokyo, 48, 87-114, 1970.

Abramowitz, M. and I. Stegun, Handbook of Mathematical Functions, 10th printing, Govt. Printing Office, Washington, D.C., 1972.

Aki, K. and H. Patton, Determination of Seismic Moment Tensor Using Surface Waves, EOS, Trans. Amer. Geophys. Union, 58, 441, 1977 (abstract).

Alterman, Z., H. Jarosch and C.L. Pekeris, Oscillations of the Earth, Proc. Roy. Soc. London, 252A, 80-95, 1959.

Anderson, D.L., The Plastic Layer of the Earth's Upper Mantle, Scientific American, 207, 52-59, 1962.

Anderson, D.L., Chemical Plumes in the Mantle, Geol. Soc. Amer. Bull., 86, 1593-1600, 1975.

Anderson, D.L., A. Ben-Menahem and C.B. Archambeau, Attenuation of Seismic Energy in the Mantle, J. Geophys. Res., 70, 1441-1448, 1965.

Anderson, D.L. and R.S. Hart, An Earth Model Based on Free Oscillations and Body Waves, J. Geophys. Res., 81, 1465-1475, 1976.

Anderson, D.L. and R.S. Hart, The Q of the Earth, Phys. Earth Plan. Inter., in press, 1978.

Anderson, D.L., H. Kanamori, R.S. Hart and H.-P. Liu, The Earth as a Seismic Absorption Band, Science, 196, 1104-1106.

Anderson, D.L. and R.L. Kovach, Attenuation in the Mantle and Rigidity of the Earth's Core from Multiply Reflected Core Phases, Proc. Nat. Acad. Sci., 51, 168-172, 1964.

Anderson, D.L. and C. Sammis, Partial Melting in the Upper Mantle, Phys. Earth Plan. Inter., 3, 41-50, 1970.

Anderson, D.L. and M.N. Toksöz, Surface Waves on a Spherical Earth: 1. Upper Mantle Structure from Love Waves, J. Geophys. Res., 68, 3483-3500, 1963.

Anderssen, R.S., J.R. Cleary and A.M. Dziewonski, Asymptotic Structure in the Eigenfrequencies of Spheroidal Modes of the Earth, Geophys. J. Roy. astr. Soc., 43, 1001-1005, 1975.

Baker, P.E., Islands in the South Atlantic, in: The Oceans, Basins and Margins, Vol. 1, pp. 493-553, Plenum, New-York, 1973.

Balakina, L.M. and A.V. Vvedenskaya, Variation of the Elastic Parameters and Density of Matter at the Boundary of the Earth's Core, Izv. Akad. Nauk SSSR, Geophys. Ser., 11, 909-917, 1962.

Benioff, H., Earthquake Source Mechanisms, Science, 143, 1399-1406, 1964.

Benioff, H, B. Gutenberg and C.F. Richter, Progress Report [for 1963] Seismological Laboratory, California Institute of Technology, Trans. Amer. Geophys. Union, 35, 979-987, 1964.

Ben-Menahem, A., Mode-Ray Duality, Bull. Seism. Soc. Amer., 54, 1315-1321, 1964.

Ben-Menahem, A., Observed Attenuation and Q values of Seismic Surface Waves in the Upper Mantle, J. Geophys. Res., 70, 4641-4651, 1965.

Berteussen, K.A., The Origin of Slowness and Azimuth Anomalies at Large Seismic Arrays, Bull. Seism. Soc. Amer., 66, 719-741, 1976.

Best, W.J., L.R. Johnson and T.V. McEvilly, ScS and the Mantle beneath Hawaii, EOS, Trans. Amer. Geophys. Union, 55, 1147, 1974 (abstract).

Bolt, B.A., M. Niazi and M.R. Somerville, Diffracted ScS and the Shear Velocity at the Core Boundary, Geophys. J. Roy. astr. Soc., 19, 299-305, 1970.

Butler, R., A Source of Bias in Multiple ScS Differential Travel-Times Determined by Cross-Correlation, Geophys. Res. Lett., 4, 593-595, 1977.

Bridgman, P.W., Polymorphic Transitions and Geological Phenomena, Amer. J. Sci., 243A, 90-97, 1945.

Brune, J.N., Travel Times, Body Waves and Normal Modes of the Earth, Bull. Seism. Soc. Amer., 54, 2099-2128, 1964.

Brune, J.N. and J. Dorman, Seismic Waves and Earth Structure in the Canadian Shield, Bull. Seism. Soc. Amer., 53, 167-210, 1963.

Buchbinder, G. and G. Poupinet, Problems Related to PcP and the Core-Mantle Boundary Illustrated by two Nuclear Events, Bull. Seism. Soc. Amer., 63, 2047-2070, 1973.

Buland, R. and J.F. Gilbert, The Theoretical Basis for the Rapid and Accurate Computation of Normal Mode Eigenfrequencies and Eigenfunctions, Unpublished Research Report, Univ. California, San Diego, 1976.

Bullen, K.E., Ellipticity Corrections to Earthquake Waves Reflected at the Central Core, Mon. Not. Roy. astr. Soc. Geophys. Supp., 4, 332-335, 1938.

Capon, J., Characterization of Crust and Upper-Mantle Structure under LASA as a Random Medium, Bull. Seism. Soc. Amer., 64, 235-266, 1974.

Chapman, C.H. and R.A. Phinney, Diffracted Seismic Signals and Their Numerical Resolution, Meth. Comp. Phys., 12, 165-230, 1972.

Choudhury, M.A. and J. Dorel, Spectral Ratio of Short-Period ScP and ScS Phases in Relation to the Attenuation in the Mantle beneath the Tasman Sea and the Antarctic Region, J. Geophys. Res., 78, 462-469, 1973.

Chung, W.-Y. and H. Kanamori, Source Process and Tectonic Implications of the Spanish Deep-Focus Earthquake of March 29, 1954, Phys. Earth Plan. Inter., 13, 85-96, 1976.

Cleary, J., The S-Velocity at the Core-Mantle Boundary from Observations of Diffracted S, Bull. Seism. Soc. Amer., 59, 1399-1405, 1969.

Cleary, J., K. Porra and L. Read, Diffracted S, Nature, 216, 905-906, 1967.

Cordani, U.G., Idade do Volcanismo no Oceamo Atlantico Sul, Ph.D. Thesis, Univ. São Paulo, São Paulo, 1968.

Dahlen, F.A., The Correction of Great-Circular Surface Wave Phase Velocity Measurements for the Rotation and Ellipticity of the Earth, J. Geophys. Res., 80, 4895-4903, 1975.

Dahlen, F.A., Reply [to Dziewonski and Sailor], J. Geophys. Res., 81, 4951, 1976.

Davies, D. and R.M. Sheppard, Lateral Heterogeneity in the Earth's Mantle, Nature, 239, 318-323, 1972.

Dennis, J.G. and C.T. Walker, Earthquakes Resulting from Metastable Phase Transitions, Tectonophysics, 2, 401-407, 1965.

Doornbos, D.J., Characteristics of Lower Mantle Inhomogeneities from Scattered Waves, E⊕S, Trans. Amer. Geophys. Union, 56, 395, 1975 (abstract).

Dorman, J., M. Ewing and J. Oliver, Study of Shear-Velocity Distribution in the Mantle by Rayleigh Waves, Bull. Seism. Soc. Amer., 50, 87-115, 1960.

Douglas, A., J.A. Hudson and V.K. Khembavi, The Relative Excitation of Seismic Surface and Body Waves by Point Sources, Geophys. J. Roy. astr. Soc., 23, 451-460, 1971.

Dratler, J., W.E. Farrell, B. Block and J.F. Gilbert, High-Q Overtone Modes of the Earth, Geophys. J. Roy.astr. Soc., 23, 399-410, 1971.

Dziewonski, A.M., On Regional Differences in Dispersion of Surface Waves, Geophys. J. Roy. astr. Soc., 22, 289-325, 1970.

Dziewonski, A.M., Upper Mantle Models from 'Pure-Path' Dispersion Data, J. Geophys. Res., 76, 2587-2601, 1971.

Dziewonski, A.M. and J.F. Gilbert, Observations of Normal Modes from 84 Records of the Alaskan Earthquake of 1964 March 28, Geophys. J. Roy. astr. Soc., 27, 393-446, 1972.

Dziewonski, A.M. and J.F. Gilbert, Observations of Normal Modes from 84 Records of the Alaskan Earthquake of 1964 March 28, Part II : Further Remarks Based on New Spheroidal Overtone Data, Geophys. J. Roy. astr. Soc., 35, 401-437, 1973.

Dziewonski, A.M. and J.F. Gilbert, Temporal Variations of the Seismic Moment Tensor and the Evidence of Precursive Compression for Two Deep Earthquakes, Nature, 247, 185-188, 1974.

Dziewonski, A.M. and R.V. Sailor, On the Effect of the Earth's Ellipticity on Velocity of Mantle Waves, J. Geophys. Res., 81, 4947-4950, 1976.

Forsyth, D.W., The Early Structural Evolution and Anisotropy of the Oceanic Upper Mantle, Geophys. J. Roy. astr. Soc., 43, 103-162, 1975.

Francis, T.J.G., Upper-Mantle Structure along the Axis of the Mid-Atlantic Ridge near Iceland, Geophys. J. Roy. astr. Soc., 17, 507-520, 1969.

Fukao, Y., Seismic Body Waves from Surface Faults, J. Phys. Earth, 19, 271-281, 1971.

Fukao, Y. and K. Abe, Multimode Love Waves Excited by Shallow and Deep Earthquakes, Bull. Earthq. Res. Inst. Univ. Tokyo, 49, 1-12, 1971.

Furumoto, M. and Y. Fukao, Seismic Moments of Great Deep Shocks, Phys. Earth Plan. Inter., 11, 352-357, 1976.

Furumoto, M., Spacio-Temporal History of the Deep Colombia Earthquake of 1970, Phys. Earth Plan. Inter., 15, 1-12, 1977.

Geller, R.J., Evidence of Precursive Compression for Two Deep Earthquakes, Nature, 252, 28-29, 1974.

Geller, R.J, Body Force Equivalents for Seismic Stress Drop Sources, Bull. Seism. Soc. Amer., 66, 1801-1804, 1976.

Geller, R.J. and S. Stein, Normal Modes of a Laterally Heteorgeneous Body : A One-Dimensional Example, Bull. Seism. Soc. Amer., 68, 103-116, 1978.

Geological Society of America, Map of the Age of the Oceans, 1974.

Gilbert, J.F., Excitation of the Normal Modes of the Earth by Earthquake Sources, Geophys. J. Roy. astr. Soc., 22, 223-226, 1970.

Gilbert, J.F., The Relative Efficiency of Earthquakes and Explosions in Exciting Surface Waves and Body Waves, Geophys. J. Roy. astr. Soc., 33, 487-488, 1973.

Gilbert, J.F., Some Asymptotic Properties of the Normal Modes of the Earth, Geophys. J. Roy. astr. Soc., 43, 1007-1011, 1975.

Gilbert, J.F. and R.P. Buland, An Enhanced Deconvolution Procedure for Retrieving the Moment Tensor from a Sparse Network, Geophys. J. Roy. astr. Soc., 47, 251-255, 1976.

Gilbert, J.F. and A.M. Dziewonski, An Application of Normal Mode Theory to the Retrieval of Structural Parameters and Source Mechanisms from Seismic Spectra, Phil. Trans. Roy. Soc. London, 278A, 187-269, 1975.

Gilman, R., Report on Some Experimental Long-Period Systems, Bull. Seism. Soc. Amer., 50, 553-559, 1960.

Girardin, N. and G. Poutpinet, Teleseismic S Travel-Time Delays for Mid-Atlantic Ridge Earthquakes, Phys. Earth Plan. Inter., 9, 306-313, 1974.

Green, D.H., Magmatic Activity as the Major Process in the Chemical Evolution of the Earth's Crust and Mantle, Tectonophysics, 13, 47-71, 1972.

Gutenberg, B. Der Aufbau der Erdkruste auf Grund geophysikalischer Beobachtungen, Z. Geophysik, 1, 94-108, 1924.

Gutenberg, B., Untersuchungen zur Frage, bis zu welcher Tiefe die Erde kristallin ist, Z. Geophysik, 2, 24-30, 1926.

Gutenberg, B., On the Layer of Relatively Low Wave Velocity at a Depth of about 180 km, Bull. Seism. Soc. Amer., 38, 121-148, 1948.

Gutenberg, B. and C.F. Richter, On Seismic Waves, II, Gerlands. Beitr. Geophys., 45, 280-360, 1935.

Hadley, D.M., G.S. Stewart and J.E. Ebel, Yellowstone : Seismic Evidence for a Chemical Mantle Plume, Science, 193, 1237-1239, 1976.

Hales, A.R. and J.L. Roberts, The Travel Times of S and SKS, Bull. Seism. Soc. Amer., 60, 461-489, 1970.

Hamilton, W.C., Statistics in Physical Science, Ronald, New-York, 1964.

Harkrider, D.G., Surface Waves in Multilayered Elastic Media. I: Rayleigh and Love Waves from Buried Sources in a Multilayered Elastic Half-Space, Bull. Seism. Soc. Amer., 54, 627-679, 1964.

Harkrider, D.G., Surface Waves in Multilayered Elastic Media. II: Higher Mode Spectra and Spectral Ratios from Point Sources in Plane Layered Earth Models, Bull. Seism. Soc. Amer., 60, 1937-1987, 1970.

Harkrider, D.G. and F. Press, The Krakatoa Air-Sea Waves : An Example of Pulse Propagation in Coupled Systems, Geophys. J. Roy. astr. Soc., 13, 149-159, 1967.

Hart, R.S., D.L. Anderson and H. Kanamori, Shear Velocity and Density of an Attenuating Earth, Earth Plan. Sci. Lett., 32, 25-34, 1976.

Hart, R.S., D.L. Anderson and H. Kanamori, The Effect of Attenuation on Gross Earth Models, J. Geophys. Res., 82, 1647-1654, 1977.

Hart, R.S. and H. Kanamori, Search for Compression before a Deep Earthquake, Nature, 253, 333-336, 1975.

Hart, R.S. and F. Press, S_n Velocities and the Composition of the Lithosphere in the Regionalized Atlantic, J. Geophys. Res., 78, 407-411, 1973.

Healy, J.H. and L.G. Peake, Seismic Velocity Structure along a Section of the San Andreas Fault near Bear Valley, California, Bull. Seism. Soc. Amer., 65, 1177-1197, 1975.

Helmberger, D.V., The Crust-Mantle Transition in the Bering Sea, Bull. Seism. Soc. Amer., 58, 179-214, 1968.

Helmberger, D.V., On the Structure of the Low-Velocity Zone, Geophys. J. Roy.astr. Soc., 34, 251-263, 1973.

Helmberger, D.V. and G.R. Engen, Upper Mantle Shear Structure, J. Geophys. Res., 79, 4017-4028, 1974.

Ibrahim, A.-B. K., The Amplitude Ratio PcP/P and the Core-Mantle Boundary, Pure Appl. Geophys., 91, 114-133, 1971.

Ibrahim, A.-B. K. and O.W. Nuttli, Travel-Time Curves and Upper-Mantle Structure from Long Period S Waves, Bull. Seism. Soc. Amer., 57, 1063-1092, 1967.

Ince, E.L., Ordinary Differential Equations, Dover, New-York, 1956.

Isacks, B. and P. Molnar, Distribution of Stresses in the Descending Lithosphere from a Global Survey of Focal-Mechanism Solutions of Mantle Earthquakes, Rev. Geophys. Space Phys., 9, 103-174, 1971.

Jacobs, J.A., The Earth's Core, Academic Press, London, 1975.

Jeffreys, H., The Times of Transmission and Focal Depths of Large Earthquakes, Mon. Not. Roy. astr. Soc. Geophys. Supp., 1, 500-521, 1928.

Jeffreys, H., Small Corrections in the Theory of Surface Waves, Geophys. J. Roy. astr. Soc., 6, 115-117, 1961.

Jeffreys, H. and K.E. Bullen, Seismological Tables, British Association for the Advacement of Science, London, 1940.

Jobert, N., Excitation des Oscillations Propres de Torsion de la Terre, Ann. Géophys., 19, 372-383, 1962.

Jordan, T.H., Lateral Heterogeneity and Mantle Dynamics, Nature, 257, 745-750, 1975a.

Jordan, T.H., The Continental Tectosphere, Rev. Geophys. Space Space, 13, (4), 1-12, 1975b.

Jordan, T.H. and D.L. Anderson, Earth Structure from Free Oscillations and Travel Times, Geophys. J. Roy. astr. Soc., 36, 411-459, 1974.

Jordan, T.H. and S.A. Sipkin, Estimation of the Attenuation Operator for Multiple ScS Waves, Geophys. Res. Lett., 4, 167-170, 1977.

Julian, B.R. and M.K. Sengupta, Seismic Travel-Time Evidence for Lateral Heterogeneities in the Deep Mantle, Nature, 242, 243-247, 1973.

Kanamori, H., Spectrum of Short-Period Core Phases in Relation to Attenuation in the Mantle, J. Geophys. Res., 72, 2181-2186, 1967.

Kanamori, H., Velocity and Q of Mantle Waves, Phys. Earth Plan. Inter., 2, 259-275, 1970.

Kanamori, H., Re-examination of the Earth's Free Oscillations Excited by the Kamchatka Earthquake of November 4, 1952, Phys. Earth Plan. Inter., 11, 216-226, 1976.

Kanamori, H., Seismic and Aseismic Slip along Subduction Zones and their Tectonic Implications, in: Island Arcs, Deep Sea Trenches and Back-Arc Basins, Maurice Ewing Series, Amer. Geophys. Union, 1, 163-174, 1977a.

Kanamori, H., The Energy Release in Great Earthquakes, J. Geophys. Res., 82, 2981-2987, 1977b.

Kanamori, H. and K. Abe, Deep Structure of Island Arcs as Revealed by Surface Waves, Bull. Earthq. Res. Inst. Univ. Tokyo, 46, 1001-1025, 1968.

Kanamori, H. and D.L. Anderson, Importance of Physical Dispersion in Surface Wave and Free Oscillation Problems : Review, Rev. Geophys. Space Phys., 15, 105-112, 1977.

Kanamori, H. and J.J. Cipar, Focal Process of the Great Chilean Earthquake of May 22, 1960, Phys. Earth Plan. Inter., 9, 128-136, 1975.

Kanamori, H. and G.S. Stewart, Mode of the Strain Release along the Gibbs Fracture Zone, Mid-Atlantic Ridge, Phys. Earth Plan. Inter., 11, 312-332, 1976.

Kanasewich, E.R., R.M. Ellis, C.H. Chapman and P.R. Gutowski, Seismic Array Evidence for a Core Boundary Origin for the Hawaiian Linear Volcanic Chain, J. Geophys. Res., 78, 1361-1370, 1973.

Katsumata, M., Seismicity and Some Related Problems in and near the Japanese Islands, Kenshin Jiho (Q.J. Seism. Jap. Meteor. Agency), 35, 75-142, 1970 [in Japanese].

Kausel, E.G., A.R. Leeds and L. Knopoff, Variations of Rayleigh-Wave Phase Velocities across the Pacific Ocean, Science, 186, 139-1414, 1974.

Kennett, B.L.N. and R.S. Simmons, An Implosive Precursor to the Colombia Earthquake of 1970 July 31, Geophys. J. Roy. astr. Soc., 44, 471-482, 1976.

Kind, R. and G. Müller, The Structure of the Outer Core from SKS Amplitudes and Travel Times, Bull. Seism. Soc. Amer., 67, 1541-1554, 1977.

Kittel, C., Quantum Theory of Solids, Wiley, New-York, 1963.

Kono, Y. and T. Yoshii, Numerical Experiments on the Thickening Plate Model, J. Phys. Earth, 23, 63-75, 1975.

Kovach, R.L. and D.L. Anderson, Attenuation of Shear Waves in the Upper and Lower Mantle, Bull. Seism. Soc. Amer., 54, 1855-1864, 1964.

Lamb, H., On the Vibrations of an Elastic Sphere, London Math. Soc. Proc., 13, 1882.

Lambeck, K, Lateral Density Anomalies in the Upper Mantle, J. Geophys. Res., 81, 6333-6340, 1976.

Landisman, M., T. Usami, Y. Satô and R. Massé, Contributions of Theoretical Seismograms to the Study of Modes, Rays and the Earth, Rev. Geophys. Space Phys., 8, 533-591, 1970.

Langston, C.A. and D.V.Helmberger, A Procedure for Modelling Shallow Dislocation Sources, Geophys. J. Roy. astr. Soc., 42, 117-130, 1975.

Leeds, A.R., Lithospheric Thickness in the Western Pacific, Phys. Earth Plan. Inter., 11, 61-64, 1975.

Leeds, A.R., E.G. Kausel and L. Knopoff, Variations of Upper Mantle Structure under the Pacific Ocean, Science, 186, 141-143, 1974.

Lehmann, I., On the Shadow of the Earth's Core, Bull. Seism. Soc. Amer., 43, 291-306, 1953.

Liu, H.-P., D.L. Anderson and H. Kanamori, Velocity Dispersion due to Anelasticity, Geophys. J. Roy. astr. Soc., 47, 41-58, 1976.

Love, A.E.H., Some Problems of Geodynamics, Camb. Univ. Press, Cambridge, 1911.

Love, A.E.H., A Treatise on the Mathematical Theory of Elasticity, Dover, New-York, 1944.

Luh, P.C. and A.M. Dziewonski, Theoretical Seismograms for the Colombian Earthquake of 1970 July 31, Geophys. J. Roy. astr. Soc., 43, 679-695, 1975.

Madariaga, R.I. and K. Aki, Spectral Splitting of Toroidal Free Oscillations due to Lateral Heterogeneity of the Earth's Structure, J. Geophys. Res., 77, 4421-4431, 1972.

Matusawa, T., Study of Earthquakes, Uno Shoten, Tokyo, 1964.

Mendiguren J.A., Source Mechanism of a Deep Earthquake from Analysis of World-Wide Observations of Free Oscillations, Ph.D. Thesis, Massachusetts Institute of Technology, Cambridge, Mass., 1972.

Mendiguren J.A., Identification of Free Oscillation Spectral Peaks for 1970 July 31, Colombian Deep Shock Using the Excitation Criterion, Geophys. J. Roy. astr. Soc., 33, 281-321, 1973.

Mendiguren, J.A., Volumetric Characteristics of the Focal Process of Deep Earthquakes Based on Free Oscillation Data, EOS, Trans. Amer. Geophys. Union, 56, 1028, 1975 (abstract).

Mendiguren, J.A., Inversion of Surface Wave Data in Source Mechanism Studies, J. Geophys. Res., 82,889-894, 1977.

Mikumo, T. and T. Kurita, Q Distribution for Long-Period P Waves in the Mantle, J. Phys. Earth, 16, 11-29, 1968.

Minster, J.B., T.H. Jordan, P. Molnar and E. Haines, Numerical Modelling of Instantaneous Plate Tectonics, Geophys. J. Roy. astr. Soc., 36, 541-576, 1974.

Mitchell, B.J. and D.V. Helmberger, Shear Velocities at the Base of the Mantle from Observations of S and ScS, J. Geophys. Res., 78, 6009-6020, 1973.

Mondt, J.C., SH Waves : Theory and Observations for Epicentral Distances Greater than 90°, Phys. Earth Plan. Inter., 15, 46-59, 1977.

Moore, R.D. and W.E. Farrell, Linearization and Calibration of Electrostatically Fedback Gravity Meters, J. Geophys. Res., 75, 928-932, 1970.

Morgan, W.J., Convection Plumes in the Lower Mantle, Nature, 230, 42-43, 1971.

Nakanishi, I., Measurements of Phase Velocities and Q, M.S. Thesis, Nagoya Univ., Nagoya, 1977.

Niazi, M., Source Dynamics of the Dasht-e-Bayāz Earthquake of August 31, 1968, Bull. Seism. Soc. Amer., 59, 1843-1861, 1969.

Noponen, I., Surface Wave Phase Velocities in Finland, Bull. Seism. Soc. Amer., 56, 1093-1104, 1966.

Noponen, I., Seismic Ray Direction Anomalies Caused by Deep Structure in Fennoscandia, Bull. Seism. Soc. Amer., 64, 1931-1941, 1974.

Okal, E.A., The Effect of Intrinsic Oceanic Upper-Mantle Heterogeneity on Regionalization of Long-Period Rayleigh Wave Phase Velocities, Geophys. J. Roy. astr. Soc., 49, 357-370, 1977.

Okal, E.A., A Physical Classification of the Earth's Spheroidal Modes, J. Phys. Earth, in press, 1978a.

Okal, E.A., Observed Very-Long Period Rayleigh Wave Phase Velocities across the Canadian Shield, Geophys. J. Roy. astr. Soc., in press, 1978b.

Okal, E.A. and D.L. Anderson, A Study of Lateral Hetrogeneities in the Upper Mantle by Multiple-ScS Travel-Time Residuals, Geophys. Res. Lett., 2, 313-316, 1975.

Okal, E.A. and R.J. Geller, On the Observability of Isotropic Sources: The July 31, 1970 Colombian Earthquake, Phys. Earth Plan. Inter., in press, 1978a.

Okal, E.A. and R.J. Geller, Shear Wave Velocity at the Base of the Mantle from Profiles of Diffracted SH Waves, Bull. Seism. Soc. Amer., submitted, 1978b.

Okal, E.A. and G. Kuster, A Teleseismic Array Study in French Polynesia : Implications for Local and Distant Structure, Geophys. Res. Lett., 2, 5-8, 1975.

Oversby, V.M., Lead in Ocean Islands : Faial, Azores and Trindade, Earth Plan. Sci. Lett., 11, 401-406, 1971.

Parker, R.L. and D.W. Oldenburg, Thermal Model of an Ocean Ridge, Nat. Phys. Sci., 242, 137-139, 1973.

Parsons, B. and J.G. Sclater, An Analysis of the Variation of Ocean Floor Bathymetry with Age, J. Geophys. Res., 82, 803-827, 1977.

Particle Data Group, Review of Particle Properties, Revs. Mod. Phys., 43, S1-S150, 1971.

Particle Data Group, Review of Particle Properties, Revs. Mod. Phys., 48, S1-S246, 1976.

Pekeris, C.L. and H. Jarosch, Free Oscillations of the Earth, Int. Ser. Monog. Earth Sci., E. Ingerson, ed., vol. 1, 171-192, 1958.

Phinney, R.A. and R. Burridge, Representation of the Elastic-Gravitational Excitation of a Spherical Earth Model by Generalized Spherical Harmonics, Geophys. J. Roy. astr. Soc., 34, 451-487, 1973.

Powell, C.A., Evidence for Mantle Heterogeneity from Two Large Seismic Arrays, Nature, 254, 40-42, 1975.

Powell, C.A., Mantle Heterogenity : Evidence from Large Seismic Arrays, Ph.D. Thesis, Princeton Univ., Princeton, N.J., 1976.

Press, F., Rigidity of the Earth's Core, Science, 124, 1204, 1956.

Press, F. and D.G. Harkrider, Air-Sea Waves from the Explosion of Krakatoa, Science, 154, 1325-1327, 1966.

Randall, M.J. and L. Knopoff, The Mechanism of the Focus of Deep Earthquakes, J. Geophys. Res., 75, 4965-4976, 1970.

Richards, P.G., A Contribution to the Theory of High Frequency Elastic Waves, with Applications to the Shadow of the Earth's Core, Ph.D. Thesis, California Institute of Technology, Pasadena, California, 1970.

Ringwood, A.E., The Pyroxene-Garnet Transformation in the Earth's Mantle, Earth Plan. Sci. Lett., 2, 255-263, 1967.

Rocard, Y., Dynamique Générale des Vibrations, Masson, Paris, 1948.

Saito, M., Excitation of Free Oscillations and Surface Waves by a Point Source in a Vertically Heterogeneous Medium, J. Geophys. Res., 72, 3689-3699, 1967.

Sasatani, T., Focal Process of the Tonga Deep-Focus Earthquake of 1967, Proc. Ann. Meet. Seism. Soc. Japan, (1), 101, 1976 (abstract)[In Japanese].

Sato, R. and A.F. Espinosa, Dissipation in the Earth's Mantle and Rigidity and Viscosity in the Earth's Core Determined from Waves Multiply Reflected from the Mantle-Core Boundary, Bull. Seism. Soc. Amer., 57, 829-856, 1967.

Satô, Y. and T. Usami, Basic Study on the Oscillation of a Homogeneous Elastic Sphere I: Frequency of the Oscillations, Geophys. Mag., 31, 15-24, 1962a.

Satô, Y. and T. Usami, Basic Study on the Oscillation of a Homogeneous Elastic Sphere II: Distribution of Displacement, Geophys. Mag., 31, 25-47, 1962b.

Satô, Y. and T. Usami, Basic Study on the Oscillation of a Homogeneous Elastic Sphere III: Boundary Conditions and the Generation of Elastic Waves, Geophys. Mag., 31, 49-62, 1962c.

Scholte, J.G.J., On Seismic Waves in a Spherical Earth, Kon. Ned. Meteorol. Inst. Meded. Ver., 65, 1-55, 1956.

Sengupta, M.K. and B.R. Julian, Mantle Velocity and its Regional Variation, EOS, Trans. Amer. Geophys. Union, 55, 330, 1974 (abstract).

Sipkin, S.A. and T.H. Jordan, Lateral Heteorgenity of the Upper Mantle Determined from the Travel Times of ScS, J. Geophys. Res., 80, 1474-1484, 1975.

Sipkin, S.A. and T.H. Jordan, Lateral Heterogeneity of the Upper Mantle Determined from the Travel Times of Multiple ScS, J. Geophys. Res., 81, 6307-6331, 1976.

Stein, S. and R.J. Geller, Time-Domain Observation and Synthesis of Split Spheroidal and Torsional Free Oscillations of the 1960 Chilean Earthquake : Preliminary Results, Bull. Seism. Soc. Amer., 68, 325-332, 1978.

Stewart, G.S., Implications for Plate Tectonics of the August 19, 1977 Indonesian Decoupling Normal-Fault Earthquake, EOS, Trans. Amer. Geophys. Union, 59, in press, 1978 (abstract).

Stoneley, R., On Deep Focus Earthquakes, Gerlands. Beitr. Geophys., 29, 417-435, 1931.

Strelitz, R.A., Source Progress of Three Complex Deep-Focus Earthquakes, Ph.D. Thesis, Princeton Univ., Princeton, N.J., 1977.

Strelitz, R.A., Moment Tensor Inversions and Source Models, Geophys. J. Roy. astr. Soc., 52, 359-364, 1978.

Stump, B., The Determination of Source Mechanisms by the Linear Inversion of Seismograms, EOS, Trans. Amer. Geophys. Union, 57, 953, 1976 (abstract).

Sykes, L.R., Deep Earthquakes and Rapidly-Running Phase Changes; A Reply to Dennis and Walker, J. Geophys. Res., 73, 1508-1510, 1968.

Takeuchi, H. and M. Saito, Seismic Surfaces Waves, Meth. Comp. Phys., 12, 217-295, 1972.

Takeuchi, H., M. Saito and N. Koyabashi, Study of Shear Wave Velocity Distribution in the Upper Mantle by Rayleigh and Love Waves, J. Geophys. Res., 67, 2831-2839, 1962.

Takeuchi, H., M. Saito and N. Koyabashi, Rigidity of the Earth's Core and Fundamental Oscillation of the Earth, J. Geophys. Res., 68, 933-936, 1963.

Toksöz, M.N. and D.L. Anderson, Phase Velocities of Long-Period Surface Waves and Structure of the Upper Mantle 1. Great Circle Love and Rayleigh Wave Data, J. Geophys. Res., 71, 1649-1658, 1966.

Toksöz, M.N. and A. Ben-Menahem, Velocities of Mantle Love and Rayleigh Waves over Multiple Paths, Bull. Seism. Soc. Amer., 53, 741-763, 1963.

Toksöz, M.N., J.W. Minear and N.H. Sleep, Temperature Field and Geophysical Effects of a Downgoing Slab, J. Geophys. Res., 76, 1113-1138, 1971.

Tréhu, A.M., J.G. Sclater and J. Nabelek, The Depth and Thickness of the Ocean Crust and Dependence upon Age, Bull. Soc. Géol. France, Ser. 7, 18, 917-930, 1976.

Tryggvason, E., Wave Velocity in the Upper Mantle below the Arctic-Atlantic Ocean and Northwest Europe, Ann. Geofis., 14, 379-392, 1961.

Utsu, T., Anomalies in Seismic Wave Velocity and Attenuation Associated with a Deep Earthquake Zone, J. Fac. Sci. Hokkaido Univ. Ser. 7 (Geophys.), 3, 1-25, 1967.

Vaišnys, J.R. and C.C. Pilbeam, Deep Earthquake Initiation by Phase Transformation, J. Geophys. Res., 81, 985-988, 1976.

Valencio, D.A. and J.E. Mendía, Paleomagnetism and K/Ar Ages of Some Igneous Rocks of the Trindade Complex and the Valado Formation from Trindade Island, Brazil, Rev. Bras. Geociênc., 4, 124-132, 1974.

Vermeulen, J.M. and D.J. Doornbos, Mantle Heterogeneity and Mislocation Patterns for Seismic Networks, Z. Geophys., 43, 545-559, 1977.

Vogt, P.R., Volcano Spacing, Fractures, and Thickness of the Lithosphere, Earth Plan. Sci. Lett., 21, 235-252, 1974a.

Vogt, P.R., Volcano Height and Plate Thickness, Earth Plan. Sci. Lett., 23, 337-348, 1974b.

Wilson, J.T., Hypothesis of Earth's Behaviour, Nature, 198, 925-929, 1963.

Wilson, J.T., Convection Currents and Continental Drift: Evidence from Ocean Islands Suggesting Movement of the Earth, Phil. Trans. Roy. Soc. London, 258A, 145-167, 1965.

Wilson, J.T., Continents Adrift and Continents Aground, Freeman, San Francisco, California, 1976.

Woodhouse, J.H, Asymptotic Results for Elastodynamic Propagator Matrices in Plane Stratified and Spherically Symmetric Earth Models, Geophys. J. Roy. astr. Soc., in press, 1978.

Wright, C., Comments on 'Seismic Array Evidence of a Core-Boundary Source for the Hawaiian Linear Volcanic Chain' by Kanasewich et al., J. Geophys. Res., 80, 1915-1919, 1975.

York, J.E. and D.V. Helmberger, Low-Velocity Zone Variations in the Southwestern United States, J. Geophys. Res., 78, 1883-1886, 1973.

Yoshida, M. and M. Tsujiura, Spectrum and Attenuation of Multiply Reflected Core Phases, J. Phys. Earth, 23, 31-42, 1975.

Yoshii, T., Regionality of Group Velocities of Rayleigh Waves in the Pacific and Thickening of the Plate, Earth Plan. Sci. Lett., 25, 305-312, 1975.